Technische Universität München
TUM School of Computation, Information and Technology

Incremental Optimal Control for Robot Manipulators: A Robust and Optimal Control Framework

Yongchao Wang

Vollständiger Abdruck der von der TUM School of Computation, Information and Technology der Technischen Universität München zur Erlangung des akademischen Grades eines

Doktors der Ingenieurwissenschaften (Dr.-Ing.)

genehmigten Dissertation.

Vorsitz: Prof. Dr.-Ing. habil. Erwin Biebl

Prüfende/-r der Dissertation:

1. Prof. Dr.-Ing. Martin Buss

2. Prof. Dr.-Ing. Rolf Findeisen
   Technische Universität Darmstadt

Die Dissertation wurde am **06.04.2022** bei der Technischen Universität München eingereicht und durch die TUM School of Computation, Information and Technology am **03.11.2022** angenommen.

To my wife and
my daughter

Preamble

The dissertation summarizes my research conducted at Chair of Automatic Control Engineering (LSR), Technical University of Munich, Germany. This dissertation would not have have been possible without numerous people whom I would like to thank here.

I would like to thank my doctoral advisor, Prof. Martin Buss, for his continuous support and the freedom. I am also very greatful to my co-supervisor Dr. Marion Leibold for her support and feedback during my research. I also want to thank Dr. Jinoh Lee with German Aerospace Center (DLR) for his constructive feedback on this work. His insightful comments and recommendations were valuable contributions to my dissertation and are highly appreciated. I also appreciate the support of Dr. Dirk Wollherr and Dr. Stefan Sosnowski.

Furthermore, I also would like to thank Prof. Lars Grune from University of Bayreuth, and Dr. Chritian Ott and Dr. Alexander Dietrich from DLR, for their useful discussions and suggestions to my research.

I would like to thank my colleagues at LSR for being supportive and helpful during my stay (in alphabetical order): Salman Bari, Tommaso Bensiolini, Tim Brudigam, Yuhong Chen, Annalena Daniels, Ni Dang, Yingwei Du, Michael Fink, Volker Gabler, Yufeng Gao, Gerold Huber, Yuchen Jiang, Sebastian Kerz, Cong Li, Run Li, Fangzhou Liu, Tong Liu, Johannes Teutsch, Hao Zhang, Zengjie Zhang, and Zhehua Zhou. The monthly discussions were constructive in improving my research. Special thanks go to Dr. Qingchen Liu and Zewen Yang at the Chair of Information-oriented Control (ITR) who helped me so much in my academic career. I also want to appreciate Wolfgang Jaschik, Thomas Lowitz, Tobias Stoeber, Kilian Weber, and Christian Ott for their assistance and help related to hardware. I am also thankful for kind and professional support in organizational matters by Larissa Schmid and Brigitta Renner.

During my research at LSR, I had the chance to work with some bright and talented students. I would like to thank Wenyan Ye, Jing Xie, Jia Lv, Yang Liu, and Bowen Song for their commitment and excellent contributions.

Finally, my family deserves my deepest gratefulness: I would like to thank my parents, sisters, brothers for their continuous support and invaluable advice in hard times. Most importantly, my beloved wife and my daughter backed my endeavors, although countless evenings and weekends were sacrificed throughout the years. Thank you very much.

Munich, March 2022 Yongchao Wang

Abstract

Robot manipulators have been widely used in scientific research and engineering applications, such as space exploration, mental spinning and polishing, cargo handling, medical surgery, etc. With low cost, they are able to effectively improve production efficiency, freed up productivity, and protect human life and health. Recently, the robot manipulator is required to execute more and more sophisticated tasks, and thus it is increasingly challenging to control a robot manipulator reliably. First, the dynamics of the robot manipulator is normally not known exactly, especially for high-degree-of-freedom ones. Moreover, input and state constraints may deteriorate instantaneous performance of the robot manipulator and can be used to describe safety requirements on control used in safety-critical applications, e.g., close to or in cooperation with humans. Unfortunately, input and state constraints are not of interest in the recent controller design. In addition, because of the inverse calculation involved in task-space control schemes, singularity problems are also challenging to be handled.

In the dissertation, an adaptive incremental sliding mode controller is firstly proposed to address modeling errors and external disturbances. The switching gains of the sliding mode controller are regulated by a novel positive semi-definite barrier function (PSDBF). The PSDBF prevents switching gains from being over/under-estimated. It results in enhancing robustness of the controller and attenuating chattering.

Secondly, an incremental model predictive controller (MPC) is developed exploiting time-delay estimation (TDE), and the concrete mathematical model is not required. This is because the continuous-time nonlinear system model is approximated by an incremental system using TDE. The input and state constraints are formulated as inequality constraints. Thus, optimal control performance is achieved while input and state constraints are taken into account. Considering the bounded error sourced from TDE as the major disturbance, local input-to-state stability (ISS) of MPC is analyzed. Different from existing ISS analysis for MPC, here continuity of the value function is used to derive the upper bound of the difference between two value functions, and the resulting cumulative error bound is not over-conservative. It is theoretically inferred from this ISS and the cumulative error bound that increasing the prediction horizon enlarges the region of attraction, and at the same time decreases tracking errors.

Finally, a robust and singularity-free task-prioritized control scheme, hierarchical incremental MPC (HIMPC), is proposed for kinematically redundant robots based on multi-layer constrained optimal control problems (OCPs), where multiple tasks are executed and ordered by priority levels. Incremental systems are developed that approximate uncertain system dynamics and also equations of motion of tasks. The task hierarchy is then realized by equality constraints on control signals for lower-priority tasks, based on dynamic consistency. Hierarchical feasibility of HIMPC and uniqueness of the solution is theoretically analyzed. The distinctive feature of this task-space controller is singularity-free. The reasons are two-fold: (1) no inverse matrix calculation is involved in the algorithm; (2) Hessian matrices of the constrained OCPs are always positive definite.

Zusammenfassung

Robotermanipulatoren sind in der wissenschaftlichen Forschung und in technischen Anwendungen weit verbreitet, z. B. in der Weltraumforschung, beim Drehen und Polieren von Metallen, beim Frachtumschlag, in der medizinischen Chirurgie usw. Sie sind kostengünstig und können die Produktionseffizienz effektiv verbessern, die Produktivität steigern und das Leben und die Gesundheit der Menschen schützen. In letzter Zeit müssen Robotermanipulatoren immer anspruchsvollere Aufgaben ausführen, so dass es immer schwieriger wird, einen Robotermanipulator zuverlässig zu regeln. Zum einen ist die Dynamik des Robotermanipulators normalerweise nicht genau bekannt, insbesondere bei Robotern mit hohem Freiheitsgrad. Darüber hinaus können Eingangs-und Zustandsbeschränkungen die instantane Performanzdes Robotermanipulators verschlechtern. Eingangs- und Zustandsbeschränkungen sind typischeSicherheitsanforderungen in sicherheitskritischen Anwendungen, z. B. bei Robotermanipulatorenin der Nähe von oder in Zusammenarbeit mit Menschen. Beschränkungen diese Art werden in Reglerentwurfsverfahren jedoch häufig nicht beachtet. Darüber hinaus sind Singularitätsprobleme aufgrund der inversen Berechnungen, die nötig sind wenn Regelungen im Task-Space erfolgen, ebenfalls eine Herausforderung.

In dieser Dissertation wird zunächst ein adaptiver inkrementeller Gleitmodusregler vorgeschlagen, um Modellierungsfehler und externe Störungen zu berücksichtigen. Die Schaltfunktionendes Gleitmodusreglerswerden durch eine neuartige positiv semi-definite Barrierefunktion (PSDBF) implementiert. Die PSDBF verhindert, dass die Schaltverstärkungüber-oder unterschätzt werden. Dadurch wird die Robustheit des Reglers erhöht und das Chattering gedämpft.

Zweitens wird ein inkrementeller modellprädiktiver Regler (MPC) entwickelt, der eine Zeitverzögerungsschätzung (TDE) nutzt, und kein konkretesmathematische erfordert. Das konkrete mathematische Modell ist nicht erforderlich, da das zeitkontinuierliche nichtlineare Systemmodell durch ein inkrementelles System mit TDE approximiert wird. Die Eingangs- und Zustandsbeschränkungen werden als Ungleichheitsbedingungen formuliert. Auf diese Weise wird eine optimale Regelperformanzerreicht, während Eingangs- und Zustandsbeschränkungen berücksichtigt werden. Unter Betrachtung des begrenzten Fehlers, der von der TDE als Hauptstörung herrührt, wird die lokale Input-to-State-Stabilität (ISS) der MPC analysiert. Anders als bei der bisherigen ISS-Analyse für MPC wird hier die Stetigkeitder Wertefunktion verwendet, um die obere Schranke der Differenz zwischen zwei Wertfunktionen abzuleiten. Dieresultierende kumulative Fehlerschranke ist damit nicht überkonservativ. Aus der ISS und der kumulativen Fehlerschranke wird theoretisch abgeleitet, dass eine Vergrößerung des Vorhersagehorizontssowohlden Attraktionsbereichals auch denNachlauffehler verringert.

Schließlich wird ein robustes und singularitätsfreiestask-priorisierendes Regelschema, hierarchische inkrementelle MPC (HIMPC), für kinematisch redundanteRoboter vorgeschlagen, das auf mehrschichtigen, beschränktenoptimalen Regelproblemen (OCPs) basiert, bei denen mehrere Tasksausgeführt und nach Prioritätsstufen geordnet werden. Es werden inkrementelle Systeme entwickelt, die die unsichere Systemdynamik und auch die Bewegungsgleichungen der Aufgabenapproximieren. Die Task-hierarchie wird durch Gleichheitsbeschränkungen für Steuersignale der Tasksniedrigerer Priorität realisiert, wobei als Grundlage die dynamische Konsistenz dient. Die hierarchische Machbarkeit von HIMPC und die Eindeutigkeit der Lösung werden theoretisch analysiert. Die Besonderheit dieses Task-Space-Reglersist die Singularitätsfreiheit. Dafür gibt es zwei Gründe: (1) der Algorithmus erfordert

keine Berechnung der inversen Matrix; (2) die Hessematrizender beschränkten OCPs sind immer positiv definit.

List of Publications

Publications resulting from the work performed during the research at Technical University of Munich with first authorship and co-authorship:

- **Yongchao Wang**, Zengjie Zhang, Cong Li, and Martin Buss, "Adaptive incremental sliding mode control for a robot manipulator", *Mechatronics*, vol.82, Apr. 2022, Art. No. 102717.
- **Yongchao Wang**, Marion Leibold, Jinoh Lee, Wenyan Ye, Jing Xie, and Martin Buss, "Incremental model predictive control exploiting time delay estimation for a robot manipulator", *IEEE Transactions on Control Systems Technology*, Early Access, `Doi: 10.1109/TCST.2022.3142629`.
- **Yongchao Wang**, Yang Liu, Jinoh Lee, Marion Leibold, and Martin Buss, "Hierarchical incremental MPC: a robust and singularity-free method", *IEEE Transactions on Robotics*, under review.
- Zengjie Zhang, **Yongchao Wang** (corresponding author), and Dirk Wollherr, "Safe tracking control of Euler-Lagrangian systems based on a novel adptive super-twisting algorithm", in *Proc. 21st IFAC world congress*, Berlin, Germany, 2020, pp. 10109-10114.
- Cong Li, **Yongchao Wang**, Fangzhou Liu, Qingchen Liu, and Martin Buss, "Model-free incremental adaptive dynamic programming based approximate robust optimal regulation", *International Journal of Robust and Nonlinear Control*, Early Access, `Doi: https://doi.org/10.1002/rnc.5964`.
- Cong Li, Fangzhou Liu, **Yongchao Wang**, and Martin Buss, "Concurrent learning-based adaptive control of an uncertain robot manipulator with guaranteed safety and performance", *IEEE Transactions on Systems, Man, and Cybernetics: System*, Early Access, `Doi: 10.1109/TSMC.2021.3064971`.

Contents

List of Figures

List of Tables

Notation

Acronyms and Abbreviations

MPC	model predictive control
IMPC	incremental model predictive control
HIMPC	hierarchical incremental model predictive control
TDE	time-delay estimation
ISS	input-to-state stability
PSDBF	positive semi-definite barrier function
OCP	optimal control problem
IBS	incremental backstepping
CT	computed torque
DOB	disturbance observer
TDC	time delay conrol
INDI	incremental nonlinear dynamic inversion
SMC	sliding mode control
AISMC	adaptive incremental sliding mode control
LQR	linear quadratic regulator
LTI	linear time-invariant
PCI	peripheral component interconnect
RMS	root-mean-square
NN	neural network
QP	quadratic-programming
OSF	operational space formulation
HQP	hierarchical quadratic programming
GP	Gaussian processes

EE	end-effector
D-H	Denavit-Hartenbe
TCP	tool center point

Symbols

$\mathbb{R}$	real set
$\mathbb{R}_{\geq 0}$	non-negative real set
$\mathbb{R}_{>0}$	positive real set
$\mathbb{R}^n$	n-dimensional vector space
$\mathbb{R}^{n\times m}$	n-dimensional matrix space
$\mathbb{I}$	integer set
$\mathbb{I}_{>0}$	positive integer set
$\mathbb{I}_{[a,b]}$	$\mathbf{I}_{[a,b]} := \{x \in \mathbb{I} : a \leq x \leq b\}$
$\mathbf{I}$	identify matrix
$\mathbf{1}$	all-one vector
$\mathbf{O}$	null matrix
$\mathbf{0}$	null vector
$\mathrm{col}(\mathbf{x}_1, \mathbf{x}_2)$	column vectors of $\mathbf{x}_1$ and $\mathbf{x}_2$, $[\mathbf{x}_1^\top, \mathbf{x}_2^\top]^\top$
$\mathbf{Q} \succ 0$	positive definite matrix $\mathbf{Q}$
$\|\mathbf{x}\|$	Euclidean norm of vector/matrix $\mathbf{x}$
$\|\mathbf{x}\|_\mathbf{Q}$	$\|\mathbf{x}\|_\mathbf{Q} = \sqrt{\mathbf{x}^\top \mathbf{Q}\mathbf{x}}$ for vector $\mathbf{x}$ and $\mathbf{Q} \succ 0$
$\lambda(\mathbf{Q})$	eigenvalue of $\mathbf{Q}$
$\lambda_{\min}(\mathbf{Q})$	minimal eigenvalue of $\mathbf{Q}$
$\lambda_{\max}(\mathbf{Q})$	maximal eigenvalue of $\mathbf{Q}$
dom	domain of one function
$\mathbf{q}$	joint position
$\dot{\mathbf{q}}$	joint velocity

$\ddot{\mathbf{q}}$	joint acceleration
$\mathbf{M}$	inertia matrix
$\hat{\mathbf{M}}$	the nominal inertia matrix
$\tilde{\mathbf{M}}$	modelling error of the inertia matrix
$\bar{\mathbf{M}}$	the constant diagonal decoupling inertia matrix
$\mathbf{C}$	matrix of centrifugal and Coriolis terms
$\hat{\mathbf{C}}$	the nominal matrix of centrifugal and Coriolis terms
$\mathbf{G}$	vector of gravitational term
$\hat{\mathbf{G}}$	the nominal vector of gravitational term
$\mathbf{F}$	viscous friction
$\hat{\mathbf{F}}$	the nominal viscous friction
$\mathbf{N}$	lumped nonlinear dynamics term ($\mathbf{C}\dot{\mathbf{q}} + \mathbf{G} + \mathbf{F}$)
$\tilde{\mathbf{N}}$	modelling error of $\mathbf{N}$
$\boldsymbol{\tau}$	torque
$\boldsymbol{\tau}_{\mathrm{d}}$	external disturbance
$\mathbf{s}$	sliding variable
$\Delta\mathbf{u}$	incremental controller
$\boldsymbol{\varepsilon}$, $\boldsymbol{\varepsilon}_*$	TDE error
$\boldsymbol{\rho}$	switching gain
$\mathbb{X}$	admissible set for state
$\mathbb{U}$	admissible set for controller
T_s	sampling period
L	delay time
$\oplus$	Minkowski sum
$\mathbb{C}_s$	$\{\mathbf{c} \in \mathbb{R}^n : -s\mathbf{1} \leq \mathbf{c} \leq s\mathbf{1}\}$
$\mathbb{B}_{\tilde{r}}$	$\{\mathbf{b} \in \mathbb{R}^{4n} : \|\mathbf{b}\| \leq \tilde{r}\}$
V	Lyapunov function
N	prediction horizon

$V_N(\mathbf{X}(k), k)$	value function
id	identity function
$\bullet_{\text{ref}}$	reference signal of the variable $\bullet$
$\bullet_{k+i\|k}$	predictions of states and control inputs at time k
$\mathbf{f}_i(\mathbf{q})$	i-th task mapping
$\mathbf{J}$, $\mathbf{J}_i$	Jacobian matrix
$\mathbf{K}_{\text{V}_i}$	damping matrix
$\mathbf{K}_{\text{P}_i}$	stiffness matrix
$\mathcal{Q}_i$	Hessian matrix
$\mathcal{L}_i$	gradient vector

1 Introduction

In this chapter, research background is first introduced. Then, challenges in control of robot manipulators are summarized and state-of-the-art controllers are reviewed. Finally, contributions and outline of this dissertation are introduced.

1.1 Research Background

Robot manipulator has attracted more and more attention from researchers, and are playing increasing significant roles in scientific researches and engineering applications, such as space exploration [1], mental spinning and polishing [2], [3], cargo handling [4], assembly [5], medical surgery [6], [7], etc.

In accordance with the above-mentioned applications, the main advantages of the robot manipulator are summarized as follows:

1) The robot manipulator improves production efficiency. In factories, repetitive and high-intensity manual labour is usually not only inefficient but also performed with low precision and safety. With the help of the robot manipulator, the work efficiency will be improved significantly and factories can also increase more profits.

2) The robot manipulator freed up productivity. With the development of control science and artificial intelligence technology, the robot manipulator is able to complete high-precision, complex and repetitive tasks independently. As a result, manual operation time is greatly reduced.

3) The robot manipulator improves surgical outcomes. With the help of tools controlled autonomously by mechanical micro-manipulators, surgeons perform operations with greater precision and tremors are reduced. It directly impact the surgical outcomes.

4) The robot manipulator protects human life and health. The robot manipulator can replace humans to do tasks in environments that are dangerous or harmful to humans such as high temperature, high humidity, radiation, poison, etc.

1.2 Challenges in Control of Robot Manipulators

Recently, the robot manipulator is required to complete more and more sophisticated tasks. To control a robot manipulator reliably in the complex environment is challenging, and the main challenges are listed as follows:

1.2.1 Uncertainties and Unmodelled Dynamics

In practice, sufficiently accurate model identification is impossible, especially for high-degree-of-freedom robot manipulators. First of all, when we construct the system dynamics, the friction function of the robot manipulator is always simplified to reduce the complexity of the controller. Linear friction models are studied in [8]. Although nonlinear friction models were constructed, such as LuGre model [9] and the integrated friction model [10], the friction function is still not accurately known. This is because the joint friction varies during operation or device wear. And also the complex mechanism of the mechanical systems and the friction is also affected by environments, such as temperature. Besides, the robot dynamics, especially the inertia matrix, undergoes severe changes when the end-effector carries or releases unknown payloads. In addition, there are also some unmodelled dynamics. For example, the high-order dynamics of the motor are always omitted in the controller design. Unfortunately, these model uncertainties and unmodelled dynamics inevitably deteriorate tracking performance of the controller. Thus, it has a strict requirement on robustness of the controller.

1.2.2 Input and State Constraints

The robotic system suffers from input saturation problems since all motors have an upper bound of torques. Input saturation is a challenge of the controller design. The nonlinear saturation of motor will deteriorate instantaneous performance of the robot manipulator, such as higher overshoot, larger tracking errors, and even instability of the closed-loop system [11], [12]. In addition, state constraints can be used to describe safety requirements on control and thus enable robot manipulators to also be used in safety-critical applications, e.g., close to or in cooperation with humans. Thus, state constraints are required to be considered in controller design to guarantee safety. Unfortunately, state constraints are usually not of interest to most of the Lyapunov-based controller design, such as computed torque and dynamic inversion controllers [13]. This is because the consideration of state constraints increases the complexity of Lyapunov functions. Although some Lyapunov-based controllers consider the state constraints, the results are conservative, i.e., the feasible region is far away from the boundary of the admissible set. As a result, the working space of the robot manipulator is "wasted".

1.2.3 Singularity

Singularity problem appears in task-space control schemes for the robot manipulator. Inverse kinematics and inverse dynamics are two main task-space control approaches, where the inversion of the term involving the Jacobian matrix is required to be computed. When the Jacobian matrix loses its rank, the kinematic singularity occurs and the system is unstable. Although we can avoid the kinematic singularity by a restriction on allowed tasks, an assumption is made on singularity-free task space. However, this assumption limits the feasible task space of the robot manipulator.

Kinematically redundant robots are able to execute multiple tasks simultaneously, and often tasks are ordered by priority levels. To enable the robot manipulator to perform multiple tasks in a prioritized manner, task-prioritized control schemes are mostly developed using the null-space projection method, and prioritized Jacobian matrices are computed. The

prioritized Jacobian matrix happens to be singular even in configurations at which Jacobian is full-rank. These kind of singularities are due to the employed control algorithm, and thus they are termed algorithmic singularities. Because of the inverse calculation involved in task-space control schemes, singularity problems are challenging to be handled.

1.3 State-of-the-Art Controllers

The challenges and problems stated in Section 1.2 have been studied although they are not well resolved, and the state-of-the-art controllers are reviewed as follows.

1.3.1 Methods to Improve Robustness

Control accuracy is an important criterion of the robot manipulator. Thus, robustness, the property to measure capabilities of controllers handle modelling errors and external disturbances, is emphasized in most of the state-of-the-art controllers. To enhance the robustness of the controller, sliding mode controllers (SMC) [14], [15] are employed. However, the chattering phenomenon of SMC deteriorates the tracking performance. Adaptive methods [16], [17] and intelligent methods, such as neural networks [18], [19], fuzzy [20], [21], and Gaussian process (GP) [22], are also applied on robot manipulators. However, these methods normally use amounts of parameters that are tuned online to approximate and identify uncertainties and external disturbances, resulting in high computational complexity. Moreover, weighting parameters are required to be tuned offline relying on empirical knowledge of the engineers.

Owing to simplicity and efficacy, disturbance observer (DOB) based controllers have been widely employed on robotic and mechanical systems [23]–[25]. Nevertheless, there are also some limitations for the DOB-based controllers in practice [26]. In case the bandwidth of the DOB is not high enough to compensate for inertia variations, the closed-loop system will be unstable. In other words, if one can increase the bandwidth of DOB and/or nominal inertia matrix, then stability will be enhanced. However, in practice, it will make the controller more noise-sensitive. To address this problem, nonlinear DOB was developed in [27], and the trade-off between robustness and noise sensitivity can be better adjusted. Nevertheless, the nominal nonlinear dynamics terms are required to design the nonlinear DOB.

Time delay control (TDC) [28] based on time-delay estimation (TDE) [28]–[36] is a robust controller, which requires less modelling information. The time-delayed signals are employed to estimate dynamics of the robot manipulator. The stability condition for TDC was established independently in [28], [36], which also provides an important criterion to select the constant diagonal decoupling inertia matrix $\bar{\mathbf{M}}$. A sufficient small $\bar{\mathbf{M}}$ can stabilize the system even when the nonlinear dynamics terms of robot manipulators are unknown. Nevertheless, with the constant $\bar{\mathbf{M}}$, the TDE-based controllers do not always guarantee high tracking accuracy in different positions. In [30], a modified Nussbaum function was employed to tune $\bar{\mathbf{M}}$ automatically. However, the modified Nussbaum function method is sensitive to measurement noises and difficult to be implemented in practice. To make the controller more practical, adaptive schemes for $\bar{\mathbf{M}}$ were developed in [32], [33]. However, the adaptive schemes in [32], [33] usually do not reflect the tracking error timely and precisely. As a result, it results in low control precision [35]. Considering TDE error as the disturbance, adaptive SMC schemes were also developed to improve tracking accuracy of TDE-based controllers

[29], [31], [34]. However, the switching gains are normally overestimated [37] or underestimated [29], [33]. When the switching gains are overestimated, it results in chattering. For underestimation, tracking accuracy will be adversely affected.

To sum up, if we can prevent the switching gains from being underestimated and overestimated simultaneously, then the combination of TDC and SMC is an effective way to address uncertainties and modelling errors and thus enhance robustness.

1.3.2 Methods to Address Input and State Constraints

Input saturation has been intensively studied, since it is critical to tracking performance. The methods to handle the input saturation are similar, where auxiliary variables are introduced and auxiliary dynamics subsystems are designed to compensate for the saturation nonlinearity [11], [12], [38]–[40]. Although the overshoot caused by the input saturation is avoided, the tracking performance is not optimal. In comparison, there are fewer research on the state constraints. In [13], [41], barrier functions were employed to address state constraints, however, the results are conservative and the design of the control Lyapunov function is challenging.

Model predictive control (MPC) [42] is an optimization-based control method addressing optimal control performance as well as input and state constraints, where the constrained optimal control problem (OCP) is considered. For MPC, the constrained OCP is solved using the state predictions generated by the nominal mathematical model in a horizon. Thus, control performance of MPC will be adversely affected by uncertainties, such as modelling errors and disturbances. To attenuate uncertainties and improve robustness, SMC [43] is combined with MPC. However, optimality of the control performance is adversely affected by SMC. Moreover, the nominal mathematical model of the robot manipulator is required. In addition, the employed mathematical model is nonlinear and thus we have to consider nonlinear MPC schemes, of which computational complexity is such high that it can not implemented in real-time. Although the nominal model of the robot manipulator are not required for NN [44], [45], data-driven methods [46], [47], GP [48]–[50], and other learning methods [51], [52] based MPC methods, they further increase the computational complexity and real-time control performance is not guaranteed.

All in all, if we can reduce dependence on the mathematical model (enhance the robustness) and adopt a linear MPC scheme, MPC can an option to address input and state constraints of the robot manipulator.

1.3.3 Methods to Handle Singularity

In the literature, damping factors [53] are commonly introduced to calculate inverse kinematics (inverse dynamics) controllers and to address kinematic singularity problems, The damping factors are either fixed or can be automatically adopted [54], [55]. However, there is a trade-off between good conditioning of the solution and tracking accuracy. Thus, tuning a reasonable damping factor is a challenging work: too low a damping factor and the control signal will be too large (undesired); too large damping factor and control performance will be deteriorated [56]. Besides introducing damping factors, there are also several methods introduced to avoid singularities. In [57], an optimization-based inverse kinematics singularity-robust solver is developed, taking advantage of the structure of the robot

manipulator. However, this method is merely applied to one robot with a spherical wrist and more than three joints before it. In [58], a singularity-robust method is introduced. In [58], [59], the singularity-robust controller consists of a joint-space position controller which is activated when the robot manipulator is near singular configurations and a task-space controller that is employed when the robot leaves the singular region. The singular regions are described by the potential energy functions. When there are multiple singular regions, a complex potential energy function is required.

In the null-space projection based task-prioritized controllers, algorithm singularity occurs especially when tasks conflict with each other. The damping factor [53] and the continuous null-space projection [60] were used to address algorithmic singularity. The result is still not satisfactory. In [61], the equality constraints on control signals are employed to realize the task hierarchy, without using the null-space projection idea and inverse matrix of the prioritized Jacobian matrix is not required to calculate. However, the dynamic consistency (or task hierarchy) will be affected since the inertial matrix is required to construct the equality constraint equations and the fact that modelling error is inevitable.

Therefore, how to address singularity in task-space control schemes is still an open problem. In accordance with the literature review, if we can avoid inverse calculation, use the equality constraints, and adopt a robust mathematical model, the singularity problems (including algorithmic singularity in task-prioritized control schemes) will be solved.

1.4 Contributions and Outline

In this dissertation, incremental optimal controllers exploiting time-delay estimation (TDE) are developed to address uncertainties and unmodlled dynamics, input and state constraints, and singularity problems. First, the main contributions of this dissertation are summarized as follows:

1) **The switching gains are not overestimated or underestimated, and robustness is enhanced.** The positive semi-definite barrier function (PSDBF) based incremental sliding mode controller is developed, where a novel PSDBF is designed to regulate switching gains. Then, switching gains increase with the rise of sliding variables, and vice versa. Thus, the PSDBF prevents switching gains of the sliding mode controllers from being over/under-estimated. It results in enhancing robustness of the controller and chattering attenuation simultaneously.

2) **The MPC is developed without concrete mathematical model.** A new incremental model predictive controller (IMPC) is proposed. The new IMPC allows for constrained control of a robot manipulator where the resulting incremental model is derived using time-delay estimation (TDE). Compared with existing MPC methods, the nominal mathematical model is not required and robustness of the controller is enhanced. Moreover, the IMPC is a linear MPC, and computational complexity dramatically decreases compared with nonlinear MPC methods, which makes it possible to realize real-time control in milliseconds.

3) **Input-to-state stability (ISS) of the incremental model predictive is analyzed, and the *cumulative error bound* is not over-conservative.** Considering the bounded error sourced from TDE as the major disturbance, local ISS of IMPC

is confirmed. Different from existing ISS analyses for MPC, here continuity of the value function is used to derive the *cumulative error bound*, and thus the *cumulative error bound* is no longer over-conservative. It is theoretically inferred from the ISS and the derived *cumulative error bound* that increasing the prediction horizon enlarges the region of attraction, and at the same time decreases tracking errors.

4) **Singularity problem in task-space control scheme is avoided.** A hierarchical incremental model predictive controller (HIMPC) is designed to execute multiple tasks simultaneously, and tasks are ordered by priority levels. The null-space projection idea is not employed, and task hierarchy is realized by imposing equality constraints on input signals. Since no inverse calculation is involved in these constraint equations, algorithmic singularity is avoided. Besides, the inverse calculation of terms w.r.t. Jacobian matrices is also not involved in the constrained OCPs, and the Hessian matrix of each constrained OCP is verified to be positive definite. Therefore, the HIMPC is also a kinematically singularity-free method.

Next, the outline of this dissertation is listed, in the order of the organisation.

Incremental sliding mode controller (Chapter 2). An adaptive incremental sliding mode control (AISMC) scheme for a robot manipulator is presented in this chapter, it prevents switching gains from being over/under-estimated. Firstly, an incremental backstepping (IBS) controller is designed using TDE to reduce dependence on the mathematical model. After substituting IBS controller into the nonlinear system, a linear system w.r.t. tracking errors is obtained while TDE error is the disturbance. Then, the AISMC scheme, including a nominal controller and an SMC, is developed for the resulted linear system to improve control performance. According to the equivalent control method, the SMC is to handle TDE error. To receive optimal control performance at the sliding manifold, an LQR controller is selected as the nominal controller. The SMC is designed based on PSDBF since it prevents switching gains from being over/under-estimated, and two practical problems are addressed in this paper: A new PSDBF is designed and conservative (large) setting bounds affecting tracking precision and/or system stability are avoided; An improved PSDBF based SMC is developed where the PSDBF and an adaptive parameter are used simultaneously to regulate switching gains, and the system is still stable when sliding variable occasionally exceeds the predefined vicinity. Moreover, the finite-time convergence property of the sliding variable is strictly analyzed. Finally, real-time experiments are conducted to verify the effectiveness of the proposed control method. The material of this chapter was published in *Mechatronics* [62].

Incremental model predictive controller (Chapter 3). A new IMPC strategy is proposed in this chapter, which allows for constrained control of a robot manipulator while the resulting incremental model is derived without a concrete mathematical system model. First, to reduce dependence on the nominal model of robot manipulators, the continuous-time nonlinear system model is approximated by an incremental system using TDE. Then, based on the incremental system, the tracking IMPC is designed in the framework of MPC without terminal ingredients. Thus, compared with existing MPC methods, the nominal mathematical model is not required. Moreover, we investigate reachable reference trajectories and confirm the local ISS of IMPC, considering the bounded TDE error as the disturbance of the incremental system. For reachable reference trajectories, the local ISS of IMPC is analyzed using the continuity of the value function, and the *cumulative error bound* is

not over-conservative. Finally, several real-time experiments are conducted to verify the effectiveness of IMPC. Experimental results show that the system can achieve optimal control performance while guaranteeing that input and state constraints are not violated. The material of this chapter was accepted by *IEEE Transactions on Control Systems Technology* [63].

Hierarchical incremental model predictive controller (Chapter 4). A hierarchical incremental model predictive controller (HIMPC) is developed for redundant robots controlling multiple hierarchical tasks formulated on multi-layer constrained optimal control problems (OCPs), and algorithmic and kinematic singularities are avoided. The proposed HIMPC method, is robust to dynamic uncertainties, untethered from kinematic/algorithmic singularities and capable of handling input and state constraints. To this end, we first derive robust incremental systems that approximate uncertain system dynamics without computing complex nonlinear functions or identifying model parameters. Then the constrained OCPs are cast as quadratic programming problems which result in linear MPC, where dynamically-consistent task priority is realized by deploying equality constraints and optimal control is attained under inequality state constraints. Thus computational complexity drastically decreases compared with nonlinear MPC-based methods. Hierarchical feasibility and uniqueness of its solution are theoretically analyzed; finally, simulations and experiments verify the effectiveness of HIMPC compared with state-of-the-art task-prioritized controllers. The material of this chapter was submitted to *IEEE Transactions on Robotics*, and now it is under review.

As a summary, the contributions and outline of the dissertation are visualized in Fig. 1.1.

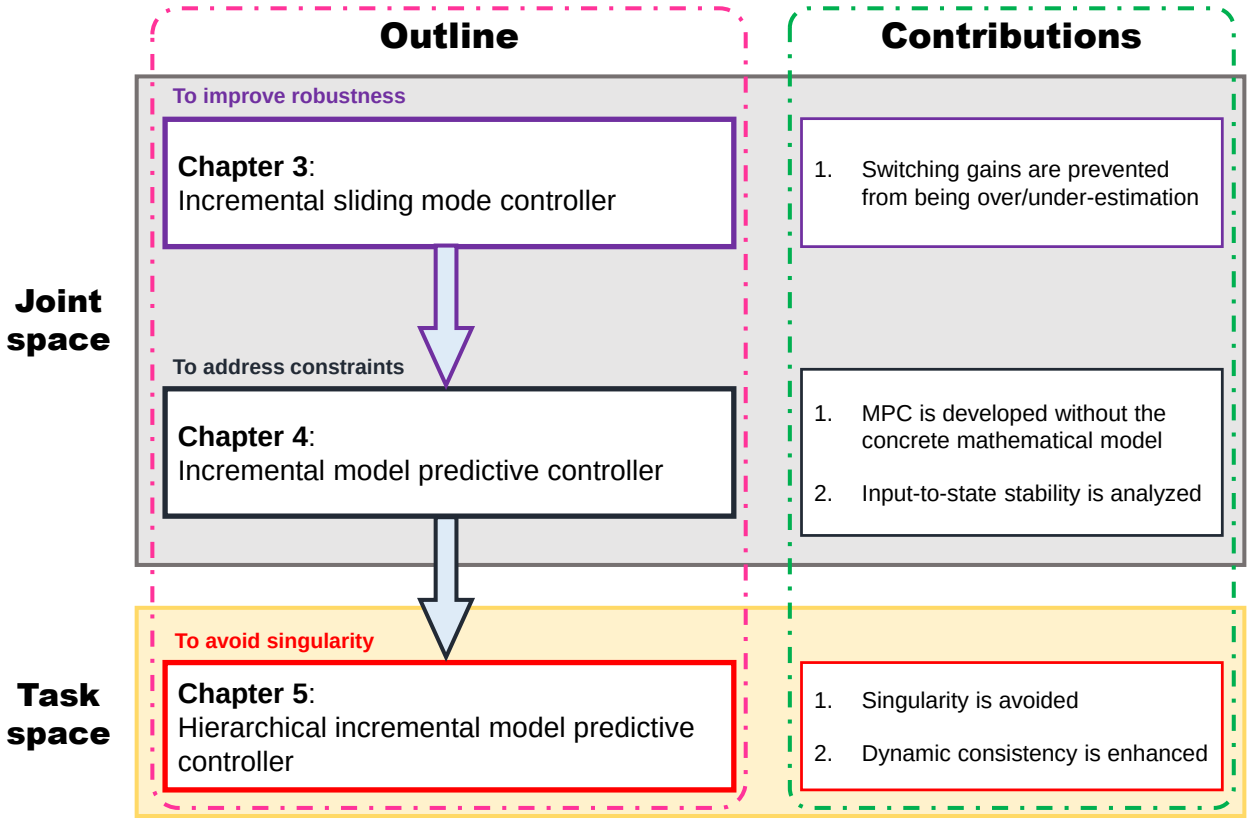

Figure 1.1: The contributions and outline of the dissertation.

2 Incremental Sliding Mode Control

The control of robot manipulators has been well investigated in the past several decades, and it attracts considerable attention [14], [64]–[67]. The major challenge in robot manipulator control, e.g., in manufacturing [68] or aerospace applications [69], is to be able to accurately track reference trajectories in joint or task space. Generally, precise control of the robot manipulator is challenging due to external disturbances and un-modelled uncertainties [70]. In this chapter, the aim is to design a robust controller using the time-delay eatimation (TDE) technique.

2.1 Overview

The robust controller developed in this chapter is a combination of TDE and SMC. TDE is used to approximate uncertain dynamics of the robot manipulator. Then to further enhance control performance, SMC is designed to address the TDE error. However, switching gains are either over-estimated or under-estimated. It is challenging to realize robustness enhancement and chattering attenuation simultaneously. Thus, in this chapter, how to prevent switching gains from being over-/under-estimated is the main focus.

2.1.1 Related Work

There are model-based and model-free approaches to control robot manipulators. The prominent model-based approaches are computed torque (CT) [71] and backstepping [72]–[74]. However, control performance of model-based controllers depends on precise identification of the system. In practice, sufficiently accurate identification is impossible because joint friction varies during operation or device wears. Besides, the robot dynamics, especially the inertia matrix, undergoes severe changes when the end-effector carries or releases unknown payloads [75], which inevitably deteriorates tracking performance. To cope with this problem, robust control [65], [76]–[78], SMC [14], [15], [79], and some techniques, such as neural networks [18], [19] and fuzzy logic systems [80], were applied in combination with CT method to improve tracking accuracy. Nevertheless, some techniques, such as neural networks, employed some parameters identified online to approximate uncertain nonlinear functions and external disturbances, resulting in high computational complexity.

Owing to its simplicity and efficacy, in the last forty years, disturbance observer (DOB) based controllers have been widely applied on robotics and mechanical systems [23], where uncertainties and external disturbances of the controlled plant are estimated [24], [25]. Especially in [26], nonlinear stability analysis for the DOB-based position control for robot manipulators was implemented. As stated in [26], there are limitations for the DOB-based

controllers in practice. In case the bandwidth of the DOB is not sufficiently high to compensate for inertia variations, the closed loop system will not be stable. In other words, if one can increase bandwidth of DOB and/or nominal inertia matrix sufficiently, then stability of the control system will be strengthened. However, in practice, it makes the DOB-based controller more noise-sensitive. To address inertia variations and to improve stability of the DOB-based controller, the inertia matrix of the robot manipulator was identified online in [81]. Nevertheless, online identification was realized using neural network, which increases computational complexity. When the known nonlinear dynamics terms are used in the design of nonlinear DOB [27], performance of the control system can be improved in practice and the trade-off between robustness and noise sensitivity can be better adjusted. However, to implement the nonlinear DOB, the nominal nonlinear dynamics terms are required.

Time delay control (TDC) [28] based TDE [28]–[36] is a typical model-free control method. TDC, similarly to incremental nonlinear dynamic inversion (INDI) [82], [83] or incremental backstepping (IBS) [84], [85], uses time-delay signals to estimate partial dynamics of the controlled system without any parameters identified online. In [28] and [36], the well known stability condition of TDE was established independently, which provides an important basis for the application of TDE and also a criterion to select the TDE parameter $\bar{\mathbf{M}}$. A sufficiently small $\bar{\mathbf{M}}$ can stabilize the system even when inertia matrix and other nonlinear dynamics terms are unknown. Besides, $\bar{\mathbf{M}}$ selected for the robot manipulator also satisfies the sufficient condition for stability under payload variations. Considering the posture of a robot manipulator changes frequently during operation, the best tuned $\bar{\mathbf{M}}$ in a particular situation may not be the best one for other situations. Thus, with constant $\bar{\mathbf{M}}$, the TDE-based controllers do not always guarantee high tracking accuracy in different positions. A modified Nussbaum function was employed in [30] to tune $\bar{\mathbf{M}}$ automatically. However, the modified Nussbaum function method is sensitive to measurement noises and difficult to be implemented directly in practical applications. To improve tracking performance, an adaptive $\bar{\mathbf{M}}$ scheme was adopted in [32], [33]. Nevertheless, the proposed adaptive laws usually do not reflect the tracking error timely and precisely. Thus, sometimes it results in low control precision [35]. Considering TDE error as the disturbance, SMC was also developed together with TDC to improve tracking accuracy in [29], [31], [34] because of its strong robustness.

For conventional SMC, the upper bound of the disturbance is selected as the switching gain. However, it is difficult to apply in practice. First, the selected upper bound is always conservative although some papers estimated it mathematically [86]. Besides, the overestimated upper bound is the main reason for chattering phenomenon. The chattering phenomenon makes various undesirable effects [80], e.g. current harmonics and torque pulsation. To address chattering, several strategies were developed. In [87], a DOB-based SMC scheme was proposed. A DOB is firstly employed to estimate disturbance, and then the SMC is designed to address the rest disturbance. Amplitudes of switching gains are decreased and it results in less chattering. Besides, robustness of the control system is also guaranteed. However, the upper bound of the estimation error is required to design the switching gain. Normally, this upper bound is overestimated. Without the upper bound of the disturbance, an adaptive SMC scheme was proposed in [37]. Nevertheless, chattering still happens since switching gains are monotonically increasing to guarantee asymptotic stability. For adaptive SMC schemes in [29], [33], the switching gain increases when the sliding variable magnitude is large, and decreases in the vicinity of sliding manifold. However, involvement of a threshold value in the adaptive laws invites potential underestimation problem of the switching

gain, and this problem compromises the controller accuracy by applying lower switching gain than the required amount [35].

A barrier function-based adaptive SMC was developed in [88], where the proposed barrier function ensures convergence of the output variable and maintains it in a predefined neighborhood around the origin. In this predefined vicinity around the origin, switching gains are regulated by the barrier function. Thus, the switching gains increase with the rise of sliding variables and vice visa. Therefore, the barrier function based adaptive SMC avoids over/under-estimation of switching gains, i.e., it achieves good tracking performance and chattering reduction simultaneously. However, it also has some limitations. In practice, sliding variables may exceed the predefined vicinity because of some severe changes of the model, some faults or some measurement noises. Then the switching gain turns to be negative and finally it results in instability. In addition, the barrier function based adaptive SMC as well as SMC schemes in [15], [18], [19], [29], [31], [33], [37], [83], [87] focus on addressing disturbances and reducing chattering, while optimal control performance at the sliding manifold is always ignored.

2.1.2 Method and Contributions

In this chapter, the IBS controller based on TDE is designed for a robot manipulator. To improve tracking performance, a *redesign* incremental control combining IBS with AISMC is developed. Because of the TDE method, a linear system is obtained after substituting IBS controller into the system and TDE error is considered as the disturbance. The AISMC scheme, including a nominal controller and an improved positive semi-definite barrier function (PSDBF) based SMC, is developed, where the PSDBF based SMC avoids over/under-estimation of switching gains. In accordance with the equivalent control method, the PSDBF based SMC is to compensate for the TDE error. To receive optimal control performance at the sliding manifold, an LQR controller is selected as the nominal controller. For the PSDBF based SMC, to avoid conservative (large) setting bound affecting tracking precision and/or system stability, a new PSDBF is designed. Besides, to keep the system stable once sliding variables exceed the predefined vicinity, an improved PSDBF based SMC structure is developed. When the sliding variable locates inside the predefined vicinity, switching gains are mainly regulated by the PSDBF. Otherwise, switching gains will be updated according to adaptive laws. Finite time convergence property of the sliding variable is strictly analyzed by Lyapunov theorem. Finally, the PSDBF based AISMC is implemented in practice.

Compared with the above mentioned articles and references herein, the main contributions of this paper are summarized as follows:

1) An improved PSDBF based SMC is developed which keeps the system stable when sliding variables occasionally exceed the predefined vicinity;

2) A new PSDBF is designed to avoid conservative (large) setting bound;

3) The system receives optimal control performance at the sliding manifold.

2.1.3 Outline of this Chapter

The rest of this chapter is organized as follows. In Section 2.2, the IBS controller based on TDE is first introduced. In Section 2.3, to further enhance tracking performance, the

AISMC scheme based on PSDBF is developed, and finite-time convergence of the sliding variable is analyzed by Lyapunov theorem. The experimental results are given in Section 2.4 followed by a short summary in Section 2.5.

2.2 Problem Formulation and Preliminaries

2.2.1 Control Objective

In this chapter, our target is to make the robot manipulator precisely and robustly track the reference signals. Before we design the controller, the following assumption about reference signals is made.

Assumption 1 (Bounded and Smooth Reference Signals [85], [89])**.** *The joint position reference signal* $\mathbf{q}_{\text{ref}}$ *is smooth and bounded, satisfying* $0 \leq \underline{r} \leq \|\mathbf{q}_{\text{ref}}\| \leq \overline{r} < \infty$*,* $0 \leq \underline{\dot{r}} \leq \|\dot{\mathbf{q}}_{\text{ref}}\| \leq \overline{\dot{r}} < \infty$*, and* $0 \leq \underline{\ddot{r}} \leq \|\ddot{\mathbf{q}}_{\text{ref}}\| \leq \overline{\ddot{r}} < \infty$*.*

Remark 1 (Reasonability of **Assumption 1**)**.** *The smoothness of reference signals is a reasonable assumption widely applied in related works, since non-smooth reference signals causes sharp actuator changes and may cause damages to mechanical systems.*

2.2.2 Incremental Backstepping based on TDE

In this subsection, an IBS controller based on TDE is presented, which is the fundamental work of this chapter.

The devloped incremental system (A.7) is in the strict-feedback form, and backstepping controller is designed.

Step 1: Let $\mathbf{e}_1 = \mathbf{x}_1 - \mathbf{q}_{\text{ref}}$ be the tracking error. For (A.7a), we design the virtual control signal $\mathbf{x}_{2\text{d}}$ as follows:

$$\mathbf{x}_{2\text{d}} = -k_1\mathbf{e}_1 + \dot{\mathbf{q}}_{\text{ref}}, \tag{2.1}$$

where $k_1 \in \mathbb{R}_{>0}$ is a design parameter.

Let $\mathbf{e}_2 = \mathbf{x}_2 - \mathbf{x}_{2\text{d}}$ be the tracking error of (A.7b), the dynamics of the tracking error $\mathbf{e}_1$ reads

$$\begin{aligned}\dot{\mathbf{e}}_1 &= \dot{\mathbf{x}}_1 - \dot{\mathbf{q}}_r = \mathbf{x}_2 - \dot{\mathbf{q}}_{\text{ref}} \\ &= \mathbf{x}_{2\text{d}} + (\mathbf{x}_2 - \mathbf{x}_{2\text{d}}) - \dot{\mathbf{q}}_{\text{ref}} = -k_1\mathbf{e}_1 + \mathbf{e}_2.\end{aligned} \tag{2.2}$$

Step 2: Consider the second subsystem (A.7b), the incremental controller $\Delta\mathbf{u}$ is designed as

$$\Delta\mathbf{u} = \bar{\mathbf{g}}^{-1}(\mathbf{v} - \dot{\mathbf{x}}_{2,0}) \tag{2.3}$$

where $\mathbf{v} = -k_2\mathbf{e}_2 + \dot{\mathbf{x}}_{2\text{d}}$ is a pseudo control law, $k_2 \in \mathbb{R}_{>0}$ is a design parameter. Substituting (2.3) into (A.6) yields

$$\dot{\mathbf{e}}_2 + k_2\mathbf{e}_2 = \boldsymbol{\epsilon}. \tag{2.4}$$

Thus, the dynamics of the tracking error $\mathbf{e}_2$ is stable if the TDE error $\boldsymbol{\epsilon}$ is bounded. Here, similarly to [31], [36], we introduce a lemma about the boundedness property of the TDE error.

Lemma 1 (Bounded TDE Error)**.** *Assume the sampling rate is sufficiently high,* $\exists\bar{\epsilon} \in \mathbb{R}_{>0}$*,* $\|\boldsymbol{\epsilon}\| \leq \bar{\epsilon}$ *holds if* $\bar{\mathbf{g}}$ *satisfies* $\|\mathbf{I} - \mathbf{g}(\mathbf{x})\bar{\mathbf{g}}^{-1}\| < 1$ *and IBS controller* (2.3) *is employed.*

Proof: Substituting (2.3) into (A.2b) yields

$$\boldsymbol{\epsilon} = \dot{\mathbf{x}}_2 - \mathbf{v} \tag{2.5}$$

Combining (A.2b), (2.3), with (2.5) yields

$$\begin{aligned}\mathbf{g}^{-1}(\mathbf{x})\boldsymbol{\epsilon} = \mathbf{g}^{-1}(\mathbf{x})\left(\dot{\mathbf{x}}_2 - \mathbf{v}\right) &\overset{(A.2b)}{=} \mathbf{g}^{-1}(\mathbf{x})\left(\mathbf{f}(\mathbf{x}) - \mathbf{v}\right) + \mathbf{u} \\ &\overset{(2.3)}{=} \mathbf{g}^{-1}(\mathbf{x})\left(\mathbf{f}(\mathbf{x}) - \mathbf{v}\right) + \mathbf{u}_0 + \bar{\mathbf{g}}^{-1}(\mathbf{v} - \dot{\mathbf{x}}_{2,0})\end{aligned} \tag{2.6}$$

From (A.4), we have $\bar{\mathbf{g}}^{-1}\dot{\mathbf{x}}_{2,0} = \mathbf{H}(\mathbf{x}_0, \dot{\mathbf{x}}_0) + \mathbf{u}_0$, then

$$\mathbf{g}^{-1}(\mathbf{x})\boldsymbol{\epsilon} = \mathbf{g}^{-1}(\mathbf{x})\mathbf{f}(\mathbf{x}) + \left(\bar{\mathbf{g}}^{-1} - \mathbf{g}^{-1}(\mathbf{x})\right)\mathbf{v} - \mathbf{H}(\mathbf{x}_0, \dot{\mathbf{x}}_0). \tag{2.7}$$

For $\mathbf{H}(\mathbf{x}_0, \dot{\mathbf{x}}_0) = \left(\bar{\mathbf{g}}^{-1} - \mathbf{g}^{-1}(\mathbf{x}_0)\right)\dot{\mathbf{x}}_{2,0} + \mathbf{g}^{-1}(\mathbf{x}_0)\mathbf{f}(\mathbf{x}_0)$, we get

$$\boldsymbol{\epsilon} = \left(\mathbf{g}(\mathbf{x})\bar{\mathbf{g}}^{-1} - \mathbf{I}\right)\mathbf{v} - \left(\mathbf{g}(\mathbf{x})\bar{\mathbf{g}}^{-1} - \mathbf{I}\right)\dot{\mathbf{x}}_{2,0} + \boldsymbol{\eta}_1 \tag{2.8}$$

where $\boldsymbol{\eta}_1 = \mathbf{g}(\mathbf{x})\left(\boldsymbol{\Delta} + \left(\mathbf{g}^{-1}(\mathbf{x}_0) - \mathbf{g}^{-1}(\mathbf{x})\right)\dot{\mathbf{x}}_{2,0}\right)$, $\boldsymbol{\Delta} = \mathbf{g}^{-1}(\mathbf{x})\mathbf{f}(\mathbf{x}) - \mathbf{g}^{-1}(\mathbf{x}_0)\mathbf{f}(\mathbf{x}_0)$. Besides, from (2.5), we obtain $\boldsymbol{\epsilon}_0 = \dot{\mathbf{x}}_{2,0} - \mathbf{v}_0$, where $\boldsymbol{\epsilon}_0$ and $\mathbf{v}_0$ are values of $\boldsymbol{\epsilon}$ and $\mathbf{v}$ at the previous sampling time respectively. Thus,

$$\boldsymbol{\epsilon} = \left(\mathbf{I} - \mathbf{g}(\mathbf{x})\bar{\mathbf{g}}^{-1}\right)\boldsymbol{\epsilon}_0 + \left(\mathbf{g}(\mathbf{x})\bar{\mathbf{g}}^{-1} - \mathbf{I}\right)(\mathbf{v} - \mathbf{v}_0) + \boldsymbol{\eta}_1. \tag{2.9}$$

In the discrete-time domain, the TDE error is expressed as follows:

$$\boldsymbol{\epsilon}(k) = \left(\mathbf{I} - \mathbf{g}(k)\bar{\mathbf{g}}^{-1}\right)\boldsymbol{\epsilon}(k-1) + \left(\mathbf{g}(k)\bar{\mathbf{g}}^{-1} - \mathbf{I}\right)\boldsymbol{\eta}_2(k) + \boldsymbol{\eta}_1(k) \tag{2.10}$$

where $\boldsymbol{\eta}_2(k) = \mathbf{v}(k) - \mathbf{v}(k-1)$. As shown in (2.3), $\mathbf{v}$ is designed to be continuous in time, thus $\lim_{T_s \to 0}\|\mathbf{v}(k) - \mathbf{v}(k-1)\| = 0$ and $\lim_{T_s \to 0}\|\boldsymbol{\eta}_1(k)\| = 0$. In other words, $\boldsymbol{\eta}_1(k)$ and $\boldsymbol{\eta}_2(k)$ are all bounded for sufficiently small T_s. Suppose there exists $\bar{\eta}_1, \bar{\eta}_2 \in \mathbb{R}_{>0}$ such that $\|\boldsymbol{\eta}_1(k)\| \leq \bar{\eta}_1$ and $\|\boldsymbol{\eta}_2(k)\| \leq \bar{\eta}_2$ hold for $k \geq 0$ [31]. Besides, $\bar{\mathbf{g}}$ satisfies $\|\mathbf{I} - \mathbf{g}(\mathbf{x})\bar{\mathbf{g}}^{-1}\| < 1$. There exists $\kappa \in \mathbb{R}_{>0}$, $0 < \kappa < 1$, such that $\|\mathbf{I} - \mathbf{g}(\mathbf{x})\bar{\mathbf{g}}^{-1}\| \leq \kappa < 1$. By induction, we get

$$\begin{aligned}\|\boldsymbol{\epsilon}(k)\| &\leq \kappa\|\boldsymbol{\epsilon}(k-1)\| + \kappa\bar{\eta}_2 + \bar{\eta}_1 \\ &\leq \kappa^2\|\boldsymbol{\epsilon}(k-2)\| + (\kappa^2 + \kappa)\bar{\eta}_2 + (\kappa + 1)\bar{\eta}_1 \\ &\leq \kappa^k\|\boldsymbol{\epsilon}(0)\| + \sum_{i=0}^{k-1}\kappa^i(\kappa\bar{\eta}_2 + \bar{\eta}_1) \\ &\leq \kappa^k\|\boldsymbol{\epsilon}(0)\| + \frac{\kappa\bar{\eta}_2 + \bar{\eta}_1}{1-\kappa} = \bar{\epsilon}\end{aligned} \tag{2.11}$$

where $\boldsymbol{\epsilon}(0)$ is the initial value of $\boldsymbol{\epsilon}(k)$.

Therefore, the TDE error is bounded by $\left(\kappa^k\|\boldsymbol{\epsilon}(0)\| + \frac{\kappa\bar{\eta}_2 + \bar{\eta}_1}{1-\kappa}\right)$ if $\|\mathbf{I} - \mathbf{g}(\mathbf{x})\bar{\mathbf{g}}^{-1}\| \leq \kappa < 1$ holds. As $k \to \infty$, $\left(\kappa^k\|\boldsymbol{\epsilon}(0)\| + \frac{\kappa\bar{\eta}_2 + \bar{\eta}_1}{1-\kappa}\right) \to \frac{\kappa\bar{\eta}_2 + \bar{\eta}_1}{1-\kappa}$.

■

Given the bounded TDE error, the stability of closed-loop system is analyzed. Consider a Lyapunov function $V : \mathbb{R}^n \times \mathbb{R}^n \mapsto \mathbb{R}$

$$V = 0.5\mathbf{e}_1^\top \mathbf{e}_1 + 0.5\mathbf{e}_2^\top \mathbf{e}_2. \tag{2.12}$$

Along with tracking error dynamics (2.2) and (2.4), $\dot{V}$ is

$$\begin{aligned} \dot{V} &= \mathbf{e}_1^\top \dot{\mathbf{e}}_1 + \mathbf{e}_2^\top \dot{\mathbf{e}}_2 \\ &= -k_1 \mathbf{e}_1^\top \mathbf{e}_1 - k_2 \mathbf{e}_2^\top \mathbf{e}_2 + \mathbf{e}_1^\top \mathbf{e}_2 + \mathbf{e}_2^\top \boldsymbol{\epsilon}. \end{aligned} \tag{2.13}$$

Through Young's inequality [90] and **Lemma 1**, we have

$$\mathbf{e}_1^\top \mathbf{e}_2 \leq 0.5\mathbf{e}_1^\top \mathbf{e}_1 + 0.5\mathbf{e}_2^\top \mathbf{e}_2 \tag{2.14}$$

$$\mathbf{e}_2^\top \boldsymbol{\epsilon} \leq 0.5\mathbf{e}_2^\top \mathbf{e}_2 + 0.5 \left\|\boldsymbol{\epsilon}\right\|_2^2 \leq 0.5\mathbf{e}_2^\top \mathbf{e}_2 + 0.5\bar{\epsilon}^2 \tag{2.15}$$

where $\bar{\epsilon}$ is the upper bound of the TDE error $\boldsymbol{\epsilon}$ (compare **Lemma 1**). Substituting (2.14) and (2.15) into (2.13) yields

$$\dot{V} \leq -\left(k_1 - 0.5\right)\mathbf{e}_1^\top \mathbf{e}_1 - \left(k_2 - 1\right)\mathbf{e}_2^\top \mathbf{e}_2 + 0.5\bar{\epsilon}^2 \tag{2.16}$$

Let $k_1 > 0.5$ and $k_2 > 1$, and define $k_0 = \min\{k_1 - 0.5, k_2 - 1\}$. Then, (2.16) is rewritten as

$$\dot{V} \leq -2k_0 V + 0.5\bar{\epsilon}^2 \tag{2.17}$$

Then, applying the comparison principle and zooming technique [91], we obtain the upper bound of tracking errors from (2.12) and (2.17):

$$\left\|\mathbf{e}_i(t)\right\| \leq \sqrt{2V(t)} \leq \sqrt{2V(0)e^{-2k_0 t} + \frac{\bar{\epsilon}^2}{2k_0}(1 - e^{-2k_0 t})}. \tag{2.18}$$

Eqs. (2.17) and (2.18) indicate tracking errors are all bounded over any time interval. Besides, tracking precision can be improved by compensating for the TDE error and/or choosing appropriate design parameters. Large design parameters decrease tracking errors and increase convergence rate, while too large design parameters cause system oscillation.

Remark 2 (Why is the Backstepping Structure Adopted?)**.** *In accordance with definitions of tracking errors (*$\mathbf{e}_1$ *and* $\mathbf{e}_2$*) and the virtual control signal* $\mathbf{x}_{2\mathrm{d}}$ *in* (2.1)*, the incremental controller* $\Delta\mathbf{u}$ *designed in* (2.3) *can be rewritten as follows:* $\Delta\mathbf{u} = \bar{\mathbf{g}}^{-1}\left(\ddot{\mathbf{q}}_{\mathrm{ref}} + \mathbf{K}_{\mathrm{D}}\dot{\mathbf{e}}_1 + \mathbf{K}_{\mathrm{P}}\mathbf{e}_1 - \ddot{\mathbf{q}}_0\right)$*, where* $\mathbf{K}_{\mathrm{D}} = (k_1 + k_2)\mathbf{I}$*,* $\mathbf{K}_{\mathrm{P}} = k_1 k_2 \mathbf{I}$*, and* $\ddot{\mathbf{q}}_0 = \dot{\mathbf{x}}_{2,0}$*. It implies the designed IBS controller is identical to the TDC developed in [12]. The backstepping control structure is adopted here since it is a systematic control method, i.e., construction of both the control law and the the associated Lyapunov function is systematic [92]. One of the benefits of a systematic approach is rigorousness of the theoretical derivation of the methods. In the backstepping control structure, an* n*-order nonlinear affine system is divided into* n *sub-systems. For each one sub-system, a control law is designed based on the dynamic inversion method where only one parameter* $k_i (i = 1, \cdots, n)$ *is involved. Employing the uniform/standard Lyapunov function* $V_i = \sum_{j=1}^{i} \frac{1}{2} z_j^2$ *(where* z_j *is the tracking error of the* j*-th sub-system), Lyapunov stability is analyzed. A series of positive design parameters (greater than 1) guarantees the closed-loop system is Lyapunov stable. The other advantage of the systematic approach is that the parameters are convenient to be tuned. For example, from* (2.18)*, one learns that increasing* k_i *appropriately, tracking performance will be enhanced.*

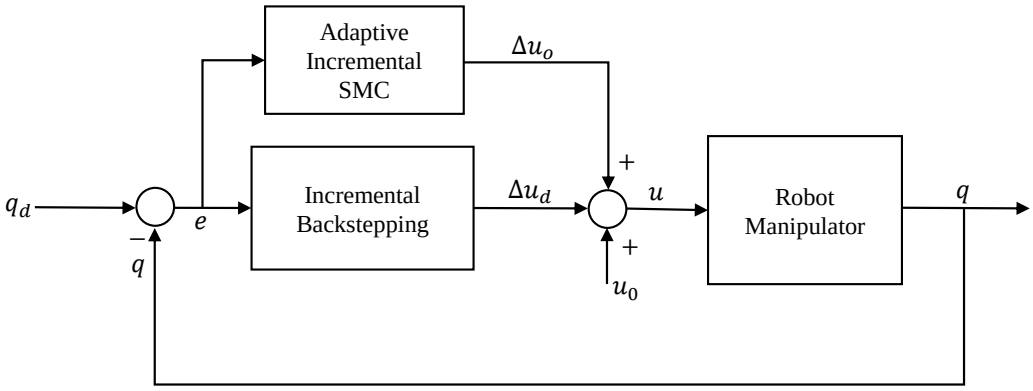

Figure 2.1: Control framework (where $\mathbf{u}_0$ is the most recent torque input).

2.3 Adaptive Incremental Sliding Mode Control

The IBS controller based on TDE is designed in Section 2.2.2, and it is shown that tracking precision is affected by the TDE error and design parameters. To address TDE error and then enhance tracking performance, the adaptive incremental sliding mode control (AISMC) scheme based on PSDBF is developed in this section.

2.3.1 Barrier Function based Adaptive Incremental SMC

As shown in Figure 2.1, the AISMC is combined with the IBS controller to improve tracking accuracy, i.e., we complete the incremental controller $\Delta\mathbf{u}$ *redesign* as follows:

$$\Delta\mathbf{u} = \Delta\mathbf{u}_{\mathrm{d}} + \Delta\mathbf{u}_{\mathrm{o}} \tag{2.19}$$

Let $\Delta\mathbf{u}_{\mathrm{d}}$ be the IBS controller (2.3), substituting the *redesign* controller $\Delta\mathbf{u}$ (2.19) into the incremental system (A.6), and then combining with the tracking error dynamics (2.2), we obtain an LTI system w.r.t. tracking errors $\mathbf{e}_1$ and $\mathbf{e}_2$:

$$\begin{cases} \dot{\mathbf{e}}_1 &= -k_1\mathbf{e}_1 + \mathbf{e}_2 \\ \dot{\mathbf{e}}_2 &= -k_2\mathbf{e}_2 + \bar{\mathbf{g}}\Delta\mathbf{u}_o + \boldsymbol{\epsilon} \end{cases} \tag{2.20}$$

Denote $\mathbf{X} := \mathrm{col}(\mathbf{e}_1, \mathbf{e}_2)$, (2.20) is rewritten as:

$$\dot{\mathbf{X}} = \mathbf{A}\mathbf{X} + \mathbf{B}(\Delta\mathbf{u}_o + \boldsymbol{\epsilon}') \tag{2.21}$$

where $\mathbf{A} = \begin{bmatrix} -k_1\mathbf{I} & \mathbf{I} \\ \mathbf{O} & -k_2\mathbf{I} \end{bmatrix}$, $\mathbf{B} = \begin{bmatrix} \mathbf{O} \\ \bar{\mathbf{g}} \end{bmatrix}$, and $\boldsymbol{\epsilon}' = \bar{\mathbf{g}}^{-1}\boldsymbol{\epsilon}$ is a new version TDE error. Note that $(\mathbf{A}, \mathbf{B})$ is stabilizable, regardless of k_1 and k_2.

In the sequel, we first determine the SMC structure. Here, we not only want to attenuate the TDE error, but also regulate the tracking performance at the sliding manifold. Thus, we design the following SMC scheme for (2.21).

$$\Delta\mathbf{u}_{\mathrm{o}} = \Delta\mathbf{u}_{\mathrm{o,noi}} + \Delta\mathbf{u}_{\mathrm{o,sm}} \tag{2.22}$$

where $\Delta\mathbf{u}_{\mathrm{o,noi}} = -\mathbf{K}\mathbf{X} = -\mathbf{R}^{-1}\mathbf{B}^{\top}\mathbf{P}\mathbf{X}$ is a linear quadratic regulator (LQR) controller designed for the nominal plant of (2.21), $\mathbf{Q} > 0$ and $\mathbf{R} > 0$ are weighting matrices, $\mathbf{P}$ is the solution of the following Riccati equation:

$$\mathbf{A}^{\top}\mathbf{P} + \mathbf{P}\mathbf{A} + \mathbf{Q} - \mathbf{P}\mathbf{B}\mathbf{R}^{-1}\mathbf{B}^{\top}\mathbf{P} = 0.$$

Note that $\Delta\mathbf{u}_{\mathrm{o,sm}}$ is the PSDBF based SMC which is given later.

Then, according to the designed SMC scheme (2.22), we design the sliding variable. Regarding the LQR controller $\Delta\mathbf{u}_{\mathrm{o,noi}}$ as the nominal controller, we define the integral sliding variable [93], [94]:

$$\mathbf{s}(t) = \mathbf{G}\left(\mathbf{X}(t) - \mathbf{X}(0) - \int_0^t \left(\mathbf{A}\mathbf{X} + \mathbf{B}\Delta\mathbf{u}_{\mathrm{o,noi}}\right) dt\right) \tag{2.23}$$

where $\mathbf{G} = \mathbf{B}^{\dagger} = (\mathbf{B}^{\top}\mathbf{B})^{-1}\mathbf{B}^{\top}$.

Finally, we will use the equivalent control method [95], [96] to determine the state equations when the state is confined to the sliding manifold. The equivalent control method is a common way to explore the nature of TDE. It consists in the following three steps:

1) *Force the derivative of* $\mathbf{s}(t)$ *equal to zero.* For (2.23), the derivative of $\mathbf{s}(t)$ is

$$\dot{\mathbf{s}}(t) = \mathbf{G}\left(\dot{\mathbf{X}}(t) - \left(\mathbf{A}\mathbf{X} + \mathbf{B}\Delta\mathbf{u}_{\mathrm{o,noi}}\right)\right) = \Delta\mathbf{u}_{\mathrm{o,sm}} + \boldsymbol{\epsilon}'. \tag{2.24}$$

2) *Determine the equivalent control.* Let $\dot{\mathbf{s}}(t) = \mathbf{0}$, the equivalent control is

$$\left(\Delta\mathbf{u}_{\mathrm{o,sm}}\right)_{\mathrm{eq}} = -\boldsymbol{\epsilon}'. \tag{2.25}$$

3) *Determine the state equations on the sliding surface.* Substituting (2.25) into (2.24), the TDE error is eliminated, and trajectories of tracking errors at the sliding manifold are given by

$$\dot{\mathbf{X}}_{\mathrm{eq}} = \mathbf{A}\mathbf{X}_{\mathrm{eq}} + \mathbf{B}\Delta\mathbf{u}_{\mathrm{o,noi}} \tag{2.26}$$

where $\mathbf{X}_{\mathrm{eq}}$ is the equivalent state (tracking errors $\mathbf{e}_1$ and $\mathbf{e}_2$) at the sliding manifold.

In accordance with the idea of equivalent control method [95], [96] and the resulting equation (2.25), we learn that $\Delta\mathbf{u}_{\mathrm{o,sm}}$ is to attenuate the TDE error. Besides, under the function of the LQR controller $\Delta\mathbf{u}_{\mathrm{o,noi}}$, the system at the sliding manifold (compare (2.26)) achieves optimal control performance with the cost function $\int_0^{\infty}\left(\mathbf{X}^{\top}\mathbf{Q}\mathbf{X} + \Delta\mathbf{u}_{\mathrm{o,noi}}^{\top}\mathbf{R}\Delta\mathbf{u}_{\mathrm{o,noi}}\right) dt$. Thus, the combination of $\Delta\mathbf{u}_{\mathrm{o,noi}}$ and $\Delta\mathbf{u}_{\mathrm{o,sm}}$ not only attenuates the TDE error, but it also regulates tracking performance at the sliding manifold.

Remark 3 (Linear Controller is Adopted.)**.** *For the nonlinear controlled plant, an LTI system w.r.t. the tracking errors is obtained after the redesign incremental controller is employed. In other words, the redesign incremental controller makes it possible to design the LQR controller to regulate the tracking errors.*

Remark 4 (Tracking Performance of Conventional SMC Depends on Parameter λ.)**.** *For most of adaptive SMC methods, their main purpose is to attenuate the disturbance. They do not guarantee the system receives optimal control performance at the sliding manifold. For example in [29], the tracking error trajectory at the sliding manifold is* $\ddot{\mathbf{e}} + 2\lambda\dot{\mathbf{e}} + \lambda^2\mathbf{e} = \mathbf{0}$*, where* λ *is a design parameter. That means the tracking error dynamics only depends on* λ *at the sliding manifold. If inappropriate* λ *is selected, the tracking performance is not improved significantly even if an effective SMC is designed later.*

Before the PSDBF based SMC $\Delta\mathbf{u}_{\mathrm{o,sm}}$, a new format PSDBF is introduced.

$$f_{BF}(x) = \frac{\varpi|x|}{\varpi - |x|},\ x \in (-\varpi, \varpi) \tag{2.27}$$

Note that for some given and fixed $\varpi \in \mathbb{R}_{>0}$, $f_{BF}(x) : (-\varpi, \varpi) \mapsto [0, \infty]$ is an even continuous function, strictly increasing on $[0, \varpi)$ and satisfying the following two properties:

1) $\lim_{|x|\mapsto\varepsilon} f_{BF}(x) = +\infty$;

2) $f_{BF}(x)$ has a minimum at zero and $f_{BF}(0) = 0$ [88].

To attenuate the TDE error and prevent swtiching gains from being over/under-estimated, we design the following PSDBF based SMC $\Delta\mathbf{u}_{\mathrm{o,sm}}$:

$$\Delta\mathbf{u}_{\mathrm{o,sm}} = -\boldsymbol{\rho}\ \mathbf{sgn}(\boldsymbol{s}(t)) \tag{2.28}$$

where $\mathbf{sgn}(\mathbf{s}(t)) = (\mathrm{sign}(s_1(t)), \cdots, \mathrm{sign}(s_n(t)))$; $\boldsymbol{\rho} = \mathrm{diag}(\rho_1, \cdots, \rho_n)$ are switching gains. To keep system stable when sliding variables occasionally exceed the predefined vicinity ϖ, the switching gain will be regulated by PSDBF (2.27) and the adaptive parameter $r_i(t)$ simultaneously:

$$\rho_i(t) = r_i(t) + \tilde{f}_{BF}(s_i(t)) \tag{2.29}$$

where

$$\tilde{f}_{BF}(s_i(t)) = \begin{cases} f_{BF}(b\varpi), & \text{if } |s_i(t)| \geq b\varpi \\ f_{BF}(s_i(t)), & \text{if } |s_i(t)| < b\varpi \end{cases},$$

$b \in \mathbb{R}_{>0}$ and $0 < b < 1$, and the updating law of parameter $r_i(t)$ is

$$\dot{r}_i(t) = \begin{cases} 0, & (|r_i(t)| \leq \varsigma) \wedge (|s_i(t)| < b\varpi) \\ \varphi\left(\mathrm{sat}\left(|s_i(t)|\right)\right)^{\theta_i(t)} \theta_i(t), & \text{otherwise} \end{cases} \tag{2.30}$$

with $r_i(0) \geq 0$,

$$\mathrm{sat}(|s_i(t)|) = \begin{cases} |s_i(t)|, & \text{if } |s_i(t)| \geq \iota \\ \iota, & \text{if } |s_i(t)| < \iota \end{cases},$$

$\iota \in \mathbb{R}_{>0}$ is a small scalar, $\theta_i(t) = \mathrm{sign}(|s_i(t)| - b\varpi)$, $\varphi \in \mathbb{R}_{>0}$ is an adaption parameter and $\varsigma \in \mathbb{R}_{>0}$ is a small scalar. Note that $r_i(t) \geq 0$ according to (2.30) and the fact $r_i(0) \geq 0$.

Remark 5 (Security Problem is Solved.)**.** *In [88], the PSDBF is directly employed to regulate the switching gain. It is theoretically verified the sliding variable converges to and stays inside a predefined vicinity around the origin. However, in practice, the sliding variables sometimes exceed the predefined vicinity because of some severe changes of the model, some faults or some measurement noises. Unfortunately the switching gain turns to be negative when sliding variable exceeds vicinity, resulting in instability. While for the proposed PSDBF based SMC scheme, the switching gain is regulated by PSDBF and an adaptive parameter simultaneously as shown in* (2.30)*. Even when the sliding variable exceeds the predefined vicinity occasionally, the switching gain updates through* (2.30) *accordingly. Thus, security of the scheme is guaranteed.*

In what follows, the behavior of the sliding variable will be analyzed. Assume $|s_i(0)| \geq b\varpi$, then switching gain ρ_i increases because of the increasing r_i, until $|s_i(t)| < b\varpi$. Once the sliding variable enters the vicinity of the sliding manifold, i.e., $|s_i(t)| < b\varpi$, $r_i(t)$ decreases and $\rho_i(t)$ is gradually regulated by the PSDBF $f_{BF}(s_i(t))$. According to (2.27), $f_{BF}(s_i(t))$ is strictly increasing on $[0, \varpi)$ and it is an even function. Thus, in the region $|s_i(t)| < b\varpi$, the switching gain falls as $|s_i(t)|$ declines, and increases with the rise of $|s_i(t)|$. It not only prevents the switching gain from being overestimated, resulting in chattering reduction, but also avoids underestimation problem. Afterwards, if $|s_i(t)|$ exceeds $b\varepsilon$, the switching gain increases fast through (2.30) to decrease $|s_i(t)|$ until $|s_i(t)|$ reaches $b\varpi$ again.

From above analysis, the design parameter ϖ plays an important role to determine the bound of the sliding variable ($|s_i(t)| < b\varpi < \varpi$). Thus, ϖ is termed as the *setting bound* for the sliding variable in this chapter.

Finally, from (2.3), (2.19), (2.22), and (2.28), the entire control law $\mathbf{u}$ is designed as follows:

$$\begin{aligned}\mathbf{u} &= \mathbf{u}_{\mathrm{o}} + \Delta\mathbf{u} \\ &= \mathbf{u}_{\mathrm{o}} + \underbrace{\bar{\mathbf{g}}^{-1}\left(-k_2\mathbf{e}_2 + \dot{\mathbf{x}}_{2\mathrm{d}} - \dot{\mathbf{x}}_{2,0}\right)}_{\Delta\mathbf{u}_{\mathrm{d}}} \underbrace{-\mathbf{R}^{-1}\mathbf{B}^{\top}\mathbf{P}\mathbf{X}}_{\Delta\mathbf{u}_{\mathrm{o,noi}}} \underbrace{-\boldsymbol{\rho}\ \mathbf{sgn}(\mathbf{s}(t))}_{\Delta\mathbf{u}_{\mathrm{o,sm}}}.\end{aligned} \tag{2.31}$$

Although the control scheme (2.31), involving IBS, LQR, and SMC is relatively complex, there is only one parameter $\boldsymbol{\rho}$ adapted online. For other parameters in (2.31), they are either measurements or can be determined offline before implementation. Thus, it will not cause heavy computational complexity.

2.3.2 Finite-Time Convergence Property of the Sliding Variable

Before analyzing finite-time convergence property of the sliding variable, the following two lemmas about boundedness properties of TDE error and switching gain are introduced.

Note that the upper bound of the TDE error is related to the controller as shown in the proof of **Lemma 1**. Owing to the introduced *redesign* controller, the upper bound of the TDE error is essential to be re-analyzed.

Lemma 2 (Bounded TDE Error)**.** *Assume the sampling rate is sufficiently high,* $\exists\bar{\epsilon}^* \in \mathbb{R}_{>0}$, $\|\boldsymbol{\epsilon}'\|_2 \leq \bar{\epsilon}^*$ *holds if* $\bar{\mathbf{g}}$ *satisfies* $\|\mathbf{I} - \mathbf{g}(\mathbf{x})\bar{\mathbf{g}}^{-1}\|_2 < 1$ *and the controller* (2.31) *is employed.*

Proof: According to the entire control law $\mathbf{u}$ in (2.31), the *redesign* incremental control law $\Delta\mathbf{u}$ can be rewritten as follows:

$$\Delta\mathbf{u} = \bar{\mathbf{g}}^{-1}(\mathbf{v}^* - \dot{\mathbf{x}}_{2,0}) \tag{2.32}$$

where $\mathbf{v}^* = -k_2\mathbf{e}_2 + \dot{\mathbf{x}}_{2\mathrm{d}} - \bar{\mathbf{g}}\mathbf{R}^{-1}\mathbf{B}^{\top}\mathbf{P}\mathbf{X} - \bar{\mathbf{g}}\boldsymbol{\rho}\mathbf{sgn}(\mathbf{s}(t))$ is the pseudo control law of the incremental system (A.6). Similarly to the pseudo control laws in [31], [83] where they also include the sliding mode controller part, $\Delta\mathbf{v}^* = \mathbf{v}^*(k) - \mathbf{v}^*(k-1)$ is bounded for sufficiently high sampling rate. Let $\bar{\eta}_2^*$ be the bound of $\|\Delta\mathbf{v}^*\|$, i.e., $\|\Delta\mathbf{v}^*\| \leq \bar{\eta}_2^*$, then analogous to **Lemma 1**, the TDE error $\boldsymbol{\epsilon}'$ is bounded by

$$\|\boldsymbol{\epsilon}'(k)\| \leq \kappa^k\|\boldsymbol{\epsilon}'(0)\| + \lambda_{\min}(\bar{\mathbf{g}})\frac{\kappa\bar{\eta}_2^* + \bar{\eta}_1}{1-\kappa} = \bar{\epsilon}^* \tag{2.33}$$

where $\lambda_{\min}(\bar{\mathbf{g}})$ is the minimum eigenvalue (element) of $\bar{\mathbf{g}}$, and $\bar{\epsilon}^*$ is the upper bound.

■

Lemma 3 (Bounded Switching Gain)**.** *Based on the bounded TDE error, the switching gain ρ_i, which is updated by* (2.29) *and* (2.30)*, is bounded by $\rho_i^* \in \mathbb{R}_{>0}$, i.e., $\rho_i(t) \leq \rho_i^*$ for any $t \geq 0$.*

Proof: Considering the "worst" case, we calculate the upper bound of switching gains.

Suppose that $|s_i(0)| > b\varpi$. Without loss of generality, we assume $s_i(0) > 0$. There are two situations for r_0: $\bar{\epsilon}^* \geq r_0 + f_{BF}(b\varpi)$ and $\bar{\epsilon}^* < r_0 + f_{BF}(b\varpi)$, where r_0 is the initial value of $r_i(t)$.

i) $\bar{\epsilon}^* \geq r_0 + f_{BF}(b\varpi)$. From the updating law of $r_i(t)$ (2.30), and given that upper bound of the TDE error exists as proved in **Lemma 2**, it follows that $\rho_i(t)$ is increasing and there exists t_1, $t_1 < \frac{\bar{\epsilon}^* - r_0 - f_{BF}(b\varpi)}{\varphi b\varpi}$, such that $\rho_i(t_1) = \bar{\epsilon}^*$. This is because $\bar{\epsilon}^* \overset{s_i(0)>b\varpi}{=} r_0 + \int_0^{t_1} \varphi s_i(t)dt + f_{BF}(b\varpi) > r_0 + \varphi b\varpi t_1 + f_{BF}(b\varpi)$. According to (2.24), $s_i(t_1) - s_i(0) = \int_0^{t_1} \dot{s}_i(t)dt \leq \int_0^{t_1} (-\rho_i(t) + \bar{\epsilon}^*)\, dt \leq (\bar{\epsilon}^* - r_0 - f_{BF}(b\varpi))\, t_1$. Thus, $s_i(t_1) < s_i(0) + \frac{(\bar{\epsilon}^* - r_0 - f_{BF}(b\varpi))^2}{\varphi b\varpi}$.

Afterwards, switching gain is large enough to make the sliding variable decrease. Then, at t_2, $s_i(t_2) = b\varpi$. According to (2.24),

$s_i(t_2) - s_i(t_1) \leq \int_{t_1}^{t_2} (-\rho_i(\tau_1) + \bar{\epsilon}^*)\, d\tau_1 = \int_{t_1}^{t_2} (-r_0 - \int_0^{\tau_1} \varphi s_i(\tau_2)d\tau_2 - f_{BF}(b\varpi) + \bar{\epsilon}^*)\, d\tau_1$

$\overset{\rho_i(t_1)=r_0+\int_0^{t_1} \varphi s_i(\tau_2)d\tau_2+f_{BF}(b\varpi)=\bar{\epsilon}^*}{=} - \int_{t_1}^{t_2} \int_{t_1}^{\tau_1} \varphi s_i(\tau_2)d\tau_2 d\tau_1 \leq -\frac{\varphi b\varpi (t_2 - t_1)^2}{2}$.

Thus, $t_2 - t_1 \leq \sqrt{\frac{2(s_i(t_1) - b\varpi)}{\varphi b\varpi}}$, where $s_i(t_1)$ is upper bounded as we discussed above. According to (2.29) and (2.30), we have

$$\rho_i(t_2) = \bar{\epsilon}^* + \int_{t_1}^{t_2} \varphi s_i(t)dt \leq \bar{\epsilon}^* + s_i(t_1)\sqrt{\frac{2\varphi(s_i(t_1) - b\varpi)}{b\varpi}}. \tag{2.34}$$

Therefore, $\rho_i(t_2)$ is upper bounded.

ii) $\bar{\epsilon}^* < r_0 + f_{BF}(b\varpi)$. At $t = 0$, the switching gain is large enough to decrease the sliding variable, and the switching gain still increase to improve the convergence of the sliding variable, according to (2.30). If $s_i(t_3) = b\varpi$, then $\rho_i(t_3) > \rho_i(t)$ for all $t < t_3$. According to (2.24) and (2.28)-(2.30), we have: $b\varpi - s_i(0) = \int_0^{t_3} \dot{s}_i(t)dt \leq \int_0^{t_3} (\bar{\epsilon}^* - r_i(t) - f_{BF}(b\varpi))\, dt \leq (\bar{\epsilon}^* - r_0 - f_{BF}(b\varpi))\, t_3$ since $r_i(t) > r_0$ for any $t \leq t_3$. Hence, $t_3 \leq \frac{s_i(0) - b\varpi}{r_0 + f_{BF}(b\varpi) - \bar{\epsilon}^*}$. According to (2.30), we have

$$\begin{aligned} \rho_i(t_3) &= r_0 + \int_0^{t_3} \varphi s_i(t)dt + f_{BF}(b\varpi) \\ &\overset{s_i(t)<s_i(0)}{\leq} r_0 + \frac{\varphi s_i(0)\,(s_i(0) - b\varepsilon)}{r_0 + f_{BF}(b\varpi) - \bar{\epsilon}^*} + f_{BF}(b\varpi). \end{aligned} \tag{2.35}$$

Therefore, $\rho_i(t_3)$ is still bounded.

After the sliding variable enters the region $|s_i(t)| \leq b\varpi$, $f_{BF}(s_i(t))$ is bounded and $r_i(t)$ is decreasing until $r_i(t) \leq \varsigma$ according to (2.30). Thus when $|s_i(t)| \leq b\varpi$ the switching gain is less than $\rho_i(t_2)$ or $\rho_i(t_3)$. Therefore, if the sliding variable is maintained in the region afterwards, $\rho_i(t)$ is bounded and ρ_i^* is obtained through (2.34) or (2.35). On the other hand, if the sliding variable exceeds the setting bound at t_4, $s_i(t_4) = b\varpi$, the rest $\rho_i(t)$ is still bounded. This is because there is a bound for $r_i(t_4)$. If we assume $r_i(t_4) > \bar{\epsilon}^* - f_{BF}(s_i(t_4))$, then $s_i(t_4)\dot{s}_i(t_4) \leq |s_i(t_4)|\,(\bar{\epsilon}^* - (r_i(t_4) + f_{BF}(s_i(t_4)))) < 0$. That means the sliding variable

will decrease. It contradicts. Therefore, $r_i(t_4) \leq \bar{\epsilon}^* - f_{BF}(s_i(t_4)) = \bar{\epsilon}^* - f_{BF}(b\varpi)$. Then, according to (2.35), we can determine the upper bound of $\rho_i(t)$ under this circumstances. All in all, $\rho_i(t)$ is bounded during the whole time horizon.

■

Based on **Lemma 2** and **Lemma 3**, we analyze finite-time convergence property of sliding variables. For simplicity, we use one sliding variable (noted as $s_i(t)$) to complete the following analysis.

Theorem 1 (Finite-Time Convergence Property)**.** *Consider the LTI system* (2.21) *controlled by the SMC* (2.28)*, with the updating law* (2.30) *for the switching gain* (2.29)*, then for any* $s_i(0)$ *and* $\varpi \in \mathbb{R}_{>0}$*, there exists* $\bar{t} > 0$ *such that for all* $t \geq \bar{t}$*,*

$$|s_i(t)| \leq \sqrt{(b\varpi)^2 + \frac{(\bar{\epsilon}^* - f_{BF}(b\varpi) - \varsigma)^2}{\varphi}}.$$

Proof: Suppose $|s_i(0)| \geq b\varpi$, the Lyapunov function $V_s : \mathbb{R} \times \mathbb{R} \mapsto \mathbb{R}$ [97] is considered

$$V_s = 0.5 s_i^2(t) + 0.5\vartheta \left(\rho_i(t) - \rho_i^*\right)^2 \tag{2.36}$$

where $\vartheta \in \mathbb{R}_{>0}$ is a design parameter, and $\vartheta > \frac{1}{\varphi}$ holds.

Considering the case $|s_i(t)| \geq b\varpi$, we have

$$\begin{aligned}
\dot{V}_s =& s_i(t)\left(-\rho_i(t)\,\mathrm{sign}(s_i(t)) + \epsilon_i'\right) + \vartheta\left(\rho_i(t) - \rho_i^*\right)\varphi|s_i(t)| \\
\leq& -\rho_i(t)|s_i(t)| + \bar{\epsilon}^*|s_i(t)| + \vartheta\varphi\left(\rho_i(t) - \rho_i^*\right)|s_i(t)| \\
=& -\rho_i(t)|s_i(t)| + \bar{\epsilon}^*|s_i(t)| + \rho_i^*|s_i(t)| - \rho_i^*|s_i(t)| \\
&+ \vartheta\varphi\left(\rho_i(t) - \rho_i^*\right)|s_i(t)| \\
=& -\left(\rho_i^* - \bar{\epsilon}^*\right)|s_i(t)| + \left(-|s_i(t)| + \vartheta\varphi|s_i(t)|\right)\left(\rho_i(t) - \rho_i^*\right)
\end{aligned} \tag{2.37}$$

From **Lemma 3**, $\rho_i(t) \leq \rho_i^*$ and $\bar{\epsilon}^* < \rho_i^*$. Besides, $\vartheta\varphi - 1 > 0$ since $\vartheta > \frac{1}{\varphi}$. Thus,

$$\begin{aligned}
\dot{V}_s \leq& -\underbrace{\left(\rho_i^* - \bar{\epsilon}^*\right)}_{\Pi_s > 0}|s_i(t)| - \underbrace{\left(-|s_i(t)| + \vartheta\varphi|s_i(t)|\right)}_{\Pi_\rho > 0}|\rho_i(t) - \rho_i^*| \\
=& -\sqrt{2}\Pi_s\frac{|s_i(t)|}{\sqrt{2}} - \sqrt{\frac{2}{\vartheta}}\Pi_\rho\frac{\sqrt{\vartheta}|\rho_i(t) - \rho_i^*|}{\sqrt{2}} \\
\leq& -\Pi\left(\frac{|s_i(t)|}{\sqrt{2}} + \frac{\sqrt{\vartheta}|\rho_i(t) - \rho_i^*|}{\sqrt{2}}\right) \leq -\Pi\sqrt{V_s}
\end{aligned} \tag{2.38}$$

where $\Pi = \min\{\sqrt{2}\Pi_s, \sqrt{\frac{2}{\vartheta}}\Pi_\rho\}$. Thus, finite-time converging to $|s_i(t_r)| = b\varpi$ is guaranteed, where t_r is the reaching time. From (2.37), we have $\frac{d}{dt}\left(2\sqrt{V_s}\right) \leq -\Pi$. Integral both sides, we get

$$\begin{aligned}
t_r \leq& \frac{2}{\Pi}\left(\sqrt{V_s(0)} - \sqrt{V_s(t_r)}\right) \\
\overset{(\rho_i(t_r) - \rho_i^*)^2 \geq 0}{\leq}& \frac{2}{\Pi}\left(\sqrt{V_s(0)} - \frac{b\varpi}{\sqrt{2}}\right).
\end{aligned} \tag{2.39}$$

Now the sliding variable enters the region $|s_i(t)| \leq b\varpi$. Afterwards, $|s_i(t)|$ still decreases because $\rho_i(t_r) > \bar{\epsilon}^*$ as discussed especially in Appendix C. That means, the sliding variable does not leave the region instantly. In the region $|s_i(t)| \leq b\varpi$, $\rho_i(t)$ is gradually regulated by PSDBF according to (2.29) and (2.30). To check whether the sliding variable leaves the region, the Lyapunov function $V_B = 0.5 s_i^2(t)$ is considered. Combining (2.24), (2.27), (2.28) with (2.29), one has

$$\begin{aligned}
\dot{V}_B &= s_i(t)\dot{s}_i(t) \\
&= s_i(t)\left(-(r_i(t) + f_{BF}(s_i(t)))\,\mathrm{sign}(s_i(t)) + \bar{\epsilon}_i'\right) \\
&\leq -r_i(t)|s_i(t)| - f_{BF}(s_i(t))|s_i(t)| + \bar{\epsilon}^*|s_i(t)| \\
&\overset{r_i(t)\geq 0}{\leq} -\underbrace{\left(f_{BF}(s_i(t)) - \bar{\epsilon}^*\right)}_{\Pi_B}|s_i(t)|
\end{aligned} \tag{2.40}$$

Eq. (2.40) shows that when $|s_i(t)| > \frac{\varpi\bar{\epsilon}^*}{\varpi+\bar{\epsilon}^*}$, $\Pi_B > 0$. If the parameter $\frac{\varpi\bar{\epsilon}^*}{\varpi+\bar{\epsilon}^*} < b\varpi$, then $\Pi_B > 0$ ($\dot{V}_B < 0$) for $|s_i(t)| \in \left(\frac{\varpi\bar{\epsilon}^*}{\varpi+\bar{\epsilon}^*}, b\varpi\right)$. The PSDBF ensures the sliding variable converges to a neighborhood around $\frac{\varpi\bar{\epsilon}^*}{\varpi+\bar{\epsilon}^*}$ in finite time t_c, and the sliding variable remains in the region $|s_i(t)| \leq \frac{\varpi\bar{\epsilon}^*}{\varpi+\bar{\epsilon}^*}$. On the contrary, if $\frac{\varpi\bar{\epsilon}^*}{\varpi+\bar{\epsilon}^*} \geq b\varpi$, then $\Pi_B < 0$ for $|s_i(t)| \in (0, b\varpi)$. With the decreasing of $r_i(t)$, $r_i(t) + \Pi_B < 0$ for $t \geq t_s$, i.e., some time later after the sliding variable enters the region $|s_i(t)| \leq b\varpi$, the switching gain $\rho_i(t) = r_i(t) + f_{BF}(s_i(t))$ will be smaller than $\bar{\epsilon}^*$. Although under this circumstances the sliding variable gradually leaves the region, the switching gain decreases when the sliding variable lies in the vicinity of the sliding manifold, resulting in chattering reduction. From the above discussion, the sliding variable trajectory is grouped into following two categories:

i) if $\frac{\varpi\bar{\epsilon}^*}{\varpi+\bar{\epsilon}^*} < b\varpi$, then $\Pi_B > 0$ for $|s_i(t)| \in \left(\frac{\varpi\bar{\epsilon}^*}{\varpi+\bar{\epsilon}^*}, b\varpi\right)$. From (2.40), we have

$$\begin{aligned}
\dot{V}_B &\leq -\Pi_B|s_i(t)| = -\sqrt{2}\Pi_B\frac{|s_i(t)|}{\sqrt{2}} \\
&= -\sqrt{2}\Pi_B\sqrt{V_B}
\end{aligned} \tag{2.41}$$

Thus, there exists $\delta \in \mathbb{R}_{>0}$ such that $\frac{\varpi\bar{\epsilon}^*}{\varpi+\bar{\epsilon}^*} + \delta < b\varpi$ holds, and $|s_i(t)|$ reaches $\left(\frac{\varpi\bar{\epsilon}^*}{\varpi+\bar{\epsilon}^*} + \delta\right)$ in finite time t_c, which satisfies

$$t_c \leq \frac{\sqrt{2}\left(\sqrt{V_B(b\varpi)} - \sqrt{V_B\left(\frac{\varpi\bar{\epsilon}^*}{\varpi+\bar{\epsilon}^*} + \delta\right)}\right)}{f_{BF}\left(\frac{\varpi\bar{\epsilon}^*}{\varpi+\bar{\epsilon}^*} + \delta\right) - \bar{\epsilon}^*}. \tag{2.42}$$

Note that Π_B takes the minimum value at $|s_i(t)| = \left(\frac{\varpi\bar{\epsilon}^*}{\varpi+\bar{\epsilon}^*} + \delta\right)$ for $|s_i(t)| \in \left(\frac{\varpi\bar{\epsilon}^*}{\varpi+\bar{\epsilon}^*} + \delta, b\varpi\right)$. The reason why we introduce a small scalar δ to determine the upper bound of t_c is that $\Pi_B = 0$ when $|s_i(t)| = \frac{\varpi\bar{\epsilon}^*}{\varpi+\bar{\epsilon}^*}$.

ii) if $\frac{\varpi\bar{\epsilon}^*}{\varpi+\bar{\epsilon}^*} \geq b\varpi$, then $\Pi_B < 0$ for $|s_i(t)| \in (0, b\varpi)$. Therefore, $|s_i(t)|$ gradually leaves the region $|s_i(t)| \leq b\varpi$. Later on, according to (2.38), $|s_i(t)|$ will converge to this region again after it leaves the region. Although $|s_i(t)|$ moves in and out of the region, $|s_i(t)|$ and $\rho_i(t)$ are all bounded according to (2.38) and **Lemma 3**. Without loss of

generality, we estimate the upper bound of the sliding variable when it moves out of the region at t_ε supposing $s_i(t_\varepsilon) = b\varpi$ and $r_i(t_\varepsilon) = \varsigma$. Considering the "worst" case [97], one gets

$$\begin{cases} \dot{s}_i(t) = -\left(r_i(t) + f_{BF}(b\varpi)\right) + \bar{\epsilon}^* \\ \dot{r}_i(t) = \varphi s_i(t),\ r_i(t_\varepsilon) = \varsigma \end{cases} \tag{2.43}$$

Then, using Laplace transform, we have

$$\begin{aligned} s_i(t) &= b\varpi \cos\left(\sqrt{\varphi}t\right) + \frac{\bar{\epsilon}^* - f_{BF}(b\varpi) - \varsigma}{\sqrt{\varphi}} \sin\left(\sqrt{\varphi}t\right) \\ &= \sqrt{(b\varpi)^2 + \frac{\left(\bar{\epsilon}^* - f_{BF}(b\varpi) - \varsigma\right)^2}{\varphi}} \sin\left(\sqrt{\varphi}t + \Theta\right) \end{aligned} \tag{2.44}$$

where $\Theta = \arctan \frac{b\varpi\sqrt{\varphi}}{\bar{\epsilon}^* - f_{BF}(b\varpi) - \varsigma}$.

Thus, the upper bound of the sliding variable is $\sqrt{(b\varpi)^2 + \frac{\left(\bar{\epsilon}^* - f_{BF}(b\varpi) - \varsigma\right)^2}{\varphi}}$. Note that (2.44) is not the real trajectory of the sliding variable. We only use it to demonstrate boundedness property of the sliding variable after the sliding variable exceeds the setting bound.

Therefore, for all $t > t_r$, $|s_i(t)|$ stays inside $(0, B(\varpi))$, where $B(\varpi) = \sqrt{(b\varpi)^2 + \frac{\left(\bar{\epsilon}^* - f_{BF}(b\varpi) - \varsigma\right)^2}{\varphi}}$.

■

Remark 6 (Conservative Setting Bound is Adopted in the Conventional PSDBF [88].)**.** *The novel PSDBF* (2.27) *is different from the one employed in [88]. As stated in [88],* $|s_i(t)|$ *ultimately converges to* $\frac{\varpi\bar{\epsilon}^*}{1+\bar{\epsilon}^*}$*. We assume the PSDBF in [88] is still applied in this paper. In practice, the TDE error is related to the sampling period, i.e., the smaller sampling period, the smaller is the TDE error. When the sampling period is sufficiently small,the TDE error can be very small and it is possible that* $\bar{\epsilon}^* << 1$ *during a long time horizon or even the entire execution time. In what follows, we will investigate whether the PSDBF introduced in [88] is suitable to be applied when* $\bar{\epsilon}^* << 1$*. If* $\bar{\epsilon}^* << 1$*, then the actual bound for* $|s_i(t)|$*,* $\frac{\varpi\bar{\epsilon}^*}{1+\bar{\epsilon}^*} (\approx \varpi\bar{\epsilon}^*)$*, is much smaller than the setting bound* ϖ*. Thus, there remains a considerable discrepancy between the actual bound and the setting one. Normally, we want to regulate the sliding variable to be as small as possible to attenuate the disturbance (TDE error in the context of this chapter). Thus, in practice, we would like to select a small setting bound* ϖ*. Sometimes* $\varpi\bar{\epsilon}^*$ *will be so small that* $|s_i(t)|$ *can not converge to it, resulting in fluctuation or even instability. This phenomenon is also verified by numerical simulations in Section 2.4.2. Thus, in practice, to guarantee stability, conservative (large) setting bounds are selected, which have bad influences on tracking precision.*

Remark 7 (Conservative Setting Bound is Avoided in the Novel PSDBF.)**.** *For the proposed PSDBF* (2.27) *in this paper,* $|s_i(t)|$ *ultimately converges to* $\frac{\varpi\bar{\epsilon}^*}{\varpi+\bar{\epsilon}^*}$*. Here is a case analysis to analyze the actual bound* $\frac{\varpi\bar{\epsilon}^*}{\varpi+\bar{\epsilon}^*}$*, and there are two situations considered.*

1) *If* $\bar{\epsilon}^* << \varpi$, *then* $\frac{\varpi\bar{\epsilon}^*}{\varpi+\bar{\epsilon}^*} < \bar{\epsilon}^* < \varpi$ *and* $\frac{\varpi\bar{\epsilon}^*}{\varpi+\bar{\epsilon}^*} \approx \bar{\epsilon}^*$. *Obviously, the sliding variable will converge to* $|s_i(t)| < \varpi$. *As mentioned in* ***Remark 6****, we normally would like to select a small setting bound to satisfy precision requirement of the control system. In this situation, the upper bound of the TDE error* $\bar{\epsilon}^*$ *is even smaller than the setting bound* ϖ. *Thus, tracking performance will not be badly influenced by the disturbance. According to the actual bound* $\frac{\varpi\bar{\epsilon}^*}{\varpi+\bar{\epsilon}^*} (\approx \bar{\epsilon}^*)$ *and the barrier function, we learn that the switching gain* $\frac{\varpi|s_i(t)|}{\varpi-|s_i(t)|} \approx \bar{\epsilon}^*$. *Therefore, it results in chattering reduction and tracking performance is nearly not affected.*

2) *If* $\bar{\epsilon}^* >> \varpi$, *then* $\frac{\varpi\bar{\epsilon}^*}{\varpi+\bar{\epsilon}^*} < \varpi (\frac{\varpi\bar{\epsilon}^*}{\varpi+\bar{\epsilon}^*} \approx \varpi)$. *In this situation,* $\bar{\epsilon}^*$ *is larger than the setting bound. Under the function of the PSDBF based on SMC, the sliding variable will converge to* $|s_i(t)| < \frac{\varpi\bar{\epsilon}^*}{\varpi+\bar{\epsilon}^*}$ *and* $\frac{\varpi\bar{\epsilon}^*}{\varpi+\bar{\epsilon}^*} \approx \varpi$. *It also means the sliding variable will converge to a predefined vicinity w.r.t.* ϖ. *In this situation, even when* $\bar{\epsilon}^* << 1$, *the actual bound will not shrink significantly. From the case study, one learns that sliding variable will converge to a predefined vicinity and conservative (large) setting bounds are avoided, regardless of* $\bar{\epsilon}^*$.

Remark 8 (How to Select the Parameter b.)**.** *If we let* b *be close to 1 infinitely, then* $\frac{\varpi\bar{\epsilon}^*}{\varpi+\bar{\epsilon}^*} < b\varpi$ *holds because* $\frac{\varpi\bar{\epsilon}^*}{\varpi+\bar{\epsilon}^*} < \varpi$ *regardless of* ϖ *and* $\bar{\epsilon}^*$. *As shown in the situation i) of* ***Theorem 1****,* $|s_i(t)|$ *is maintained in the region* $[0, b\varpi]$ *independent of* $\bar{\epsilon}^*$. *This is also why we keep* b *as close as possible to 1 in the following experiments.*

Remark 9 (Over- and Underestimation of Switching Gains are Avoided Simultaneously.)**.** *If the sliding variable is maintained in the region* $|s_i(t)| \leq b\varpi$, *the switching gain eventually changes following the PSDBF. Thus the switching gain increases with the rise of sliding variable and vice versa. Therefore, this scheme avoids over- and underestimation of the switching gains simultaneously. While in [29], the switching gain sometimes is underestimated because the switching gain merely decreases in the vicinity of the sliding manifold.*

2.4 Simulation and Experiments

To validate effectiveness of the proposed control scheme, a 3-DoF robot manipulator (see Figure 2.2), created by Chair of Automatic Control Engineering (LSR), Technical University of Munich (TUM), is considered. The identified mathematical model of the robot manipulator can be referred to Table II, III, and IV in [94]. The manipulator is actuated by 3 Maxon torque motors with a turn ration of 1.25×10^{-3} deg. The incremental encoders offer the joint position measurement with a resolution of 2000. The sensors and actuators are connected with the computer using a peripheral component interconnect (PCI) communication card. The executable algorithm is created by MATLAB 2017a in Ubuntu 14.04 LTS, using the first-order Euler solver with the sampling rate of 1 kHz.

2.4.1 Tracking Accuracy in Experiments

To verify the high tracking accuracy of the proposed controller, we compare three conventional control methods, the adaptive backstepping [72], the adaptive SMC [29], and the IBS developed in Section 2.2.2, with our AISMC scheme in Section 3.1, in this experiment. For

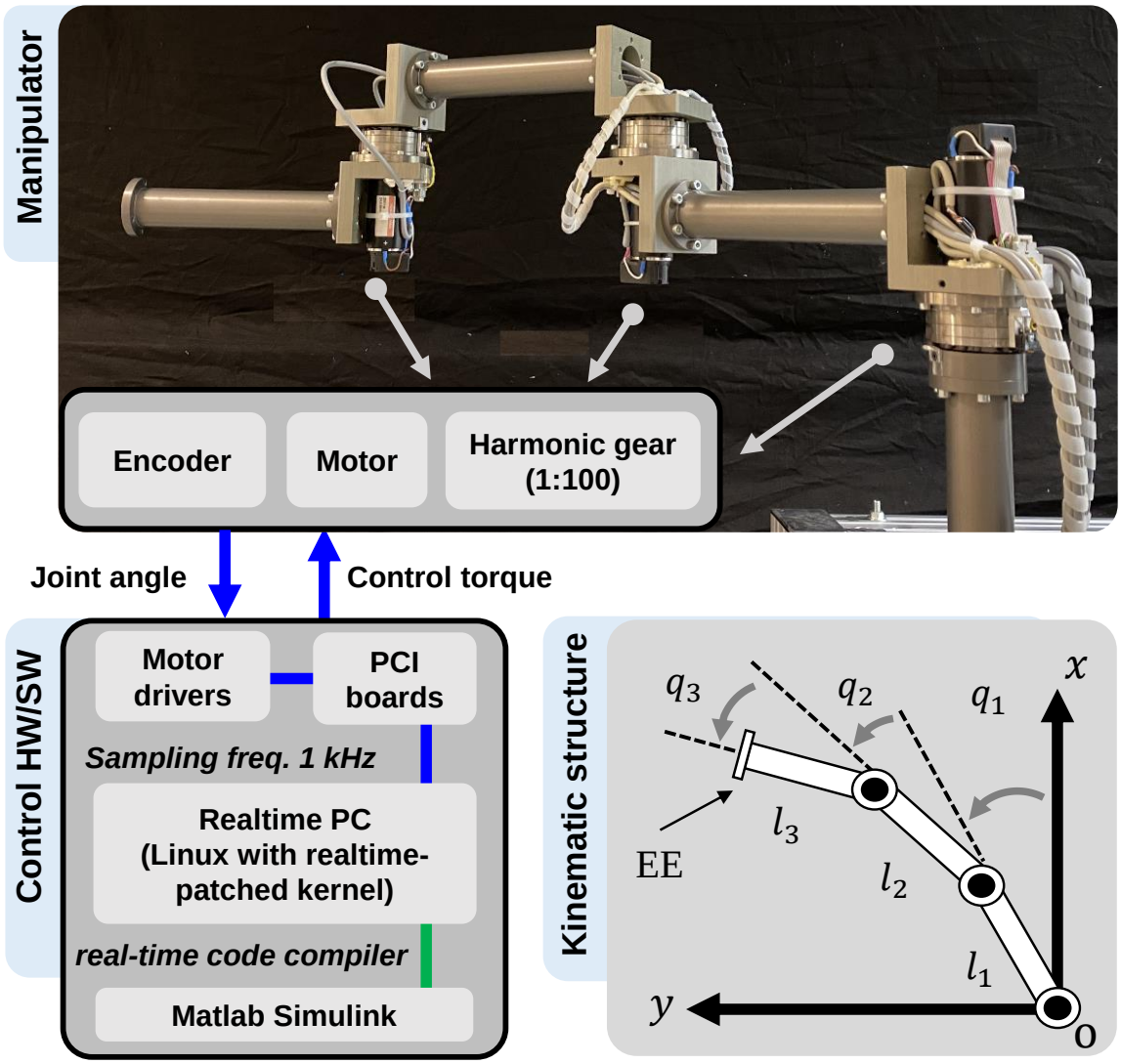

Figure 2.2: Experimental setup of the 3-DoF planar robot manipulator with control hardware and software architectures and its kinematic structure ($l_1 = l_2 = l_3 = 0.3$ m).

simplicity, we will use the abbreviation ABS, ASMC, IBS and AISMC to respectively refer these methods.

Parameters of Controllers: To ensure objectivity, design parameters are determined for four controllers in accordance with following steps.

S1 : $\bar{\mathbf{g}} = \text{diag}(14, 32, 80)$ for ASMC, IBS, and the proposed AISMC. As stated in [98], lowering the elements of $\bar{\mathbf{M}}$ attenuates signal noises, having the same effect as using the first-order digital low-pass-filter. Besides, the TDE based controller does not pose strict requirements on the selection of TDE gains. A sufficiently small $\bar{\mathbf{M}}$ can also guarantee the stability condition holds (compare **Remark 23**). As stated in (A.4), $\bar{\mathbf{g}} = \bar{\mathbf{M}}^{-1}$. Thus, a large $\bar{\mathbf{g}}$ is selected.

S2 : $k_1 = k_2 = 8$ for ABS, IBS, and the proposed AISMC. As analyzed in Section 2.2.2, IBS controller in nature is a TDC and $\mathbf{K}_\text{P} = k_1 k_2 \mathbf{I}$ and shaping factors $\mathbf{K}_\text{D} = (k_1 + k_2)\mathbf{I}$. Then, $\mathbf{K}_\text{P} = 64\mathbf{I}$ and $\mathbf{K}_\text{D} = 16\mathbf{I}$ for ASMC. To avoid input saturation, we do not select

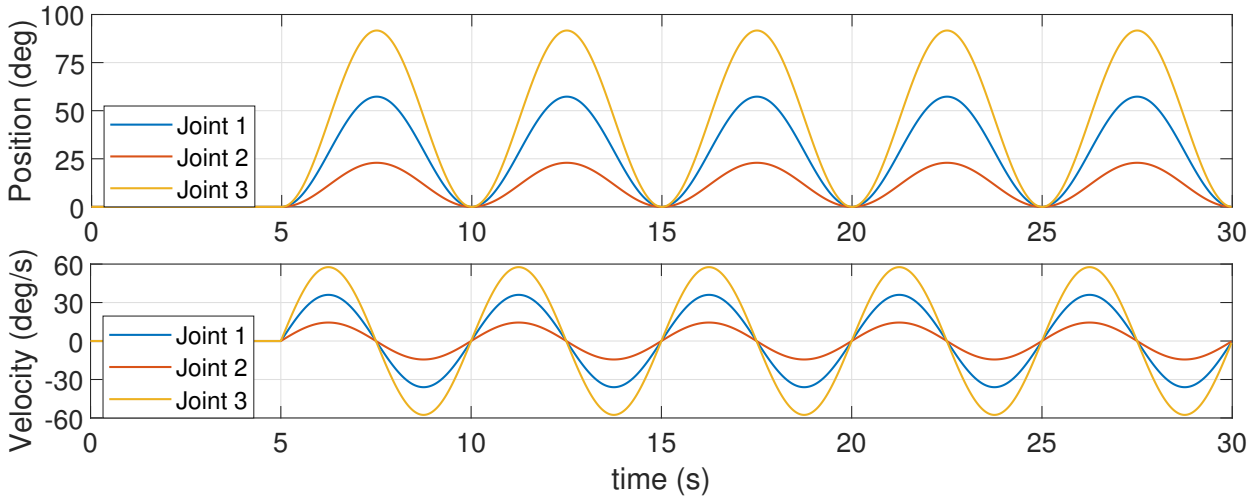

Figure 2.3: Reference trajectories for the three joints.

high gains in this step.

S3 : $b = \frac{10}{11}$ for the proposed AISMC since b should be close to 1 as stated in **Remark 8**. The setting bound $\boldsymbol{\varpi} = [0.002, 0.001, 0.001]$ for ASMC and the proposed AISMC. Normally, the setting bound $\boldsymbol{\varpi}$ is determined according to precision requirement of the control system and designers' experience. Meanwhile, one method to determine a reasonable $\boldsymbol{\varpi}$ is shown in Section 2.4.2.

S4 : For the proposed ASMC, $\alpha_i = 50$ and $\varphi_i = 2.5 \times 10^3$ $(i = 1, 2, 3)$. According to the updating law (2.30) in this article and (11) in [29], the design parameter φ in this article is corresponding to $\frac{\varphi_i}{\alpha_i}$ in [29]. Thus, $\varphi = 50$ for the proposed AISMC.

For AISMC, weighting matrices $\mathbf{Q} = 20\mathbf{I}$ and $\mathbf{R} = \mathbf{I}$, and small scalar parameters $\varsigma = \iota = 10^{-5}$. Note that according design parameters $\bar{\mathbf{g}}$, k_1, k_2, $\mathbf{Q}$ and $\mathbf{R}$, we can obtain matrix $\mathbf{P}$.

From the above steps to determine parameters for controllers, we learn that the practical design procedure of the proposed controller is not much more complex than that of existing methods, almost the same as that of ASMC.

Because of the limited availability of sensors, we use the following difference models to estimate $\dot{\mathbf{q}}(k)$ and $\ddot{\mathbf{q}}(k)$ [99], [100]: $\dot{\mathbf{q}}(k) = \frac{\mathbf{q}(k)-\mathbf{q}(k-1)}{T_s}$, $\ddot{\mathbf{q}}(k) = \frac{\mathbf{q}(k)-2\mathbf{q}(k-1)+\mathbf{q}(k-2)}{T_s^2}$ where T_s is the sampling period, and $T_s = 1\,\text{ms}$.

Experimental Results: The reference trajectories for the three joints are displayed in Figure 2.3, and experimental results are displayed in Figures 2.4-2.9 and Table 2.1.

As shown in Figure 2.4 and Table 2.1, the tracking errors increase with the rise of the reference signal amplitudes when ABS and IBS are employed (For clarity, we only give the root-mean-square (RMS) values of ABS). ASMC and AISMC show smaller tracking errors than IBS, because the TDE error is compensated for by the additional SMC. The proposed AISMC scheme shows the smallest tracking errors, and the maximum tracking errors of the three joints are all about 0.01 deg regardless of the reference signal amplitudes. Figure 2.5 displays the torques generated by ASMC, IBS, and AISMC, respectively. It is observed that three controllers are all affected by the inherent noises almost in the same degree.

Figures 2.6-2.7 show sliding variables and switching gains generated by ASMC and AISMC schemes. For the ASMC scheme, there are some fluctuations around the setting bound. This

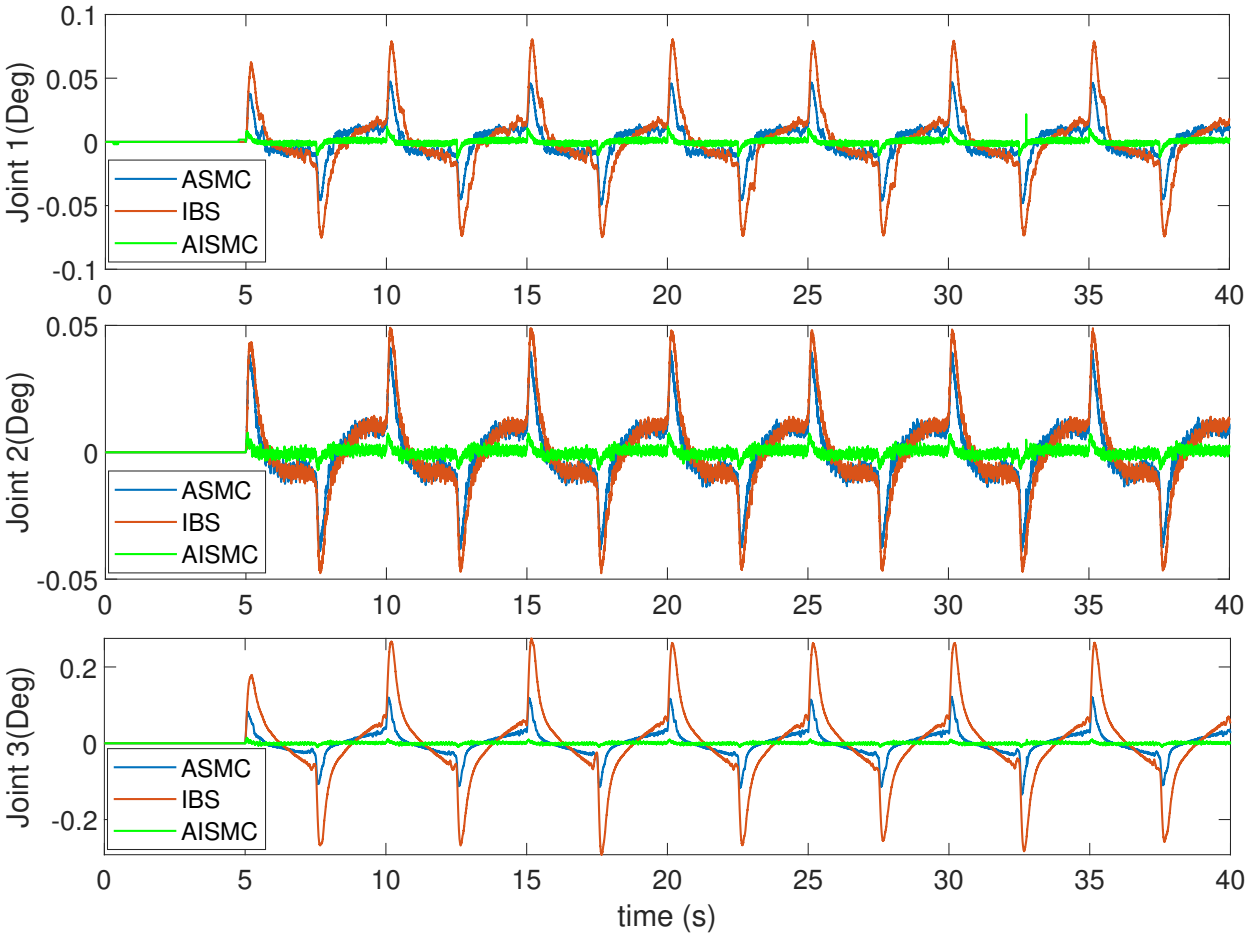

Figure 2.4: Experimental results: Tracking errors of the three joints.

is because the switching gain merely decreases when the sliding variable enters the bound, and then the switching gain increases when the sliding variable moves outside the bound, as shown in Fig. 2.7. While, the sliding variables are nearly maintained inside the setting bounds for the AISMC scheme. Because of measurement noises, the sliding variables exceed the bounds temporarily for some short periods. When the sliding variable lies inside the bound, the switching gains increase or decrease whenever the sliding variables increase or decrease.

To further verify effectiveness of AISMC, we conducted the experiments with different payloads, and the payloads are installed to the end-effector of the manipulator. As shown in Figure 2.8 (taking joint 2 for example) and Table 2.1, the tracking accuracy for IBS and ABS controllers decrease, and tracking errors rise as the payload weights increase. This is because the robot dynamics is affected by the payload. For ASMC, it attenuates the external disturbance effectively while the tracking errors generated by IBS increases with the rise of the payloads (see the enlarged parts). As expected, there are no apparent differences for the AISMC scheme with different payloads, except for a short time around the starting time (see the enlarged part). During these time, switching gains are adapted to attenuate the disturbances, and the longer time is taken for the heavier payloads, resulting in larger tracking errors only around the starting time.

Figure 2.9 shows the effectiveness of the LQR controller. Here, we select $k_1 = k_2 = 3$ to do

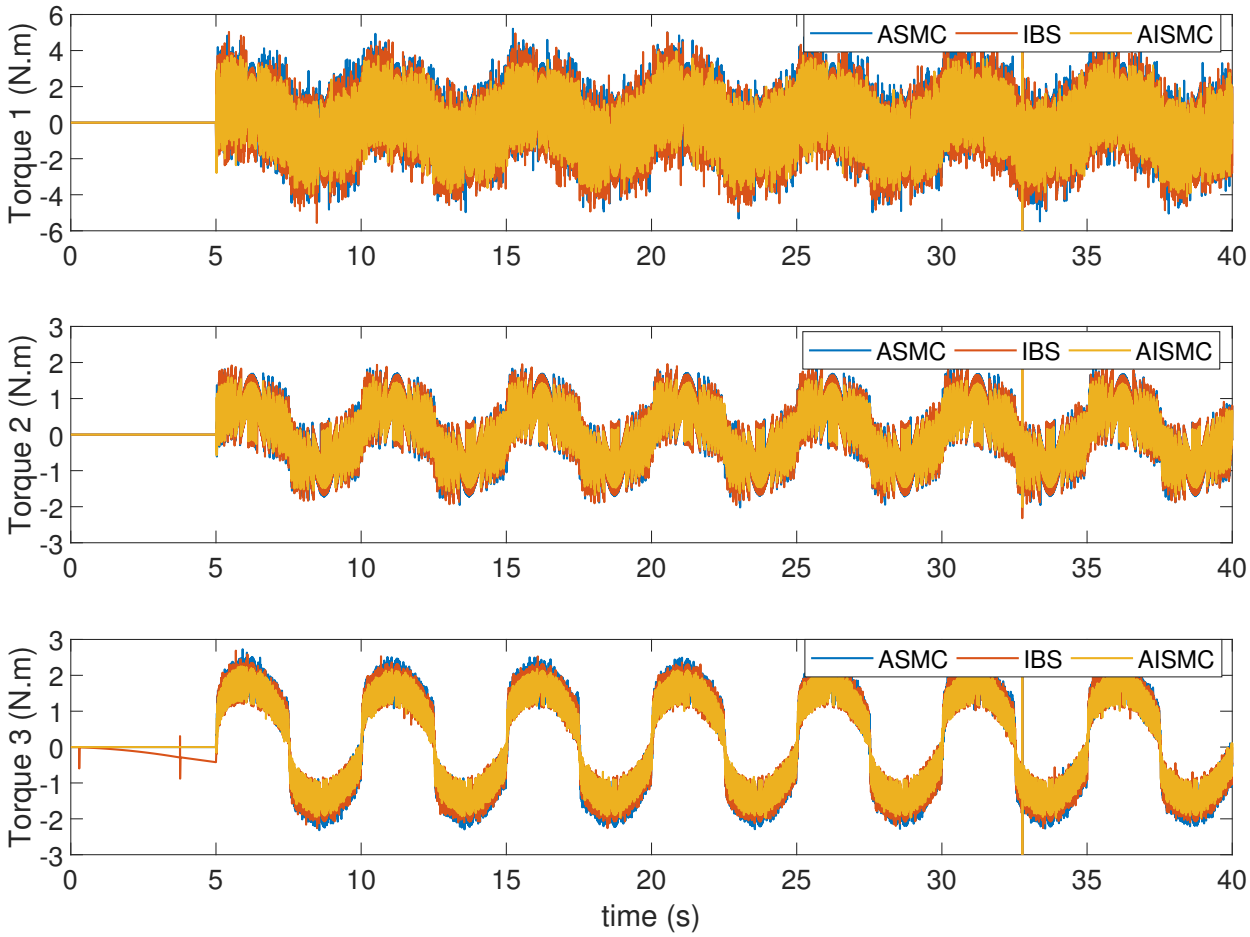

Figure 2.5: Experimental results: Torque inputs for three joints.

comparison experiments. Without the LQR controller, we design the sliding variable letting the $\Delta \mathbf{u}_{\mathrm{o,noi}} = \mathbf{0}$ following (2.23). Thus, there are four schemes are considered, i.e.,

1) : no LQR, $k_1 = k_2 = 3$;

2) : AISMC, $k_1 = k_2 = 3$;

3) : no LQR, $k_1 = k_2 = 8$;

4) : AISMC, $k_1 = k_2 = 8$.

As shown in Figure 2.9, tracking performance of Scheme 1 ($k_1 = k_2 = 3$) is worse than that of Scheme 3 ($k_1 = k_2 = 8$). It is attributed to the difference of design parameters. In Schemes 1 and 3, after the TDE error is addressed by SMC $\Delta \mathbf{u}_{\mathrm{o,sm}}$, tracking error dynamics is only affected by design parameters (k_1 and k_2) at the sliding manifold. If inappropriate design parameters are selected, tracking performance is not satisfied although the TDE error is handled by SMC. Moreover, design parameters are selected according to trial and error. In general, the larger k_1 and k_2 are selected, the better tracking performance is received. However, in practice, we could not increase k_1 and k_2 infinitely because large parameters will cause input saturation and/or fluctuation of the system. Besides, tracking performance of Schemes 1 and 3 is worse than that of their counterparts (Scheme 2 or 4). This is because for

Table 2.1: Experimental results: RMS Values of the Tracking Errors of the Three Joints (10^{-2} Deg) with or without Payloads

	Weight (g)	**ABS**	**ASMC**	**IBS**	**AISMC**
	0	92.13	2.08	3.45	0.20
Joint 1	200	92.34	2.11	3.58	0.20
	500	92.60	2.14	3.69	0.21
	1000	92.94	2.15	3.87	0.21
	Weight (g)	**ABS**	**ASMC**	**IBS**	**AISMC**
	0	28.93	1.18	1.53	0.18
Joint 2	200	29.02	1.22	1.60	0.18
	500	29.29	1.25	1.65	0.19
	1000	30.27	1.35	1.75	0.20
	Weight (g)	**ABS**	**ASMC**	**IBS**	**AISMC**
	0	227.1	3.11	8.82	0.21
Joint 3	200	227.2	3.14	8.83	0.24
	500	227.3	3.15	8.87	0.26
	1000	227.5	3.16	8.92	0.26

Schemes 2 and 4 (AISMC schemes), their tracking performance is regulated further at the sliding manifold because of LQR controllers. In addition, for Schemes 2 and 4, they display almost the same tracking performance regardless of k_1 and k_2. This is also because LQR controllers make the system receive optimal control performance at the sliding manifold. It also implies the proposed AISMC scheme does not pose strict requirements on k_1 and k_2.

Note that for existing methods, such as IBS (or TDC) and ASMC, tracking performance can be enhanced if elements of $\bar{\mathbf{M}}$ (or $\bar{\mathbf{g}}^{-1}$) increase appropriately. The larger $\bar{\mathbf{M}}$ generally suppresses TDE error faster so that control performance can be enhanced. However, the large value of $\bar{\mathbf{M}}$ amplifies the signal noise effect and invokes control chattering. For the sake of attenuating the signal noise, we select a small $\bar{\mathbf{M}}$ (or large $\bar{\mathbf{g}}$) in this study.

Note that the proposed control scheme does not take input saturation into account. When control signals are highly saturated, control performance will be degraded. As displayed in Figure 2.9, the conventional TDE-based controller normally select high gains to improve tracking performance. However, large k_1 and k_2 also can cause input saturation and/or fluctuation of the system. For our method, we can set relatively small k_1 and k_2 when we design IBS. Then, LQR controller is designed later to obtain a satisfactory control performance. Besides, when we design the LQR controller, the corresponding cost function also considers the input variable, which prevents control signals from being too large. Moreover, the sliding mode controller is developed based on PSDBF. The PSDBF avoids over/under-estimation of switching gains. Thus, our proposed control scheme prevents input signals from being saturated to some extent.

2.4.2 Effectiveness of the Barrier Function

As discussed in **Remark 6**, the previous PSDBF introduced in [88] may not be safe. Here, it is dangerous to do experiments using the previous PSDBF (introduced in [88]) based

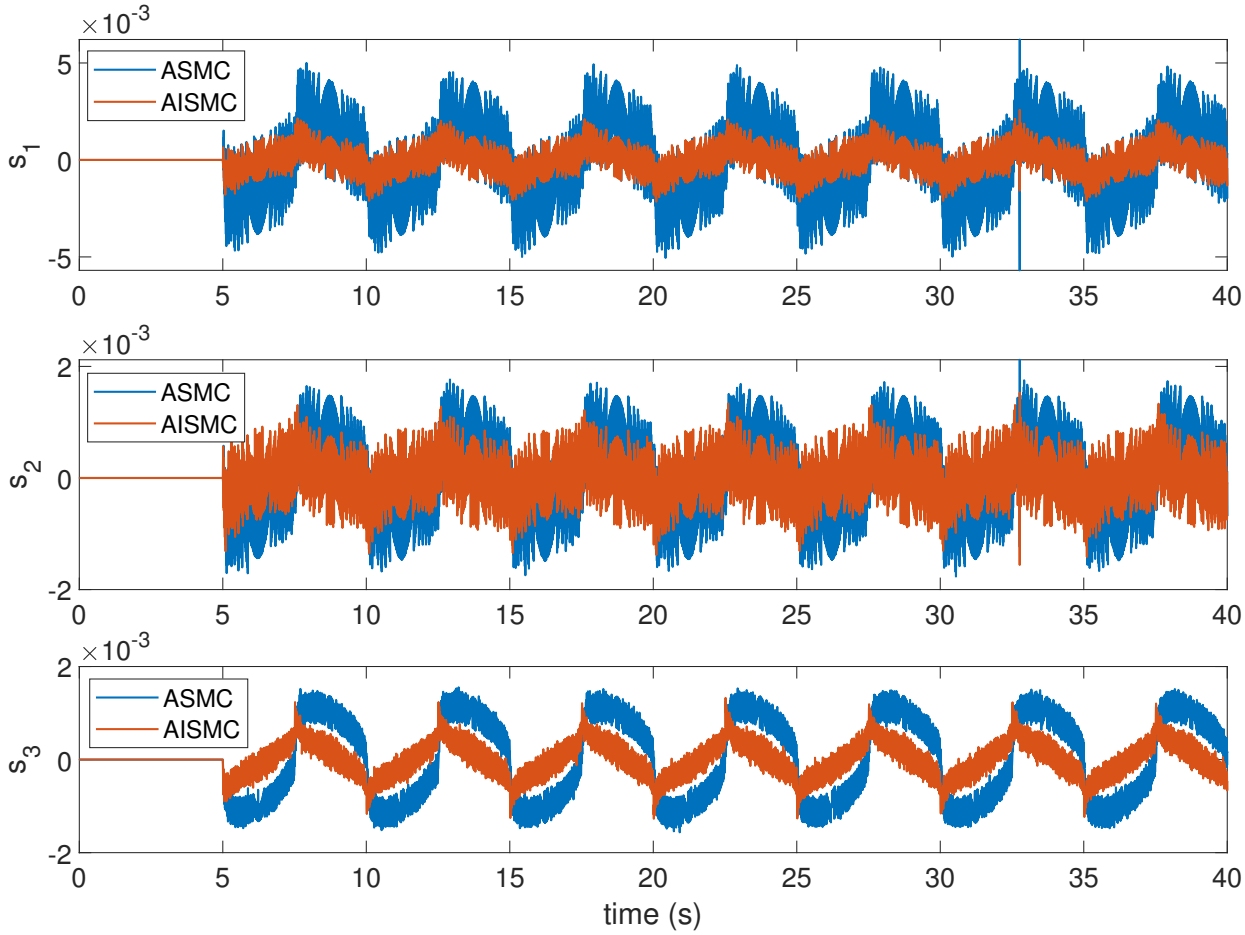

Figure 2.6: Experimental results: Sliding variables.

incremental sliding mode controller, e.g. it may break the robot when fluctuation or even instability occurs. Thus we did simulations here. We set $\varpi = 0.02$, and the other parameters are same to the Section 2.4.1.

As shown in Figure 2.10, the system is unstable. As discussed in **Remark 6**, we intend to make the sliding variable converge to a bound ϖ while the controller makes it converge to the bound $\varpi\bar{\epsilon}^*$ in nature. Because $\bar{\epsilon}^*$ is relatively small (compare Figure 2.11), the actual bound $\varpi\bar{\epsilon}^*$ is too small such that it is beyond the controller capabilities, resulting in instability. Note that the TDE error is also affected by the controller. Normally, we need to provide the TDE error curves under the action of the previous PSDBF (introduced in [88]) based incremental sliding mode controller. However, the system is not stable. In this situation, the system function suffers from sudden and drastic changes. The aim of displaying the TDE error curves under the action of the IBS controller (compare Figure 2.11) is to show the amplitude of the TDE error is relatively small under the current simulation environment.

To show effectiveness of the novel PSDBF based AISMC, a series of simulations are conducted. As shown in Figure 2.12, the sliding variables converge to and maintain inside the setting bound when $\varpi = 0.5$ or 0.0004, corresponding to situation i) of **Theorem 1**, the ultimate $|s_i(t)|$ is maintained in the region $(0, b\varpi)$. When we select $\varpi = 0.5$ which is obviously larger than the upper bound of TDE error $\bar{\epsilon}^*$, the sliding variable is smaller than that generated by IBS plus LQR. That means, it also attenuates the disturbance even when we

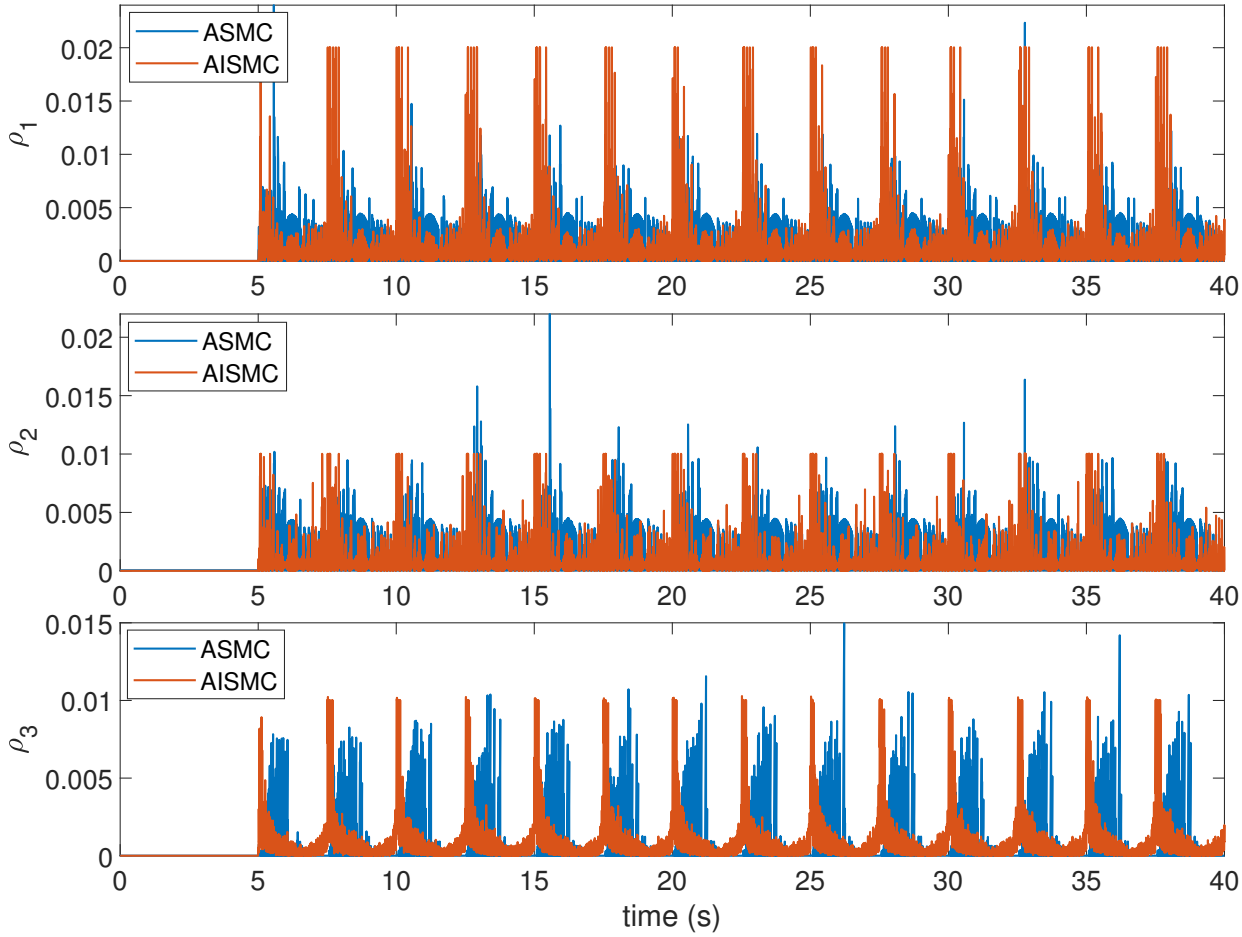

Figure 2.7: Experimental results: Switching gains.

select a large setting bound. For $\varpi = 0.0002$, corresponding to the situation ii) of **Theorem 1**, $|s_i(t)|$ converges to a bound σ $\left(\sigma < \sqrt{(b\varpi)^2 + \frac{(\bar{\epsilon}^* - f_{BF}(b\varpi) - \varsigma)^2}{\varphi}}\right)$ although sometimes the output exceeds the bound ϖ. In this situation, there are some slight fluctuations of the sliding variable around the setting bound. It also implies the smaller setting bound ϖ may not generate better tracking performance. When too small ϖ is selected, it causes fluctuation of the sliding variable although the system is still stable. This is the limitation of this study.

In practice, to avoid fluctuation of the sliding variables, we also can determine b and ϖ as follows. As discussed in **Remark 8**, we keep b as close as possible to 1. Then, motivated by finite-time convergence of the sliding variable we analyzed in Section 2.3.2, we can determine ϖ hereafter. We first apply a large setting bound. As discussed in **Remark 6**, the sliding variable converges to the bound $\frac{\varpi\bar{\epsilon}^*}{\varpi+\bar{\epsilon}^*}$ which can be measured from simulation/experimental results. Then, we can determine the upper bound of TDE error $\bar{\epsilon}^*$. According to the precision requirement, we select appropriate ϖ and let $\frac{\varpi\bar{\epsilon}^*}{\varpi+\bar{\epsilon}^*} < b\varpi$, corresponding to the situation i). Thus, the sliding variable converges to and stays in the region $|s_i(t)| \leq b\varpi$, and there are no fluctuations of the sliding variable around the setting bound. In this situation, the switching gain increases or decreases whenever the sliding variable increases or decreases, and it protects the switching gains from being overestimated or underestimated. As a future development, the setting bound ϖ will be updated employing data-driven and/or learning

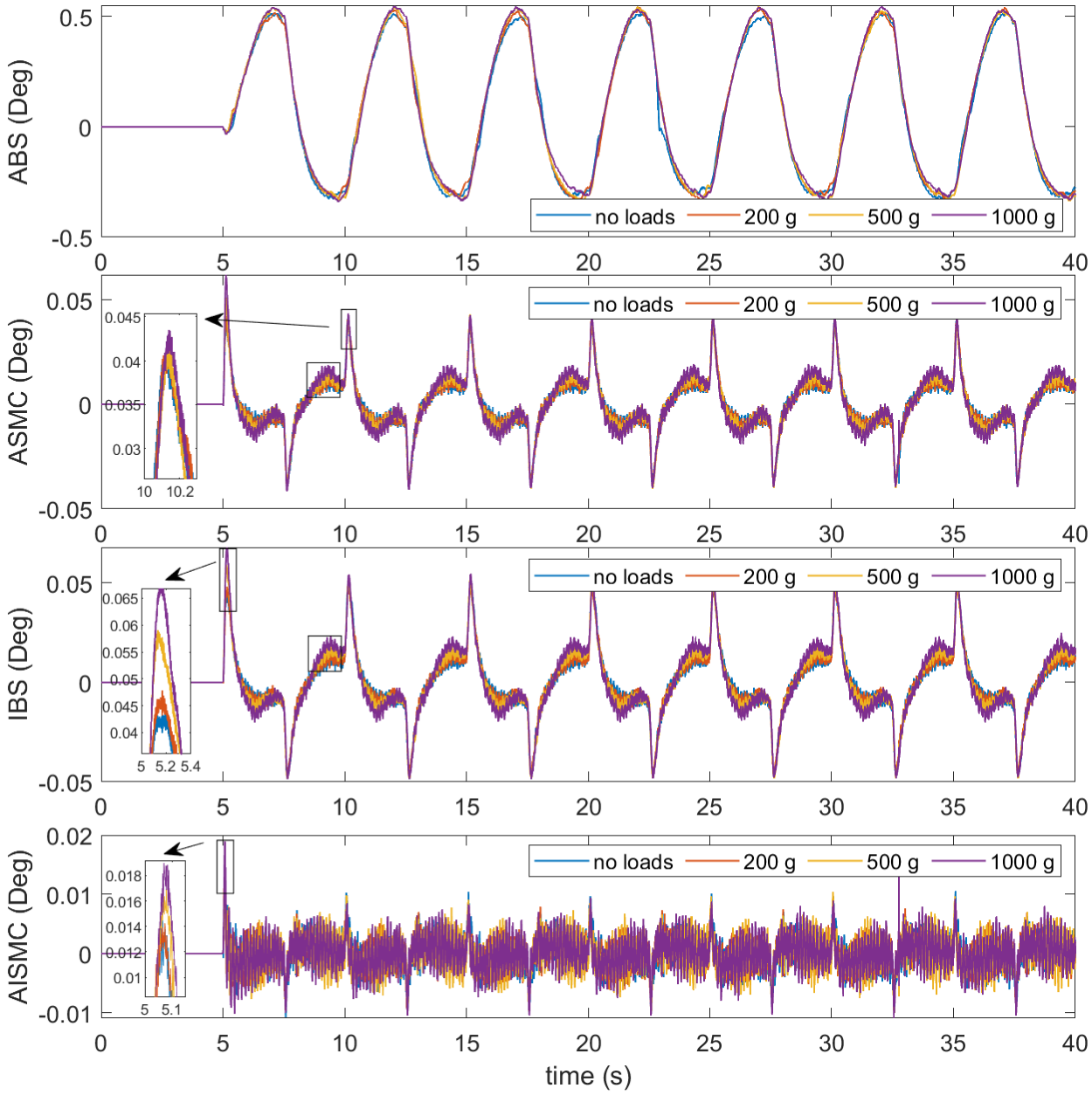

Figure 2.8: Experimental results: Tracking errors of Joint 2 with different payloads generated by ABS, ASMC, IBS, and AISMC.

techniques to avoid fluctuation of the sliding variable and enhance control performance.

2.5 Summary

In this chapter, an adaptive incremental sliding mode controller (AISMC) is developed for a robot manipulator under the framework of incremental backstepping (IBS) using time-delay estimation (TDE). The AISMC consists of the IBS controller and an integral SMC.

The IBS controller is the base of AISMC. First, to reduce dependency on the concrete mathematical model of the robot manipulator and also address modeling uncertainties and

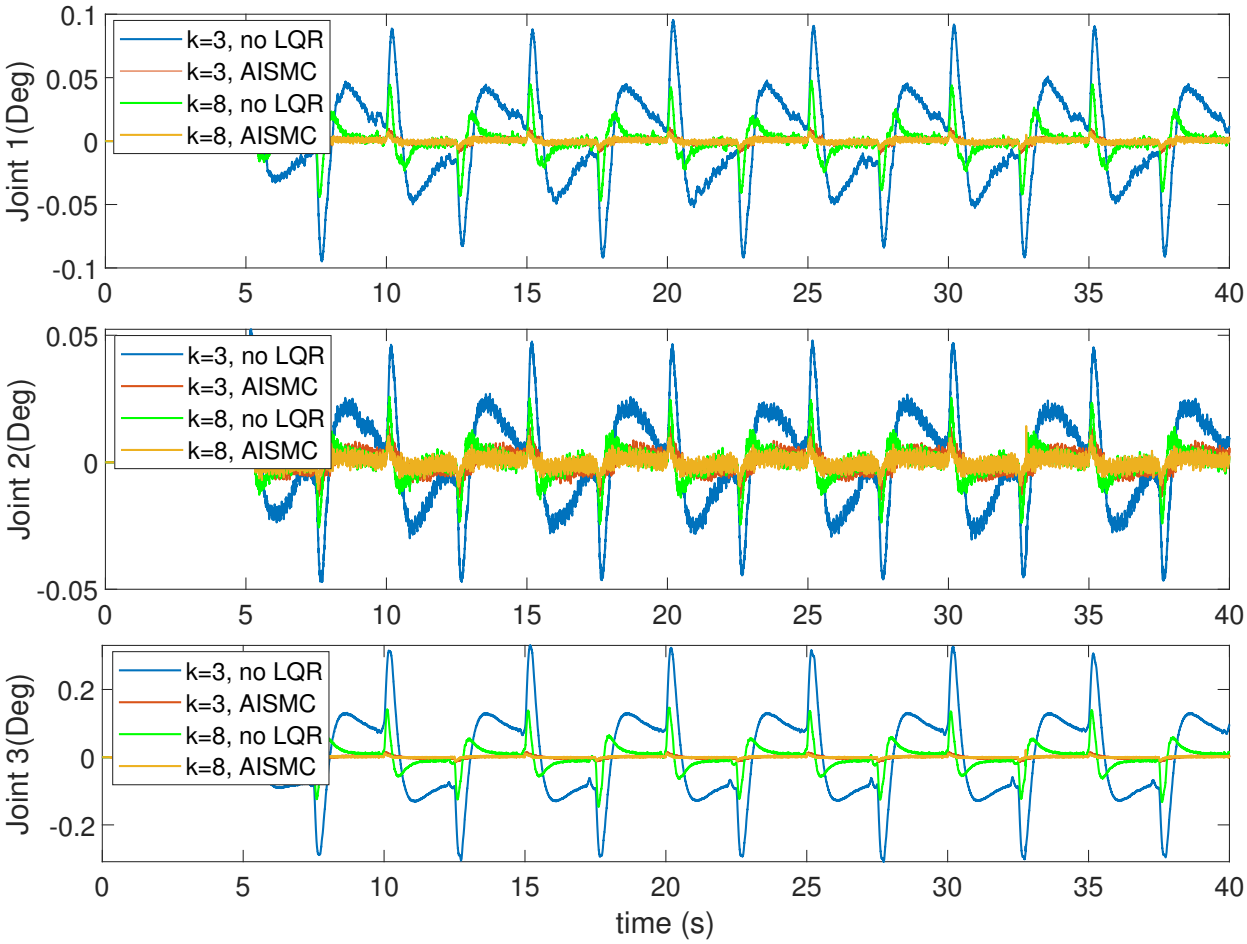

Figure 2.9: Experimental results: Tracking errors for the three joints with or without the LQR controller.

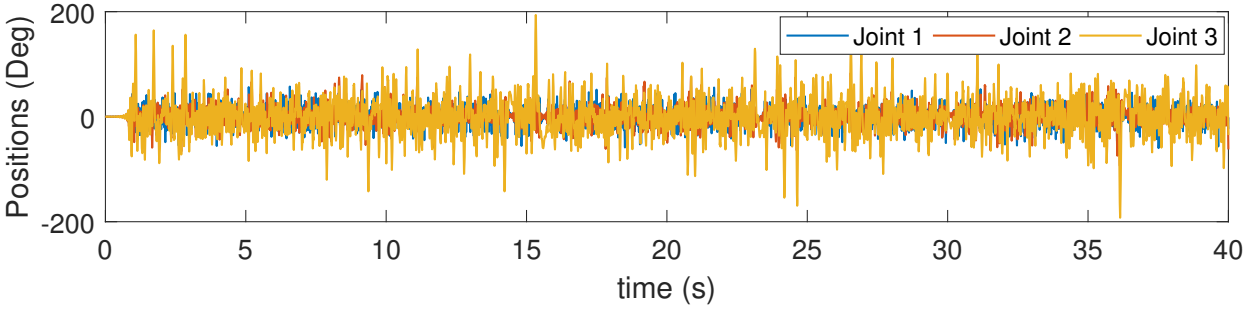

Figure 2.10: Simulation results: Positions of the joints under the PSDBF in [88] based SMC when $\varpi = 0.02$.

external disturbances, the TDE technique is employed to approximate the dynamics equation. As a result, the incremental system in the strict-feedback form is obtained. To track the reference signal, the IBS controller is first designed for the incremental system. The Lyapunov theorem is used to theoretically analyze stability of the closed-loop system. However, from the stability analysis, it is shown that the tracking error is adversely effected by the TDE error. Although the tracking performance can be improved by increasing the

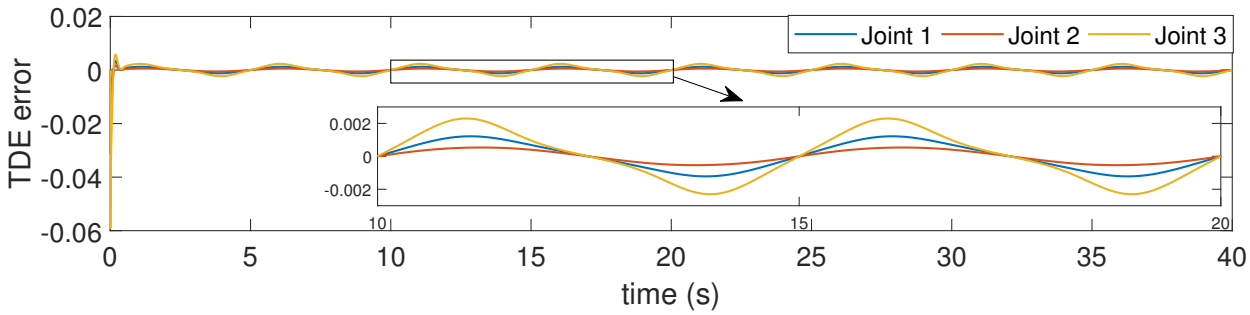

Figure 2.11: Simulation results: TDE errors under the action of the IBS controller.

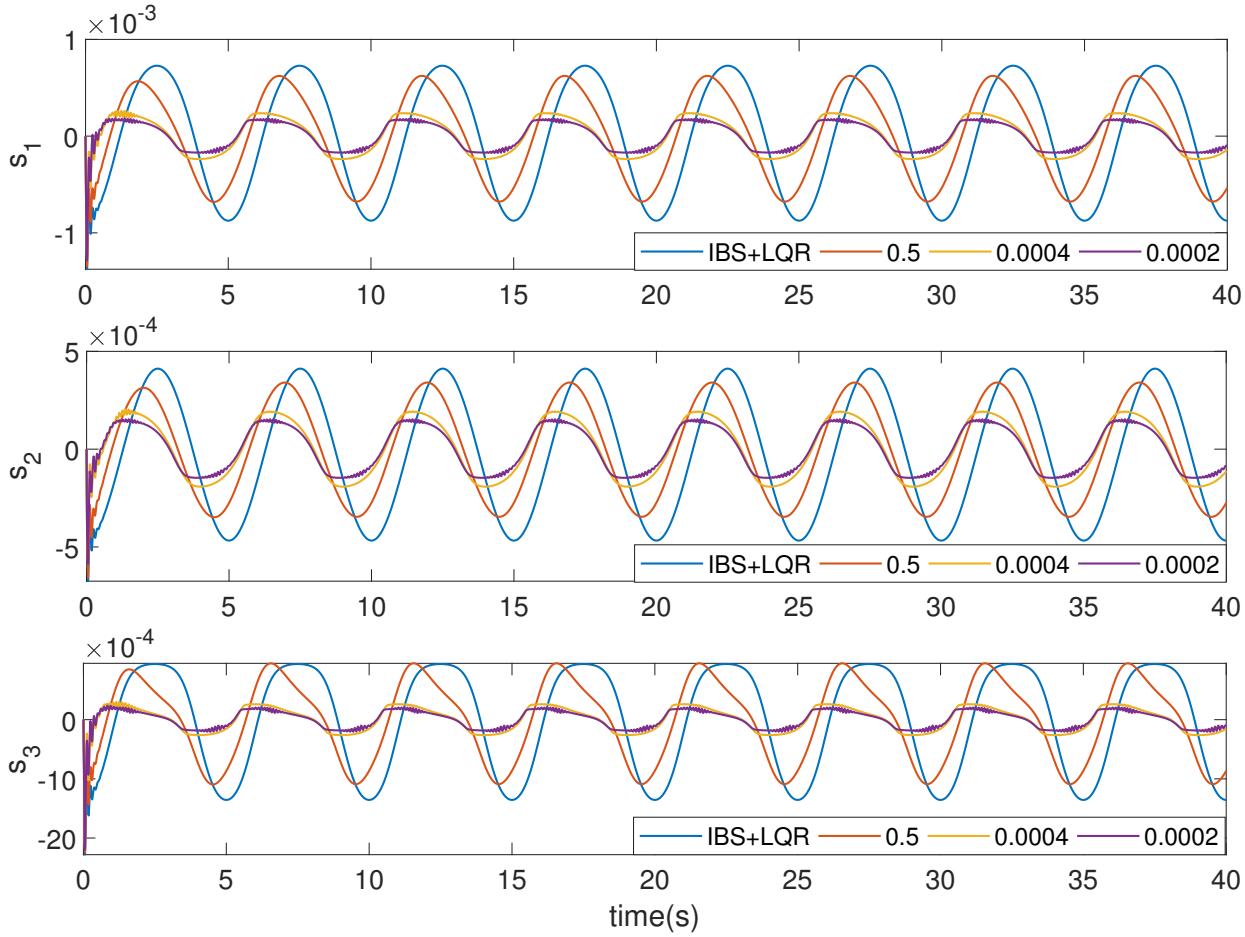

Figure 2.12: Simulation results: Sliding variables of the joints under the PSDBF based sliding mode controller when $\varpi = 0.5, 0.0004$, and 0.0002.

control gains, too large control gains may cause system oscillation. Thus, SMC is designed to address the TDE error.

After substituting IBS into the nonlinear system, the resulting system is a linear time-invariant (LTI) system w.r.t. tracking errors. An AISMC is designed for the LTI system to address the TDE error and then improve tracking performance further. The SMC is designed into an integral form since it not only attenuates the TDE error, but also regulates the tracking performance at the sliding manifold. Thus, the AISMC scheme involves the nominal

controller and the sliding mode controller. The linear LQR controller is designed as the nominal controller to guarantee the system receive optimal control performance at the sliding manifold. The sliding mode controller is designed on the basis of a novel positive semi-definite barrier function, which avoids overestimation and underestimation of the switching gains simultaneously, resulting in high tracking accuracy and slight chattering simultaneously. The finite-time convergence of the sliding variable to a vicinity around the origin is theoretically analyzed by the Lyapunov theorem.

Simulation and comparison experiments are conducted to verify the effectiveness of the proposed control scheme. There are three schemes involved. First, the developed AISMC is compared with state-of-the-art nonlinear controllers and it is proven that tracking errors of AISMC decrease without chattering of control signals. Robustness of the controller is enhanced. Then, AISMC is compared with the adaptive SMC and it is shown that switching gains of AISMC avoids underestimation and overestimation simultaneously. In addition, the performance of the system at the sliding manifold is also investigated. The system exhibits optimal performance at the sliding manifold regardless of control gains.

However, as discussed in simulation and experiments in Section 2.4, input and state constraints, which either affect tracking performance of the control system or can be be described as safety requirements, are not considered in this chapter. To make the controller more practical, the robust controller while satisfying input and state constraints will be studied in the following chapters.

Incremental Model Predictive Control (IMPC)

3

In Chapter 2, robustness of the controller is enhanced by developing one TDE-based controller. Nevertheless, optimality of controllers and accounting for input and state constraints were not yet thoroughly addressed together, while constraints can be used to describe safety requirements on control and thus enable robot manipulators to also be used in safety critical applications, e.g., close to or in cooperation with humans. To fill in this gap, in this chapter, we will design a robust and optimal controller while satisfying input and state constraints.

3.1 Overview

In this chapter, an incremental model predictive controller is developed exploiting TDE, without the concrete mathematical model. Considering the TDE error as the disturbance, practical stability of IMPC is analyzed. Finally, effectiveness of the controller is validated by experimental results.

3.1.1 Related Work

Nonlinear control approaches, such as computed torque [101] or backstepping [73], are able to deliver high-performance controllers for robot manipulators. However, a precise model is needed and performance is deteriorated in the presence of model uncertainties and disturbances. To address the robustness issue, disturbance observers [102], SMC [15], [103], and adaptive control methods [74] are employed and often combined with computed torque or backstepping. Nevertheless, the nominal model of the robot manipulator and its parameters still need to be identified. To alleviate the need of the concrete mathematical modeling and parameter identification, intelligent control techniques, such as fuzzy logic systems [104] and neural networks (NNs) [105], are proposed to approximate unknown/uncertain system dynamics. Yet, these approaches also pay more attention to robustness, not to optimal tracking performance. In addition, input and state constraints are usually not of interest.

Model predictive control (MPC) [42], or receding horizon control[106], is an optimization-based control addressing optimal tracking control performance and input and state constraints such as saturation of control inputs and physical limits of workspace and speed. The distinct feature of MPC lies in its capability of systematically handling input and state constraints within the controller design. For MPC, the constrained optimal control problem is solved using the state predictions generated by the nominal mathematical model in a horizon [107]–[111], where the difference between the nominal and real mathematical models due to uncertainties and disturbances may degrade tracking performance [112]. Besides, when some dynamics terms are unknown, MPC algorithms in [107]–[112] are not able to be implemented.

A robust MPC was proposed for a helicopter in [113] where an extended high-gain observer estimates model uncertainties and disturbances. However, the nominal mathematical model is required. Learning-based MPC methods are proposed [114]–[116] to deal with uncertain/unknown system dynamics, where Gaussian process (GP) and NNs are used to identify nonlinear models online which can reduce dependence on the concrete mathematical model. A data-driven model predictive control was developed in [117], where a non-parametric machine learning technique is used to estimate a prediction model. Unfortunately, learning and data-driven techniques further increase the computational complexity of MPC, and selection of parameters is empirical. Other robust MPC schemes including min-max optimization [118], [119] and sliding mode techniques [120], [121] are also employed to improve robustness without significant increase of complexities. Alternatively, MPC is formulated with an incremental model which generates the state predictions by using both present and previous states[122]. However, since the incremental system is obtained from linearization of the nonlinear system, the concrete mathematical model is required and the controller is only effective locally around equilibrium points.

Model uncertainties and disturbances not only increase the computational complexity of MPC, but they also make stability analysis more challenging. Due to uncertainties and/or disturbances, the Lyapunov stability that was established for the nominal system is not simply transferable [110], [111], and input-to-state stability (ISS), also known as practical Lyapunov stability, is required to be considered. In [123], [124], ISS of MPC with terminal ingredients was analyzed where a feasible control sequence, which guarantees that input and state constraints are not violated, was employed. However, the derived *cumulative error bound* increases with increasing the prediction horizon. It results in an over-conservative *cumulative error bound*, which conveys that the tracking error increases for increasing the prediction horizon. However, in practice, increasing prediction horizon appropriately will decrease tracking errors [125]. Thus, the derived over-conservative *cumulative error bound* provides a wrong guidance to improve tracking accuracy.

For MPC without terminal ingredients, the ISS property was investigated in [126], where time-variant sets of admissible predicted states are used. In [127], [128], for linear systems, the continuity property of the value function was applied to estimate *cumulative error bounds* and then verify ISS. Feasible control sequences were not required and time-invariant input and state constraints could be used. Unfortunately, if the eigenvalue of the system matrix (also known as coefficient matrix) is greater than one, it still results in the rise of the *cumulative error bound* with increasing the prediction horizon.

3.1.2 Method and Contributions

In this chapter, an incremental model predictive control (IMPC) method is developed for a robot manipulator modelled by Euler-Lagrange equations. To obtain optimal performance in the presence of input and state constraints as well as the robustness against uncertainties and disturbances, we first design a robust incremental model in the global set of admissible states exploiting the time-delay estimation (TDE) technique[28], [36]. TDE is a model-free method, which uses time-delayed input and output signals to estimate partial dynamics of the system without concrete mathematical model, laborious parameter identification, and linearization around equilibrium points of the system[29], [32], [33]. Then, a MPC problem is formulated, where the state predictions are generated from the discretized incremental

control system derived by TDE.

In particular, a reachable reference trajectory is defined, for which ISS of the proposed IMPC is analyzed. Using continuity of the value function, ISS is verified and over-conservative *cumulative error bound* is avoided. ISS is shown for all horizon lengths that are larger than a specific threshold derived recursively. The contributions are summarized as follows:

1) *No concrete mathematical model required.* Different from existing MPC methods, the concrete mathematical model of the robot manipulator is not required. This is because the continuous-time nonlinear system model is approximated by an incremental system using TDE, and the state predictions are generated using the linear discretized incremental system.

2) *Optimal performance for TDE based control.* The TDE based incremental controller is developed in the framework of MPC without terminal ingredients, and input and state constraints are formulated as inequality constraints. Thus, optimal control performance is achieved while input and state constraints are taken into account, which has not been considered in existing TDE-based controllers[28], [29], [32], [33], [36].

3) *No over-conservative cumulative error bound.* Considering the bounded error sourced from TDE as the major disturbance, local ISS of IMPC is confirmed. Different from existing ISS analyses for MPC, here continuity of the value function is used to derive the upper bound of the difference between two value functions, and the resulting *cumulative error bound is not over-conservative*. It is theoretically inferred from this ISS and the *cumulative error bound* that increasing the prediction horizon enlarges the region of attraction, and at the same time decreases tracking errors.

3.1.3 Outline of this Chapter

The rest of this chapter is organized as follows: Section 3.2 presents the proposed IMPC. The local ISS property of IMPC is theoretically analyzed in Section 3.3. A series of real-time experiments is performed on a robot manipulator and effectiveness of the proposed IMPC is verified in Section 3.4 followed by a short summary in Section 3.5.

3.2 Reference Tracking IMPC

In this section, the control objective is first introduced, which is a prerequisite to formulate the MPC problem. Then, discretizing the incremental system derived by TDE, an approximated discrete-time linear system is obtained. Based on the approximated discrete-time linear system, the reference tracking IMPC is developed through formulating a constrained optimal control problem.

3.2.1 Control Objective

The control objective is to make the robot manipulator track the given reference signal $\mathbf{x}_{\text{ref}}$ and impose the following point-wise constraints on state and input:

$$(\mathbf{x}, \mathbf{u}) \in \mathbb{Z} = \mathbb{X} \times \mathbb{U}, \tag{3.1}$$

where $\mathbb{X}$, $\mathbb{U}$, and $\mathbb{Z}$ are all compact sets containing the origin in their interior.

Constraints are imposed on state and input in (3.1), i.e., $\mathbf{x} \in \mathbb{X}$, and $\mathbf{u} \in \mathbb{U}$. In the context of the robot manipulator, the joint position, velocity, and torque are constrained by $|q_i| \leq q_{i,\max},\ |\dot{q}_i| \leq \dot{q}_{i,\max},\ |\tau_i| \leq \tau_{i,\max}$ with $q_{i,\max}, \dot{q}_{i,\max}, \tau_{i,\max} \in \mathbb{R}_{>0}$ being specified limits.

In this dissertation, only smooth reference trajectories $\mathbf{x}_{\text{ref}}$ are considered, since non-smooth reference trajectories can cause damage to mechanical systems due to sharp actuator changes. Without loss of generality, reference trajectories are assumed to be smooth and bounded (See Assumption 1).

Note that according to the definition in (A.2), the reference signal $\mathbf{x}_{\text{ref}} := (\mathbf{x}_{1,\text{ref}}, \mathbf{x}_{2,\text{ref}}) := (\mathbf{q}_{\text{ref}}, \dot{\mathbf{q}}_{\text{ref}})$.

3.2.2 Formulation of the Proposed IMPC

In this subsection, the IMPC is developed. Firstly, a discrete-time linear system is obtained by discretizing the incremental system (A.7) derived by TDE. Then, the stage cost function will be defined. Finally, IMPC is developed by formulating a constrained optimal control problem (OCP).

Discrete-Time Linear System

Discretizing the incremental system (A.7) using the following Euler numerical differentiation

$$\dot{\mathbf{x}}_*(k) = \frac{\mathbf{x}_*(k+1) - \mathbf{x}_*(k)}{T_s} + \boldsymbol{\omega}_*(k),$$

where $\boldsymbol{\omega}_*(k)$ is the dicretization error. Replacing $\dot{\mathbf{x}}_1$, $\dot{\mathbf{x}}_2$, and $\dot{\mathbf{x}}_{2,0}$ by $\dot{\mathbf{x}}_1(k)$, $\dot{\mathbf{x}}_2(k)$, and $\dot{\mathbf{x}}_2(k-1)$ respectively, (A.7) is transformed into the discrete-time form:

$$\begin{aligned}\mathbf{x}_1(k+1) &= \mathbf{x}_1(k) + T_s\mathbf{x}_2(k) - T_s\boldsymbol{\omega}_1(k)\\ \mathbf{x}_2(k+1) &= 2\mathbf{x}_2(k) - \mathbf{x}_2(k-1) + \bar{\mathbf{g}}T_s(\Delta\mathbf{u}(k) + \boldsymbol{\epsilon}') + T_s\bar{\boldsymbol{\omega}}_2(k),\end{aligned} \tag{3.2}$$

where $\boldsymbol{\epsilon} = \bar{\mathbf{g}}\boldsymbol{\epsilon}'$, $\bar{\boldsymbol{\omega}}_2(k) := \boldsymbol{\omega}_2(k-1) - \boldsymbol{\omega}_2(k)$, and T_s is the sampling period. Note that it is reasonable to assume that discretization errors are bounded, and the smaller T_s, the smaller are discretization errors.

Let $\mathbf{x}(k) := \text{col}\,(\mathbf{x}_1(k), \mathbf{x}_2(k))$, then (3.2) is rewritten as

$$\mathbf{x}(k+1) = \mathbf{A}_1\mathbf{x}(k) + \mathbf{A}_2\mathbf{x}(k-1) + \mathbf{B}_1\Delta\mathbf{u}(k) + \bar{\boldsymbol{\epsilon}}_1 \tag{3.3}$$

with $\mathbf{A}_1 := \begin{bmatrix}\mathbf{I} & T_s\mathbf{I}\\ \mathbf{O} & 2\mathbf{I}\end{bmatrix}$, $\mathbf{A}_2 := \begin{bmatrix}\mathbf{O} & \mathbf{O}\\ \mathbf{O} & -\mathbf{I}\end{bmatrix}$, $\mathbf{B}_1 := \begin{bmatrix}\mathbf{O}\\ \bar{\mathbf{g}}T_s\end{bmatrix}$, and $\bar{\boldsymbol{\epsilon}}_1 := \begin{bmatrix}-T_s\boldsymbol{\omega}_1(k)\\ \bar{\mathbf{g}}T_s\boldsymbol{\epsilon}' + T_s\bar{\boldsymbol{\omega}}_2(k)\end{bmatrix}$.

Let $\mathbf{X}(k) := \text{col}\,(\mathbf{x}(k), \mathbf{x}(k-1))$, equation (3.3) is then rewritten as a first-order discrete-time system with disturbance $\bar{\boldsymbol{\epsilon}}_2$ given by

$$\mathbf{X}(k+1) = \mathbf{A}\mathbf{X}(k) + \mathbf{B}\Delta\mathbf{u}(k) + \bar{\boldsymbol{\epsilon}}_2 \tag{3.4}$$

with $\mathbf{A} := \begin{bmatrix}\mathbf{A}_1 & \mathbf{A}_2\\ \mathbf{I} & \mathbf{O}\end{bmatrix}$, $\mathbf{B} := \begin{bmatrix}\mathbf{B}_1\\ \mathbf{O}\end{bmatrix}$, and $\bar{\boldsymbol{\epsilon}}_2 := \begin{bmatrix}\bar{\boldsymbol{\epsilon}}_1\\ \mathbf{O}\end{bmatrix}$.

For $\bar{\boldsymbol{\epsilon}}_2 = 0$, we obtain the nominal system of (3.4), a discrete-time linear system:

$$\mathbf{X}(k+1) = \mathbf{A}\mathbf{X}(k) + \mathbf{B}\Delta\mathbf{u}(k). \tag{3.5}$$

Note that the linear system $(\mathbf{A}, \mathbf{B})$ is controllable. Different from conventional linearization methods, such as Taylor series [122], [129] and Carleman approaches [130], the linear system (3.5) is obtained without concrete mathematical model. Besides, it is effective in the whole set $\mathbb{D}_{\mathbf{x}}$, not only locally around equilibrium points.

Stage Cost Function

The stage cost function will be defined in the following. Besides $\mathbf{x}_{\text{ref}}$, the reference control signal $\mathbf{u}_{\text{ref}}$ is required to define a reference tracking stage cost function. For nonlinear MPC [131], [132], $\mathbf{u}_{\text{ref}}$ is usually calculated from the nominal model. Since it is assumed that prior knowledge of the nominal model is not available (see Section A.1), the discrete-time linear approximation (3.5) is used to calculate an approximated incremental reference control signal $\Delta\hat{\mathbf{u}}_{\text{ref}}(k)$:

$$\Delta\hat{\mathbf{u}}_{\text{ref}}(k) = \mathbf{B}^{\dagger}\left(\mathbf{X}_{\text{ref}}(k+1) - \mathbf{A}\mathbf{X}_{\text{ref}}(k)\right) \tag{3.6}$$

with $\mathbf{B}^{\dagger} := (\mathbf{B}^{\top}\mathbf{B})^{-1}\mathbf{B}^{\top}$, $\mathbf{X}_{\text{ref}}(k) := \text{col}(\mathbf{x}_{\text{ref}}(k), \mathbf{x}_{\text{ref}}(k-1))$.

Constrained OCP

Consider the full reference trajectory of the manipulator is predefined. The reference trajectories over a finite horizon after time instance k are thus priorly known, and the tracking stage cost function is defined as follows:

$$\ell(\mathbf{X}_{k+i|k}, \Delta\mathbf{u}_{k+i|k}, k+i) = \left\|\mathbf{X}_{k+i|k} - \mathbf{X}_{\text{ref}}(k+i)\right\|_{\mathbf{Q}}^2 + \left\|\Delta\mathbf{u}_{k+i|k} - \Delta\hat{\mathbf{u}}_{\text{ref}}(k+i)\right\|_{\mathbf{R}}^2, \tag{3.7}$$

where $\mathbf{Q} \succ 0$ and $\mathbf{R} \succ 0$ are weighting matrices and $\bullet_{k+i|k}$ denotes predictions of states and control inputs, in particular, $\mathbf{X}_{k|k} = \mathbf{X}(k)$, and $\mathbf{X}_{k+i|k}$ is calculated using (3.5), i.e.,

$$\mathbf{X}_{k+i|k} = \mathbf{A}\mathbf{X}_{k+i-1|k} + \mathbf{B}\Delta\mathbf{u}_{k+i-1|k}. \tag{3.8}$$

Based on the stage cost function (3.7), the cost function $J_N(\mathbf{X}(k), \Delta\bar{\mathbf{u}}(k), k) : \mathbb{R}^{4n} \times \mathbb{R}^{n\times N} \times \mathbb{I}_{\geq 0} \to \mathbb{R}$ w.r.t. an input sequence $\Delta\bar{\mathbf{u}}(k) := [\Delta\mathbf{u}_{k|k}, \cdots, \Delta\mathbf{u}_{k+N-1|k}]$ at time k, is defined as follows:

$$J_N(\mathbf{X}(k), \Delta\bar{\mathbf{u}}(k), k) = \sum_{i=0}^{N-1} \ell(\mathbf{X}_{k+i|k}, \Delta\mathbf{u}_{k+i|k}, k+i) \tag{3.9a}$$

$$\text{s.t. } \mathbf{X}_{k+i+1|k} = \mathbf{A}\mathbf{X}_{k+i|k} + \mathbf{B}\Delta\mathbf{u}_{k+i|k} \tag{3.9b}$$

$$\mathbf{u}_{k+i+1|k} = \left(\mathbf{u}(k) + \sum_{m=0}^{i} \Delta\mathbf{u}_{k+m|k}\right) \in \mathbb{U} \tag{3.9c}$$

$$\mathbf{X}_{k+i|k} \in \bar{\mathbb{X}} \tag{3.9d}$$

where $\bar{\mathbb{X}} := \{\mathbf{X} = \text{col}(\mathbf{x}', \mathbf{x}'') \in \mathbb{R}^{4n} : \mathbf{x}' \in \mathbb{X}, \mathbf{x}'' \in \mathbb{X}\}$, $i \in \mathbb{I}_{[0,N-1]}$, and $N \in \mathbb{I}_{>0}$ is the prediction horizon.

Finally, the IMPC is developed in the framework of MPC without terminal ingredients, i.e., the reference tracking IMPC is developed through formulating the following constrained OCP:

$$V_N(\mathbf{X}(k), k) = \min_{\Delta\bar{\mathbf{u}}(k)} J_N\left(\mathbf{X}(k), \Delta\bar{\mathbf{u}}(k), k\right). \tag{3.10}$$

The solution to OCP (3.10) is an optimal state and input sequence $(\bar{\mathbf{X}}_k^*, \Delta\bar{\mathbf{u}}_k^*)$, where $\bar{\mathbf{X}}_k^* := [\mathbf{X}_{k|k}^*, \cdots, \mathbf{X}_{k+N-1|k}^*]$ and $\Delta\bar{\mathbf{u}}_k^* := [\Delta\mathbf{u}_{k|k}^*, \cdots, \Delta\mathbf{u}_{k+N-1|k}^*]$. The first column of the optimal input trajectory $\Delta\bar{\mathbf{u}}_k^*$, denoted by $\Delta\mathbf{u}^*(k)$ or $\Delta\mathbf{u}_{k|k}^*$, is applied to the system combined with the current control law $\mathbf{u}(k)$. In other words, the feedback control law at time $k+1$ is $\mathbf{u}^*(k+1) := \mathbf{u}(k) + \Delta\mathbf{u}^*(k)$.

Remark 10 (Convex Optimization Problem)**.** *For this chapter the cost function is defined in* (3.9)*, to account for the incremental control signal* $\Delta\mathbf{u}$ *and do not consider the absolute control signal* $\mathbf{u}$*. Obviously, the cost function* $J_N(\mathbf{X}(k), \Delta\bar{\mathbf{u}}(k), k)$ *is a convex function because of its quadratic form. Besides, (3.9b) is an affine system and* $\bar{\mathbb{X}}$*,* $\mathbb{U}$ *are convex sets. Therefore, OCP* (3.10) *is a convex optimization problem, and a unique optimal solution exists for non-empty admissible sets.*

Remark 11 (Nominal Model is not Required)**.** *In existing MPC without terminal ingredients, compare [110], [111], the prediction is based on a nominal model. This requires to first identify the nominal model of the plant with high precision. The proposed IMPC approach employs the incremental model based on TDE and thus it is not necessary to identify the model of* $\mathbf{f}(\mathbf{x})$ *and* $\mathbf{g}(\mathbf{x})$ *in (A.2b). Accordingly, the predictions are generated by the discrete-time linear system* (3.5)*, where only* $\bar{\mathbf{g}}$ *is associated with the system model because* $\bar{\mathbf{g}}$ *is selected such that* $\|\mathbf{I} - \mathbf{g}(\mathbf{x})\bar{\mathbf{g}}^{-1}\| < 1$*. As stated in* ***Remark 23****, the sufficient condition for* $\|\mathbf{I} - \mathbf{g}(\mathbf{x})\bar{\mathbf{g}}^{-1}\| < 1$ *can be fulfilled by a large positive* $\bar{g}_i$ *even though the exact expression of* $\mathbf{g}(\mathbf{x})$ *is unknown.*

3.3 Input-to-State Stability Analysis

In Section 3.2, the IMPC is developed without the concrete mathematical model, where the approximated discrete-time linear system (3.5) is used to generate predictions. However, the TDE error is inevitable and stability will be affected by this error. Stability will be investigated in the ISS framework and it is shown that for a large enough horizon a bounded TDE error will allow that the reference trajectory is stabilized but not asymptotically reached. In this section, a definition of the reachable reference trajectory is first given. Then, some preliminary results are introduced, such as a local upper bound of the value function, an upper bound of the TDE error, and local continuity of the value function. Finally, ISS of the proposed IMPC in local regions around reachable reference trajectories is investigated.

3.3.1 Reachable Reference Trajectory

In this subsection, a locally optimal incremental controller is developed for the discrete-time linear system (3.5), which is used to define the reachable reference trajectory.

Locally Optimal Incremental Controller

Let $\mathbf{E}(k) := \mathbf{X}(k) - \mathbf{X}_{\text{ref}}(k)$ be the tracking error. Assuming input and state constraints are not violated, a locally optimal incremental control signal $\Delta\mathbf{u}_{\text{OI}}(\mathbf{X}(k), \mathbf{X}_{\text{ref}}(k))$ is designed considering (3.9a) as the cost function:

$$\Delta\mathbf{u}_{\text{OI}}(\mathbf{X}(k), \mathbf{X}_{\text{ref}}(k)) = \Delta\hat{\mathbf{u}}_{\text{ref}}(k) + \mathbf{K}_0\mathbf{E}(k), \tag{3.11}$$

where $\mathbf{K}_0 = -(\mathbf{R}+\mathbf{B}^\top\mathbf{P}\mathbf{B})^{-1}\mathbf{B}^\top\mathbf{P}\mathbf{A}$, and $\mathbf{P} \succ 0$ is the solution to the following Riccati equation:

$$\mathbf{P} = \mathbf{A}^\top\mathbf{P}\mathbf{A} - \mathbf{A}^\top\mathbf{P}\mathbf{B}(\mathbf{R}+\mathbf{B}^\top\mathbf{P}\mathbf{B})^{-1}\mathbf{B}^\top\mathbf{P}\mathbf{A} + \mathbf{Q}.$$

To study stability of the system under the action of locally optimal incremental controller (3.11), $V(\mathbf{E}(k)) := \|\mathbf{E}(k)\|^2_{\mathbf{P}}$ is considered as the Lyapunov function. Then, the difference is

$$\begin{aligned}\Delta V(\mathbf{E}(k+1)) &= V(\mathbf{E}(k+1)) - V(\mathbf{E}(k)) \\ &= \|\mathbf{E}(k+1)\|^2_{\mathbf{P}} - \|\mathbf{E}(k)\|^2_{\mathbf{P}} \\ &= -\mathbf{E}^\top(k)\left(\mathbf{Q}+\tilde{\mathbf{R}}\right)\mathbf{E}(k) \le 0\end{aligned} \tag{3.12}$$

where $\tilde{\mathbf{R}} := \mathbf{A}^\top\mathbf{P}\mathbf{B}(\mathbf{R}+\mathbf{B}^\top\mathbf{P}\mathbf{B})^{-1}\mathbf{R}(\mathbf{R}+\mathbf{B}^\top\mathbf{P}\mathbf{B})^{-1}\mathbf{B}^\top\mathbf{P}\mathbf{A}$ and $\tilde{\mathbf{R}} \succ 0$.

Definition of Reachable Reference Trajectory

Based on the locally optimal incremental controller, the definition of the reachable reference trajectory is introduced.

Definition 1 (Reachable Reference Trajectory)**.** *A reference trajectory* $(\mathbf{X}_{\text{ref}}, \Delta\hat{\mathbf{u}}_{\text{ref}})$ *is reachable if* $\mathbf{X}_{\text{ref}}(k+i) \in \bar{\mathbb{X}}$ *and* $\left\|\mathbf{E}_{k+i|k}\right\|^2_{\mathbf{Q}} \le c$ *implies* $\mathbf{u}(k) \in \mathbb{U},\ \mathbf{X}_{k+i|k} \in \bar{\mathbb{X}}$,

$$\mathbf{u}_{\text{ref}}(k), \mathbf{u}_{\text{ref}}(k+i+1) := \mathbf{u}(k) + \sum_{m=0}^{i} \Delta\hat{\mathbf{u}}_{\text{ref}}(k+m) \in \mathbb{U}_{\text{ref}},$$

$$\mathbf{u}_{k+i+1|k} = \left(\mathbf{u}(k) + \sum_{m=0}^{i} \Delta\mathbf{u}_{\text{OI}}(\mathbf{X}_{k+m|k}, \mathbf{X}_{\text{ref}}(k+m))\right) \in \mathbb{U},$$

for $i \in \mathbb{I}_{[0,N-1]}$, $\mathbb{U}_{\text{ref}} \bigoplus \mathbb{C}_s \subseteq \mathbb{U}$ *and* $\mathbb{C}_s \subseteq \mathbb{R}^n := \{\mathbf{c} \in \mathbb{R}^n : -s1 \le \mathbf{c} \le s1\}$, *where* $c, s \in \mathbb{R}_{\ge 0}$ *are positive scalars and* $\bigoplus$ *denotes Minkowski sum. Otherwise, it is unreachable.*

Similar to the definition of the reachable reference trajectory in [111], **Definition 1** also requires that the trajectory can be tracked and lies strictly in the tightened constraint sets. However, it is not guaranteed that such a reachable reference trajectory still exists when the incremental control structure is adopted. Assuming $\bar{\mathbf{g}}$ is selected such that $\|\mathbf{I} - \mathbf{g}(\mathbf{x})\bar{\mathbf{g}}^{-1}\| \le \delta < 1$, the following **Lemma 4** is given, which verifies the reachable reference trajectory exists and provides sufficient conditions of reachable reference trajectories.

Lemma 4 (Existence of Reachable Reference Trajectories)**.** *Suppose that there exists* $c_x \in \mathbb{R}_{>0}$ *such that* $\|\mathbf{X}^i - \mathbf{X}_{\text{ref}}(k+i)\|^2_{\mathbf{Q}} \le c_x$ $(i \in \mathbb{I}_{[0,N-1]})$ *implies* $\mathbf{X}^i \in \bar{\mathbb{X}}$. *If the reference trajectory satisfies* $\mu_2\left(k_1 r_{b1} + f_{\max} r_{b2} + \omega_{2,\max} + f_0\right) < \tau_{\max}$, *and* $\left(f_{\max} r_{b2} + \bar{\bar{r}} + \omega_{2,\max} + f_0\right)/\bar{g}_{\min} < (1-\delta)\tau_{\max}$, *and* $\|\mathbf{E}(k)\|^2_{\mathbf{Q}} \le c$, *then, for* $i \in \mathbb{I}_{[0,N-1]}$, $\mathbf{u}(k) \in \mathbb{U}, \mathbf{X}_{k+i|k} \in \bar{\mathbb{X}}$,

$$\mathbf{u}_{\text{ref}}(k), \mathbf{u}_{\text{ref}}(k+i+1) := \mathbf{u}(k) + \sum_{m=0}^{i} \Delta\hat{\mathbf{u}}_{\text{ref}}(k+m) \in \mathbb{U}_{\text{ref}},$$

$$\mathbf{u}_{k+i+1|k} = \left(\mathbf{u}(k) + \sum_{m=0}^{i} \Delta\mathbf{u}_{\text{OI}}\Big(\mathbf{X}_{k+m|k}, \mathbf{X}_{\text{ref}}(k+m)\Big)\right) \in \mathbb{U},$$

and $\mathbb{U}_{\text{ref}} \bigoplus \mathbb{C}_s \subseteq \mathbb{U}$, *where* $c := \min\{c_u, \frac{c_x}{\tilde{\lambda}}\}$, $s := \min\{s_1, s_2\}$, $c_u := \min\{c_1, c_2\}$, $\tilde{\lambda} := \frac{\lambda_{\max}(\mathbf{Q})\lambda_{\max}(\mathbf{P})}{\lambda_{\min}(\mathbf{Q})\lambda_{\min}(\mathbf{P})}$, $k_1 := \|\mathbf{K}_1\|$, $\mathbf{K}_1 := \frac{1}{T_s}[\mathbf{O}, \mathbf{I}, \mathbf{O}, -\mathbf{I}]$, $r_{b1} := 2\sqrt{(\bar{r}^2 + \dot{\bar{r}}^2)}$, $r_{b2} := \sqrt{2(\bar{r}^2 + \dot{\bar{r}}^2)}$, $\omega_{2,\max} := \max_{k\in\mathbb{I}_{>0}} \|\boldsymbol{\omega}_2(k)\|$, $\tau_{\max} := \min_{i\in\mathbb{I}_{[1,n]}} \tau_{i,\max}$, *and* $\bar{g}_{\min} := \lambda_{\min}(\bar{\mathbf{g}})$.

Note that s_1, c_1, s_2 *and* c_2 *are given in* (3.21), (3.22), (3.34), *and* (3.35) *respectively.*

Proof: Through exploring the working mechanism of the locally optimal incremental controller in the horizon, it is verified that reachable reference trajectories satisfying Definition 1 exist.

First, a sufficient condition for $\mathbf{u}(k) \in \mathbb{U}$ is derived. The state $\mathbf{x}(k) := \text{col}(\mathbf{x}_1(k), \mathbf{x}_2(k))$ satisfies the following differential equation, see (A.2b).

$$\dot{\mathbf{x}}_2(k) = \mathbf{f}(\mathbf{x}(k)) + \mathbf{g}(\mathbf{x}(k))\mathbf{u}(k). \tag{3.13}$$

Discretizing $\dot{\mathbf{x}}_2(k)$ with the discretization error $\boldsymbol{\omega}_2(k)$ yields

$$\left(\mathbf{x}_{2,k|k} - \mathbf{x}_{2,k-1|k}\right)/T_s = \dot{\mathbf{x}}_2(k) + \boldsymbol{\omega}_2(k). \tag{3.14}$$

Replacing $\dot{\mathbf{x}}_2(k)$ in (3.13) by (3.14) yields

$$\mathbf{u}(k) = \mathbf{g}^{-1}(\mathbf{x}(k)) \left[\left(\mathbf{x}_{2,k|k} - \mathbf{x}_{2,k-1|k}\right)/T_s - \boldsymbol{\omega}_2(k) - \mathbf{f}\left(\mathbf{x}(k)\right)\right]. \tag{3.15}$$

According to **Property 1** and **Assumption 5**, one has

$$\|\mathbf{u}(k)\| \leq \mu_2 \left(\|\mathbf{K}_1\mathbf{X}(k)\| + \omega_{2,\max} + f_{\max}\|\mathbf{x}(k)\| + f_0\right) \tag{3.16}$$

In accordance with **Assumption 1**, it is obtained that

$$\|\mathbf{K}_1\mathbf{X}(k)\| \leq \|\mathbf{K}_1\| \left(\|\mathbf{E}(k)\| + \|\mathbf{X}_{\text{ref}}(k)\|\right) \leq k_1 \left(\|\mathbf{E}(k)\| + r_{b1}\right), \tag{3.17}$$

$$\|\mathbf{x}(k)\| \leq \|\mathbf{e}(k)\| + \|\mathbf{x}_{\text{ref}}(k)\| \leq \|\mathbf{E}(k)\| + r_{b2}. \tag{3.18}$$

Substituting (3.17) and (3.18) into (3.16) yields

$$\|\mathbf{u}(k)\| \leq \mu_2 \left((k_1 + f_{\max})\|\mathbf{E}(k)\| + k_1 r_{b1} + f_{\max} r_{b2} + \omega_{2,\max} + f_0\right). \tag{3.19}$$

In Section 3.2.1, $|\tau_i| \leq \tau_{i,\max}$ is specified. Thus, from (3.19), the following sufficient conditions are derived such that $\|\mathbf{u}(k)\| \leq \tau_{\max}$ and $\|\mathbf{u}_{\text{ref}}(k)\| \leq \tau_{\max} - s$, i.e., $\mathbf{u}(k) \in \mathbb{U}$, $\mathbf{u}_{\text{ref}}(k) \in \mathbb{U}_{\text{ref}}$, and $\mathbb{U}_{\text{ref}} \bigoplus \mathbb{C}_s \subseteq \mathbb{U}$.

$$\mu_2 \left(k_1 r_{b1} + f_{\max} r_{b2} + \omega_{2,\max} + f_0\right) < \tau_{\max} \tag{3.20}$$

$$s \leq \underbrace{\tau_{\max} - \mu_2 \left(k_1 r_{b1} + f_{\max} r_{b2} + \omega_{2,\max} + f_0\right)}_{s_1 \in \mathbb{R}_{>0}} \tag{3.21}$$

$$\|\mathbf{E}(k)\|_{\mathbf{Q}}^2 \leq \underbrace{\lambda_{\min}(\mathbf{Q}) \left(\frac{\tau_{\max} - \mu_2 \left(k_1 r_{b1} + f_{\max} r_{b2} + \omega_{2,\max} + f_0\right)}{\mu_2(k_1 + f_{\max})}\right)^2}_{c_1 \in \mathbb{R}_{>0}}. \tag{3.22}$$

Secondly, incremental control signals and predicted states in the horizon are calculated by recursion.

Introducing $\bar{\mathbf{g}}$, $\mathbf{u}(k)$ is expressed as follows using (3.13):

$$\mathbf{u}(k) = \bar{\mathbf{g}}^{-1}[\dot{\mathbf{x}}_2(k) - \mathbf{f}\left(\mathbf{x}(k)\right) - (\mathbf{g}(\mathbf{x}(k)) - \bar{\mathbf{g}})\mathbf{u}(k)]\,. \tag{3.23}$$

Replacing $\dot{\mathbf{x}}_2(k)$ in (3.23) by (3.14) yields

$$\mathbf{u}(k) = \bar{\mathbf{g}}^{-1}\left[\left(\mathbf{x}_{2,k|k} - \mathbf{x}_{2,k-1|k}\right)/T_s - \boldsymbol{\omega}_2(k) - \mathbf{f}\left(\mathbf{x}(k)\right)\right] - \bar{\mathbf{g}}^{-1}\left(\mathbf{g}(\mathbf{x}(k)) - \bar{\mathbf{g}}\right)\mathbf{u}(k). \tag{3.24}$$

Recall $\Delta\mathbf{u}_{\mathrm{OI}}(\mathbf{X}(k), \mathbf{X}_{\mathrm{ref}}(k))$ in (3.11), (3.11) is rewritten as:

$$\Delta\mathbf{u}_{\mathrm{OI}}(\mathbf{X}(k),\mathbf{X}_{\mathrm{ref}}(k)) = \bar{\mathbf{g}}^{-1}\left(\ddot{\mathbf{q}}_{\mathrm{ref}}(k+1) - \hat{\ddot{\mathbf{x}}}_2(k) + \mathbf{K}_2\mathbf{E}(k)\right), \tag{3.25}$$

where $\hat{\ddot{\mathbf{x}}}_2(k) := \left(\mathbf{x}_{2,k|k} - \mathbf{x}_{2,k-1|k}\right)/T_s$ is the approximated derivative, and $\mathbf{K}_2 := \bar{\mathbf{g}}\mathbf{K}_0 + \mathbf{K}_1$. Thus, $\mathbf{u}_{k+1|k}$ is

$$\begin{aligned}\mathbf{u}_{k+1|k} =& \mathbf{u}(k) + \Delta\mathbf{u}_{\mathrm{OI}}(\mathbf{X}(k), \mathbf{X}_{\mathrm{ref}}(k)) \\ =& \bar{\mathbf{g}}^{-1}\left[-\mathbf{f}(\mathbf{x}(k)) + \mathbf{K}_2\mathbf{E}(k) + \ddot{\mathbf{q}}_{\mathrm{ref}}(k+1) - \boldsymbol{\omega}_2(k)\right] - \bar{\mathbf{g}}^{-1}[\mathbf{g}(\mathbf{x}(k)) - \bar{\mathbf{g}}]\mathbf{u}(k).\end{aligned} \tag{3.26}$$

Applying $\Delta\mathbf{u}_{\mathrm{OI}}(\mathbf{X}(k), \mathbf{X}_{\mathrm{ref}}(k))$ to (3.5), $\dot{\mathbf{x}}_{2,k+1|k}$ is

$$\begin{aligned}(\mathbf{x}_{2,k+1|k} - \mathbf{x}_{2,k|k})/T_s =& \left(\mathbf{x}_{2,k|k} - \mathbf{x}_{2,k-1|k}\right)/T_s + \bar{\mathbf{g}}\Delta\mathbf{u}_{\mathrm{OI}}(\mathbf{X}(k), \mathbf{X}_{\mathrm{ref}}(k)) \\ \overset{(3.13),(3.14)}{=}& \mathbf{f}(\mathbf{x}(k)) + \bar{\mathbf{g}}\mathbf{u}_{k+1|k} + (\mathbf{g}(\mathbf{x}(k)) - \bar{\mathbf{g}})\mathbf{u}(k) + \boldsymbol{\omega}_2(k).\end{aligned} \tag{3.27}$$

From (3.27), $\mathbf{u}_{k+1|k}$ is expressed using $\mathbf{x}_{2,k+1|k}$ and $\mathbf{x}_{2,k|k}$:

$$\begin{aligned}\mathbf{u}_{k+1|k} =& \bar{\mathbf{g}}^{-1}\left[\left(\mathbf{x}_{2,k+1|k} - \mathbf{x}_{2,k|k}\right)/T_s - \boldsymbol{\omega}_2(k) - \mathbf{f}\left(\mathbf{x}(k)\right)\right] \\ & - \bar{\mathbf{g}}^{-1}(\mathbf{g}(\mathbf{x}(k)) - \bar{\mathbf{g}})\mathbf{u}(k).\end{aligned} \tag{3.28}$$

Similarly, at time $k+i$, the predicted control signal is

$$\begin{aligned}\mathbf{u}_{k+i|k} =& \bar{\mathbf{g}}^{-1}\left(-\mathbf{f}(\mathbf{x}(k)) + \mathbf{K}_2\mathbf{E}_{k+i-1|k} + \ddot{\mathbf{q}}_{\mathrm{ref}}(k+i) - \boldsymbol{\omega}_2(k)\right) \\ & - \bar{\mathbf{g}}^{-1}(\mathbf{g}(\mathbf{x}(k)) - \bar{\mathbf{g}})\mathbf{u}(k).\end{aligned} \tag{3.29}$$

Finally, sufficient conditions for that input and state constraints in the horizon are not violated are determined.

As assumed, $\bar{\mathbf{g}}$ is selected such that $\|\mathbf{I} - \mathbf{g}(\mathbf{x})\bar{\mathbf{g}}^{-1}\| \leq \delta < 1$. Besides, according to (3.12), the following inequalities are obtained:

$$\|\mathbf{E}_{k+i|k}\|^2 \leq \bar{\lambda}\rho^{i-1}\|\mathbf{E}(k)\|^2 \tag{3.30}$$

$$\|\mathbf{E}_{k+i|k}\|_{\mathbf{Q}}^2 \leq \tilde{\lambda}\rho^{i-1}\|\mathbf{E}(k)\|_{\mathbf{Q}}^2 \tag{3.31}$$

with $\bar{\lambda} := \frac{\lambda_{\max}(\mathbf{P})}{\lambda_{\min}(\mathbf{P})}$, and $\rho := 1 - \frac{\lambda_{\min}\left(\mathbf{Q}+\tilde{\mathbf{R}}\right)}{\lambda_{\max}(\mathbf{P})} < 1$.

In accordance with **Assumption 1**, **Assumption 5**, (3.18), (3.29), and (3.30), one has

$$\|\mathbf{u}_{k+i|k}\| \leq \frac{\left(f_{\max}+k_{\max}\sqrt{\bar{\lambda}}\right)\|\mathbf{E}(k)\|+f_{\max}r_{b2}+\bar{\bar{r}}+\omega_{2,\max}+f_0}{\bar{g}_{\min}}+\delta\tau_{\max}, \tag{3.32}$$

where $k_{\max}:=\|\mathbf{K}_2\|$. According to (3.32), a sufficient condition for $\mathbf{u}_{k+i|k}\in\mathbb{U}$ and $\mathbf{u}_{\mathrm{ref}}(k+i)\in\mathbb{U}_{\mathrm{ref}}$ is obtained:

$$\left(f_{\max}r_{b2}+\bar{\bar{r}}+\omega_{2,\max}+f_0\right)/\bar{g}_{\min}<(1-\delta)\tau_{\max} \tag{3.33}$$

$$s\leq\underbrace{\tau_{\max}-\left(f_{\max}r_{b2}+\bar{\bar{r}}+\omega_{2,\max}+f_0\right)/(\bar{g}_{\min}(1-\delta))}_{s_2\in\mathbb{R}_{>0}} \tag{3.34}$$

$$\|\mathbf{E}(k)\|_{\mathbf{Q}}^2\leq\underbrace{\lambda_{\min}(\mathbf{Q})\left(\frac{(1-\delta)\bar{g}_{\min}\tau_{\max}-f_{\max}r_b-\bar{\bar{r}}-\omega_{2,\max}-f_0}{f_{\max}+k_{\max}\sqrt{\bar{\lambda}}}\right)^2}_{c_2\in\mathbb{R}_{>0}}. \tag{3.35}$$

From (3.20), (3.22), (3.33), and (3.35), it is concluded that, if the reference trajectory satisfies (3.20) and (3.33), and $\|\mathbf{E}(k)\|_{\mathbf{Q}}^2\leq c_u$, then $\forall i\in\mathbb{I}_{[0,N]}$, $\mathbf{u}_{k+i|k}\in\mathbb{U}$ and $\mathbf{u}_{\mathrm{ref}}(k+i)\in\mathbb{U}_{\mathrm{ref}}$.

Besides, if $\|\mathbf{E}(k)\|_{\mathbf{Q}}^2\leq\frac{c_x}{\bar{\lambda}}$, according to (3.31), then $\|\mathbf{E}_{k+i|k}\|_{\mathbf{Q}}^2\leq c_x,\forall i\in\mathbb{I}_{[0,N-1]}$, that is, $\mathbf{X}_{k+i|k}\in\bar{\mathbb{X}}$.

Therefore, if the reference trajectory satisfies (3.20) and (3.33), $\|\mathbf{E}(k)\|_{\mathbf{Q}}^2\leq c$ guarantees local controllability of (3.5).

■

Note that **Lemma 4** is introduced to show existence of the reachable reference trajectory. Zooming techniques are used to derive the sufficient conditions of the reachable reference trajectory and it results in conservative results. In other words, even though the sufficient conditions are not satisfied, often some reference trajectories are nevertheless reachable. Moreover, the sufficient conditions in **Lemma 4** are not related to the prediction horizon N. Hence, if the assumption ($\exists c_x\in\mathbb{R}_{>0}$ such that $\|\mathbf{X}^i-\mathbf{X}_{\mathrm{ref}}(k+i)\|\leq c_x$ implies $\mathbf{X}^i\in\bar{\mathbb{X}}$) holds regardless of N, then **Lemma 4** still holds when a large N is selected. In addition, it is not required to determine or construct reachable reference trajectories when the IMPC is implemented in practice. No matter for reachable or unreachable reference trajectory, the controller is obtained through solving the constrained OCP (3.10). The introduction of the reachable reference trajectory is merely a basis for local ISS analysis.

3.3.2 Preliminary Results

In this subsection, some preliminary results to analyze ISS of IMPC are developed. Considering the locally optimal incremental controller (3.11) as the auxiliary control law, a local upper bound of the value function $V_N(\mathbf{X}(k),k)$ is derived for a reachable reference trajectory. Then, an upper bound of the TDE error is determined. At last, the continuity of $V_N(\mathbf{X}(k),k)$ is shown, which is used to avoid an over-conservative *cumulative error bound* during ISS analysis.

Local Upper Bound of Value Function

Considering a reachable reference trajectory, a local upper bound of $V_N(\mathbf{X}(k),k)$ is determined in **Lemma 5**.

Lemma 5 (Local Upper Bound of Value Function)**.** *For a small enough tracking error* $\|\mathbf{E}(k)\|_{\mathbf{Q}}^2 \leq c$*, there exists* $\kappa \in \mathbb{R}_{>0}$ *such that* $V_N(\mathbf{X}(k),k)$ *is bounded by*

$$V_N(\mathbf{X}(k),k) \leq \kappa \|\mathbf{E}(k)\|_{\mathbf{Q}}^2. \tag{3.36}$$

Proof: Given a reachable reference trajectory, a small enough tracking error $\|\mathbf{E}(k)\|_{\mathbf{Q}}^2 \leq c$ will allow to apply the locally optimal incremental controller (3.11) without violation of input or state constraints. Besides, due to optimality principle, $V_N(\mathbf{X}(k),k) \leq J_N(\mathbf{X}(k),\bar{\mathbf{u}}(k),k)$. Thus, if it is shown that the cost function $J_N(\mathbf{X}(k),\bar{\mathbf{u}}(k),k)$ is bounded under the function of the locally optimal incremental controller, then boundedness of the value function $V_N(\mathbf{X}(k),k)$ is also found.

For the locally optimal incremental controller (3.11), upper bounds for the tracking errors are obtained (cf. (3.31) in **Lemma 4**), and for the control signals in the prediction horizon

$$\begin{aligned}\left\|\tilde{\Delta}\mathbf{u}_{k+i|k}\right\|_{\mathbf{R}}^2 &= \left\|\Delta\mathbf{u}_{\mathrm{OI}}(\mathbf{X}_{k+i|k},\mathbf{X}_{\mathrm{ref}}(k+i)) - \Delta\mathbf{u}_{\mathrm{ref}}(k+i)\right\|_{\mathbf{R}}^2 \\ &\leq K_{\max}\left\|\mathbf{E}_{k+i|k}\right\|_{\mathbf{Q}}^2,\end{aligned} \tag{3.37}$$

where $i \in \mathbb{I}_{[0,N-1]}$, $K_{\max} := \frac{\lambda_{\max}(\mathbf{R})\|\mathbf{K}_0\|_{\mathbf{R}}^2}{\lambda_{\min}(\mathbf{Q})}$.

Thus, one has

$$\begin{aligned}V_N(\mathbf{X}(k),k) &\leq J_N(\mathbf{X}(k),\Delta\bar{\mathbf{u}}(k),k) \\ &= \sum_{i=0}^{N-1}\left(\|\mathbf{E}_{k+i|k}\|_{\mathbf{Q}}^2 + \|\tilde{\Delta}\mathbf{u}_{k+i|k}\|_{\mathbf{R}}^2\right) \\ &\overset{0<\rho<1}{\leq} \kappa\|\mathbf{E}(k)\|_{\mathbf{Q}}^2,\end{aligned} \tag{3.38}$$

where $\kappa := \frac{(1+K_{\max})\lambda_{\max}(\mathbf{Q})\lambda_{\max}(\mathbf{P})}{(1-\rho)\lambda_{\min}(\mathbf{Q})\lambda_{\min}(\mathbf{P})}$.

■

Upper Bound of TDE Error

In the sequel, an upper bound for the difference between state predictions using the approximated nominal dynamics (3.5) and the real state trajectory that results from (3.4) is quantified. To determine this upper bound, an upper bound of TDE error is firstly determined.

In[7], [28], [29], [32], [33], [36], [133], the TDE error is verified to be bounded if a TDE-based controller is employed. However, in our approach the incremental controller $\Delta\mathbf{u}(k)$ is obtained by solving the constrained OCP (3.10), and an analytic expression for $\Delta\mathbf{u}(k)$ is not available. In the following **Lemma 6**, local continuity of uncertain functions and the input constraint will be used to analyze boundedness of the TDE error.

Lemma 6 (Bounded TDE Error)**.** *There exists* $\epsilon^* \in \mathbb{R}_{>0}$ *such that* $\|\boldsymbol{\epsilon}'\| \leq \epsilon^*$ *for a sufficiently small sampling period.*

Proof: According to (A.4) and (A.5), $\boldsymbol{\epsilon}'$ is rewritten as

$$\begin{aligned}\boldsymbol{\epsilon}' = &\left(\bar{\mathbf{g}}^{-1} - \mathbf{g}^{-1}(\mathbf{x})\right)(\dot{\mathbf{x}}_2 - \dot{\mathbf{x}}_{2,0}) + \left(\mathbf{g}^{-1}(\mathbf{x}_0) - \mathbf{g}^{-1}(\mathbf{x})\right)\dot{\mathbf{x}}_{2,0} \\ &+ \mathbf{g}^{-1}(\mathbf{x})\mathbf{f}(\mathbf{x}) - \mathbf{g}^{-1}(\mathbf{x}_0)\mathbf{f}(\mathbf{x}_0).\end{aligned} \tag{3.39}$$

Since $\dot{\mathbf{x}}_2 = \mathbf{f}(\mathbf{x}) + \mathbf{g}(\mathbf{x})\mathbf{u}$, one has

$$\dot{\mathbf{x}}_2 - \dot{\mathbf{x}}_{2,0} = \mathbf{f}(\mathbf{x}) - \mathbf{f}(\mathbf{x}_0) + \mathbf{g}(\mathbf{x})\Delta\mathbf{u} + (\mathbf{g}(\mathbf{x}) - \mathbf{g}(\mathbf{x}_0))\,\mathbf{u}_0. \tag{3.40}$$

Substituting (3.40) into (3.39) yields

$$\boldsymbol{\epsilon}' = \left(\bar{\mathbf{g}}^{-1}\mathbf{g}(\mathbf{x}) - \mathbf{I}\right)\Delta\mathbf{u} + \left(\bar{\mathbf{g}}^{-1}\mathbf{g}(\mathbf{x}) - \mathbf{I}\right)\mathbf{g}^{-1}(\mathbf{x})\mathbf{r}_1 + \mathbf{r}_2 \tag{3.41}$$

with $\mathbf{r}_1 := \mathbf{f}(\mathbf{x}) - \mathbf{f}(\mathbf{x}_0) + (\mathbf{g}(\mathbf{x}) - \mathbf{g}(\mathbf{x}_0))\,\mathbf{u}_0$, $\mathbf{r}_2 := (\mathbf{g}^{-1}(\mathbf{x}_0) - \mathbf{g}^{-1}(\mathbf{x}))\,\dot{\mathbf{x}}_{2,0} + \mathbf{g}^{-1}(\mathbf{x})\mathbf{f}(\mathbf{x}) - \mathbf{g}^{-1}(\mathbf{x}_0)\mathbf{f}(\mathbf{x}_0)$.

For a sufficiently small sampling period, $\mathbf{r}_1$ and $\mathbf{r}_2$ are all bounded, i.e., there exist r_1, $r_2 \in \mathbb{R}_{>0}$ such that $\|\mathbf{r}_1\| \leq r_1$ and $\|\mathbf{r}_2\| \leq r_2$ [7].

According to **Property 1** and the fact that $\mathbf{g}^{-1}(\mathbf{x}) = \mathbf{M}(\mathbf{q})$, one obtains $\|\mathbf{g}^{-1}(\mathbf{x})\| \leq \mu_2$. Moreover, as stated in Section 2.2.2, $\bar{\mathbf{g}}$ is selected such that $\|\mathbf{I} - \mathbf{g}(\mathbf{x})\bar{\mathbf{g}}^{-1}\| \leq \delta < 1$. Thus,

$$\begin{aligned}\|\boldsymbol{\epsilon}\| \leq &\|\left(\bar{\mathbf{g}}^{-1}\mathbf{g}(\mathbf{x}) - \mathbf{I}\right)\|\|\Delta\mathbf{u}\| + \|\left(\bar{\mathbf{g}}^{-1}\mathbf{g}(\mathbf{x}) - \mathbf{I}\right)\|\|\mathbf{g}^{-1}(\mathbf{x})\|\|\mathbf{r}_1\| + \|\mathbf{r}_2\| \\ \leq &\delta\|\Delta\mathbf{u}\| + \delta\mu_2 r_1 + r_2.\end{aligned} \tag{3.42}$$

For IMPC, $\Delta\mathbf{u}$ is obtained solving the constrained OCP (3.10) such that $\mathbf{u} \in \mathbb{U}$. As stated in Section 3.2.1, $\|\mathbf{u}\| \leq u_{\max}$. Thus, $\Delta u_{\max} := \max\|\Delta\mathbf{u}\| = \max\|\mathbf{u} - \mathbf{u}_0\| \leq 2u_{\max}$. Therefore, the TDE error is bounded by

$$\|\boldsymbol{\epsilon}'\| \leq 2\delta u_{\max} + \delta\mu_2 r_1 + r_2 := \epsilon^*. \tag{3.43}$$

■

Remark 12 (Supplementary Notes to **Lemma 6**). *Note that ϵ^* derived in **Lemma 6** is over-estimated. $\mathbf{H}(\mathbf{x}, \dot{\mathbf{x}})_{t-L}$ is used to approximate $\mathbf{H}(\mathbf{x}, \dot{\mathbf{x}})$ and L is usually selected as the sampling period. In practice, a digital control system can be regarded as a continuous system when the sampling rate is faster than 30 times the system bandwidth [134]. Thus, the smaller the sampling period, the smaller is the TDE error. In other words, for any choice of $\bar{\epsilon}^*$, a sufficiently small sampling period can be chosen such that $\|\boldsymbol{\epsilon}'\| \leq \bar{\epsilon}^*$.*

Thus using (3.4), (3.5), and **Lemma 6**, one obtains that

$$\|\mathbf{X}(k+1) - \mathbf{X}^*_{k+1|k}\| \leq \|\bar{\boldsymbol{\epsilon}}_2\| \leq \bar{\epsilon}^* \tag{3.44}$$

with $\bar{\epsilon}^* := \sqrt{2\left(\omega_{1,\max}^2 + (\bar{g}_{\max}\epsilon^* + 2\omega_{2,\max})^2\right)}T_s$ and $\omega_{1,\max} := \max_{k\in\mathbb{I}_{\geq 0}}\|\boldsymbol{\omega}_1(k)\|$.

Continuity of Value Function

In the following, continuity property of the value function will be verified, based on local controllability of the system (3.5). At first, a set $\mathbb{D}$ ($\mathbb{D} \subseteq \bar{\mathbb{X}}$) will be introduced in **Lemma 7**, to show if $\mathbf{X} \in \mathbb{D}$, then the optimal solutions lie strictly in the tightened constraint sets.

Lemma 7 (Tightened Constraint Sets)**.** *There exist constants $V_{\max}$, $\tilde{s}$, $\tilde{r}_1 \in \mathbb{R}_{>0}$ such that optimal solutions starting from $\mathbf{X}$ ($\mathbf{X} \in \mathbb{D}$, $\mathbb{D} := \{\mathbf{X} \in \bar{\mathbb{X}} : V_N(\mathbf{X}, k) \leq V_{\max}\}$) satisfy tightened constraints, i.e., $\mathbf{X}^*_{k+i|k} \in \bar{\mathbb{X}}'$ and $\mathbf{u}^*_{k+i|k} \in \mathbb{U}'$ for all $i \in \mathbb{I}_{[0,N-1]}$, where $\bar{\mathbb{X}}' \bigoplus \mathbb{B}_{\tilde{r}_1} \subseteq \bar{\mathbb{X}}$ and $\mathbb{U}' \bigoplus \mathbb{C}_{\tilde{s}} \subseteq \mathbb{U}$.*

Proof: First, it is verified that the reachable reference trajectory lies in the tightened constraint sets. According to the definition of the reachable reference trajectory (Definition 1), $\|\mathbf{E}_{k+i|k}\|^2_{\mathbf{Q}} \leq c$ implies $\mathbf{X}_{k+i|k} \in \bar{\mathbb{X}}$ for all $i \in \mathbb{I}_{[0,N-1]}$. Thus, $\mathbf{X}_{\text{ref}}(k+i) \in \mathbb{X}_{\text{ref}}$ and $\mathbb{X}_{\text{ref}} \bigoplus \mathbb{B}_{\tilde{r}} \subseteq \bar{\mathbb{X}}$, where $\mathbb{B}_{\tilde{r}} \subseteq \mathbb{R}^{4n} := \{\mathbf{b} \in \mathbb{R}^{4n} : \|\mathbf{b}\| \leq \tilde{r}\}$ denotes a unitary ball with the radius $\tilde{r}$, and $\tilde{r} = \sqrt{\frac{c}{\lambda_{\max}(\mathbf{Q})}}$. Besides, $\mathbf{u}_{\text{ref}}(k+i) \in \mathbb{U}_{\text{ref}}$ and $\mathbb{U}_{\text{ref}} \bigoplus \mathbb{C}_s \subseteq \mathbb{U}$. Thus, the reachable reference trajectory lies strictly in the tightened constraint sets.

Then, the possibility that optimal solutions $\mathbf{X}^*_{k+i|k}$ and $\mathbf{u}^*_{k+i|k}$ also lie strictly in the tightened constraint sets is demonstrated using an extreme value. When $\|\mathbf{E}(k)\|^2_{\mathbf{Q}} \leq \xi$ ($\xi \leq c$), the system is controllable. If ξ is sufficiently small, then the optimal solutions $\mathbf{X}^*_{k+i|k}$ and $\mathbf{u}^*_{k+i|k}$ converge and get close to the reference trajectory. Thus, it is reasonable to assume that when $\|\mathbf{E}(k)\|^2_{\mathbf{Q}} \leq \xi$, $\mathbf{X}^*_{k+i|k}$ and $\mathbf{u}^*_{k+i|k}$ strictly lie in the tightened constraint sets, i.e., there exist $\tilde{s}$, $\tilde{r}_1 \in \mathbb{R}_{>0}$ such that $\mathbf{X}^*_{k+i|k} \in \bar{\mathbb{X}}'$ and $\mathbf{U}^*_{k+i|k} \in \mathbf{U}'$ where $\bar{\mathbb{X}}' \bigoplus \mathbb{B}_{\tilde{r}_1} \subseteq \bar{\mathbb{X}}$ and $\mathbb{U}' \bigoplus \mathbb{C}_{\tilde{s}} \subseteq \mathbb{U}$.

In addition, when $\|\mathbf{E}(k)\|^2_{\mathbf{Q}} \leq c$, $V_N(\mathbf{X}(k), k)$ is a *decrescent* function, i.e., $\|\mathbf{E}(k)\|^2_{\mathbf{Q}} \leq V_N(\mathbf{X}(k), k) \leq \kappa \|\mathbf{E}(k)\|^2_{\mathbf{Q}}$ (cf. **Lemma 5**). Thus, $V_N(\mathbf{X}(k), k) \leq \xi$ guarantees $\|\mathbf{E}(k)\|^2_{\mathbf{Q}} \leq \xi$. Therefore, $V_{\max} \in \mathbb{R}_{>0}$ exists.

■

Lemma 7 implies if $\mathbf{X} \in \mathbb{D}$, then the optimal solutions lie strictly in the tightened constraint sets. Besides, the trajectory constituted by the optimal solutions starting from $\mathbf{X}$ can be tracked. Thus, the optimal solutions starting from $\mathbf{X}$ ($\mathbf{X} \in \mathbb{D}$), can be regarded as a reachable reference trajectory. If the initial error between $\mathbf{X}$ and $\mathbf{Y}$ is sufficiently small, then predictions starting from $\mathbf{Y}$ generated by the locally optimal incremental controller lie in feasible sets, in accordance with **Definition 1**. Thus, it is reasonable to make the following assumption.

Assumption 2 (Optimal Solutions can be regarded as Reachable Reference Trajectories.)**.** *For $\mathbf{X} \in \mathbb{D}$ and $\mathbf{Y} \in \mathbb{R}^{4n}$, $\|\mathbf{Y} - \mathbf{X}\|^2_{\mathbf{Q}} \leq c_d$ ($c_d \in \mathbb{R}_{>0}$) implies $\forall i \in [0, N-1]$, $\mathbf{Y}_{k+i|k} \in \bar{\mathbb{X}}$ and $\mathbf{u}^{\mathbf{Y}}_{k+i|k} \in \mathbb{U}$, where $\mathbf{Y}_{k+i|k}$ and $\mathbf{u}^{\mathbf{Y}}_{k+i|k}$ are predictions generated by the locally optimal incremental controller $\Delta\mathbf{u}(\mathbf{Y}_{k+i}, \mathbf{X}^*_{k+i|k})$:*

$$\Delta\mathbf{u}(\mathbf{Y}_{k+i}, \mathbf{X}^*_{k+i|k}) = \Delta\mathbf{u}^*_{\mathbf{X},k+i|k} + \mathbf{K}_0(\mathbf{Y}_{k+i} - \mathbf{X}^*_{k+i|k}) \tag{3.45}$$

with $\Delta\mathbf{u}^*_{\mathbf{X},k+i|k}$ is optimal control signal corresponding to $\mathbf{X}$.

Based on **Lemma 7** and **Assumption 2**, **Lemma 8** about continuity of value function is proposed, which will be used to determine the *cumulative error bound* when ISS is analyzed.

Lemma 8 (Continuity of Value Function)**.** *If* $\mathbf{X} \in \mathbb{D}$, $\mathbf{Y} \in \bar{\mathbb{X}}$, *and* $\|\mathbf{X}-\mathbf{Y}\|_{\mathbf{Q}}^2 \leq c_d$, *then*

$$V_N(\mathbf{Y},k)-V_N(\mathbf{X},k) \leq \frac{K_\ell(1+\|\mathbf{K}_0\|_{\mathbf{P}})}{1-\sqrt{\rho}}\sqrt{\frac{\lambda_{\max}(\mathbf{P})}{\lambda_{\min}(\mathbf{Q})}c_d} \tag{3.46}$$

with a constant $K_\ell \in \mathbb{R}_{>0}$.

Proof: Since the stage cost (3.7) is quadratic, one obtains the following Lipschitz property of the stage cost function with a constant $K_\ell \in \mathbb{R}_{>0}$:

$$\begin{aligned}&|\ell(\mathbf{X}_{k+i|k},\Delta\mathbf{u}_{\mathbf{X},k+i|k},k+i)-\ell(\mathbf{Y}_{k+i|k},\Delta\mathbf{u}_{\mathbf{Y},k+i|k},k+i)|\\&\leq K_\ell\left(\|\mathbf{X}_{k+i|k}-\mathbf{Y}_{k+i|k}\|_{\mathbf{P}}+\|\Delta\mathbf{u}_{\mathbf{X},k+i|k}-\Delta\mathbf{u}_{\mathbf{Y},k+i|k}\|_{\mathbf{P}}\right)\end{aligned} \tag{3.47}$$

where $\Delta\mathbf{u}_{\mathbf{X},k+i|k}$ and $\Delta\mathbf{u}_{\mathbf{Y},k+i|k}$ are predicted control signals corresponding to $\mathbf{X}$ and $\mathbf{Y}$, respectively.

Considering $\mathbf{X}^*_{k+i|k}$ and $\Delta\mathbf{u}^*_{\mathbf{X},k+i|k}$ are the optimal solutions starting from $\mathbf{X}$ and the fact that $\|\mathbf{X}-\mathbf{Y}\|_{\mathbf{Q}}^2 \leq c_d$, it is concluded that if the locally optimal incremental controller designed in (3.45) is employed, the generated predicted variables corresponding to $\mathbf{Y}$ will not violate constraints, according to **Assumption 2**. Thus, the following upper bound of the difference between $V_N(\mathbf{Y},k)$ and $V_N(\mathbf{X},k)$ is derived, employing $\Delta\mathbf{u}(\mathbf{Y}_{k+i},\mathbf{X}^*_{k+i|k})$ (3.45) as the auxiliary control law:

$$\begin{aligned}&V_N(\mathbf{Y},k)-V_N(\mathbf{X},k)\\&\leq J_N\left(\mathbf{Y},\Delta\mathbf{u}_{\mathrm{OI}}(\mathbf{Y}_{k+i},\mathbf{X}^*_{k+i|k})\right)-V_N(\mathbf{X},k)\\&\leq K_\ell\sum_{i=0}^{N-1}\|\mathbf{Y}_{k+i|k}-\mathbf{X}^*_{k+i|k}\|_{\mathbf{P}}\\&\quad+K_\ell\sum_{i=0}^{N-1}\|\Delta\boldsymbol{u}(\mathbf{Y}_{k+i},\mathbf{X}^*_{k+i|k})-\Delta\mathbf{u}^*_{\mathbf{X},k+i|k}\|_{\mathbf{P}}\\&\overset{(3.45),(3.12)}{\leq} K_\ell(1+\|\mathbf{K}_0\|_{\mathbf{P}})\sum_{i=0}^{N-1}(\sqrt{\rho})^i\|\mathbf{X}-\mathbf{Y}\|_{\mathbf{P}}\\&\leq\frac{K_\ell(1+\|\mathbf{K}_0\|_{\mathbf{P}})}{1-\sqrt{\rho}}\sqrt{\frac{\lambda_{\max}(\mathbf{P})}{\lambda_{\min}(\mathbf{Q})}c_d}.\end{aligned} \tag{3.48}$$

From (3.48), it is concluded that, if $\mathbf{X} \in \mathbb{D}$, $\mathbf{Y} \in \bar{\mathbb{X}}$, and $\|\mathbf{X}-\mathbf{Y}\|_{\mathbf{Q}}^2 \leq c_d$, then the difference between $V_N(\mathbf{Y},k)$ and $V_N(\mathbf{X},k)$ is upper bounded, regardless of N.

■

3.3.3 ISS of the Proposed IMPC

The concept of ISS has been widely used in stability analysis of systems with bounded additive uncertainties [123], [124], [135]. Definitions and criteria for ISS that will be used later are referred to **Definition 2**, **Definition 3** and **Proposition 1**.

Definition 2 (Input-to-State Stable [123], [135]). *Consider a system given by*

$$\mathbf{x}(k+1) = \mathbf{F}(\mathbf{x}(k), \mathbf{w}(k)), \tag{3.49}$$

where $\mathbf{x}(k) \in \mathbb{R}^n$ *and* $\mathbf{w}(k) \in \mathbb{R}^m$ *($m \leq n$) are the state and disturbance of the system* (3.49)*, respectively. Besides, there exists a constant* $\gamma \in \mathbb{R}_{>0}$ *such that* $\|\mathbf{w}(k)\| \leq \gamma$ *for all* k*. Then the system* (3.49) *is input-to-state stable if there exist* $\beta(\cdot,\cdot) \in \mathcal{KL}$ *and* $\eta(\cdot) \in \mathcal{K}$ *such that*

$$\|\mathbf{x}(k)\| \leq \beta(\mathbf{x}(0), k) + \eta(\gamma) \tag{3.50}$$

with $\mathbf{x}(0)$ *being the initial value.*

Definition 3 (ISS Lyapunov Function [123], [135]). *A continuous function* $V(\cdot)$ *is an ISS Lyapunov function for the system (3.49) if there exist functions* $\alpha_1(\cdot)$*,* $\alpha_2(\cdot)$*,* $\alpha_3(\cdot) \in \mathcal{K}_\infty$ *and* $\varphi(\cdot) \in \mathcal{K}$ *such that*

$$\alpha_1(\|\mathbf{x}(k)\|) \leq V(\mathbf{x}(k)) \leq \alpha_2(\|\mathbf{x}(k)\|), \tag{3.51}$$

$$V(\mathbf{F}(\mathbf{x}(k), \mathbf{w}(k)) - V(\mathbf{x}(k)) \leq -\alpha_3(\|\mathbf{x}(k)\|) + \varphi(\gamma), \tag{3.52}$$

where $\varphi(\gamma)$ *is the* cumulative error bound*.*

Note that definitions and properties of comparison functions $\mathcal{K}$, $\mathcal{K}_\infty$ and $\mathcal{KL}$ in **Definition 2** and **Definition 3** are introduced in Appendix C.

Proposition 1 (The Method to Determine ISS of the System [123], [135]). *If the system (3.49) admits an ISS Lyapunov function, then it is ISS.*

Motivated by [127], [128], the continuity of the value function will be employed to complete the ISS analysis. In contrast to ISS analyses in [123], [124], feasible control sequences are not required in this article. The continuity of the value function has been proved in Section 3.3.2, which is also different from [127], [128]. Our approach has the advantage that when the difference between states $\mathbf{X}$ and $\mathbf{Y}$ is sufficiently small (i.e., $\|\mathbf{X} - \mathbf{Y}\|_{\mathbf{Q}}^2 \leq c_d$), the estimated upper bound of the difference between $V_N(\mathbf{X}, k)$ and $V_N(\mathbf{Y}, k)$ does not increase with increasing N.

In the following **Theorem 2**, considering a reachable reference trajectory, ISS of the IMPC w.r.t. the TDE error is analyzed. Finally, ISS of IMPC is proved by showing that $V_N(\mathbf{X}(k), k)$ is an ISS Lyapunov function.

Theorem 2 (ISS of IMPC). *Let* ***Assumption 2****,* ***Assumption 2****, and* ***Assumption 5*** *hold and suppose* $\bar{\epsilon}^*$ *satisfies*

$$\bar{\epsilon}^* \leq \sqrt{\frac{c_d}{\lambda_{\max}(\mathbf{Q})}}, \tag{3.53}$$

$$\epsilon_N := \frac{K_\ell(1 + \|\mathbf{K}_0\|_{\mathbf{P}})}{1 - \sqrt{\rho}} \sqrt{\frac{\lambda_{\max}(\mathbf{P})\lambda_{\max}(\mathbf{Q})}{\lambda_{\min}(\mathbf{Q})}} \bar{\epsilon}^* \leq \alpha_V(V_{\max}). \tag{3.54}$$

Considering a reachable reference trajectory, there exists $N_1 \in \mathbb{I}_{>0}$*, such that for all* $N > N_1$*,* $V_N(\mathbf{X}(k), k)$ *with the initial value* $V_N(\mathbf{X}(k_0), k_0) \leq V_{\max}$*, satisfies*

$$\alpha_1\left(\|\mathbf{E}(k)\|\right) \leq V_N(\mathbf{X}(k), k) \leq \alpha_2\left(\|\mathbf{E}(k)\|\right) \tag{3.55}$$

$$V_N(\mathbf{X}(k+1), k+1) - V_N(\mathbf{X}(k), k) \leq -\alpha_N(\|\mathbf{E}(k)\|) + \epsilon_N \tag{3.56}$$

where $\alpha_V(\cdot) \in \mathcal{K}$ *and* $\alpha_N(\cdot) \in \mathcal{K}_\infty$*, i.e.,* $V_N(\mathbf{X}(k), k)$ *is an ISS Lyapunov function.*

Proof: It consists of 3 parts. Assuming $V_N(\mathbf{X}(k),k) \leq V_{\max}$, *Part I* confirms that $V_N(\mathbf{X}(k),k)$ is a *decrescent function*, and *Part II* confirms that $V_N(\mathbf{X}(k),k)$ is decreasing regionally. At last, *Part III* demonstrates that, for a large enough prediction horizon N, $V_N(\mathbf{X}(k),k) \leq V_{\max}$ holds recursively.

Part I : A lower bound for $V_N(\mathbf{X}(k),k)$ is straight-forwardly obtained from

$$V_N(\mathbf{X}(k),k) \geq \|\mathbf{E}(k)\|_{\mathbf{Q}}^2 \geq \lambda_{\min}(\mathbf{Q})\|\mathbf{E}(k)\|^2. \tag{3.57}$$

Define $\gamma_{V_{\max}} \in \mathbb{R}_{>0} := \max\{\kappa, \frac{V_{\max}}{c}\}$. $V_N(\mathbf{X}(k),k)$ is upper bounded according to **Lemma 5** and the definition of $\gamma_{V_{\max}}$.

$$V_N(\mathbf{X}(k),k) \leq \gamma_{V_{\max}}\|\mathbf{E}(k)\|_{\mathbf{Q}}^2 \leq \gamma_{V_{\max}}\lambda_{\max}(\mathbf{Q})\|\mathbf{E}(k)\|^2. \tag{3.58}$$

Therefore, from (3.57) and (3.58), $V_N(\mathbf{X}(k),k)$ is a *decrescent function*, i.e., $V_N(\mathbf{X}(k),k)$ satisfies (3.55), which is the first criterion of ISS Lyapunov function in **Definition 3** (compare (3.51)) with $\alpha_1(x) := \lambda_{\min}(\mathbf{Q})x^2, \alpha_2(x) := \gamma_{V_{\max}}\lambda_{\max}(\mathbf{Q})x^2$.

Part II: In this part, the regional decreasing property of $V_N(\mathbf{X}(k),k)$ is analyzed, i.e., the relationship between $V_N(\mathbf{X}(k{+}1),k{+}1)$ and $V_N(\mathbf{X}(k),k)$ is constructed. To be able to analyze stability similar to [110], [111], the value function $V_N(\mathbf{X}^*_{k+1|k},k{+}1)$ is selected as an auxiliary value function, and the relationship between $V_N(\mathbf{X}^*_{k+1|k},k{+}1)$ and $V_N(\mathbf{X}(k),k)$ is investigated for a large enough N. To avoid an over-conservative *cumulative error bound*, the continuity of the value function is used to upper bound the difference between $V_N(\mathbf{X}(k{+}1),k{+}1)$ and $V_N(\mathbf{X}^*_{k+1|k},k{+}1)$. Finally, the relationship between $V_N(\mathbf{X}(k{+}1),k{+}1)$ and $V_N(\mathbf{X}(k),k)$ is determined.

Following [110], [111], the relation between $V_N(\mathbf{X}^*_{k+1|k},k{+}1)$ and $V_N(\mathbf{X}(k),k)$ is determined for a large enough prediction horizon N ($N \geq N_1$):

$$V_N(\mathbf{X}^*_{k+1|k},k{+}1) \leq V_N(\mathbf{X}(k),k) - \phi_N\lambda_{\min}(\mathbf{Q})\|\mathbf{E}(k)\|^2 \tag{3.59}$$

where $\phi_N := 1 - \frac{(\kappa-1)^M}{\kappa^{M-2}}$, $M \in \mathbb{I}_{>0} \geq \lceil 2\frac{\ln\kappa}{\ln\kappa - \ln(\kappa-1)}\rceil$, and $N_1 \in \mathbb{I}_{>0} := \lceil M + \gamma_{V_{\max}} - 1\rceil$.

Note that the basic idea of the proof of (3.59) can be summarized as follows. For a large enough N, there exists a constant $k_x \in \mathbb{I}_{[0,N-M]}$ such that $\ell(\mathbf{X}^*_{k+k_x|k}, \Delta\mathbf{u}^*_{k+k_x|k}, k+k_x) \leq c$. Then, based on the local upper bound of the value function established in **Lemma 5** and the dynamic programming principle, (3.59) is obtained. For the detailed proof, see [110], [111].

To construct the relation between $V(\mathbf{X}(k{+}1),k{+}1)$ and $V_N(\mathbf{X}^*_{k+1|k},k+1)$ using **Lemma 8**, the following **Lemma 9** is introduced.

Lemma 9. *Assuming* $\bar{\epsilon}^* \leq \sqrt{\frac{c_d}{\lambda_{\max}(\mathbf{Q})}}$, *if* $\mathbf{X}(k) \in \mathbb{D}$ *and* $N \geq N_1$, *then* $\mathbf{X}^*_{k+1|k} \in \mathbb{D}$ *and* $\mathbf{X}(k+1) \in \bar{\mathbb{X}}$.

Proof: First, $\mathbf{X}^*_{k+1|k} \in \mathbb{D}$ is verified. According to (3.59), if $N \geq N_1$, then $V_N(\mathbf{X}^*_{k+1|k},k{+}1) \leq V_N(\mathbf{X}(k),k)$.

Given that $\mathbf{X} \in \mathbb{D}$, i.e., $V_N(\mathbf{X}(k),k) \leq V_{\max}$, one obtains that $V_N(\mathbf{X}^*_{k+1|k},k{+}1) \leq V_N(\mathbf{X}(k),k) \leq V_{\max}$, which implies $\mathbf{X}^*_{k+1|k} \in \mathbb{D}$.

Then, $\mathbf{X}(k+1) \in \bar{\mathbb{X}}$ is confirmed. According to the TDE error bound in **Lemma 6**, one has $\|\mathbf{X}(k{+}1) - \mathbf{X}^*_{k+1|k}\| \leq \bar{\epsilon}^*$ (cf. (3.44)). Thus, $\|\mathbf{X}(k{+}1) - \mathbf{X}^*_{k+1|k}\|_{\mathbf{Q}}^2 \leq \lambda_{\max}(\mathbf{Q})(\bar{\epsilon}^*)^2$. Since $\bar{\epsilon}^* \leq \sqrt{\frac{c_d}{\lambda_{\max}(\mathbf{Q})}}$, one obtains $\|\mathbf{X}(k{+}1) - \mathbf{X}^*_{k+1|k}\|_{\mathbf{Q}}^2 \leq c_d$. Therefore, according to **Assumption 2**, $\mathbf{X}(k+1) \in \bar{\mathbb{X}}$ is obtained.

■

In accordance with **Lemma 8** and **Lemma 9**, one has

$$V_N(\mathbf{X}(k+1),k+1) \leq V_N(\mathbf{X}^*_{k+1|k},k+1)+\epsilon_N. \tag{3.60}$$

Finally, the relation between $V_N(\mathbf{X}(k+1),k+1)$ and $V_N(\mathbf{X}(k),k)$ is confirmed. Substituting (3.59) into (3.60) yields (3.56):

$$V_N\left(\mathbf{X}(k+1),k+1\right)-V_N(\mathbf{X}(k),k) \leq -\alpha_N\left(\|\mathbf{E}(k)\|\right)+\epsilon_N$$

with $\alpha_N(\|\mathbf{E}(k)\|) := \phi_N\lambda_{\min}(\mathbf{Q})\|\mathbf{E}(k)\|^2$.

Thus, as shown in (3.56), $V_N(\mathbf{X}(k),k)$ satisfies the second criterion of ISS Lyapunov function in **Definition 3** (compare (3.52)) with

$$\alpha_3(x) := \phi_N\lambda_{\min}(\mathbf{Q})x^2, \varphi(x) := \frac{K_\ell(1+\|\mathbf{K}_0\|_{\mathbf{P}})}{1-\sqrt{\rho}}\sqrt{\frac{\lambda_{\max}(\mathbf{P})\lambda_{\max}(\mathbf{Q})}{\lambda_{\min}(\mathbf{Q})}}x.$$

Therefore, $V_N(\mathbf{X}(k),k)$ is an ISS Lyapunov function.

Part III: In this part, it will be verified that $V_N(\mathbf{X}(k),k) \leq V_{\max}$ holds recursively, for a large enough N.

From (3.55) and (3.56), one has

$$V_N(\mathbf{X}(k+1),k+1)-V_N(\mathbf{X}(k),k) \leq -\alpha_V(V_N(\mathbf{X}(k),k))+\epsilon_N \tag{3.61}$$

where $\alpha_V(\cdot) := \alpha_N \circ {\alpha_r}^{-1}(\cdot)$ and $\alpha_r(x) := \lambda_{\max}(\mathbf{Q})x^2$ are $\mathcal{K}_\infty$ functions.

If $\mathbf{X}(k) \in \mathbb{D}$, then $V_N(\mathbf{X}(k),k) \leq V_{\max}$. Thus, combining with the above analysis and assumption, one has

$$\begin{aligned} V_N(\mathbf{X}(k+1),k+1) &\overset{(3.61)}{\leq} (\mathrm{id}-\alpha_V)(V_N(\mathbf{X}(k),k))+\epsilon_N \\ &\overset{(3.54)}{\leq} (\mathrm{id}-\alpha_V)(V_{\max})+\alpha_V(V_{\max}) \\ &\leq V_{\max}, \end{aligned} \tag{3.62}$$

where id is the identity function, i.e., $\mathrm{id}(x) = x$, for all $x \in \mathbb{R}$. Thus, if $\mathbf{X}(k) \in \mathbb{D}$, then $\mathbf{X}(k+1) \in \mathbb{D}$. Using induction, it is shown that $V_N(\mathbf{X}(k+j),k+j) \leq V_{\max}$ for all $j \in \mathbb{I}_{>0}$. Thus, $\mathbb{D}$ is a *positive invariant set*. Therefore, $V_N(\mathbf{X}(k),k) \leq V_{\max}$ holds recursively.

According to (3.62), $V_N(\mathbf{X}(k),k) \leq V_{\max}$ holds recursively if $N > N_1$. Given that $V_N(\mathbf{X}(k_0),k_0) \leq V_{\max}$, $V_N(\mathbf{X}(k),k) \leq V_{\max}$ holds for all $k \in \mathbb{I}_{[k_0,\infty)}$.

In conclusion, it is demonstrated that for all $N > N_1$ and initial state $\mathbf{X}(k_0)$ with $V_N(\mathbf{X}(k_0),k_0) \leq V_{\max}$, the system is local ISS for a reachable reference trajectory.

■

Remark 13 (Assumptions (3.53) and (3.54) can be Satisfied.)**.** *The ISS analysis is based on the assumptions* (3.53) *and* (3.54) *for the TDE error. If the combined TDE and discretization error $\bar{\epsilon}^*$ is sufficiently small, these assumptions can be satisfied. According to* (3.44)*, the magnitude of $\bar{\epsilon}^*$ mainly depends on the upper bound of the TDE error ϵ^*. As stated in* ***Remark 12****, by reducing the sampling period, the TDE error can be regulated as small as necessary. It is consistent with simulations in Section 3.4.3 which displays the influences of the sampling period on the stability of the closed-loop system.*

Remark 14 (Conservative Cumulative Error Bound is Avoided.)**.** *Different from the* cumulative error bound $\left(L_s\frac{{L_\mathbf{f}}^{N-1}-1}{L_\mathbf{f}-1}+L_t{L_\mathbf{f}}^{N-1}\right)d$ *(where* $L_\mathbf{f}$*,* L_s*, and* L_t *are Lipschitz constants, and* d *is the upper bound of the disturbance) derived in [123], [124], the* cumulative error bound *in this article* $\epsilon_N := \frac{K_\ell(1+\|\mathbf{K}_0\|_\mathbf{P})}{1-\sqrt{\rho}}\sqrt{\frac{\lambda_{\max}(\mathbf{P})\lambda_{\max}(\mathbf{Q})}{\lambda_{\min}(\mathbf{Q})}}\bar{\epsilon}^*$ *does not increase as* N *increases. Similar to our approach, the continuity property of the value function is also used to investigate local ISS of the MPC method in [127], [128]. Unfortunately, for* $\mathbf{A}$ *in* (3.5)*, its eigenvalue* $\lambda(\mathbf{A})>1$*. It still results in the rise of the* cumulative error bound *with increasing* N*, if the method in [127], [128] is applied.*

Remark 15 (Increasing the Prediction Horizon Enlarges the Region of Attraction.)**.** *Simply increasing the prediction horizon* N *can enlarge the region of attraction* $\{\mathbf{X}\in\bar{\mathbb{X}}: V_N(\mathbf{X},k)\leq V_{\max}\}$*. This is because* $N_1:=\lceil M+\gamma_{V_{\max}}-1\rceil$ *increases as* $\gamma_{V_{\max}}:=\frac{V_{\max}}{c}$ *increases. It is also verified by experiments in Section 4.5.*

Remark 16 (Increasing the Prediction Horizon Decreases Tracking Errors.)**.** *According to* Part 3*, the system ultimately converges to* $\mathbb{D}_t:=\{\mathbf{X}\in\bar{\mathbb{X}}: V_N(\mathbf{X},k)\leq\alpha_V^{-1}(\epsilon_N)\}$*. Thus,* $\|\mathbf{E}(k)\|\leq\sqrt{\alpha_V^{-1}(\epsilon_N)/\lambda_{\min}(\mathbf{Q})}$ *according to (3.55). If we increase* M *(or* N*) properly, both* $\alpha_N(\cdot)$ *and* $\alpha_V(\cdot)$ *increase. Thus, the tracking error decreases if* N *increases properly. But it does not asymptotically converge to zero because of the non-zero TDE error. The effects of* N *on the tracking errors are also investigated by experiments in Section 4.5.*

Remark 17 (How to Determine the Prediction Horizon.)**.** *To guarantee ISS of IMPC in local regions around the reachable reference trajectory, the minimal prediction horizon* $N_1\in\mathbb{I}_{>0}:=\lceil M+\gamma_{V_{\max}}-1\rceil$ *is determined. Due to the zooming technique, this minimal* N *is very conservative (normally over-estimated, compare [111]). However, a too large prediction horizon causes heavier computation such that the real-time control capability will be affected. Thus, a balance between ISS and computing efficiency has to be found in practice. To this end, based on current computing resources, the prediction horizon is selected as large as possible.*

3.4 Experiment

In this section, the proposed IMPC is validated on the 3-DoF robot manipulator shown in Section 2.4.1. Firstly, to validate optimal control performance of IMPC, comparison experiments with state-of-the-art TDE based controllers are conducted. Then, to show capabilities to address input and state constraints, experiments are performed where step by step, the constraints are tightened. Finally, there is a discussion of the experimental results.

3.4.1 Experimental Setup

The sampling period $T_s=1$ms. The parameters for IMPC are chosen as follows: diagonal matrix $\bar{\mathbf{g}}=\text{diag}(14,32,80)$; weighting matrices $\mathbf{Q}=\text{diag}\{500\mathbf{I}_3,10\mathbf{I}_3,50\mathbf{I}_3,\mathbf{I}_3\}$, $\mathbf{R}=\text{diag}\{5,5,5\}$. Owing to the TDE technique, the nonlinear system is approximated by a linear system (3.5) and then the constrained OCP (3.10) is a quadratic-programming (QP) problem. Thus, the constrained OCP (3.10) is calculated by the active-set QP solver,

Table 3.1: Input and state constraints of Scenarios 1-5

Scenario No.	Angular constraint	Velocity constraint	Input constraint
1	114.59 deg	114.59 deg/s	4 N·m
2	114.59 deg	114.59 deg/s	2 N·m
3	63.03 deg	114.59 deg/s	4 N·m
4	114.59 deg	45.84 deg/s	4 N·m
5	63.03 deg	114.59 deg/s	2 N·m

`qpOASES` [136]. The prediction horizon N =15 unless noted otherwise. Note that $\bar{\mathbf{g}}$ is selected by a manual tuning process following the procedures in **Remark 23**.

For the experimental study, 6 scenarios are considered. The reference trajectories for the three joints are chosen as given in Figure 2.3. They are all sinusoidal reference trajectories. The period is 5s and amplitudes are 28.65 deg (0.5 rad), 11.46 deg (0.2 rad), and 45.86 deg (0.8 rad), respectively. Then, reference velocity amplitudes are 36.11 deg/s (0.63 rad/s), 14.40 deg/s (0.25 rad/s), and 57.60 deg/s (1.01 rad/s), respectively.

Scenario 1: Comparison with TDE based controllers. To verify optimal tracking performance of the proposed IMPC, it is compared to the time delay control (TDC) [36] and TDC combined with sliding mode controller [29]. For simplicity, these controllers are referred to as IMPC, TDC, and TSMC, respectively. For IMPC, the input and state constraints are shown in Table 3.1; For TDC and TSMC, the design parameters k_P and k_D are in general determined by the desired natural frequency ω_n and the damping ratio ζ, i.e., $k_P = \omega_n^2$ and $k_D = 2\zeta\omega_n$. Here, we set $\omega_n = 8$ rad/s and $\zeta = 1$. Thus, k_P =64 and k_D =16; Besides, for TSMC, $\boldsymbol{\varepsilon}$ =[0.002, 0.001, 0.001], α =50, and φ =2.5×10^4 where $\boldsymbol{\varepsilon}$, α, and φ are all design parameters for the sliding mode controller. To quantify tracking performance of these three controllers, the following average cost function is employed:

$$J = \frac{1}{N_t}\sum_{k=0}^{N_t}\left(\|\mathbf{E}(k)\|_{\mathbf{Q}}^2 + \|\tilde{\Delta}\mathbf{u}(k)\|_{\mathbf{R}}^2\right) \tag{3.63}$$

where $N_t = t_s/T_s$, t_s is the terminal time.

Given that the reference signals varying flatly lie strictly in the state set of Scenario 1, reference signals can be regarded as reachable reference trajectories in Scenario 1.

In Scenarios 2-5, the capability of IMPC to handle input and state constraints is verified, through tightening input and state constraints (see Table 3.1). Note that 114.59 deg=2 rad, 63.03 deg=1.1 rad, and 45.84 deg=0.8 rad.

In Scenario 6, Scenario 1 (only IMPC part) and Scenario 3 are repeated with N =8, 12, 15, respectively, to study the effect of different prediction horizons on tracking performance.

3.4.2 Experimental Results

The experimental results of Scenario 1 are depicted in Figures. 3.1-3.3 and Table 3.2. As shown in Figure 3.1 and Table 3.2, tracking errors of IMPC are smaller than that of TDC and TSMC. As shown in Figure 3.2, especially the first subfigure, torque trajectories generated by

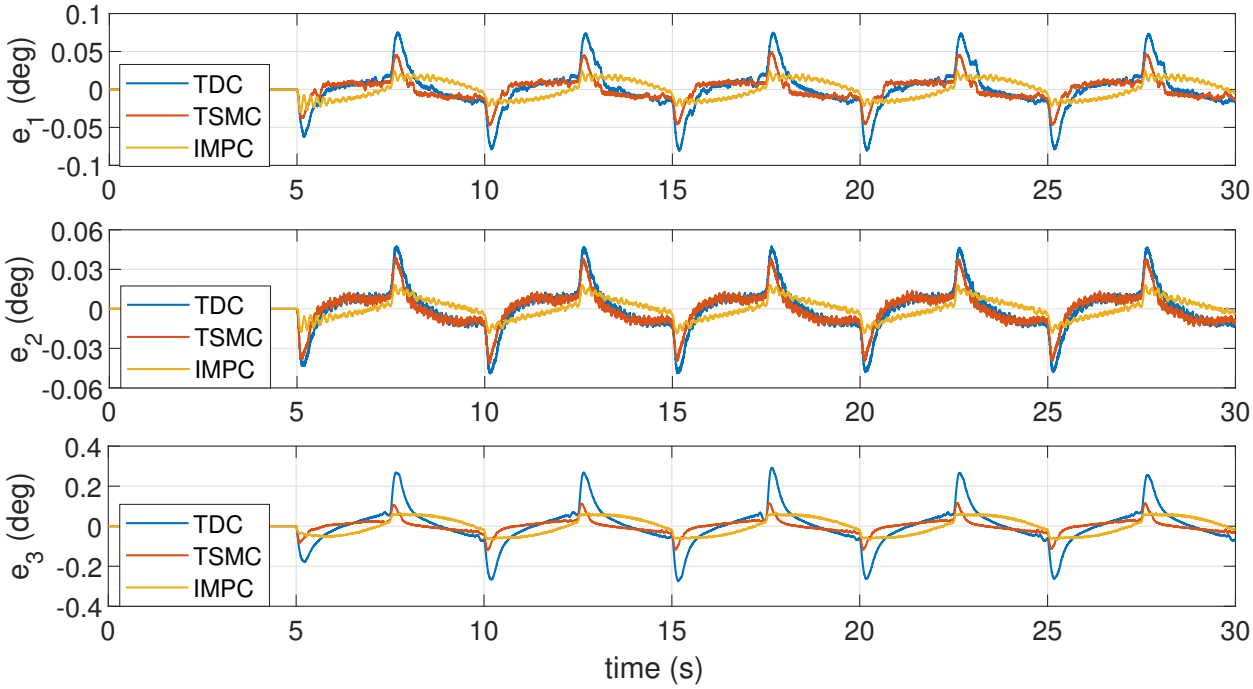

Figure 3.1: Experimental results of Scenario 1: Tracking errors for the three joints.

Table 3.2: Experimental results of Scenario 1: RMS Values of the Tracking Errors of the Three Joints (10^{-2}deg)

Joint No.	TDC	TSMC	IMPC
1	2.38	1.36	1.17
2	1.50	1.16	0.68
3	8.56	3.05	3.93

IMPC are smoother than that of TDC and TSMC. This is because acceleration information, which is easily affected by measurement noise, is used to calculate torques directly for TDC and TSMC. For IMPC, the torques are generated by solving an OCP. The costs for the three controllers, calculated from (3.63) are 16.2475, 16.1185, and 3.3716, respectively. As expected, the cost for IMPC is much smaller than that of TDC and TSMC. Although tracking errors of TSMC are smaller than that of TDC, the related costs are almost equal. This is because nonsmooth torque trajectories result in large values for $\Delta\mathbf{u}$, and costs for TDC and TSMC mainly depend on variations of torque. As shown in Figure 3.3, most of the computing time for each prediction horizon are smaller than 0.2 ms, which verifies real-time control capability.

The experimental results of Scenario 2 are depicted in Figure 3.4. As shown in Figure 3.4, input constraints are not violated and the system is still stable, although the tracking errors are larger than that in Scenario 1.

The experimental results of Scenario 3 are depicted in Figure 3.5. It can be observed that the reference trajectory of joint 3 does sometimes leave the admissible set. Nevertheless, the closed-loop system is still stable. For the tracking errors, there are no apparent differences

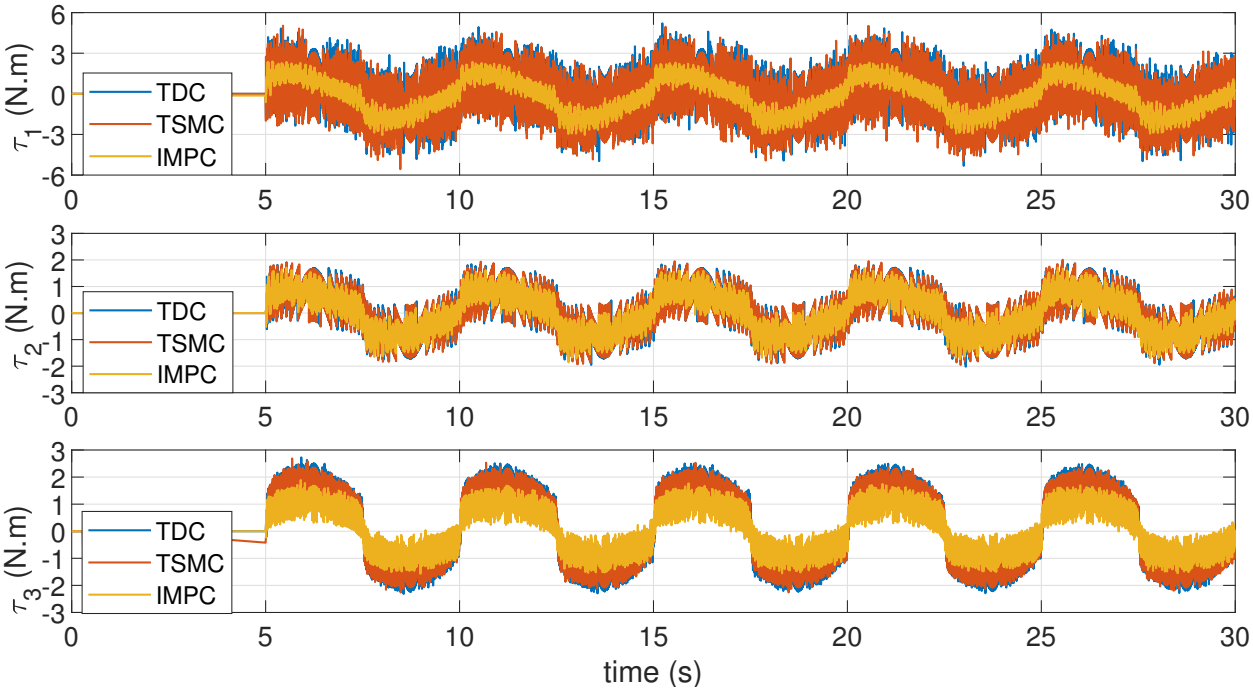

Figure 3.2: Experimental results of Scenario 1: Torques for three joints.

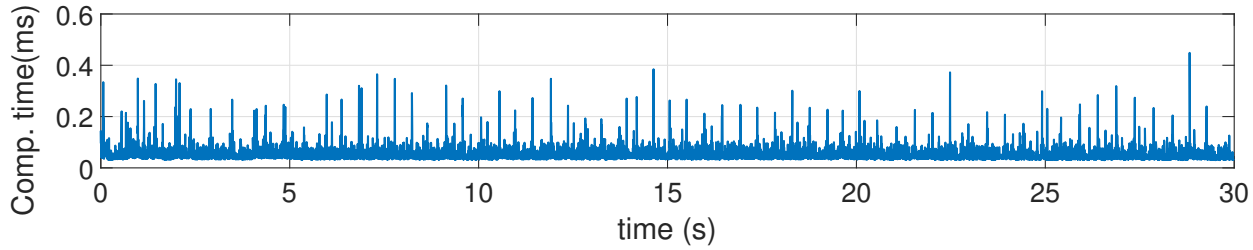

Figure 3.3: Experimental results of Scenario 1: Computation time.

for joint 1 and joint 2, in comparison with Scenario 1. For joint 3, because of the strict state constraint, the tracking error is larger when reference signals are unreachable. It is also observed that during time intervals [8s,10s], $\cdots$, [28s,30s], the tracking error of joint 3 gradually converges to a small neighborhood of the origin. There are two reasons for this phenomenon. One is that the reference trajectory is getting closer and finally approaches the feasible sets, the other is that when the reference trajectory becomes reachable again, the tracking error ultimately converges to a small neighborhood around the origin. This coincides to the local ISS of the proposed IMPC analyzed in Section 3.3. For the torques of joint 3, there are severe variations for short periods when the positions are close to the boundary of the constraints. This is to avoid state constraint violation. On the other hand, joint 3 nearly stops moving while joint 1 and joint 2 continue to move. The movement of joint 1 and joint 2 is regarded as the disturbance to joint 3. Despite of severe variations, the whole closed-loop system is stable.

In Scenario 4, the state constraints are tightened for the angular velocity. The experimental results of Scenario 4 are depicted in Figure 3.6. For joint 1 and 2, there are no significant differences in tracking errors and tracking velocities between Scenario 1 and 4. For joint

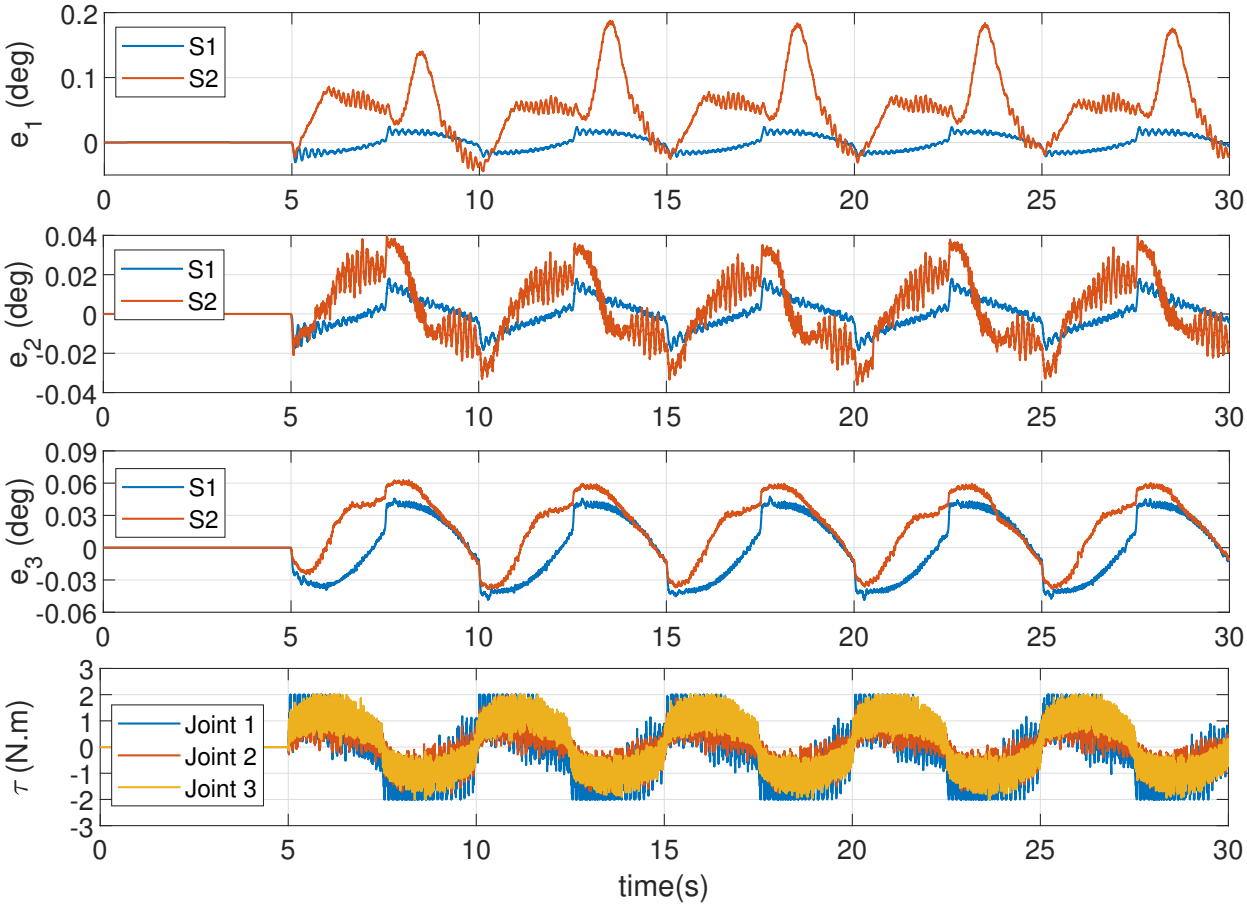

Figure 3.4: Experimental results of Scenario 2: Tracking errors and torques for three joints. Note that 'S1' and 'S2' represent variables generated in Scenarios 1 and 2, respectively.

3, the velocity is limited because of the new constraint, resulting in a larger tracking error. As displayed in the fifth subfigure of Figure 3.6, the torque of joint 3 changes significantly during some time horizons, such as [6s, 7s], [8s, 9s], $\cdots$ [28s, 29s]. During these time horizons, controller tries to avoid violation of the velocity constraints.

As displayed in Figures. 3.5 and 3.6, especially the fourth subfigure of Figure 3.5 and the fourth subfigure of Figure 3.6, state constraints are slightly violated. This is because the TDE error and measurement noises are not considered when predictions are generated in the constrained OCP (3.10). Comparing Figure 3.5 with Figure 3.6, one learns that it is more difficult to constrain velocities because velocities are easily affected by measurement noise. Although the violation phenomenon occurs around the constraint boundary, the proposed IMPC scheme still has the capability to regulate states to a large extend.

The experimental results of Scenario 5 are depicted in Figure 3.7. In comparison with Scenario 1, the tracking error of joint 1 increases slightly because of the tightened input constraint. For joint 2, there are no significant differences. Joint 3 operates stably similar to Scenario 3.

The experimental results of Scenario 6 are depicted in Figures 3.8-3.9. For Scenario 1 with N =8, 12, 15, experimental results are depicted in Figure 3.8. The tracking error decreases

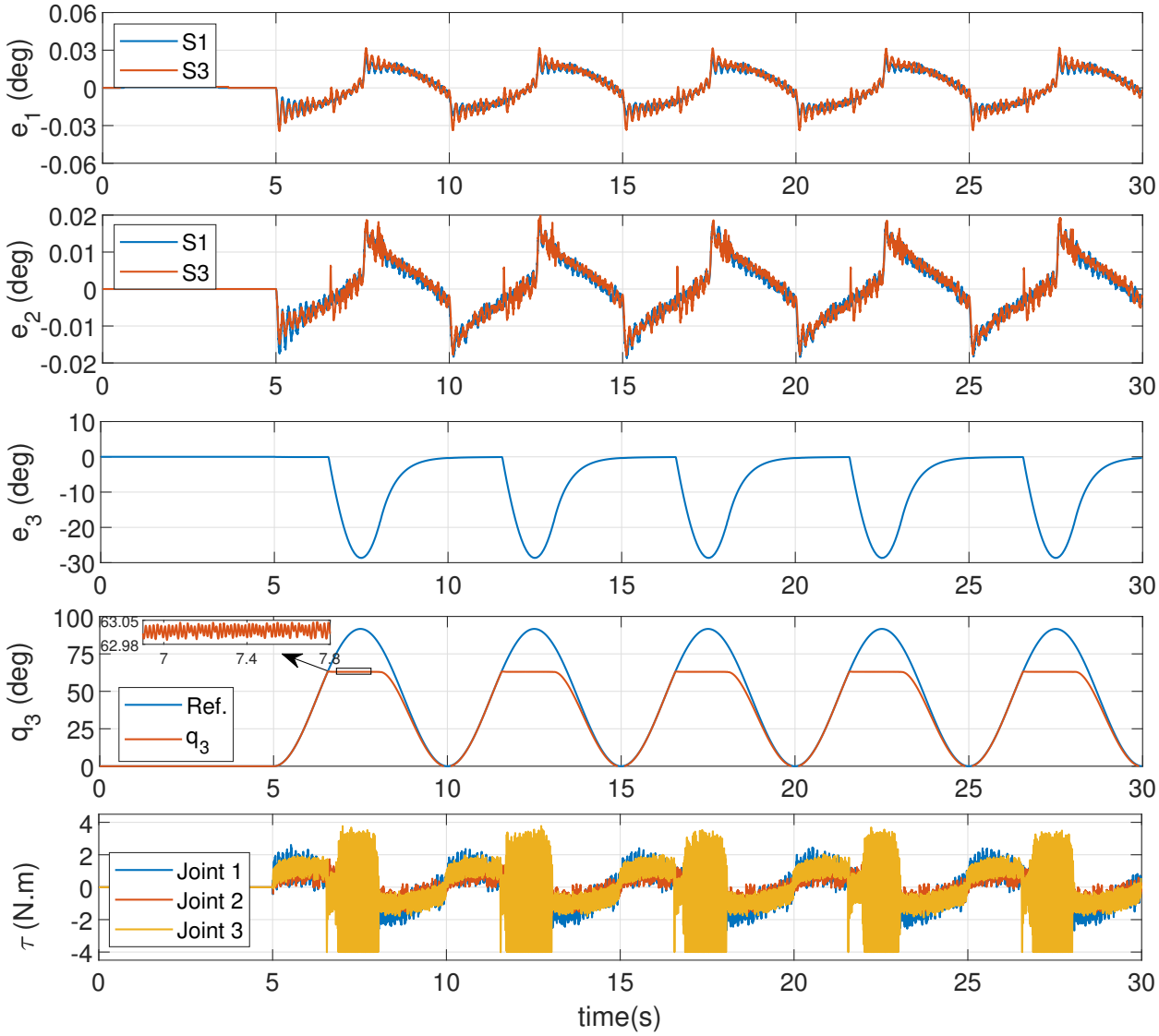

Figure 3.5: Experimental results of Scenario 3: Tracking errors, position of joint 3, and torques. Note that 'S3' represent variables generated in Scenario 3, respectively.

for a longer horizon N. It coincides with the ISS analysis in Section 3.3.3. For N =12 and 15, there are no significant differences in tracking errors. Due to the TDE error, the tracking error does not converge to zero even if N continues to increase.

The experimental results of Scenario 3 with different horizons are shown in Figure 3.9. For joints 1 and 2, the reference is reachable and tracking errors decrease with increasing the horizon N. The reference trajectory for joint 3 is not always reachable. Although ISS for unreachable reference trajectories is not considered in the presented theory, system outputs stay close to reference signals. During the time intervals [8s, 10s], $\cdots$, [28s, 30s], the unreachable reference trajectory switches to a reachable reference trajectory. As shown in Figure 3.9, especially the fourth subfigure, as the horizon N increases, the output is closer to the reference signal. This is because the region of attraction increases and the tracking error decreases with larger N, as analyzed in **Remark 15** and **Remark 16**.

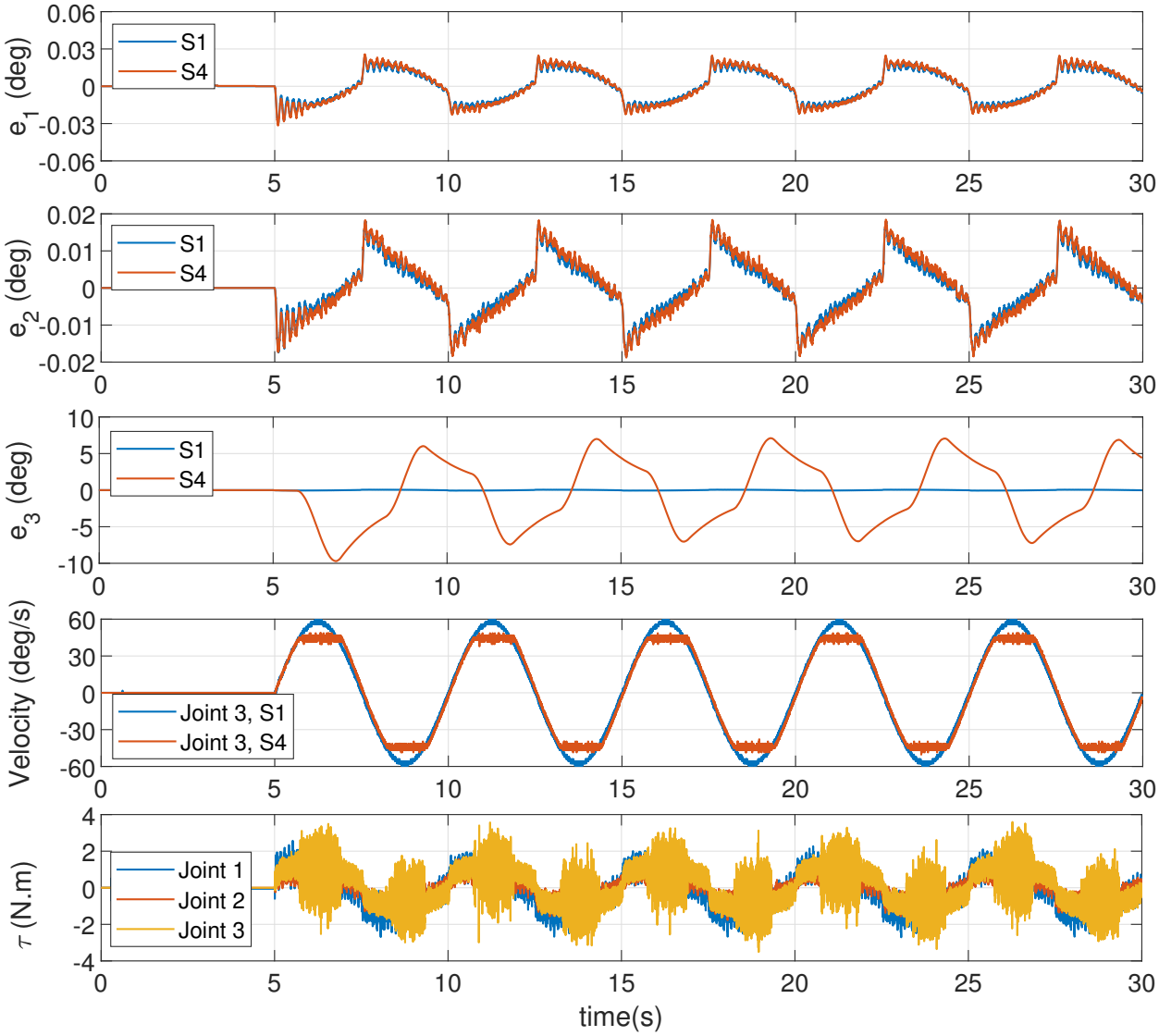

Figure 3.6: Experimental results of Scenario 4: Tracking errors, velocity of joint 3, and torques. Note that 'S4' represent variables generated in Scenario 4, respectively.

3.4.3 Discussion

Prediction Horizon N

In Section 3.3, the minimal prediction horizon $N_1 := \lceil M + \gamma_{V_{\max}} - 1 \rceil$ can guarantee local ISS of IMPC for reachable reference tracking. Using the zooming technique, the method in Section 3.3 to determine the prediction horizon N is very conservative. This phenomenon is illustrated using the following example. Assuming $\|\mathbf{E}(k)\|_{\mathbf{Q}}^2 \leq c$, we obtain the theoretical minimal prediction horizon $N = 5.02 \times 10^{12}$. However, in Scenarios 1-6, yet $N = 8$ allows for stability of the system. Thus, the minimal prediction horizon in ISS analysis is more of a conceptual nature.

Besides, the statement in **Remark 16** is verified by Scenario 6, i.e., tracking errors decrease with increasing the prediction horizon N. To this end, one would try to select a larger prediction horizon. On the other hand, increasing N causes heavier computation. Thus, in

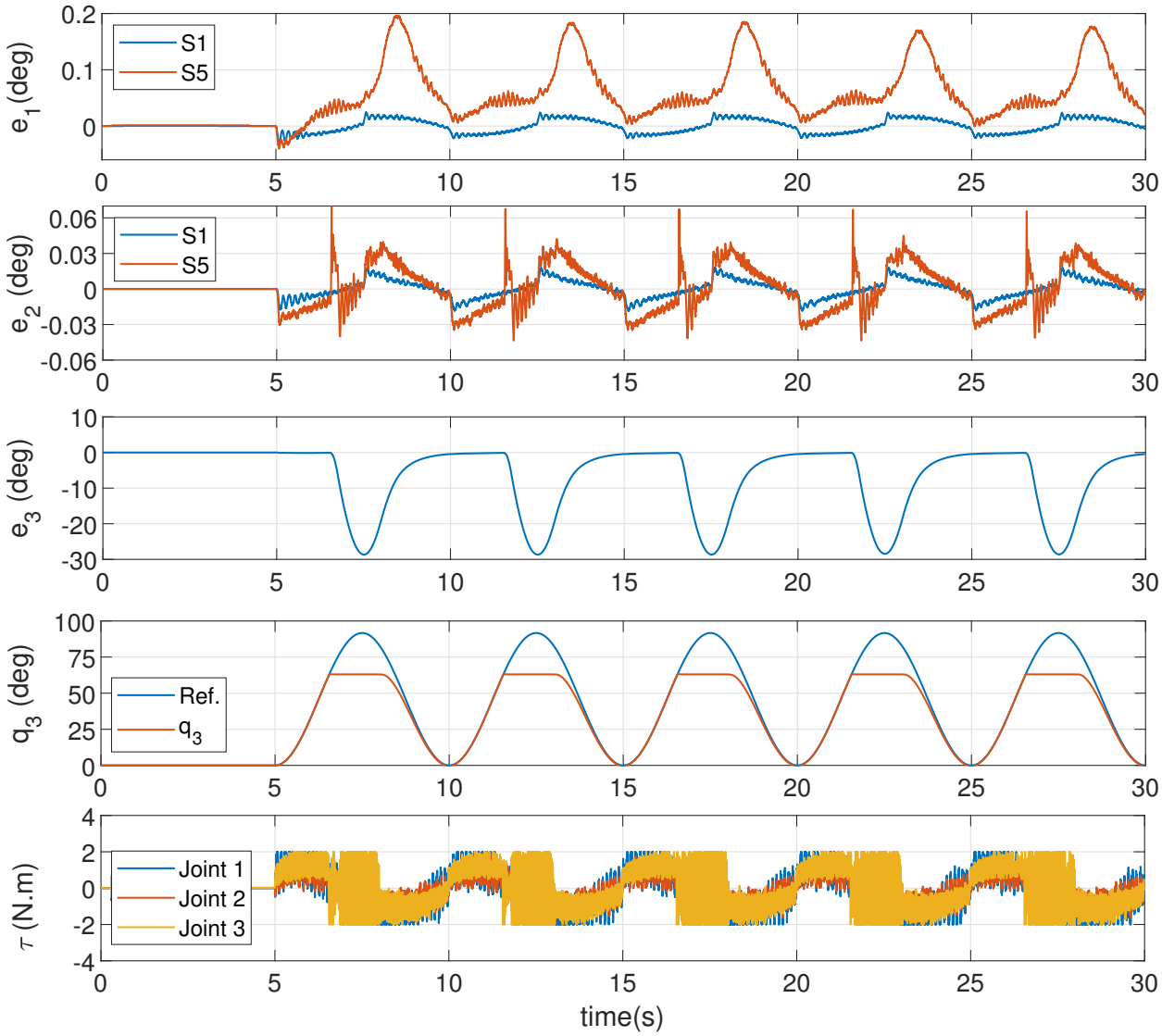

Figure 3.7: Experimental results of Scenario 5: Tracking errors, position of joint 3, and torques. Note that 'S5' represent variables generated in Scenario 5, respectively.

practice, one needs to find a compromise between tracking errors and computing efficiency. When the prediction horizon exceeds 15, real-time control cannot be realized because of the limited computational capability of our computer. As shown in Figure 3.3, for reachable trajectories, there is still room to increase the prediction horizon. However, for unreachable trajectories, iterative number of the `qpOASES` solver increases to keep constraints satisfaction, and it will also increase the computing time at the same time. Taking all factors discussed above into consideration, we find that for our application N =15 is a reasonable selection because it not only allows for real-time implementation but also guarantees precise enough tracking.

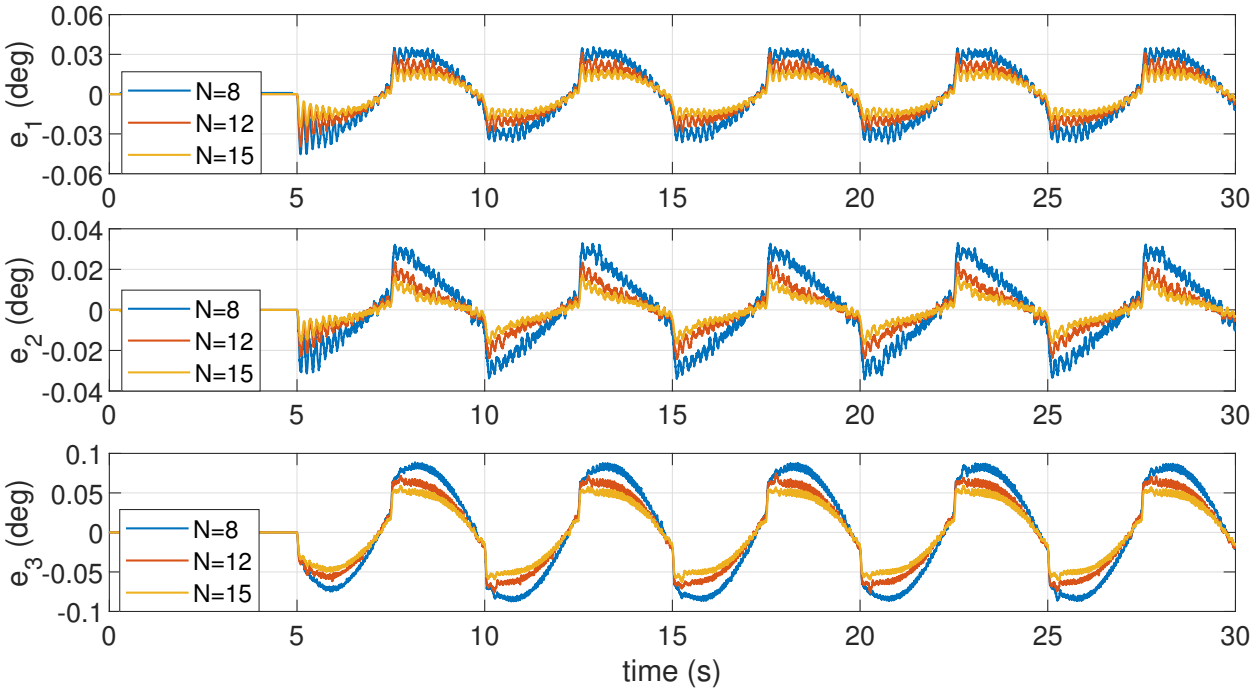

Figure 3.8: Experimental results of Scenario 6: Tracking errors with different prediction horizons.

Reachable or Unreachable Reference Trajectory

During the implementation, one does not need to justify whether the reference trajectory is reachable or unreachable. We only need to solve the constrained OCP (3.10).

As shown in **Lemma 4**, if the set of admissible states are enlarged enough, an unreachable reference trajectory can be changed into a reachable reference trajectory. In other words as shown in Scenarios 1-5, the reachable reference trajectory in Scenario 1 is changed into unreachable reference trajectories in Scenarios 2-4 after tighter input and/or state constraints are introduced. Although ISS of IMPC is not theoretically proven for unreachable reference trajectories, the reference trajectory is tracked as close as possible and the closed-loop system is still stable (as shown in Scenarios 2-5).

Limitations in Practice

To satisfy the assumptions w.r.t. the TDE error mentioned in **Remark 13**, a small enough sampling period is required. In our experiments, 0.001s is used because of the setting of our experimental system, which is also commonly used in robotic systems, such as [7], [29], [32], [65], [74], [94], [137]. If the sampling period increases, the tracking error increases and finally the closed-loop system becomes unstable. To check the influence of the sampling period on control performance and considering safety issues, simulations of Scenario 1 with different sampling periods (T_s= 0.001s, 0.005s, 0.01s, 0.02s) are implemented. Tracking errors of joint 1 are displayed. As shown in Figure 3.10, when T_s = 0.001s, 0.005s, and 0.01s, tracking errors are very small. The tracking error increases as the sampling period increases since the TDE error increases with increasing the sampling period as analyzed in Section 3.3.2. For T_s = 0.02s, the tracking error trajectory starts to oscillate because a larger TDE error

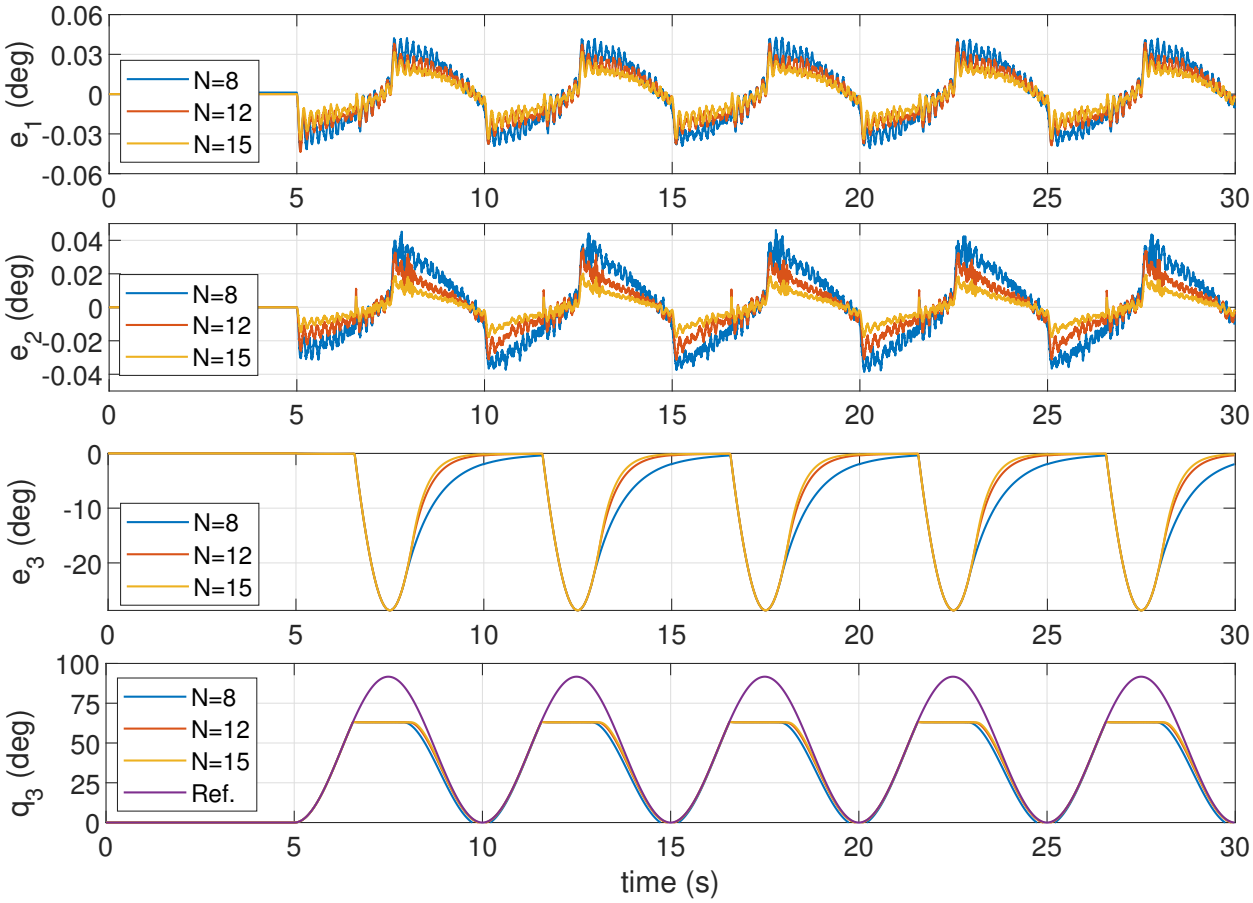

Figure 3.9: Experimental results of Scenario 6: Tracking errors and positions of joint 3 with different prediction horizons.

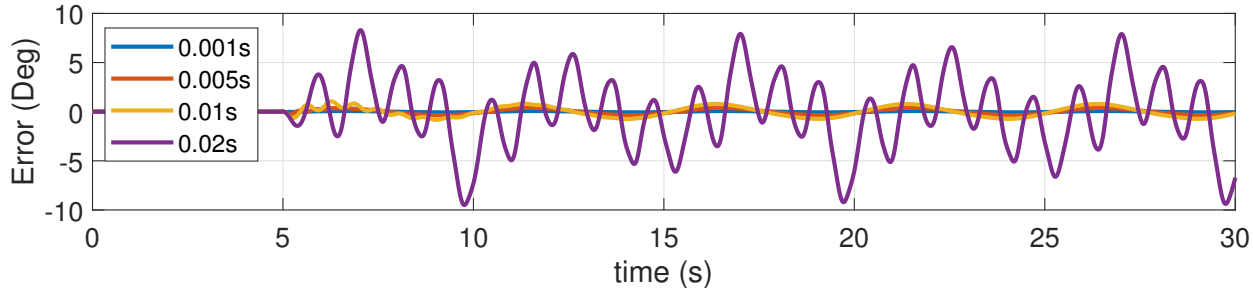

Figure 3.10: Simulation results: Tracking errors of Joint 1 with sampling periods $T_s = 0.001$s, 0.005s, 0.01s, 0.02s.

affects solutions of the constrained OCP (3.10) and the system becomes unstable. Therefore, to receive reliable control performance, the sampling period should be smaller than 0.01s. Besides, we need to take into account real-time computation capability since the smaller sampling period, the heavier the burden of computing. In the experiment of the paper, based on the simulation study, we select 0.001s to ensure both the real-time computation and the tracking performance.

3.5 Summary

In this chapter, an incremental model predictive controller (IMPC) for robot manipulators was proposed. IMPC provides a control framework which obtains optimal control performance without concrete mathematical model.

The design process of IMPC involves three steps. First, using time delay estimation (TDE) and discretization, an approximated discrete-time linear system with incremental control signal was derived. Then, the cost function is designed taking into account tracking errors and control signals. Finally, with the approximated discrete-time linear system and cost function, IMPC was developed, where the concrete mathematical model of the robot manipulator was no longer required. This is the main contribution of this chapter.

The second major contribution of this chapter is the local input-to-state stability (ISS) analysis of IMPC. First, we introduce the definition of reachable reference trajectory using the local optimal incremental controller. In a small neighborhood around the reachable reference trajectory, there exists local optimal incremental controller which stabilizes the system and guarantees input and state constraints are not violated. Then, using this local controllability of the system, a local region around the reachable reference trajectory is defined, and in this region, continuity of the value function is proved. Finally, the *cumulative error bound* is calculated using the continuity property of the value function, and the resulting *cumulative error bound* is not over-conservative. It is theoretically inferred from this local ISS analysis that increasing the prediction horizon enlarges the region of attraction and decreases tracking errors.

To validate the proposed IMPC, a set of real-time experiments was performed. The results demonstrate the efficacy of the proposed IMPC in realizing optimal control performance while guaranteeing input and state constraints are not violated. In practice, tasks are usually defined in task-space and task-space control is more intuitive. Thus, in Chapter 4, we will extend IMPC to the task-space control schemes.

Hierarchical IMPC for Task Space Control

4

In Chapters 2 and 3, joint-space controllers have been studied. Nevertheless, in the control of robot manipulators, tasks to be executed are usually given in the task space [138]. For existing task-space controllers, the most important performance criteria, such as robustness, singularity-avoidance, optimality, and constraint admissibility, are not yet considered simultaneously. Concurrently addressing these issues is challenging given the inevitable modeling errors, inherent inversion operation in algorithms and limited computing power of systems. In this chapter, we aim at developing a task-prioritized control scheme taking into account all these criteria simultaneously.

4.1 Overview

In this chapter, a task-space controller is developed in the framework of MPC, where equations of motion of tasks and system dynamics are approximated by linear incremental systems using TDE. As a result, the optimal control perfromance is realized while constraints are not violated and robustness is enhanced. Multiple tasks are considered simultaneously and performed in a prioritized order. The task priority is realized based on the *dynamic consistency* principle. In the algorithm, inversion of matrices w.r.t. Jacobian is avoided. It is a singularity-free method.

4.1.1 Related Work

Mechanical or robotic systems (e.g. high-degree-of-freedom robot manipulator and humanoid robots) which are kinematically redundant to a given task, enable execution of additional tasks simultaneously. Usually, the primary task of the robot manipulator is to realize accurate end-effector (EE) trajectory tracking. The primary task is assigned the highest priority while the additional tasks, such as maintaining the orientation of EE, can be performed by utilizing redundancy of the robot manipulator. Although multiple tasks can be controlled if they are concatenated into a single task vector, all the conflicting tasks will be adversely affected if a control conflict occurs.

To ensure conflict resolution, the operational space control framework has been employed to bestow control capability of multiple tasks in a strictly prioritized manner for redundant robots, mostly with the null-space projection method [139]–[144]. These task-prioritized controllers are grouped into three categories, where either the desired joint velocities [139], [140], or accelerations[141], or forces/torques [142], [143] are computed respectively [144]. Since most of commercial robots do not allow for a torque-level control interface, the velocity-based scheme is preferred in robotic applications. Nevertheless, for tracking with a second-order system such as a rigid body dynamics robot, the acceleration-based and force/torque-

based schemes are more appealing owing to the explicit incorporation of accelerations. The force/torque-based scheme brings significant advantages in applications where manipulation in contact with environments is required, and constraints on torques are imposed to guarantee security. In the last few decades, a variety of force/torque-based methods, such as operational space formulation (OSF) [142]–[150], hierarchical quadratic programming (HQP) [61], [151]–[153], and MPC [154], [155] were developed.

1) OSF schemes: The OSF [142] relying on null-space projections [156] has been widely used and became a popular tool for task-prioritized control since it was introduced to robotics decades ago. It provides dynamically decoupled control of multiple tasks based on a property known as *dynamic consistency*: forces/torques for lower priority tasks do not affect the execution of high-priority tasks [143], where model-based feedback linearization is applied on all hierarchical levels and decoupled control behavior of each task is obtained. The formal null-space stability, which is difficult to be proven [144], [157], is theoretically analyzed in [148], [149] for regulation control and [150] for tracking control, respectively. Nevertheless, both the novel hierarchical controller and OSF are vulnerable to modeling errors [144] since the mathematical model is required to be precisely identified to realize feedback linearization and controller design. Unfortunately, modeling errors are inevitable in practice. Besides, dynamics terms, especially the inertia matrix, undergo severe changes when the robotic system carries or releases unknown payloads. Therefore, desired control performance naturally deteriorates.

To deal with modeling errors, adaptive methods [158] and learning techniques [159] were employed in operational space controls, where uncertain/unknown functions are identified or optimal control is found online that maximizes an immediate reward. Although the robustness of the controllers is improved, the computational complexity is such high that it is difficult to apply them in practice. Besides, some parameters have to be heuristically selected, which also increases the complexity of these methods. As an alternative, time-delay estimation (TDE) based OSF methods were developed in [145]–[147]. TDE [7], [28], [33], [36], [133] is a model-free controller design method, which uses time-delayed input and output signals to estimate system dynamics without a concrete mathematical model, laborious parameter identification, and linearization around equilibrium points of the system. It results in enhanced accuracy in terms of *dynamic consistency* and control performance along with enhanced computational efficiency.

Nevertheless, the null-space projection-based OSF methods [142]–[150] result in algorithmic singularity problems especially when tasks conflict with each other which finally result in unstable behavior. Although a damping factor [53] and a continuous null-space projection [60] were introduced to address the singularity problem, there is a trade-off between good conditioning of the solution and tracking accuracy. Besides, physical limitations, such as input and state constraints, are also not considered in all approaches until here. Constraints are generally used to describe safety requirements not only for the environment but also for the robot and should be considered in safety-critical applications, e.g., close to or in cooperation with humans.

2) HQP schemes: Considering input and/or state (motion) constraints, HQP was developed in the framework of multiple quadratic programs (QPs) ordered hierarchically [61], [151]–[153], where the task hierarchy is realized using the hierarchical structure of the QPs [140], [160]. In [151], the robustness of HQP is addressed with a combination of sliding mode control (SMC). However, to realize task hierarchy simultaneously, the null-space projection

idea is adopted to design the sliding variable, which has the risk of algorithmic singularity. In [152], task hierarchy is realized by solving the cascaded QP in lexicographic order, and in [61], [153], equality constraints are imposed to guarantee strict task hierarchy without using the null-space projection method. Thus, in [61], [152], [153], algorithmic singularity is avoided. However, once the Jacobian matrix is singular, Hessian matrices of QPs in [152], [153] are no longer positive definite, and kinematic singularity occurs. This is because, for QP solvers, numerical weakness increases with the rise of the condition number of the Hessian matrix. When the Hessian matrix is positive semi-definite, undesired (large-value) control signals are computed and the system becomes unstable. Although the Hessian matrix is always positive definite in [61], the risk of kinematic singularity is still not avoided since the algorithm in [61] involves the inverse calculation of the terms w.r.t. Jacobian matrix. Besides, solutions of the HQP are optimal to the current robot configuration, but not w.r.t. global tasks. In other words, the locally optimal controllers might drive the controlled robotic systems to disadvantageous configurations in the context of global tasks [161]. Finally, the HQP control structure may cause torque peaks and oscillations [141], attributed to its limited (one step) prediction.

3) MPC schemes: Model predictive controllers have been proposed to address drawbacks of locally optimal controllers [161], [162]. Given that control performance is considered over a finite-time horizon [163], [164], model predictive control (MPC) provides a more powerful option to fulfill control objectives of multiple tasks while constraints are not violated. Nevertheless, task hierarchy in [161], [162] is realized by a weight-prioritized optimization problem [165]. It results in a soft task-prioritized inverse kinematics control scheme. When tasks conflict with each other, the highest-priority task, which is usually the primary or security-related work, will be adversely affected.

The torque-based task-prioritized MPC schemes were developed independently in [154], [155] for robotic systems. A single convex constrained optimization problem is constructed in [155] where the task hierarchy is addressed by a quadratic inequality constraint that tracking errors of high-priority tasks must be less than or equal to that of low-priority tasks. This results in a soft task hierarchy. Besides, the desired joint position and velocities are calculated using the null-space projection method, resulting again in risk of algorithmic singularity. In addition, predictions are generated based on the nominal mathematical equations of robotic systems while uncertainties and/or disturbances are not considered. For a single-task control problem, learning-based MPC methods [114], [116] were developed to improve robustness, where Gaussian processes (GP) and neural networks (NN) are employed to identify nonlinear models online. Unfortunately, GP and NN learning techniques further increase the computational complexity of MPC. SMC, being robust against uncertainties and efficient in computation, is combined with MPC in [43] to address modeling errors and external disturbances for one single task. However, when multiple tasks are considered, task hierarchy will be adversely affected by the compensating SMC method. To guarantee task hierarchy, the task-prioritized sliding variable for each layer is designed and then an operational space model predictive SMC was developed in [154]. Nevertheless, the task-prioritized sliding variable is designed using the null-space projection method, which means it still suffers from the risk of algorithmic singularity. Besides, the nominal mathematical model is needed. In addition, due to the introduced pseudo control law, constraints imposed on torques are nonlinear and non-convex and thus the considered optimal control problems (OCPs) are general nonlinear programming (NLP) problems whose convexity is not guaranteed. The Non-convex program-

ming problem whose solution is easy to fall into local optimum, is usually computationally demanding.

The permitted sampling period of robotic systems is usually down to hundreds or even thousands of a second, and thus with the general NLP solvers, such as IPOPT [166] and LOQO [167], it is hard to guarantee real-time control, finally causing feedback delays. The most popular and commonly used method is sequential quadratic programming (SQP) [168], [169], where a series of approximated QP problems is solved sequentially until the solution converges. SQP has been successfully applied on robotic systems [169], [170]. In [170], to simplify the calculation, inequalities are treated as soft constraints. Owing to the efficient SQP, the computational time is down to the order of milliseconds or tens of milliseconds [168]–[170]. However, for high-precision robotics systems, the sampling period is 1 ms [7], [33], [65], [94], [133], [137], [145]–[147], [171] since the control accuracy is in line with the sampling rate. The approximated algorithm which trades control performance for speed, such as real-time iteration (RTI), was developed [172] to avoid solving NLP iteratively. In RTI, a single convex QP that locally approximates the original optimization problem is solved per feedback step. It reduces computational time and has been applied on robot manipulators in practice [171]. Nevertheless, application of RTI and SQP, relies on accurate model of the controlled plant and stability problems arise in the presence of reference changes and/or large external disturbances [173]. In contrast to NLP solvers, QP solvers which are running at microseconds deliver solutions in a more reliable and efficient way [174], [175]. Therefore, it is appealing that the task-prioritized MPC scheme can be formulated into a linear form whose OCP can be cast to a QP.

4.1.2 Method and Contributions

In this chapter, a task-prioritized control scheme, hierarchical incremental MPC (HIMPC) is proposed for robotic systems modeled by uncertain Euler-Lagrange equations. To improve the robustness against uncertainties and disturbances, we first develop a robust incremental model in the global set of admissible states exploiting the TDE method. Then, the HIMPC is formulated with multi-level constrained optimal control problems (OCPs) sequentially ordered in accordance with task priorities. The state predictions are generated from the discretized incremental model. Task hierarchy is fulfilled through equality constraints on control signals for lower-priority tasks, based on the *dynamic consistency* principle. Moreover, each constrained OCP of the HIMPC is cast to a QP. The hierarchical feasibility of the HIMPC is investigated, and the existence and uniqueness properties of the solution are verified theoretically relying on the strict convexity of the QPs.

The contributions of this chapter are summarized as follows:

1) *Robust.* Different from existing task-prioritized MPC [154], [155] and optimization-based methods [61], [140], [151]–[153], system dynamics of the robotic system will not be required for the proposed controller. We will approximate both system dynamics and equations of motion of tasks using TDE. This model-free nature improves robustness against uncertainties and disturbances. Besides, TDE will allow that task priority constraints are set independent of the accurate inertia matrix. Thus, robustness of the controller in terms of tracking accuracy and also *dynamic consistency* is enhanced.

2) *Computationally Efficient.* Relying on the TDE method will not only improve the

robustness of the proposed method but also simplify the nonlinear equations to linear ones. The proposed HIMPC is essentially a linear MPC and each constrained OCP can be cast to a QP. Compared with the nonlinear task-prioritized MPC schemes developed in [154], [155], the proposed HIMPC decreases computational complexity dramatically, which makes it possible to realize real-time control in milliseconds.

3) *Singularity-Free.* The null-space projection idea will not be employed in this approach, and task hierarchy is realized by imposing equality constraints on input signals for lower-priority tasks. Since no inverse calculation is involved in these equality constraint equations, algorithmic singularity is avoided. Besides, the inverse calculation of terms w.r.t. Jacobian matrices is also not involved in the constrained OCPs, and the Hessian matrix of each constrained OCP is verified to be positive definite. Thus, the proposed HIMPC is also a kinematically singularity-free method.

4.1.3 Outline of this Chapter

The rest of this chapter is organized as follows. In Section 4.2, control objective is introduced. In Section 4.3, equations of motion of tasks and system dynamics are approximated by incremental systems using TDE. Further, accuracy of this approximation method is analyzed. Section 4.4 presents the HIMPC. The hierarchical feasibility of HIMPC is analyzed and the existence and uniqueness properties of the solution are investigated. In Sections 4.6 and 4.5, simulation and experimental results are described and the effectiveness of the proposed method is verified. Finally, Section 4.7 draws conclusion and discussion on future research directions.

4.2 Control Objective

For a robot manipulator modeled by (A.1), a control task hierarchy including $r \in \mathbb{I}_{>0}$ levels is introduced and it is assumed that i-th task has a lower priority level than all previous $(i-1)$ tasks [150]. Especially, the first and r-th tasks have the highest and lowest priority level, respectively. The task-space coordinate $\mathbf{x}_i \in \mathbb{R}^{m_i}$ of the i-th task is

$$\mathbf{x}_i = \mathbf{f}_i(\mathbf{q}), \quad i \in \mathbb{I}_{[1,r]}, \tag{4.1}$$

where $\mathbf{f}_i(\mathbf{q}) : \mathbb{R}^n \to \mathbb{R}^{m_i}$ is the task mapping, on which the following assumption is made.

Assumption 3 (Certain and Continuously Differentiable Task Mapping)**.** *The considered task mapping functions are known exactly and also continuously differentiable.*

With this differentiability assumption, the Jacobian $\mathbf{J}_i(\mathbf{q}) \in \mathbb{R}^{m_i \times n}$ corresponding to the coordinate $\mathbf{x}_i$ is defined as

$$\mathbf{J}_i(\mathbf{q}) = \frac{\partial \mathbf{f}_i(\mathbf{q})}{\partial \mathbf{q}}. \tag{4.2}$$

Using **Assumption 3**, we conclude that all Jacobians are known functions with no uncertainties.

In this chapter, the task i is to make $\mathbf{x}_i$ track a desired reference trajectory $\mathbf{x}_{i\mathrm{d}}$ and realize the following target motion dynamics in free space [145]:

$$\ddot{\tilde{\mathbf{x}}}_i + \mathbf{K}_{\mathrm{V}_i}\dot{\tilde{\mathbf{x}}}_i + \mathbf{K}_{\mathrm{P}_i}\tilde{\mathbf{x}}_i = 0, \tag{4.3}$$

where $\tilde{\mathbf{x}}_i := \mathbf{x}_i - \mathbf{x}_{i\mathrm{d}}$ is the tracking error, and $\mathbf{K}_{\mathrm{V}_i} \succ 0$ and $\mathbf{K}_{\mathrm{P}_i} \succ 0$ denote damping and stiffness matrices respectively, both of which are in diagonal forms in this chapter.

Non-smooth reference trajectories can cause damage to mechanical systems due to sharp actuator changes. Thus, the reference trajectory $\mathbf{x}_{i\mathrm{d}}$ is assumed to be bounded and smooth.

Assumption 4 (Bounded and Smooth Reference Trajectory,[89])**.** *The reference trajectory* $\mathbf{x}_{i\mathrm{d}}$ *is bounded and smooth, satisfying* $0 \leq \underline{r}_i \leq \|\mathbf{x}_{i\mathrm{d}}\| \leq \overline{r}_i < \infty$, $0 \leq \underline{\dot{r}}_i \leq \|\dot{\mathbf{x}}_{i\mathrm{d}}\| \leq \overline{\dot{r}}_i < \infty$, *and* $0 \leq \underline{\ddot{r}}_i \leq \|\ddot{\mathbf{x}}_{i\mathrm{d}}\| \leq \overline{\ddot{r}}_i < \infty$.

Note that exact values of $\underline{r}_i$, $\overline{r}_i$, $\underline{\dot{r}}_i$, $\overline{\dot{r}}_i$, $\underline{\ddot{r}}_i$ and $\overline{\ddot{r}}_i$ in **Assumption 4** are not required for the controller design.

We aim to design a strict task-prioritized controller which is robust and singularity-free while physical constraints of the robot manipulator, such as constraints on joint positions, velocities, and torques, are satisfied. The following box constraints are considered: $\mathbf{q}_{\min} \leq \mathbf{q} \leq \mathbf{q}_{\max}$, $\dot{\mathbf{q}}_{\min} \leq \dot{\mathbf{q}} \leq \dot{\mathbf{q}}_{\max}$, and $\boldsymbol{\tau}_{\min} \leq \boldsymbol{\tau} \leq \boldsymbol{\tau}_{\max}$, where $\bullet_{\min}, \bullet_{\max}$ denote specific lower/upper bounds of $\bullet$.

Remark 18 (Reasonability of **Assumption 3**)**.** *In this chapter, the task-space position coordinate of a specified point on the link, joint, or end-effector of the robot manipulator is considered for one task. Thus, if the Denavit-Hartenberg (D-H) parameters of the robotic system are obtained, mapping functions are known exactly and in general are continuously differentiable. Therefore,* ***Assumption 3*** *is reasonable.*

Remark 19 (Release Assumptions on Singularity-Free Task Space)**.** *We will not add an assumption here on the tasks to be executable without running into singularities. The proposed method will allow to execute singular combinations of tasks. In literature, it is common to avoid singularities by restricting allowed tasks, and one assumption is made that task space is singularity-free. However, this assumption delimits the feasible task space of the robot manipulator. In this chapter, to ensure sufficient task space for the robotic system and to guarantee safety, we will strive for designing a singularity-free control method. Thus, the assumption on singularity-free task space is released.*

4.3 Robust Incremental Systems

In this section and the following Section 3.2, a task-prioritized control scheme is developed. We aim at taking into account optimality, input and state constraints, robustness, and strict task hierarchy, simultaneously. To realize optimality and address input and state constraints, the task-prioritized control scheme is developed in the framework of MPC. Taking into account the unknown system dynamics and also the computational complexity of the algorithm, the TDE method is used to approximate equations of motion of tasks and system dynamics to avoid online identification or other time-consuming operations. Besides, the approximation accuracy of the resulting TDE-based incremental systems is analyzed.

4.3.1 Derivation of the Incremental Systems

In this subsection, uncertain equations of motion of tasks and system dynamics will be approximated using TDE, and incremental systems are obtained, which are used to generate state predictions.

As stated in control objective (see Section 4.2), we aim to impose constraints on torques. Thus, the torque is selected as the control variable in the proposed task-prioritized controller. First, the equations of motion of tasks are derived with the torques being the inputs. With (A.1) and (4.2), the equation of motion of the i-th task is obtained:

$$\ddot{\mathbf{x}}_i \overset{(4.2)}{=} \dot{\mathbf{J}}_i\dot{\mathbf{q}} + \mathbf{J}_i\ddot{\mathbf{q}} \overset{(A.1)}{=} \dot{\mathbf{J}}_i\dot{\mathbf{q}} + \mathbf{J}_i\mathbf{M}^{-1}\left(\boldsymbol{\tau} - \mathbf{C}(\mathbf{q},\dot{\mathbf{q}}) - \mathbf{G}(\mathbf{q}) - \mathbf{F}(\dot{\mathbf{q}})\right). \tag{4.4}$$

According to (4.4), the equation of motion is also uncertain. This is because it includes uncertain system dynamics terms and external disturbance. To deal with these uncertainties and reduce dependency on the concrete mathematical model, the TDE technique[7], [28], [33], [36], [133] is employed to approximate the equation of motion (4.4), which involves two steps.

Step 1: Separating Uncertain Terms from Known Terms. It is observed that uncertainties of the equation of motion (4.4) are originated from the system dynamics (A.1). Thus, we will consider (A.1) first. Introducing a diagonal positive definite matrix $\bar{\mathbf{M}}$, (A.1) is transformed into the following form:

$$\bar{\mathbf{M}}\ddot{\mathbf{q}} + \underbrace{\left(\mathbf{M} - \bar{\mathbf{M}}\right)\ddot{\mathbf{q}} + \mathbf{C}(\mathbf{q},\dot{\mathbf{q}})\dot{\mathbf{q}} + \mathbf{G}(\mathbf{q}) + \mathbf{F}(\dot{\mathbf{q}})}_{\mathbf{H_q}} = \boldsymbol{\tau}. \tag{4.5}$$

Using (4.5), the equation of motion (4.4) is rewritten as:

$$\ddot{\mathbf{x}}_i = \underbrace{\dot{\mathbf{J}}_i\dot{\mathbf{q}} - \mathbf{J}_i\bar{\mathbf{M}}^{-1}\mathbf{H_q}}_{\mathbf{H_x}} + \mathbf{J}_i\bar{\mathbf{M}}^{-1}\boldsymbol{\tau} \tag{4.6}$$

where $\mathbf{H_x}$ is also uncertain/unknown because of the lumped uncertain nonlinear function $\mathbf{H_q}$ in (4.5).

Step 2: Using the Time-Delay Signals/Functions to Approximate the Unknown Terms. The value of $\mathbf{H_x}$ at time t is approximated by that of $\mathbf{H_x}$ at time $(t-L)$ for a sufficiently small delay time L [7], [33], [133]:

$$(\mathbf{H_x})_t \cong (\mathbf{H_x})_{(t-L)}. \tag{4.7}$$

We abbreviate $\ddot{\mathbf{x}}_{i,0} := (\ddot{\mathbf{x}}_i)_{(t-L)}$, $\boldsymbol{\tau}_0 := \boldsymbol{\tau}_{(t-L)}$, and $\mathbf{J}_{i,0} = (\mathbf{J}_i)_{(t-L)}$ for simplicity. From (4.6) and (4.7), one obtains TDE of $\mathbf{H_x}$, $(\mathbf{H_x})_{(t-L)}$ as follows [133]:

$$(\mathbf{H_x})_{(t-L)} = \ddot{\mathbf{x}}_{i,0} - \mathbf{J}_{i,0}\bar{\mathbf{M}}^{-1}\boldsymbol{\tau}_0. \tag{4.8}$$

Comparing (4.6) with (4.8), we learn that input matrices ($\mathbf{J}_i\bar{\mathbf{M}}^{-1}$ and $\mathbf{J}_{i,0}\bar{\mathbf{M}}^{-1}$) are different. We will unify input matrices, considering the fact that variations of Jacobian $\mathbf{J}_i$ in a short period is negligible. In other words, for a sufficiently small L,

$$\mathbf{J}_{i,0} \cong \mathbf{J}_i. \tag{4.9}$$

Now, taking into account (4.9), we have an alternative TDE of $\mathbf{H_x}$, $\hat{\mathbf{H}}_\mathbf{x}$ as follows:

$$\hat{\mathbf{H}}_\mathbf{x} = \ddot{\mathbf{x}}_{i,0} - \mathbf{J}_i\bar{\mathbf{M}}^{-1}\boldsymbol{\tau}_0. \tag{4.10}$$

Finally, we obtain the incremental version of (4.4) with the combination of (4.6) and (4.10):

$$\ddot{\mathbf{x}}_i = \ddot{\mathbf{x}}_{i,0} + \mathbf{J}_i\bar{\mathbf{M}}^{-1}\Delta\boldsymbol{\tau} + \boldsymbol{\varepsilon}_{\mathbf{x}} \tag{4.11}$$

where $\Delta\boldsymbol{\tau} := \boldsymbol{\tau} - \boldsymbol{\tau}_0$ is the incremental control signal, and $\boldsymbol{\varepsilon}_{\mathbf{x}} := \mathbf{H}_{\mathbf{x}} - \hat{\mathbf{H}}_{\mathbf{x}}$ is the TDE error which is considered as a disturbance to the incremental system (4.11). Note that only current values of $\ddot{\mathbf{x}}_i$ and $\boldsymbol{\tau}$ are used in (4.10) to complete the approximation while complex and uncertain functions, such as $\mathbf{M}(\mathbf{q})$, $\mathbf{C}(\mathbf{q}, \dot{\mathbf{q}})$, $\mathbf{G}(\mathbf{q})$, and $\mathbf{F}(\mathbf{q})$, are not required.

For $\boldsymbol{\varepsilon}_{\mathbf{x}} = \mathbf{0}$, the nominal incremental system is obtained:

$$\ddot{\mathbf{x}}_i = \ddot{\mathbf{x}}_{i,0} + \mathbf{J}_i\bar{\mathbf{M}}^{-1}\Delta\boldsymbol{\tau}. \tag{4.12}$$

In what follows, the Euler method is used to obtain a discrete-time version of the nominal incremental system, which is used to generate predictions of $\mathbf{x}_i$. In accordance with [133], to guarantee the delay time is sufficiently small, the sampling period T_s is selected as L. Considering the sufficiently high sampling rate, discretization error is ignored. Thus, we have

$$\bar{\mathbf{x}}_i(k+1) = \mathbf{A}_{11}\bar{\mathbf{x}}_i(k) + \mathbf{A}_{12}\bar{\mathbf{x}}_i(k-1) + \mathbf{B}_{1,i}\Delta\boldsymbol{\tau}(k) \tag{4.13}$$

where

$$\bar{\mathbf{x}}_i := \mathrm{col}\,(\mathbf{x}_i, \dot{\mathbf{x}}_i, \ddot{\mathbf{x}}_i),\ \mathbf{A}_{11} := \begin{bmatrix} \mathbf{I} & T_s\mathbf{I} & \mathbf{O} \\ \mathbf{O} & 2\mathbf{I} & \mathbf{O} \\ \mathbf{O} & \mathbf{O} & \mathbf{I} \end{bmatrix},\ \mathbf{A}_{12} := \begin{bmatrix} \mathbf{O} & \mathbf{O} & \mathbf{O} \\ \mathbf{O} & -\mathbf{I} & \mathbf{O} \\ \mathbf{O} & \mathbf{O} & \mathbf{O} \end{bmatrix},\ \mathbf{B}_{1,i} := \begin{bmatrix} \mathbf{O} \\ \mathbf{J}_i\bar{\mathbf{M}}^{-1}T_s \\ \mathbf{J}_i\bar{\mathbf{M}}^{-1} \end{bmatrix}.$$

We define a stack variable $\vec{\mathbf{x}}_i(k+1) := \mathrm{col}\,(\bar{\mathbf{x}}_i(k+1), \bar{\mathbf{x}}_i(k))$, and rewrite (4.13) as a canonical linear equation:

$$\vec{\mathbf{x}}_i(k+1) = \mathbf{A}_1\vec{\mathbf{x}}_i(k) + \mathbf{B}_{1i}\Delta\boldsymbol{\tau}(k) \tag{4.14}$$

with $\mathbf{A}_1 := \begin{bmatrix} \mathbf{A}_{11} & \mathbf{A}_{12} \\ \mathbf{I} & \mathbf{O} \end{bmatrix}$, $\mathbf{B}_{1i} := \begin{bmatrix} \mathbf{B}_{1,i} \\ \mathbf{O} \end{bmatrix}$.

In addition to predictions of task-space coordinates ($\mathbf{x}_i$), we will need to predict joint space behavior ($\mathbf{q}$ and $\dot{\mathbf{q}}$) to be able to evaluate constraints in joint space during predictions. Unfortunately, as we assumed in Section A.1, the system dynamics (A.1) is uncertain in this article. Alternatively, the TDE method will also be used to approximate the system dynamics.

Same to procedures in [133], using TDE method, i.e., $\mathbf{H}_{\mathbf{q}} \cong (\mathbf{H}_{\mathbf{q}})_{(t-L)}$, the following incremental system is obtained from (4.5).

$$\ddot{\mathbf{q}} = \ddot{\mathbf{q}}_0 + \bar{\mathbf{M}}^{-1}\left(\Delta\boldsymbol{\tau} + \boldsymbol{\varepsilon}_{\mathbf{q}}\right) \tag{4.15}$$

where $\boldsymbol{\varepsilon}_{\mathbf{q}} := (\mathbf{H}_{\mathbf{q}})_{(t-L)} - \mathbf{H}_{\mathbf{q}}$ is also the TDE error.

Let $\boldsymbol{\varepsilon}_{\mathbf{q}} = \mathbf{0}$, we also obtain the nominal incremental system from (4.15):

$$\ddot{\mathbf{q}} = \ddot{\mathbf{q}}_0 + \bar{\mathbf{M}}^{-1}\Delta\boldsymbol{\tau}. \tag{4.16}$$

Let $\bar{\mathbf{q}} := \mathrm{col}(\mathbf{q}, \dot{\mathbf{q}})$, similar to (4.13), discritizing (4.16) yields the following discrete-time system:

$$\bar{\mathbf{q}}(k+1) = \mathbf{A}_{21}\bar{\mathbf{q}}(k) + \mathbf{A}_{22}\bar{\mathbf{q}}(k-1) + \mathbf{B}_{21}\Delta\boldsymbol{\tau}(k) \tag{4.17}$$

with
$\mathbf{A}_{21} := \begin{bmatrix} \mathbf{I} & T_s\mathbf{I} \\ \mathbf{O} & 2\mathbf{I} \end{bmatrix}$, $\mathbf{A}_{22} := \begin{bmatrix} \mathbf{O} & \mathbf{O} \\ \mathbf{O} & -\mathbf{I} \end{bmatrix}$, $\mathbf{B}_{21} := \begin{bmatrix} \mathbf{O} \\ T_s\bar{\mathbf{M}}^{-1} \end{bmatrix}$.

Similar to (4.14), let $\vec{\mathbf{q}}(k+1) := \mathrm{col}\,(\bar{\mathbf{q}}(k+1), \bar{\mathbf{q}}(k))$, a canonical linear equation is also obtained:

$$\vec{\mathbf{q}}(k+1) = \mathbf{A}_2\vec{\mathbf{q}}(k) + \mathbf{B}_2\Delta\boldsymbol{\tau}(k) \tag{4.18}$$

with $\mathbf{A}_2 := \begin{bmatrix} \mathbf{A}_{21} & \mathbf{A}_{22} \\ \mathbf{I} & \mathbf{O} \end{bmatrix}$, $\mathbf{B}_2 := \begin{bmatrix} \mathbf{B}_{21} \\ \mathbf{O} \end{bmatrix}$.

Now finally, using an auxiliary matrix $\bar{\mathbf{M}}$, we found discrete-time approximations of equations of motion and system dynamics (cf. (4.14) and (4.18)). We will use (4.14) and (4.18) to generate state predictions over the prediction horizon while TDE errors are ignored.

Remark 20 (How Does This TDE Formulation Avoid Singularity?)**.** *In [145], the TDE method was yet applied to task-space control. Unfortunately, kinematic and algorithmic singularities are not avoided. In the presented TDE formulation (see* (4.12)*), any inversion of the terms involving Jacobian matrices is not required. Thus, the presented TDE formulation has the potential for avoiding singularity.*

Remark 21 (Why Including $\dot{\mathbf{J}}_i\dot{\mathbf{q}}$ in the Lumped Function $\mathbf{H}_\mathbf{x}$)**.** *According to* ***Assumption 3****, the mapping function* $\mathbf{f}_i(\mathbf{q})$ *is known exactly, which also delivers a certain time derivative of Jacobian (*$\dot{\mathbf{J}}_i$*). Thus, it would be not necessary to include the term* $\dot{\mathbf{J}}_i\dot{\mathbf{q}}$ *in the lumped function* $\mathbf{H}_\mathbf{x}$*. However, if the term* $\dot{\mathbf{J}}_i\dot{\mathbf{q}}$ *is excluded in* $\mathbf{H}_\mathbf{x}$*, we can not obtain a canonical linear system approximation (compare* (4.14)*) and the linear MPC framework that is introduced in Section 3.2 has to be replaced by a nonlinear MPC framework. However, nonlinear MPC is computationally often so demanding that real-time execution is impossible. Besides, a linear formulation will allow more in-depth and more accessibly theoretical analysis of the controller performance. In addition, in accordance with its continuity property, the term* $\dot{\mathbf{J}}_i\dot{\mathbf{q}}$ *can be accurately approximated by time-delay signals with a sufficiently high sampling rate. Thus,* $\dot{\mathbf{J}}\dot{\mathbf{q}}$ *is included in the lumped function* $\mathbf{H}_\mathbf{x}$*.*

4.3.2 Analysis of Approximation Accuracy

Although the exact mathematical model of the controlled robotic system is not required, there is a discrepancy between real equations ((A.1) and (4.4)) and the nominal incremental systems ((4.12) and (4.16)) because of inevitable TDE errors. In this subsection, we will show that incremental systems exhibit higher approximation accuracy than that of the nominal nonlinear mathematical model (abbreviated as nominal model in Section 4.3.2).

Denote the nominal inertial matrix, Coriolis/centrifugal matrix, gravitational matrix, and viscous matrix as $\hat{\mathbf{M}}$, $\hat{\mathbf{C}}$, $\hat{\mathbf{G}}$, and $\hat{\mathbf{F}}$, respectively. According to (4.4), the following approximated equation of motion of the i-th task is obtained:

$$\ddot{\hat{\mathbf{x}}}_i = \dot{\mathbf{J}}_i\dot{\mathbf{q}} - \mathbf{J}_i\hat{\mathbf{M}}^{-1}\hat{\mathbf{N}} + \mathbf{J}_i\hat{\mathbf{M}}^{-1}\boldsymbol{\tau} \tag{4.19}$$

where $\hat{\mathbf{x}}_\mathrm{i}$ is the approximation generated by the nominal model, and $\hat{\mathbf{N}} := \hat{\mathbf{C}}\dot{\mathbf{q}} + \hat{\mathbf{G}} + \hat{\mathbf{F}}$. To obtain the approximation error, we recall the real system dynamics (A.1) and transform (A.1) into the following form using $\hat{\mathbf{M}}$ [145]:

$$\hat{\mathbf{M}}\ddot{\mathbf{q}} + \tilde{\mathbf{M}}\ddot{\mathbf{q}} + \mathbf{N} = \boldsymbol{\tau} \tag{4.20}$$

where $\tilde{\mathbf{M}} := \mathbf{M} - \hat{\mathbf{M}}$ is the modeling error of the inertial matrix $\mathbf{M}$, and $\mathbf{N} := \mathbf{C}\dot{\mathbf{q}} + \mathbf{G} + \mathbf{F}$ is a lumped nonlinear dynamics term. Then, according to (4.4) and (4.20), the equation of motion of the i-th task is rewritten as

$$\ddot{\mathbf{x}}_i = \dot{\mathbf{J}}_i\dot{\mathbf{q}} - \mathbf{J}_i\hat{\mathbf{M}}^{-1}\left(\tilde{\mathbf{M}}\ddot{\mathbf{q}} + \mathbf{N}\right) + \mathbf{J}_i\hat{\mathbf{M}}^{-1}\boldsymbol{\tau}. \tag{4.21}$$

From (4.19) with (4.21), the approximation error $\boldsymbol{\beta}_i := \ddot{\hat{\mathbf{x}}}_i - \ddot{\mathbf{x}}_i$ is obtained:

$$\boldsymbol{\beta}_i = \mathbf{J}_i\hat{\mathbf{M}}^{-1}\left(\tilde{\mathbf{M}}\ddot{\mathbf{q}} + \tilde{\mathbf{N}}\right) \tag{4.22}$$

where $\tilde{\mathbf{N}} := \mathbf{N} - \hat{\mathbf{N}}$ is the modelling error of $\mathbf{N}$.

Next, the approximation error of the incremental system (4.12) is derived. Similar to (4.21), we obtain the equation of motion with the constant positive definite diagonal matrix $\bar{\mathbf{M}}$ in (4.6). Comparing (4.11) with (4.12), one can observe that the approximation error of (4.12) is the TDE error $\boldsymbol{\varepsilon}_{\mathbf{x}}$. Besides, for a sufficiently small sampling period, one has

$$\dot{\mathbf{J}}_i\dot{\mathbf{q}} \approx \left(\dot{\mathbf{J}}_i\dot{\mathbf{q}}\right)_{(t-L)}. \tag{4.23}$$

Thus, combining (4.6), (4.8), (4.9), (4.10), and (4.23) results in

$$\begin{aligned}\boldsymbol{\varepsilon}_{\mathbf{x}} = \mathbf{H}_{\mathbf{x}} - \hat{\mathbf{H}}_{\mathbf{x}} &\overset{(4.8),(4.9),(4.10)}{\approx} \mathbf{H}_{\mathbf{x}} - (\mathbf{H}_{\mathbf{x}})_{(t-L)} \\ &\overset{(4.6),(4.23)}{\approx} \mathbf{J}_i\bar{\mathbf{M}}^{-1}\left[\left(\mathbf{M}-\bar{\mathbf{M}}\right)\ddot{\mathbf{q}} - \left(\mathbf{M}_{(t-L)}-\bar{\mathbf{M}}\right)\ddot{\mathbf{q}}_{(t-L)} + \boldsymbol{\varepsilon}_{\mathbf{N}}\right]\end{aligned} \tag{4.24}$$

where $\boldsymbol{\varepsilon}_{\mathbf{N}} := \mathbf{N} - \mathbf{N}_{(t-L)}$ is the TDE error of $\mathbf{N}$.

In what follows, the approximation error for predictions of joint space coordinates is derived. If the nominal model is available, in accordance with (A.1), the following nominal system dynamics (4.25) is used to estimate $\mathbf{q}$ and $\dot{\mathbf{q}}$, where $\hat{\mathbf{q}}$ is the approximation.

$$\ddot{\hat{\mathbf{q}}} = -\hat{\mathbf{M}}^{-1}\hat{\mathbf{N}} + \hat{\mathbf{M}}^{-1}\boldsymbol{\tau}. \tag{4.25}$$

From (4.20) and (4.25), the dynamics approximation error $\boldsymbol{\gamma} := \ddot{\hat{\mathbf{q}}} - \ddot{\mathbf{q}}$ for the nominal case is obtained:

$$\boldsymbol{\gamma} = \hat{\mathbf{M}}^{-1}\left(\tilde{\mathbf{M}}\ddot{\mathbf{q}} + \tilde{\mathbf{N}}\right). \tag{4.26}$$

In an analogous manner, from (4.15) with (4.16), the approximation error of (4.16), $\boldsymbol{\delta} := \ddot{\hat{\mathbf{q}}}_{\text{inc}} - \ddot{\mathbf{q}}$ (where $\hat{\mathbf{q}}_{\text{inc}}$ is the joint position approximation using (4.16)), is obtained

$$\boldsymbol{\delta} = \bar{\mathbf{M}}^{-1}\left[\left(\mathbf{M} - \bar{\mathbf{M}}\right)\ddot{\mathbf{q}} - \left(\mathbf{M}_{(t-L)} - \bar{\mathbf{M}}\right)\ddot{\mathbf{q}}_{(t-L)} + \boldsymbol{\varepsilon}_{\mathbf{N}}\right]. \tag{4.27}$$

For the TDE approximation (cf. (4.24) and (4.27)), we learn that, if the delay time L (sampling period T_s) is sufficiently small, the inertia modelling error $\left(\mathbf{M} - \bar{\mathbf{M}}\right)\ddot{\mathbf{q}}$ is compensated by their time-delay values $\left(\mathbf{M}_{(t-L)} - \bar{\mathbf{M}}\right)\ddot{\mathbf{q}}_{(t-L)}$ effectively, and the smaller is the sampling period, the smaller is the TDE error. While for nominal model cases, there are no terms to compensate for modelling error. Besides, if the sampling period is sufficiently small, then the value of $\boldsymbol{\varepsilon}_{\mathbf{N}}$ (TDE error of $\mathbf{N}$) will be less than that of $\tilde{\mathbf{N}}$ (the modeling error of $\mathbf{N}$). In practice, a digital control system can be regarded as a continuous system when the sampling rate is faster than 30 times the system bandwidth [134]. According to the

continuity property, $\boldsymbol{\varepsilon_N}$ is small enough if the sampling rate is sufficiently high. Therefore, for a sufficiently small sampling period, the incremental systems derived using TDE exhibit high approximation accuracy and show strong robustness against inertia modeling error.

So far, we have derived incremental systems which will be used to determine state predictions and also verified their high approximation accuracy if a sufficiently small sampling period is employed. Then, the task-prioritized MPC scheme will be developed in Section 3.2.

4.4 Hierarchical Incremental Model Predictive Control

In this section, the task-prioritized control scheme, hierarchical incremental MPC (HIMPC), is developed as a series of constrained OCPs, where appropriate constraints are used to enforce the task hierarchy. Then, the hierarchical feasibility of the proposed HIMPC and existence and uniqueness of the OCP solutions are shown.

4.4.1 Method

In this subsection, at first, the stage cost for one task is first introduced, which is a basis to develop the following constrained OCPs.

The stage cost is designed to take into account the target motion dynamics (4.3) as well as controller oscillations, energy efficiency, and actuator protection. Thus, the predicted motion dynamics error and the control signal are considered in the stage cost.

In accordance with (4.3), the predicted motion dynamics error $\mathbf{e}(\vec{\mathbf{x}}_{i,k+j+1|k})$ at time k is defined as

$$\begin{aligned}\mathbf{e}(\vec{\mathbf{x}}_{i,k+j+1|k}) :=& \ddot{\tilde{\mathbf{x}}}_{i,k+j+1|k} + \mathbf{K}_{\mathrm{V}_i}\dot{\tilde{\mathbf{x}}}_{i,k+j+1|k} + \mathbf{K}_{\mathrm{P}_i}\tilde{\mathbf{x}}_{i,k+j+1|k} \\ =& \bar{\mathbf{K}}_i\vec{\mathbf{x}}_{i,k+j+1|k} - \mathbf{K}_i\bar{\mathbf{x}}_{i\mathrm{d}}(k+j+1)\end{aligned} \tag{4.28}$$

Here $\vec{\mathbf{x}}_{i,k+j+1|k} := \mathrm{col}\left(\bar{\mathbf{x}}_{i,k+j+1|k}, \bar{\mathbf{x}}_{i,k+j|k}\right)$, $\tilde{\mathbf{x}}_{i,k+j|k} := \mathbf{x}_{i,k+j+1|k} - \mathbf{x}_{i\mathrm{d}}(k+j+1)$, $\bar{\mathbf{K}}_i := [\mathbf{K}_i, \mathbf{O}]$, $\mathbf{K}_i := [\mathbf{K}_{\mathrm{P}_i}, \mathbf{K}_{\mathrm{V}_i}, \mathbf{I}]$, $\bar{\mathbf{x}}_{i\mathrm{d}} := \mathrm{col}(\mathbf{x}_{i\mathrm{d}}, \dot{\mathbf{x}}_{i\mathrm{d}}, \ddot{\mathbf{x}}_{i\mathrm{d}})$, $j \in \mathbb{I}_{[0,N-1]}$ is an intermediate variable for time instance, N is the length of the prediction horizon, and $\bullet_{k+j|k}$ stands for the predicted variables, in particular, $\bullet_{k|k} := \bullet(k)$, and $\mathbf{x}_{i,k+j+1|k}$ is calculated using the discrete-time incremental system (4.14). I.e., for all $j \in \mathbb{I}_{[0,N-1]}$,

$$\vec{\mathbf{x}}_{i,k+j+1|k} = \mathbf{A}_1\vec{\mathbf{x}}_{i,k+j|k} + \mathbf{B}_{1i}\Delta\boldsymbol{\tau}_{k+j|k} \tag{4.29}$$

with $\vec{\mathbf{x}}_{i,k|k} := \mathrm{col}\left(\bar{\mathbf{x}}_{i,k|k}, \bar{\mathbf{x}}_{i,k-1|k}\right)$ and $\bar{\mathbf{x}}_{i,k-1|k} := \bar{\mathbf{x}}_i(k-1)$. To obtain a canonical linear system, the matrix $\mathbf{B}_{1i}$ is considered as a constant matrix over the current prediction horizon and it will be updated in the next prediction horizon according to the new measurement $\mathbf{q}(k+1)$. Note that this simplification is reasonable since variations of the joint position in a short period can be ignored (see **Remark 22**).

Here, the incremental control signal $\Delta\boldsymbol{\tau}$, not $\boldsymbol{\tau}$, is considered in the stage cost, since the equations of motion of tasks and system dynamics are all approximated by incremental systems. Thus, at time k, the following stage cost for task i is defined:

$$\ell\left(\vec{\mathbf{x}}_{i,k+j+1|k}, \Delta\boldsymbol{\tau}_{k+j|k}\right) = \|\mathbf{e}(\vec{\mathbf{x}}_{i,k+j+1|k})\|^2_{\mathbf{Q}_i} + \|\Delta\boldsymbol{\tau}_{k+j|k}\|^2_{\mathbf{R}_i} \tag{4.30}$$

where $\mathbf{Q}_i \succ 0$ and $\mathbf{R}_i \succ 0$ are weighting matrices.

Now the stage costs of tasks are combined and deliver the hierarchical MPC framework, HIMPC. Therefore, a constrained OCP for each task is introduced, starting with the task 1 (highest-priority task). The task hierarchy will be realized by constraints to the OCPs of lower-priority tasks.

Defining an admissible input trajectory $\Delta\bar{\boldsymbol{\tau}}_1 := \left[\Delta\boldsymbol{\tau}_{1,k|k}, \cdots, \Delta\boldsymbol{\tau}_{1,k+N-1|k}\right]$, the constrained OCP (**Problem** 1) for task 1 is introduced.

Problem 1**:**

$$\Delta\bar{\boldsymbol{\tau}}_1^* = \arg\min_{\Delta\bar{\boldsymbol{\tau}}_1} \sum_{j=0}^{N-1} \ell\left(\vec{\mathbf{x}}_{1,k+j+1|k}, \Delta\boldsymbol{\tau}_{1,k+j|k}\right) \tag{4.31a}$$

s.t.

$$\vec{\mathbf{x}}_{1,k+j+1|k} = \mathbf{A}_1\vec{\mathbf{x}}_{1,k+j|k} + \mathbf{B}_{11}\Delta\boldsymbol{\tau}_{1,k+j|k} \tag{4.31b}$$

$$\vec{\mathbf{q}}_{1,k+j+1|k} = \mathbf{A}_2\vec{\mathbf{q}}_{1,k+j|k} + \mathbf{B}_2\Delta\boldsymbol{\tau}_{1,k+j|k} \tag{4.31c}$$

$$\mathbf{q}_{\min} \leq \mathbf{q}_{1,k+j+1|k} \leq \mathbf{q}_{\max} \tag{4.31d}$$

$$\dot{\mathbf{q}}_{\min} \leq \dot{\mathbf{q}}_{1,k+j+1|k} \leq \dot{\mathbf{q}}_{\max} \tag{4.31e}$$

$$\boldsymbol{\tau}_{\min} \leq \boldsymbol{\tau}_0 + \sum_{s=0}^{j} \Delta\boldsymbol{\tau}_{1,k+s|k} \leq \boldsymbol{\tau}_{\max} \tag{4.31f}$$

where $j \in \mathbb{I}_{[0,N-1]}$, $\vec{\mathbf{q}}_{1,k+j+1|k}$ is the joint state prediction under the action of the control signal $\Delta\boldsymbol{\tau}_{1,k+j|k}$. Equality constraints (4.31b) and (4.31c) are employed to generate predictions $\vec{\mathbf{x}}_{1,k+j+1|k}$ and $\vec{\mathbf{q}}_{1,k+j+1|k}$ over the horizon while constraints (4.31d), (4.31e), and (4.31f) are imposed on joint position, velocity, and torques, respectively. For **Problem** 1, $\Delta\bar{\boldsymbol{\tau}}_1^*$ is the optimal input trajectory. In case there is only one task, the first column of the optimal input trajectory is applied to the system directly. For multiple tasks, $\Delta\boldsymbol{\tau}_{1,k|k}^*$ is just an auxiliary control input that will be considered in the constrained OCPs of lower-priority tasks while only task r, the lowest priority task, will finally deliver a control input that is applied to the system.

To realize task hierarchy, relying on the *dynamic consistency* principle [143] (i.e., high-priority tasks will not be affected by the torques designed for low-priority tasks), the following equality constraints will be imposed on control signals when **Problem** i ($i \in \mathbb{I}_{[2,r]}$) is formulated for task i:

$$\mathbf{J}_{p,k}\bar{\mathbf{M}}^{-1}\Delta\bar{\boldsymbol{\tau}}_p^* = \mathbf{J}_{p,k}\bar{\mathbf{M}}^{-1}\Delta\bar{\boldsymbol{\tau}}_i, \forall p \in \mathbb{I}_{[1,i-1]} \tag{4.32}$$

Here $\Delta\bar{\boldsymbol{\tau}}_p^*$ and $\Delta\bar{\boldsymbol{\tau}}_i$ are the optimal input trajectory and one admissible input trajectory for the p-th and i-th layer constrained OCPs respectively, and $\mathbf{J}_{p,k}$ is the Jacobian matrix for task p at time k. From (4.12) and (4.32), it is observed that the optimal motion of task p will not be disturbed by optimal controllers determined for lower-priority tasks. It is worth mentioning that no null-space projections are used and thus matrix inversion to determine the prioritized Jacobian is not necessary here. Thus, the algorithmic singularity problem is avoided.

With the task priority constraint (4.32), the following **Problem** i for task i ($i \in \mathbb{I}_{[2,r]}$) is introduced:

Problem i ($i \in \mathbb{I}_{[2,r]}$):

$$\Delta\bar{\boldsymbol{\tau}}_i^* = \arg\min_{\Delta\bar{\boldsymbol{\tau}}_i} \sum_{j=0}^{N-1} \ell\left(\vec{\mathbf{x}}_{i,k+j+1|k}, \Delta\boldsymbol{\tau}_{i,k+j|k}\right) \tag{4.33a}$$

s.t.

$$\vec{\mathbf{x}}_{i,k+j+1|k} = \mathbf{A}_1\vec{\mathbf{x}}_{i,k+j|k} + \mathbf{B}_{1i}\Delta\boldsymbol{\tau}_{i,k+j|k} \tag{4.33b}$$

$$\vec{\mathbf{q}}_{i,k+j+1|k} = \mathbf{A}_2\vec{\mathbf{q}}_{i,k+j|k} + \mathbf{B}_2\Delta\boldsymbol{\tau}_{i,k+j|k} \tag{4.33c}$$

$$\mathbf{q}_{\min} \leq \mathbf{q}_{i,k+j+1|k} \leq \mathbf{q}_{\max} \tag{4.33d}$$

$$\dot{\mathbf{q}}_{\min} \leq \dot{\mathbf{q}}_{i,k+j+1|k} \leq \dot{\mathbf{q}}_{\max} \tag{4.33e}$$

$$\boldsymbol{\tau}_{\min} \leq \boldsymbol{\tau}_0 + \sum_{s=0}^{j} \Delta\boldsymbol{\tau}_{i,k+s|k} \leq \boldsymbol{\tau}_{\max} \tag{4.33f}$$

$$\mathbf{J}_{p,k}\bar{\mathbf{M}}^{-1}\Delta\boldsymbol{\tau}^*_{p,k+j|k} = \mathbf{J}_{p,k}\bar{\mathbf{M}}^{-1}\Delta\boldsymbol{\tau}_{i,k+j|k}, \forall p \in \mathbb{I}_{[1,i-1]} \tag{4.33g}$$

It holds that $j \in \mathbb{I}_{[0,N-1]}$ and $\vec{\mathbf{q}}_{i,k+j+1|k}$ is the joint state prediction under the action of $\Delta\boldsymbol{\tau}_{i,k+j|k}$. Similar to **Problem** 1, (4.33b) and (4.33c) are equality constraints and (4.33d), (4.33e), and (4.33f) are inequality constraints. The difference between **Problem** 1 and **Problem** i ($i \in \mathbb{I}_{[2,r]}$) is the series of equality constraints (4.33g), which allows the enforcement of task hierarchy. $\mathbf{J}_{p,k}$ is considered as a constant matrix over the current prediction horizon. In this way, the equality constraint (4.33g) is an affine linear system, which is also the basis for analyzing the existence and uniqueness of the solution to **Problem** i.

The optimal control sequence $\Delta\bar{\boldsymbol{\tau}}_r^*$ is obtained after a series of constrained OCPs (from **Problem** 1 to **Problem** r) are solved. $\Delta\bar{\boldsymbol{\tau}}_r^*$ is not only the optimal solution to **Problem** r, but it also guarantees that optimal motion of tasks 1 to $(r-1)$ are not affected owing to the equality constraint (4.33g). Thus, $\Delta\bar{\boldsymbol{\tau}}_r^*$ is considered as the optimal control sequence to the proposed HIMPC. Combined with the recent control input $\boldsymbol{\tau}_0$, the first column of $\Delta\bar{\boldsymbol{\tau}}_r^*$ is applied to the system, i.e., $\boldsymbol{\tau}(k+1) = \boldsymbol{\tau}_0 + \Delta\boldsymbol{\tau}^*_{r,k|k}$.

As a summary, Fig. 4.1 visualizes the structure and the control signal flow of HIMPC.

Remark 22 (Why Considering a Constant $\mathbf{B}_{1i}$ Over the Current Prediction Horizon?)**.** *In* (4.13)*, the matrix* $\mathbf{B}_{1i}$ *is derived using the Jacobian matrix* $\mathbf{J}_i(\mathbf{q})$*. With* (4.18) *(or (4.33c)),* $\mathbf{J}_i(\mathbf{q})$ *can also be updated over the prediction horizon. However in this case,* (4.29) *will be a nonlinear equation, and consequently a nonlinear MPC framework is required to be considered, which is computational demanding. For simplicity,* $\mathbf{B}_{1i}$ *is considered as a constant matrix over the current prediction horizon and it will be updated in the next prediction horizon according to the new measurement* $\mathbf{q}(k+1)$*. This is because during a short period,* $\mathbf{q}$ *varies slighter compared with time derivative variables, such as* $\dot{\mathbf{q}}$*,* $\ddot{\mathbf{q}}$*,* $\dot{\mathbf{x}}$*, and* $\ddot{\mathbf{x}}$*. In other words, the variation of* $\mathbf{J}_i(\mathbf{q})$ *during a short period is negligible. In this way,* (4.29) *used to generate predictions of* $\vec{\mathbf{x}}_i$*, which is originally a nonlinear equation, is approximated by a canonical linear equation.*

4.4.2 Analysis

The developed HIMPC framework is only logical if each constrained OCP is feasible for every time, that means the set $\boldsymbol{\mathcal{D}_i}$ ($1 \leq i \leq r$) of admissible input trajectories $\Delta\bar{\boldsymbol{\tau}}_i$ for **Problem** i is non-empty. In this subsection, this hierarchical feasibility is proven. Based on hierarchical feasibility, we further demonstrate that the solution to HIMPC exists and is unique.

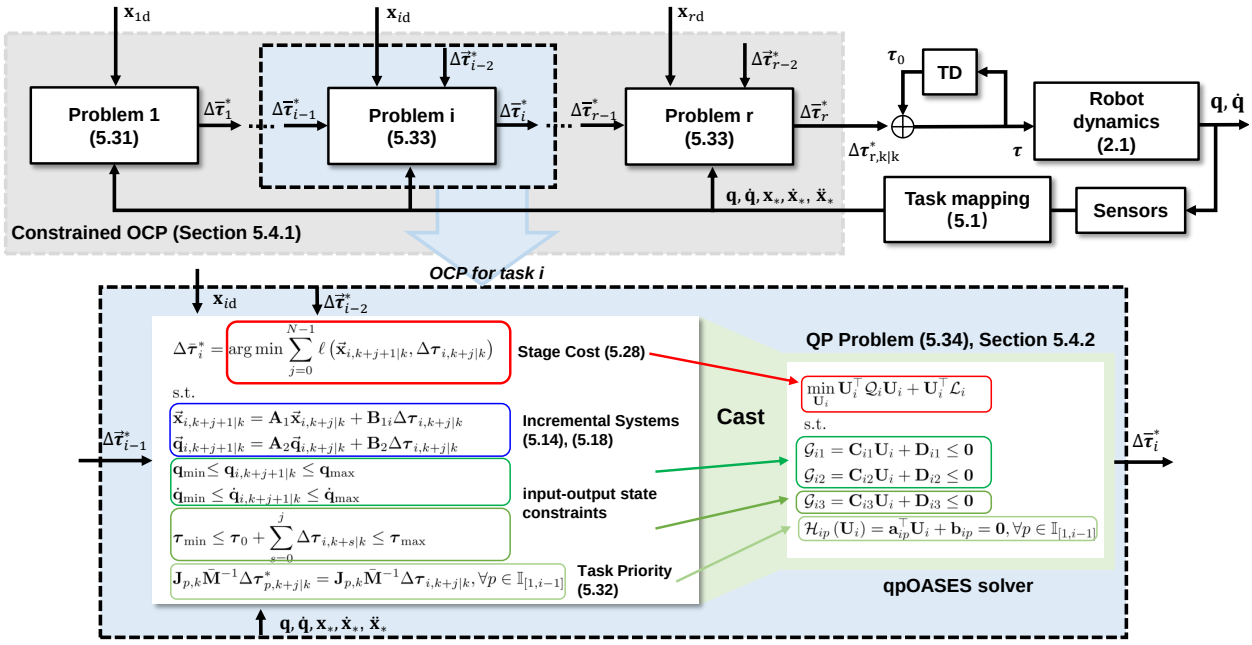

Figure 4.1: Control structure of the HIMPC, where "TD" denotes time delay of one sampling period, and $\Delta\bar{\boldsymbol{\tau}}_i^* := [\Delta\bar{\boldsymbol{\tau}}_1^*, \cdots, \Delta\bar{\boldsymbol{\tau}}_i^*]$. Problems are solved sequentially following the task priority order, and the optimal control law can only be obtained after all problems are solved.

Due to the hierarchical structure and the equality constraint (4.33g), admissible sets of low-priority constrained OCPs are affected by that of high-priority ones. To analyze the feasibility of this hierarchical MPC, the definition of hierarchical feasibility is introduced.

Definition 4 (Hierarchical Feasibility,[176]). *The hierarchical MPC (a series of constrained OCPs ordered hierarchically) admits hierarchical feasibility at time k if the feasibility of the i-th constrained OCP implies the feasibility of the $(i+1)$-th constrained OCP for all $i \in \mathbb{I}_{[1,r-1]}$.*

Before proving the hierarchical feasibility of HIMPC, we show existence and uniqueness of solutions to **Problem** i using convex optimization theory.

It is obvious that **Problem** i $(1 \leq i \leq r)$ is a standard quadratic program (QP):

$$\min_{\mathbf{U}_i} \mathbf{U}_i^\top \mathcal{Q}_i \mathbf{U}_i + \mathbf{U}_i^\top \mathcal{L}_i \tag{4.34a}$$

s.t.

$$\mathcal{G}_{i1} = \mathbf{C}_{i1}\mathbf{U}_i + \mathbf{D}_{i1} \leq 0 \tag{4.34b}$$

$$\mathcal{G}_{i2} = \mathbf{C}_{i2}\mathbf{U}_i + \mathbf{D}_{i2} \leq 0 \tag{4.34c}$$

$$\mathcal{G}_{i3} = \mathbf{C}_{i3}\mathbf{U}_i + \mathbf{D}_{i3} \leq 0 \tag{4.34d}$$

$$\mathcal{H}_{ip}(\mathbf{U}_i) = \mathbf{a}_{ip}^\top \mathbf{U}_i + \mathbf{b}_{ip} = 0, \forall p \in \mathbb{I}_{[1,i-1]} \tag{4.34e}$$

where $\mathbf{U}_i := \text{col}(\Delta\boldsymbol{\tau}_{i,k|k}, \cdots, \Delta\boldsymbol{\tau}_{i,k+N-1|k})$ and (4.34b)-(4.34e) are joint position, velocity, input, and task priority constraints in (4.33), respectively. The equality constraints (4.33b) and (4.33c), which are used to generate predictions, are omitted here since the predictions of task coordinates $\vec{\mathbf{x}}_i$ and joint angles $\vec{\mathbf{q}}$ can be expressed by functions of the input $\mathbf{U}_i$

and recent states ($\vec{\mathbf{x}}_i(k)$ and $\vec{\mathbf{q}}(k)$). For detailed expressions of Hessian matrix $\mathcal{Q}_i$, gradient vector $\mathcal{L}_i$, and other parameters in (4.34), refer to Appendix B. Note that for $i = 1$, the task priority constraint (4.34e) does not exist.

We are interested in existence and uniqueness of solutions. As preparation, the following lemma about the Hessian matrix $\mathcal{Q}_i$ is given.

Lemma 10. *The Hessian matrix $\mathcal{Q}_i$ is positive definite.*

Proof: As shown in Appendix B, $\mathcal{Q}_i := \bar{\mathbf{B}}_{1i}^\top \bar{\mathbf{Q}}_i \bar{\mathbf{B}}_{1i} + \bar{\mathbf{R}}_i$, where $\bar{\mathbf{Q}}_i := \operatorname{diag}\left(\bar{\mathbf{K}}_i^\top \mathbf{Q}_i \bar{\mathbf{K}}_i, \cdots, \bar{\mathbf{K}}_i^\top \mathbf{Q}_i \bar{\mathbf{K}}_i\right)$ is a positive semi-definite matrix since $\mathbf{Q}_i \succ 0$. Then for any vector $\mathbf{X} \in \mathbb{R}^{nN\times 1}$, we obtain that

$$\mathbf{X}^\top \bar{\mathbf{B}}_{1i}^\top \bar{\mathbf{Q}}_i \bar{\mathbf{B}}_{1i} \mathbf{X} = \left(\bar{\mathbf{B}}_{1i}\mathbf{X}\right)^\top \bar{\mathbf{Q}}_i \left(\bar{\mathbf{B}}_{1i}\mathbf{X}\right) \geq 0.$$

Thus, $\bar{\mathbf{B}}_{1i}^\top \bar{\mathbf{Q}}_i \bar{\mathbf{B}}_{1i}$ is also positive semi-definite.
Besides, $\bar{\mathbf{R}}_i := \operatorname{diag}(\mathbf{R}_i, \cdots, \mathbf{R}_i) \succ 0$ since $\mathbf{R}_i \succ 0$.
Therefore, $\mathcal{Q}_i := \bar{\mathbf{B}}_{1i}^\top \bar{\mathbf{Q}}_i \bar{\mathbf{B}}_{1i} + \bar{\mathbf{R}}_i$ is positive definite, i.e., $\mathcal{Q}_i \succ 0$.

■

Then, assuming $\boldsymbol{\mathcal{D}}_i$ is nonempty, a theorem about the properties of the solution to **Problem** i is concluded with the positive definite Hessian matrix $\mathcal{Q}_i$.

Theorem 3 (Existence and Uniqueness of the Solution,[165], [177])**.** *Given that $\boldsymbol{\mathcal{D}}_i$ is nonempty, the solution to **Problem** i exists and is unique.*

Proof: Since $\boldsymbol{\mathcal{D}}_i$ for the admissible input trajectory $\Delta\bar{\boldsymbol{\tau}}_i$ is non-empty, the admissible set $\boldsymbol{\mathcal{U}}_i$ for the argument $\mathbf{U}_i$ of the QP (4.34) is also non-empty. In the following, we will use convexity of the QP (4.34) to verify existence and uniqueness of the solution to the **Problem** i.

As shown in (4.34), the non-empty admissible set $\boldsymbol{\mathcal{U}}_i$ for $\mathbf{U}_i$ is written as

$$\boldsymbol{\mathcal{U}}_i = \left(\bigcap_{p=1}^{i-1} \mathbf{dom}\ \mathcal{H}_{ip}\right) \bigcap \left(\bigcap_{l=0}^{3} \mathbf{dom}\ \mathcal{G}_{il}\right) \tag{4.35}$$

i.e., $\boldsymbol{\mathcal{U}}_i$ is composed of $i-1$ hyperplanes $\left\{\mathbf{U}_i : \mathbf{a}_{ip}^\top \mathbf{U}_i + \mathbf{b}_{ip} = 0\right\}$ $(p \in \mathbb{I}_{[0,i-1]})$ and 3 sublevel sets $\{\mathbf{U}_i : \mathcal{G}_{il} \leq 0\}$ $(l = 1, 2, 3)$. The equality constraint functions $\mathcal{H}_{ip}(\mathbf{U}_i)$ $(p \in \mathbb{I}_{[1,i-1]})$ are linear and affine, and inequality constraint functions $\mathcal{G}_{i1}$, $\mathcal{G}_{i2}$, and $\mathcal{G}_{i3}$ are all linear and convex. Thus, the admissible set $\boldsymbol{\mathcal{U}}_i$ is convex.

Besides, the cost function $\mathbf{U}_i^\top \mathcal{Q}_i \mathbf{U}_i + \mathbf{U}_i^\top \mathcal{L}_i$ is in a quadratic form and is also convex. Thus, (4.34) is a convex optimization problem and solutions exist.

Moreover, as shown in **Lemma 10**, the Hessian matrix $\mathcal{Q}_i$ is positive definite, thus the cost function $\mathbf{U}_i^\top \mathcal{Q}_i \mathbf{U}_i + \mathbf{U}_i^\top \mathcal{L}_i$ is strictly convex. Therefore, the solution to **Problem** i is unique given that the admissible set $\boldsymbol{\mathcal{D}}_i$ is non-empty.

■

Finally, hierarchical feasibility of HIMPC is proved in **Theorem 4**.

Theorem 4 (Hierarchical Feasibility of HIMPC)**.** *The proposed HIMPC admits hierarchical feasibility at each time k.*

Proof: Assume **Problem** i is feasible. Then the admissible set $\boldsymbol{\mathcal{D}}_i$ is nonempty, and in accordance with **Theorem 3** there exists the optimal input trajectory $\Delta\bar{\boldsymbol{\tau}}_i^*$ such that the state, input, and task priority constraints (task priority constraints are not required when $i = 1$)

$$\mathbf{J}_{p,k}\bar{\mathbf{M}}^{-1}\Delta\boldsymbol{\tau}^*_{p,k+j|k} = \mathbf{J}_{p,k}\bar{\mathbf{M}}^{-1}\Delta\boldsymbol{\tau}^*_{i,k+j|k}$$

for all $p \in \mathbb{I}_{[1,i-1]}$ and $j \in \mathbb{I}_{[0,N-1]}$, are not violated.

Next, feasibility of **Problem** $(i+1)$ will be investigated through inspecting whether $\Delta\bar{\boldsymbol{\tau}}_i^*$ is an admissible input trajectory also for **Problem** $(i+1)$. Substituting $\Delta\bar{\boldsymbol{\tau}}_i^*$ into **Problem** $(i+1)$, obviously the state and input constraints, as well as priority constraints for $p \in \mathbb{I}_{[1,i-1]}$ are not violated because these constraints are identical to that in **Problem** i. Besides, the priority constraint when $p = i$ is also fulfilled, i.e., if $\Delta\bar{\boldsymbol{\tau}}_{i+1} = \Delta\bar{\boldsymbol{\tau}}_i^*$, then

$$\mathbf{J}_{i,k}\bar{\mathbf{M}}^{-1}\Delta\boldsymbol{\tau}^*_{i,k+j|k} \equiv \mathbf{J}_{i,k}\bar{\mathbf{M}}^{-1}\Delta\boldsymbol{\tau}_{i+1,k+j|k}, \forall j \in \mathbb{I}_{[0,N-1]}.$$

It shows all constraints are not violated and thus $\Delta\bar{\boldsymbol{\tau}}_i^*$ is a feasible control trajectory to **Problem** $(i+1)$. Thus, **Problem** $(i+1)$ is feasible if **Problem** i is feasible, i.e., the proposed HIMPC admits the hierarchical feasibility.

■

Assume **Problem** 1 is feasible at time k. By induction, we conclude that **Problems** 2 to r are also feasible at time k. Therefore, from **Theorem 4**, it is concluded that the admissible set $\boldsymbol{\mathcal{D}}_i$ $(1 \leq i \leq r)$ is not empty if **Problem** 1 is feasible.

In accordance with **Theorem 3** and **Theorem 4**, we conclude that the solution to HIMPC exists and is also unique if **Problem** 1 is feasible.

4.4.3 Discussion

In this subsection, the advantages of the proposed HIMPC over state-of-the-art task-prioritized controllers are discussed. Besides, limitations of the proposed method are analyzed.

Strengths of HIMPC

Low Requirements on Modeling. In existing MPC based task-prioritized control schemes [154], [155], state predictions are generated using nominal models. This requires performing time-consuming identification of the mathematical model parameters of the plant. The proposed HIMPC approach employs incremental systems to obtain state predictions and thus it is not necessary to identify parameters of the model. For incremental systems (cf. (4.12) and (4.16)), only $\bar{\mathbf{M}}$ is associated with the dynamics model because $\bar{\mathbf{M}}$ is selected such that $\|\mathbf{I}-\mathbf{M}^{-1}\bar{\mathbf{M}}\| < 1$. As discussed in **Remark 23**, the sufficient condition for $\|\mathbf{I}-\mathbf{M}^{-1}\bar{\mathbf{M}}\| < 1$ is fulfilled by a sufficiently small positive $\bar{M}_i$ even though the exact expression of inertia matrix $\mathbf{M}$ is unknown. Therefore, the proposed HIMPC has low requirements for modeling.

Robustness. As shown in Section 4.3.2, the incremental systems show high approximation accuracy and strong robustness against inertia modelling errors and external disturbances. This is because the inertia modelling error and external disturbances are compensated by time-delay signals. Robustness of this proposed method is also reflected in terms of *dynamic consistency*. In [61], a nominal inertia matrix $\mathbf{M}$ is used to construct equality constraints (similar to (4.33g)), and it is obvious that *dynamic consistency* is deteriorated when there

are inertia modelling errors. In HIMPC, $\mathbf{M}$ is replaced by a pre-determined $\bar{\mathbf{M}}$ in the task priority constraints (equality constraint (4.33g)). Thus, enhanced *dynamic consistency* is received. This advantage of HIMPC is also visible in the simulations and experiments presented in Sections 4.6 and 4.5.

Computational Efficiency. The TDE method not only improves robustness of the control scheme, but it also simplifies equations of motion of tasks and system dynamics. As shown in (4.14) and (4.18), both equation of motion and system dynamics are approximated by linear time-invariant systems, where online calculation of the complex nonlinear system dynamics terms is not required. As a result, each constrained OCP is a QP problem, and computational complexity will decrease dramatically, allowing for real-time control in milliseconds. In comparison, the MPC frameworks in [154], [155] are nonlinear since nonlinear equations are employed to generate state predictions. For a general nonlinear MPC scheme, heavy computational complexity restricts its real-time application [172].

Singularity Handling. Different from null-space projection based methods [142]–[150], we employ equality constraint (4.33g) to guarantee task hierarchy. No matrix inversion is required and algorithmic singularity is avoided. Besides, also kinematic singularity is avoided. In our approach, the cost function (4.30) is designed relying on target motion dynamics (4.3), where inverse calculation of the terms w.r.t. Jacobian matrices is not necessary. In contrast, e.g. in [61], Cartesian forces that are calculated using the equivalent Cartesian mass matrix $(\mathbf{J}\mathbf{M}^{-1}\mathbf{J}^{\top})^{-1}$ are involved in the stage costs, and kinematic singularity occurs when the Jacobian matrix loses its rank. Also, different from the approach in [152], [153], Hessian matrices of the constrained OCPs are always positive definite (see Lemma 1). This allows to relax the common assumption that singularity-free tasks are defined and gives more flexibility in defining tasks. The simulations and experiments in Sections 4.6 and 4.5 will further discuss singularity handling.

Limitations of HIMPC

Sampling. To guarantee the required approximation accuracy of the incremental systems, the sampling period has to be chosen sufficiently small. If the sampling period increases, the tracking errors will increase and the closed loop system may even become unstable. Unfortunately, there are no systematic methods to determine the maximum allowable sampling period. Note that in [7], [33], [133], [145]–[147], TDE methods have been successfully applied for robot manipulator control, where sampling periods of 1 ms and 2 ms are used. The tracking accuracy of TDE based controllers is in general better than that of state-of-the-art controllers. In simulations and experiments, described in Sections 4.6 and 4.5, we use $T_s = 1$ ms which from our experience is suitable to achieve high enough approximation accuracy.

Prediction Horizon. For MPC without terminal ingredients, a sufficiently large prediction horizon is required to guarantee recursive feasibility (system convergence) and global optimality of solutions[164]. It also implies that the larger the prediction horizon, the better is control performance. However, our framework does not allow for large prediction horizons. The reason is that we set the Jacobians constant by ignoring variations of the joint positions over the prediction horizon. The larger is the prediction horizon, the larger is the discrepancy between real equations of motion and the derived incremental systems, which will deteriorate the approximation accuracy of incremental systems. Besides, a large prediction horizon is challenging for real-time control performance. Considering the above-mentioned factors, a

Table 4.1: Task Definitions and Control Gains for Experiments

Level	Task Definition	Stiffness	Damping
1	EE in x	200 N/m	10 Ns/m
1	EE in y	200 N/m	10 Ns/m
2	Joint position q_1	50 Nm/rad	5 Nms/rad

reasonable prediction horizon is tuned manually in practice. In the following simulations and experiments, $N = 5$ is selected, which not only ensures realizability of real-time control, but also guarantees that control performance is satisfactory.

TDE Error. In the constrained OCPs from Section 3.2, equality constraints (compare (4.33g)) are imposed on control signals to realize task hierarchy. However, the TDE error is ignored in the nominal incremental system (4.12). Consequently, task hierarchy will be inevitably deteriorated, which is also visible in simulation and experimental results, see Sections 4.6 and 4.5. Besides, joint position and velocity constraints are imposed in the constrained OCPs. Nevertheless, in practice, we are not able to guarantee that state constraints are strictly satisfied. Given that the TDE error and measurement noise are ignored in this article, there are prediction errors of state variables. As a result, the system suffers from the risk of state constraint violation. After all, huge deterioration of task hierarchy and strongly violating state constraints are avoided. This is because the derived incremental systems exhibit high approximation accuracy as analyzed in Section 4.3.2. To deal with TDE error and strict state constraints, tube-based MPC and learning techniques [178], [179] might be useful.

Task Levels. The computational complexity of HIMPC increases as the number of tasks increases. For a task hierarchy with n tasks, there will be n constrained OCPs to be solved. In this article, the constrained OCPs are solved by a QP solver which is possible efficiently. Nevertheless, the computing time increases with an increasing number of tasks because of the serial connection of constrained OCPs. Fortunately, this increase is only linear.

4.5 Experiment on a 3-DoF Robot Manipulator

The effectiveness of the proposed HIMPC is investigated in experiments. The controller is therefore compared to other state-of-the-art controllers, such as operational space formulation (OSF) [150], TDE enhanced OSF (TDEOSF) [145], and hierarchical QP (HQP) [61].

4.5.1 Experimental Setup

The custom-built 3-DoF planar robot manipulator, shown in Figure 2.2, is used throughout the experimental verification. A task hierarchy with 2 priority levels is implemented. The task definition and the corresponding stiffness and damping gains are shown in Table 4.1.

For HQP and HIMPC, `qpOASES` is used to solve the constrained OCPs. For HIMPC, the prediction horizon is $N = 5$, and weighting matrices are chosen as $\mathbf{Q}_i := 200\mathbf{I}$ and $\mathbf{R}_i := 10\mathbf{I}$ for $i = 1, 2$. The upper and lower bounds of joint position, velocity, and torques are given

Table 4.2: Boundaries of Input and State for the 3-DoF Planar Robot Manipulator

$q_{\min}$ ($q_{\max}$)	$\dot{q}_{\min}$ ($\dot{q}_{\max}$)	$\tau_{\min}$ ($\tau_{\max}$)
-150 (150) deg	-100 (100) deg/s	-4 (4) N·m

in Table 4.2. For TDEOSF and HIMPC, $\bar{\mathbf{M}} = \text{diag}(0.033, 0.033, 0.033)$ is manually tuned, compare **Remark 23**.

Two scenarios are implemented to verify the performance of the proposed method with respect to control accuracy, optimality, task hierarchy, singularity handling, and constraint handling.

4.5.2 Scenario 1: Control Accuracy and Optimality

Setting

The reference trajectory RT1 is considered (see Figure 4.2) in the scenario and we choose $\mathbf{q}_0 = [0, 90, -90]^\top$deg as the initial configuration.

i) *Control Accuracy.* OSF, HQP, TDEOSF, and the proposed HIMPC are implemented for comparison. The discrepancy between the identified and the real mathematical model is considered as a disturbance. The robustness of tracking performance is analyzed by investigation of control accuracy.

ii) *Optimality (qualitative).* We take into account tracking errors and control signals in the cost function (4.30). Thus, tracking error and control signals are inspected to investigate the optimality of the control methods. We will first compare HIMPC and TDEOSF and analyze how optimality in HIMPC improves performance. Then, we introduce HIQP, i.e., a synonym of hierarchical incremental QP control which denotes HIMPC with prediction horizon $N = 1$, and compare this to HIMPC with $N = 5$ to investigate local optimality of the controller.

iii) *Optimality (quantitative).* We will calculate the average cost when applying each of the controllers. With the stage cost for the predictions, see (4.30), we now introduce the average cost (4.36) for tasks to evaluate the closed loop performance during a period $[0, t_s]$ (iterations $N_t = t_s/T_s$) where t_s is the terminal time.

$$C_i = \frac{1}{N_t} \sum_{k=0}^{N_t} \left(\|\mathbf{e}(\mathbf{x}_i(k))\|^2_{\mathbf{Q}_i} + \|\Delta\boldsymbol{\tau}(k)\|^2_{\mathbf{R}_i} \right) \tag{4.36}$$

where C_i is the average cost for task i. Note that $\mathbf{e}(\mathbf{x}_i(k))$ in (4.36) is calculated using the real-time measurements, not predictions.

Results

The experimental results are shown in Figures 4.3-4.7 and Table 4.3.

i) All of the controllers, OSF, HQP, TDEOSF, and HIMPC, allow to realize the two hierarchic tasks, but the tracking accuracy is different. As shown in Figure 4.3, and Table

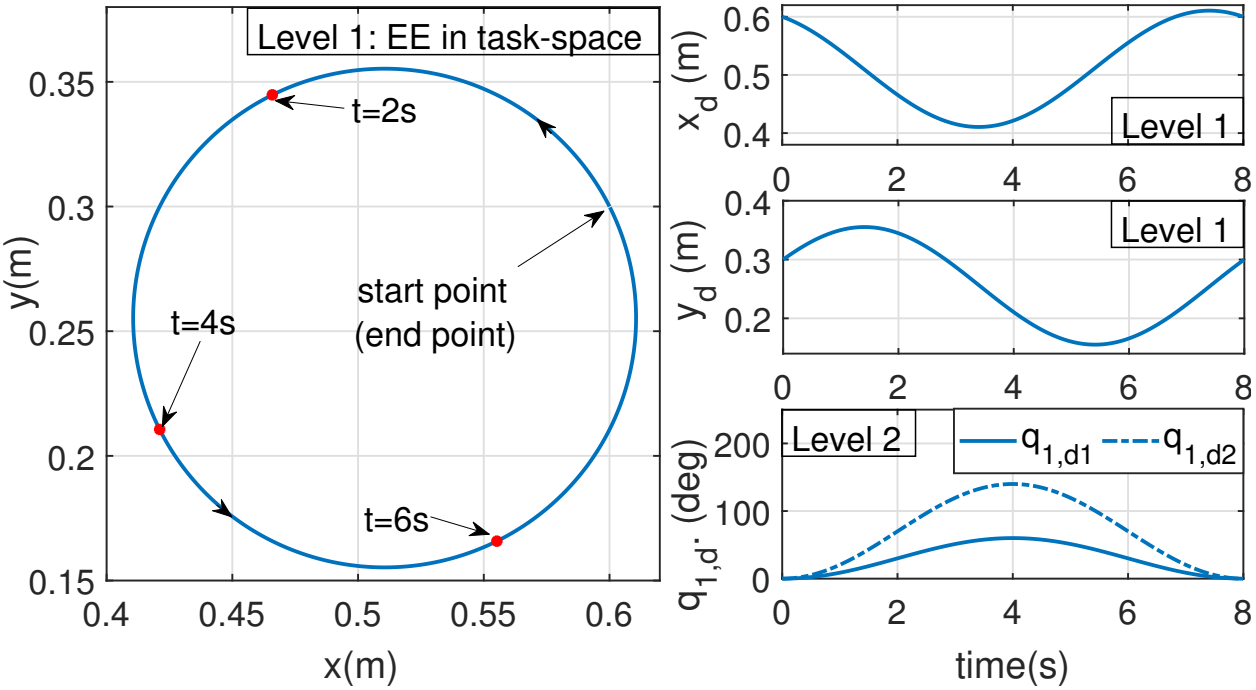

Figure 4.2: Reference trajectories RT1 and RT2. x_d and y_d are reference signals for coordinates x and y of the EE in the task-space, respectively, and the reference geometric curve of the EE is a "circle". $q_{1,\mathrm{d}1}$ and $q_{1,\mathrm{d}2}$ are reference signals for q_1. RT1 includes x_d, y_d, and $q_{1,\mathrm{d}1}$, and RT2 involves x_d, y_d, and $q_{1,\mathrm{d}2}$.

Table 4.3: Experimental Results of *Scenario 1*: Root-Mean-Square-Errors (RMSE) of Different Controllers

Task	**OSF**	**TDEOSF**	**HQP**	**HIMPC**
L1:x_EE(m)	3.81×10^{-3}	9.58×10^{-5}	3.11×10^{-3}	9.09×10^{-5}
L1:y_EE(m)	2.78×10^{-3}	8.89×10^{-5}	2.39×10^{-3}	9.43×10^{-5}
L2:q_1(deg)	0.36	8.02×10^{-3}	1.05	2.07×10^{-2}

4.3, tracking performance of the model-based methods (OSF and HQP) is inferior. This is because of the model discrepancy. Tracking performance of OSF and HQP might still be improved with a more accurate model, though its accurate identification is time-consuming and modeling errors are inevitable as we analyzed in Section 4.1.1. TDE-based methods (TDEOSF and HIMPC) are model-free ones. Thus, they are not sensitive to the model discrepancy and show strong robustness against disturbances. This allows for high tracking precision.

ii) For further analysis, the tracking errors of TDEOSF and HIMPC are again displayed in Figures 4.4 and Table 4.3, and we can conclude that the tracking performance of both methods, TDEOSF and HIMPC, is satisfactory. The tracking errors of TDEOSF are the smallest. This is because, in HIMPC, the cost function (4.30) does not only take into account the desired tracking error dynamics but also the control signal to avoid controller oscillations and to realize energy efficiency and actuator protection. Thus, the superiority of HIMPC is only visible when we in addition look at input trajectories. In Figure 4.5, it is observed

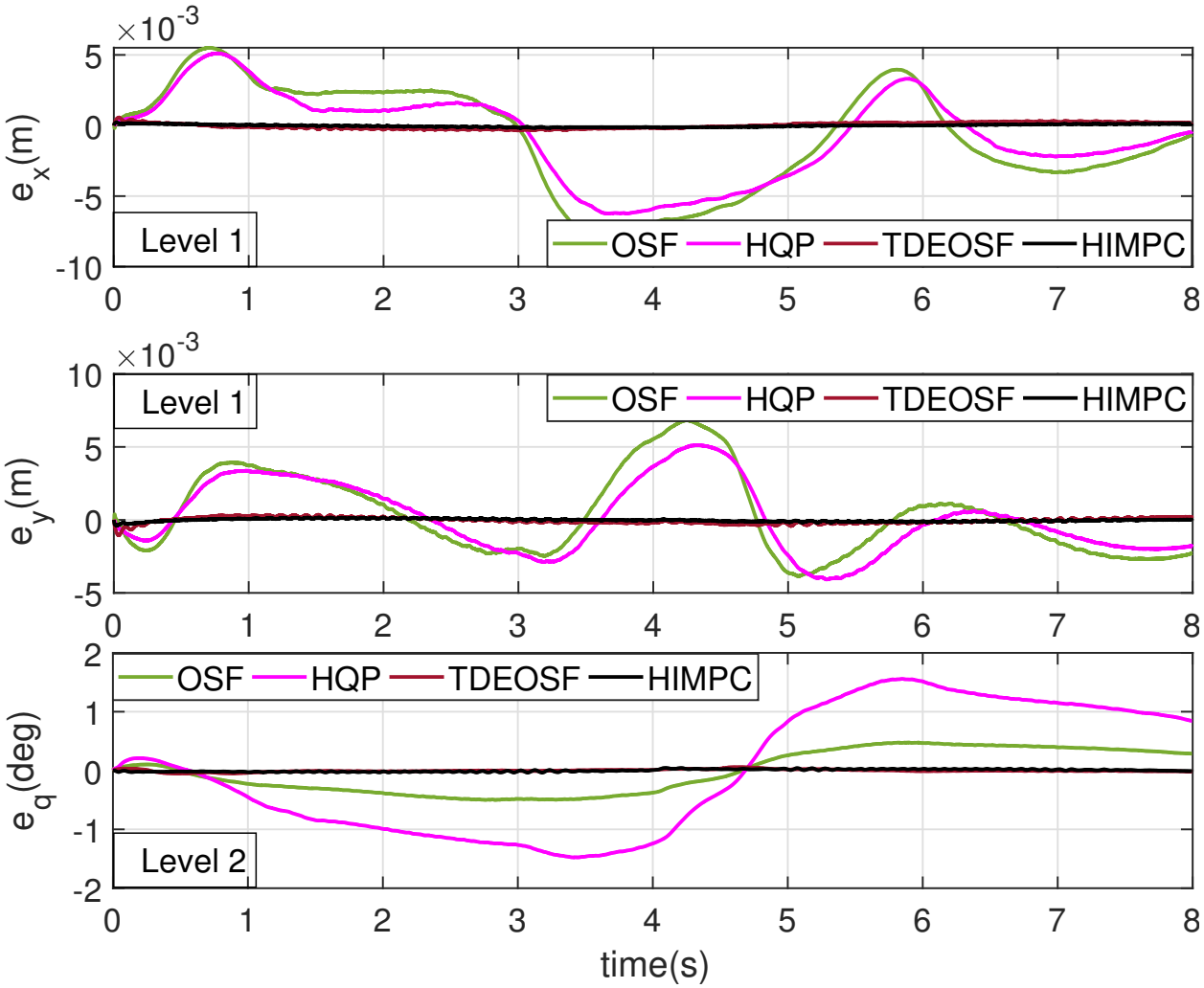

Figure 4.3: Experimental results of *Scenario 1*: Tracking errors of OSF, HQP, TDEOSF, and HIMPC.

that in comparison to TDEOSF, control signals of HIMPC are smoother. There are many "glitches" in the control signal trajectories of TDEOSF. This is because the control signal of HIMPC is obtained through solving OCPs. In contrast, for TDEOSF, the control signal is calculated from analytic expressions, focusing on addressing tracking errors, while optimality is not considered.

A final comparison between HIQP and HIMPC analyzes the local optimality of the controller, and experimental results are shown in Figures 4.4 and 4.6. For HIQP and HIMPC, the tracking errors of task 1 are very similar. However, for task 2, the tracking errors of HIQP are larger than those of HIMPC during some periods (eg. [2s, 3s]). In addition, we observe that the control signals of HIMPC are smoother than those of HIQP (see rectangular symbols in Figure 4.6). This is because control signals of HIMPC are obtained by solving OCPs over a longer prediction horizon, while HIQP only takes into account a one-step-ahead prediction resulting in torque peaks and oscillations, especially for a noisy environment.

iii) Figure 4.7 shows that the average cost of tasks 1-2 is the lowest for HIMPC. This quantitatively verifies the superior optimality of HIMPC. Although the control signals of

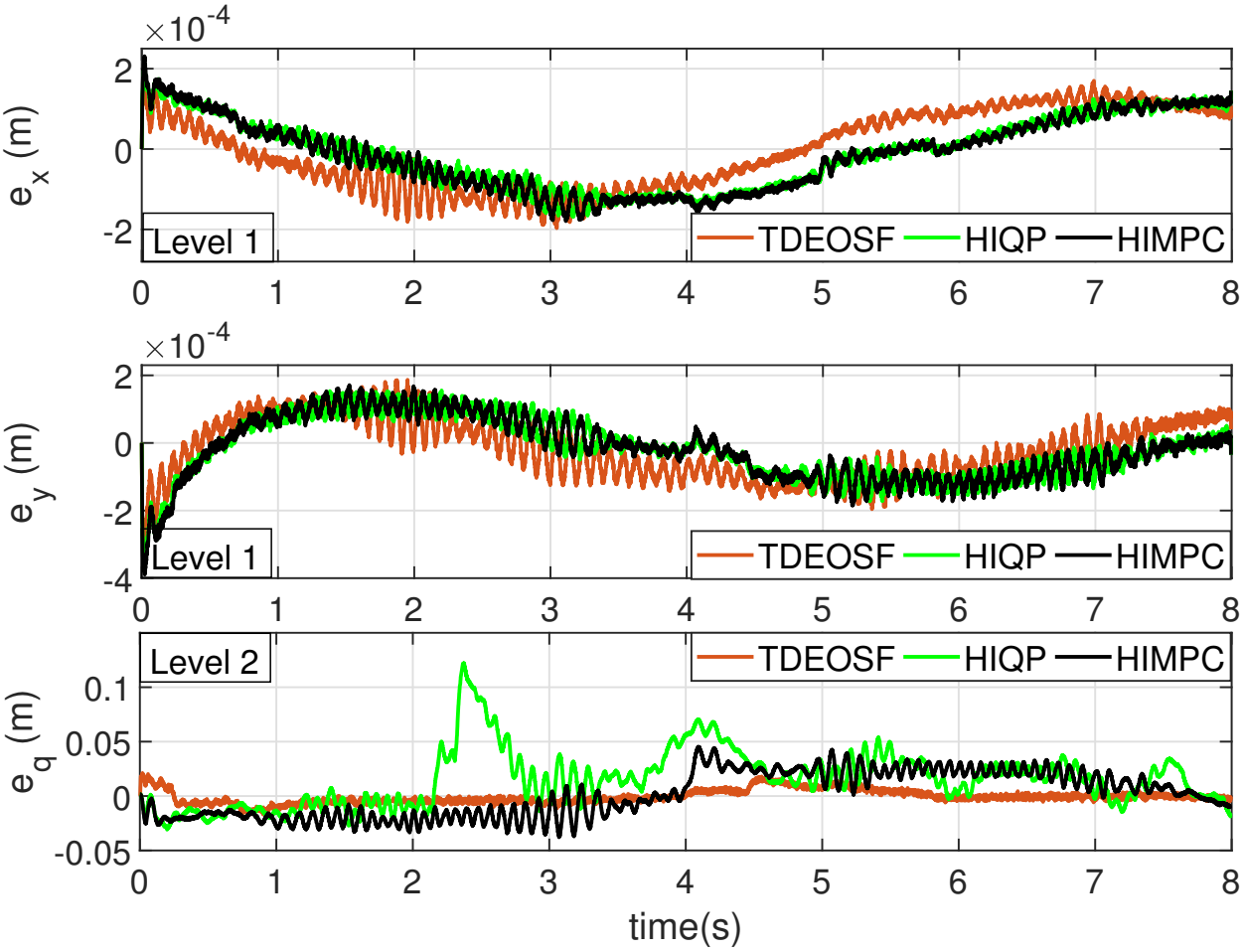

Figure 4.4: Experimental results of *Scenario 1*: Tracking errors of TDE-based methods (TDEOSF, HIQP, and HIMPC).

HIQP are also obtained through solving constrained OCPs, the average cost of task 2 under the action of HIQP is even higher than that of TDEOSF. Due to its one-step prediction, the HIQP controller is locally optimal. Thus, over a time horizon, the average cost of HIQP may be even higher than that of TDEOSF, though optimality is not considered for TDEOSF controller design.

4.5.3 Scenario 2: Task Hierarchy, Constraint Admissibility, and Singularity Handling

Setting

The reference trajectories RT2 and RT3 (see Figures 4.2 and 4.8, respectively) are considered in this scenario. The initial configuration is $\mathbf{q}_0 = [0, 90, -90]^\top$deg when RT2 is considered, while for RT3, $\mathbf{q}_0 = [0, 0, 0]^\top$deg is chosen.

i) *Task Hierarchy and Constraint Admissibility.* As long as the amplitude of the reference trajectory of task 2 (q_1) is small, task 1 and task 2 are non-conflicting. For increasing amplitude, tasks become more and more conflicting. We verify task hierarchy by

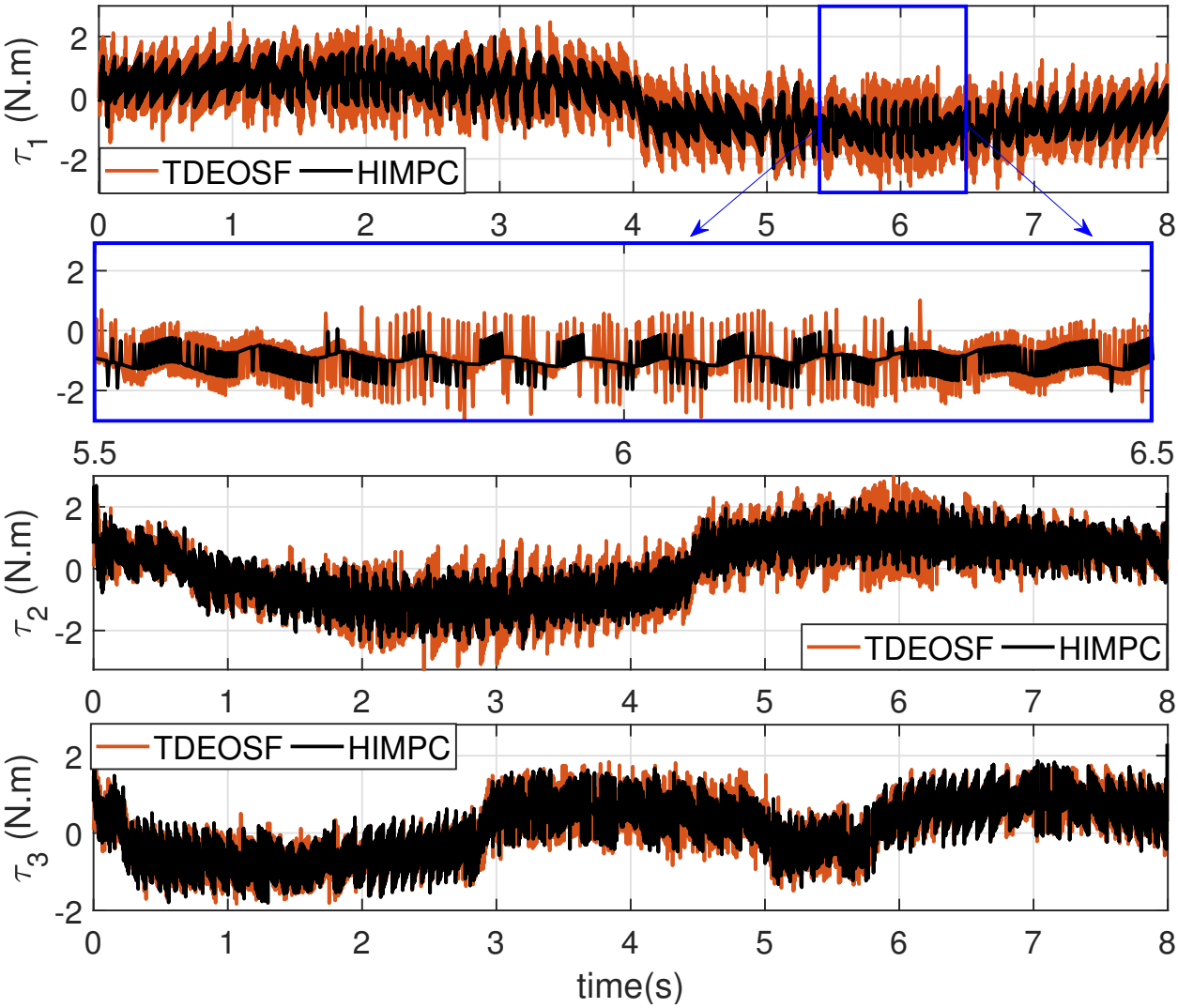

Figure 4.5: Experimental results of *Scenario 1*: Control signals of TDEOSF and HIMPC.

investigating whether tracking performance of high-priority tasks will be affected when high and low-priority tasks conflict with each other, and the reference trajectory RT2 is employed. RT2 is also used to investigate the capability of HIMPC to guarantee that input and state constraints are not violated.

ii) *Algorithmic Singularity Handling.* The reference trajectory RT2 is used to demonstrate that algorithmic singularity is avoided in HQP and HIMPC. Null-space projection based methods (OSF and TDEOSF) are likely to suffer from algorithmic singularity problems when tasks conflict with each other. To ensure safety, OSF and TDEOSF are implemented only in numerical simulation when RT2 is employed.

iii) *Kinematic Singularity Handling.* Moreover, RT3 is used to verify that kinematic singularity is avoided in HIMPC. For RT3, the robot manipulator is straightened and is kinematically singular at the start, end, and intersection between the two circles.

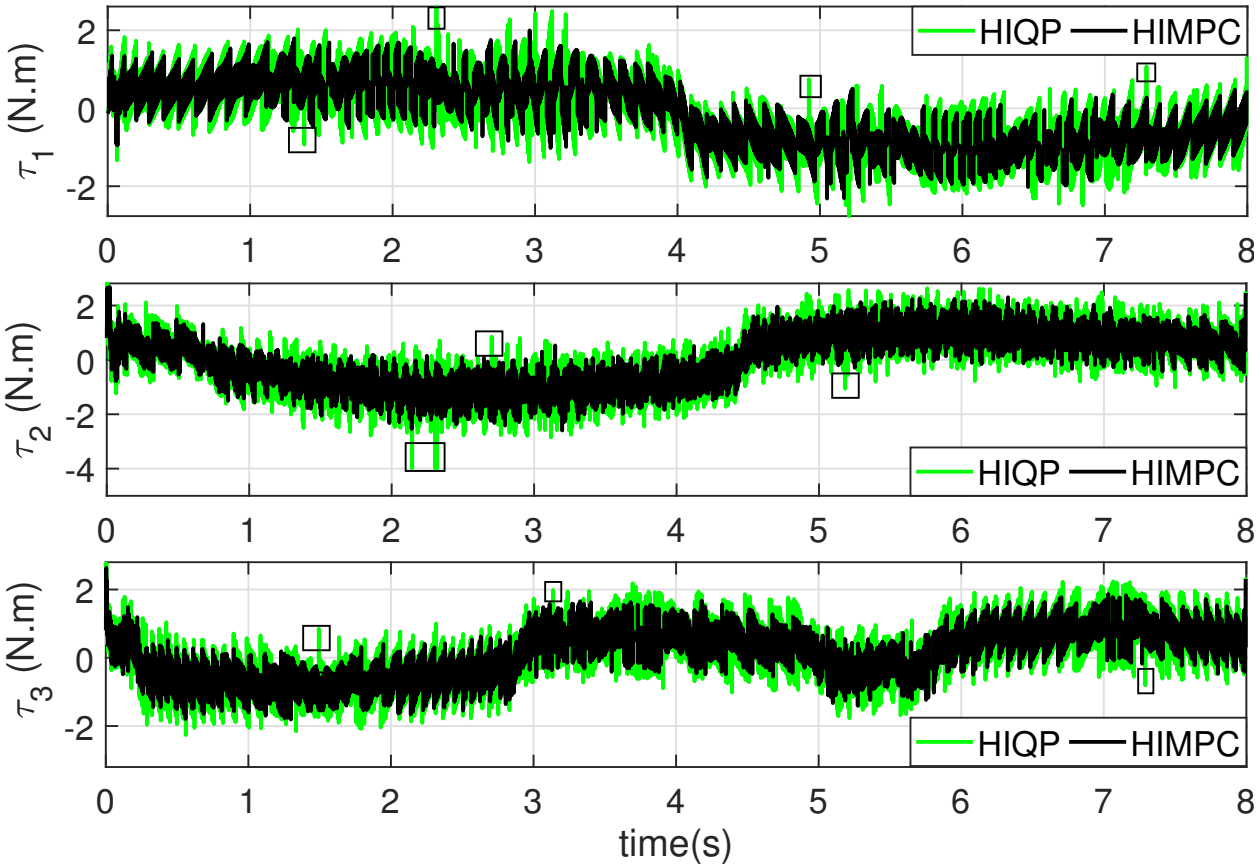

Figure 4.6: Experimental results of *Scenario 1*: Control signals of HIQP and HIMPC.

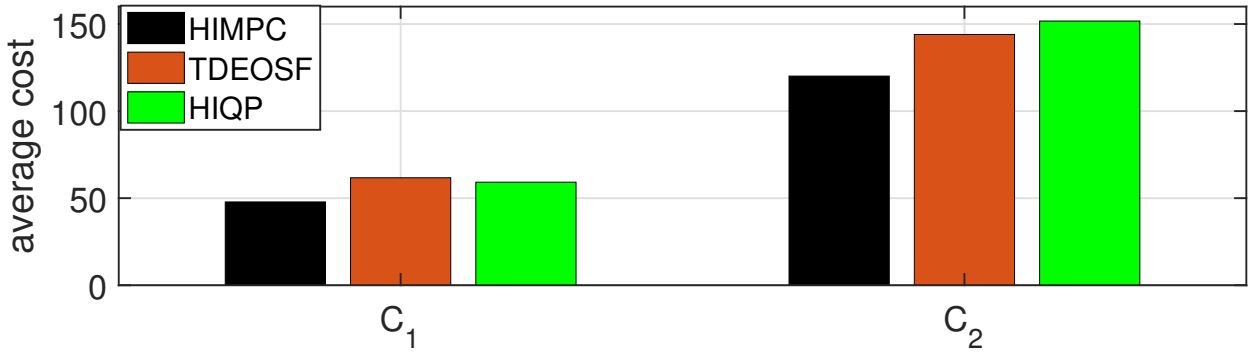

Figure 4.7: Experimental results of *Scenario 1*: Average cost (4.36) of HIMPC, TDEOSF, and HIQP.

Results

The results of *Scenario 2* are shown in Figs. 4.9-4.14.

i) Tracking errors of HQP and HIMPC are displayed in Figure 4.9, and we observe that tracking errors of q_1 (task 2) are large in the time period [3.2s, 6s]. This is because, during this period, tasks conflict with each other. The low-priority task (task 2) has to "sacrifice" itself to guarantee satisfactory tracking performance of the high-priority task. Thus, for HQP and HIMPC, task hierarchy is guaranteed. Besides, because HQP is a model-based

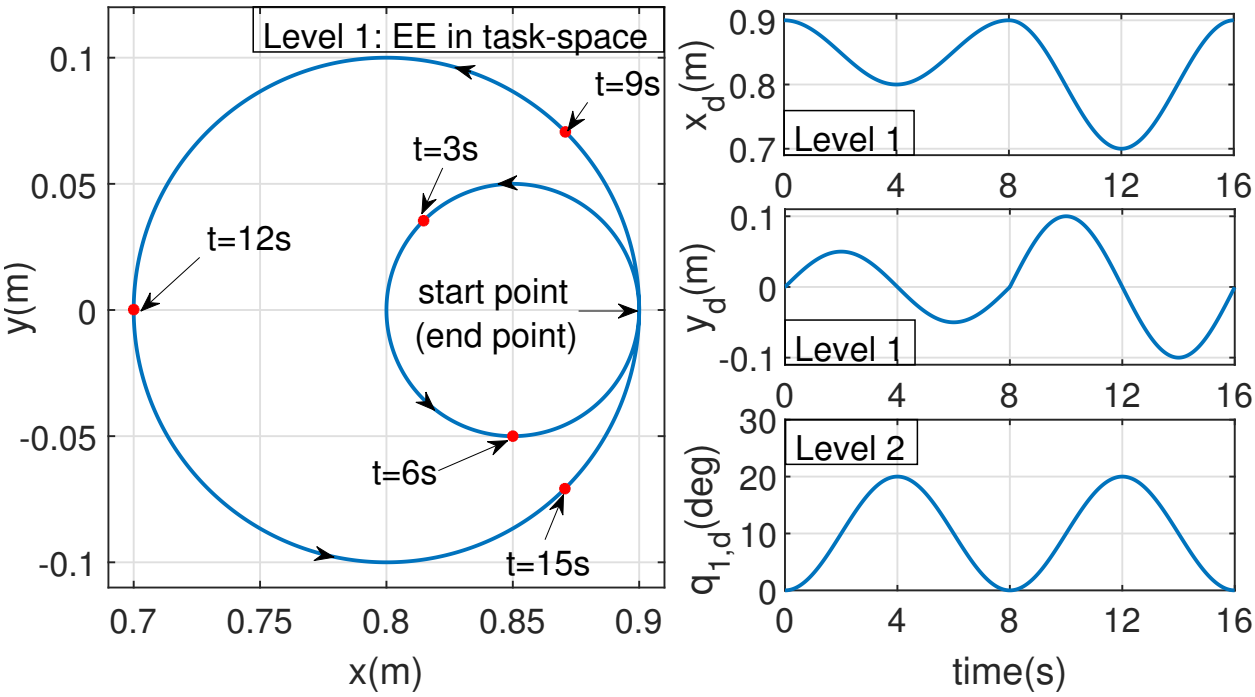

Figure 4.8: Reference trajectory RT3. The reference curve of the EE consists of two tangent circles. At $t = 0$s, 8s, and 16s, the reference configuration of the planar robot manipulator is straightened.

method, the tracking error of HQP is higher than that of HIMPC. This further verifies the robustness of HIMPC.

Besides, *dynamic consistency* can be verified by investigating whether tracking errors of the highest-priority task (task 1) are affected when different reference trajectories (RT1 and RT2) are employed. For the convenience of comparison, tracking errors of task 1 when RT1 and RT2 are employed are summarized in Figure 4.10, where one can observe that for HQP, tracking performance of task 1 deteriorates when tasks conflict. This is because the nominal inertia matrix is used in HQP to construct task priority constraints and *dynamic consistency* is adversely affected by the inertia modeling error. In contrast, for HIMPC, tracking performance of task 1 is nearly not affected no matter whether tasks conflict or not. This is because the TDE method is used to approximate equations of motion of tasks and the inertia matrix is replaced by a predetermined diagonal matrix in the task priority constraints (compare (4.33g)). Thus, enhanced *dynamic consistency* of HIMPC is obtained due to the TDE approximation.

In Figure 4.11 it is shown that input constraints are not violated. During the period [3.5s, 5.2s], the input torques of HIMPC are relatively large. This is because here tasks conflict. The control signal not only needs to guarantee the priority of task 1, but it also regulates tracking performance of low-priority tasks as well as possible. As we discussed in Section 4.4.3, the TDE error and measurement noise are not considered for state predictions in HIPMC, and it results in small prediction errors, see Figure 4.12, where joint velocity constraints are slightly violated for short periods. This is common in MPC with uncertainty. Though, at least we observe in our study that state constraints are not strongly violated. This is because the incremental systems exhibit high approximation accuracy.

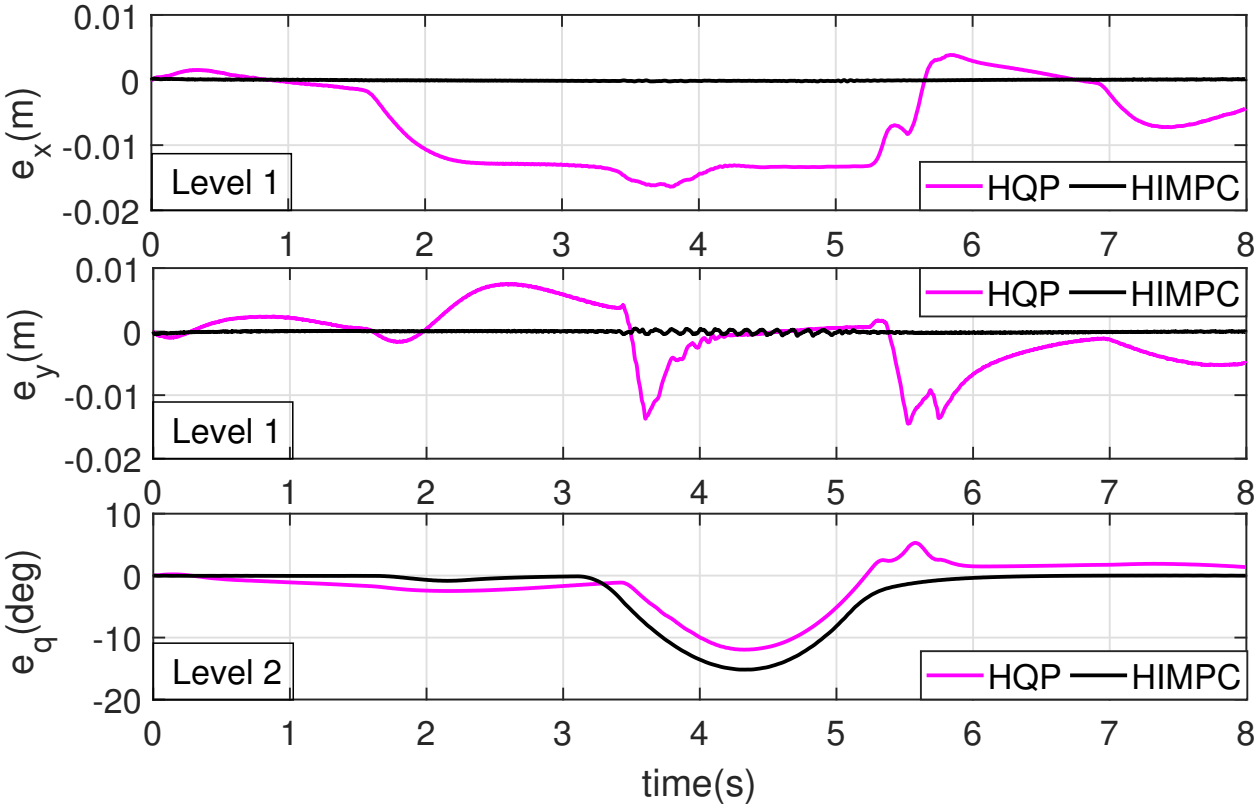

Figure 4.9: Experimental results of *Scenario 2*: Tracking errors of HQP and HIMPC (the reference trajectory is RT2).

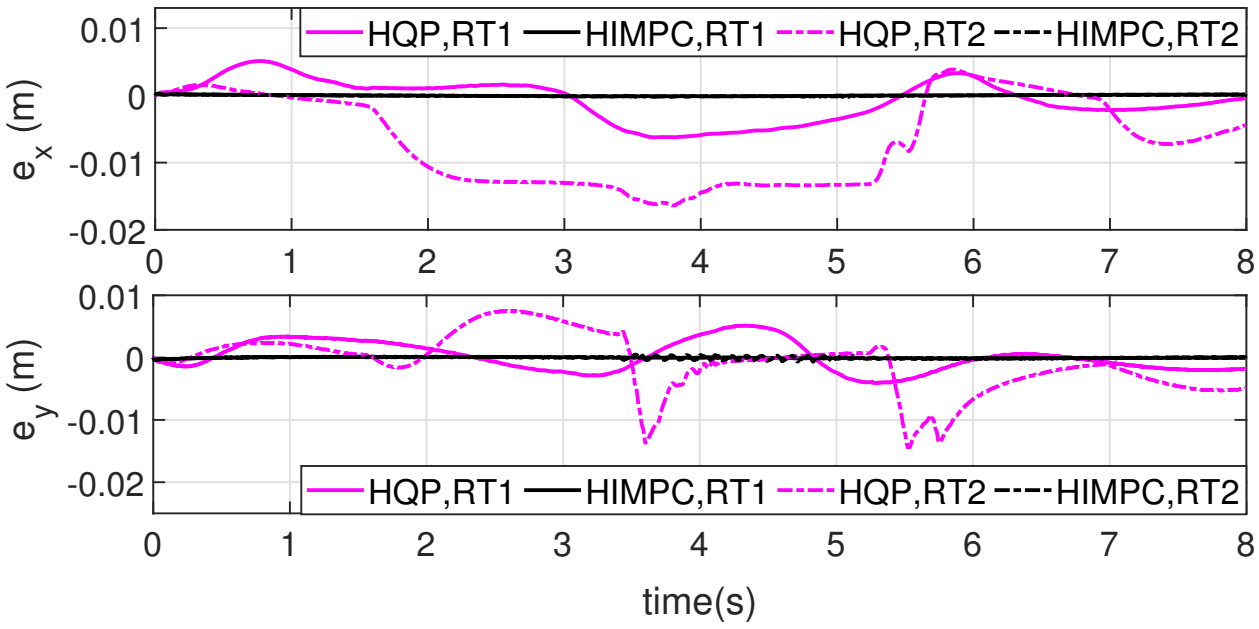

Figure 4.10: Experimental results of *Scenario 2*: Tracking errors of task 1 (RT1 and RT2 are employed).

ii) As stated in Section 4.1.1, null-space projection based methods, such as OSF and

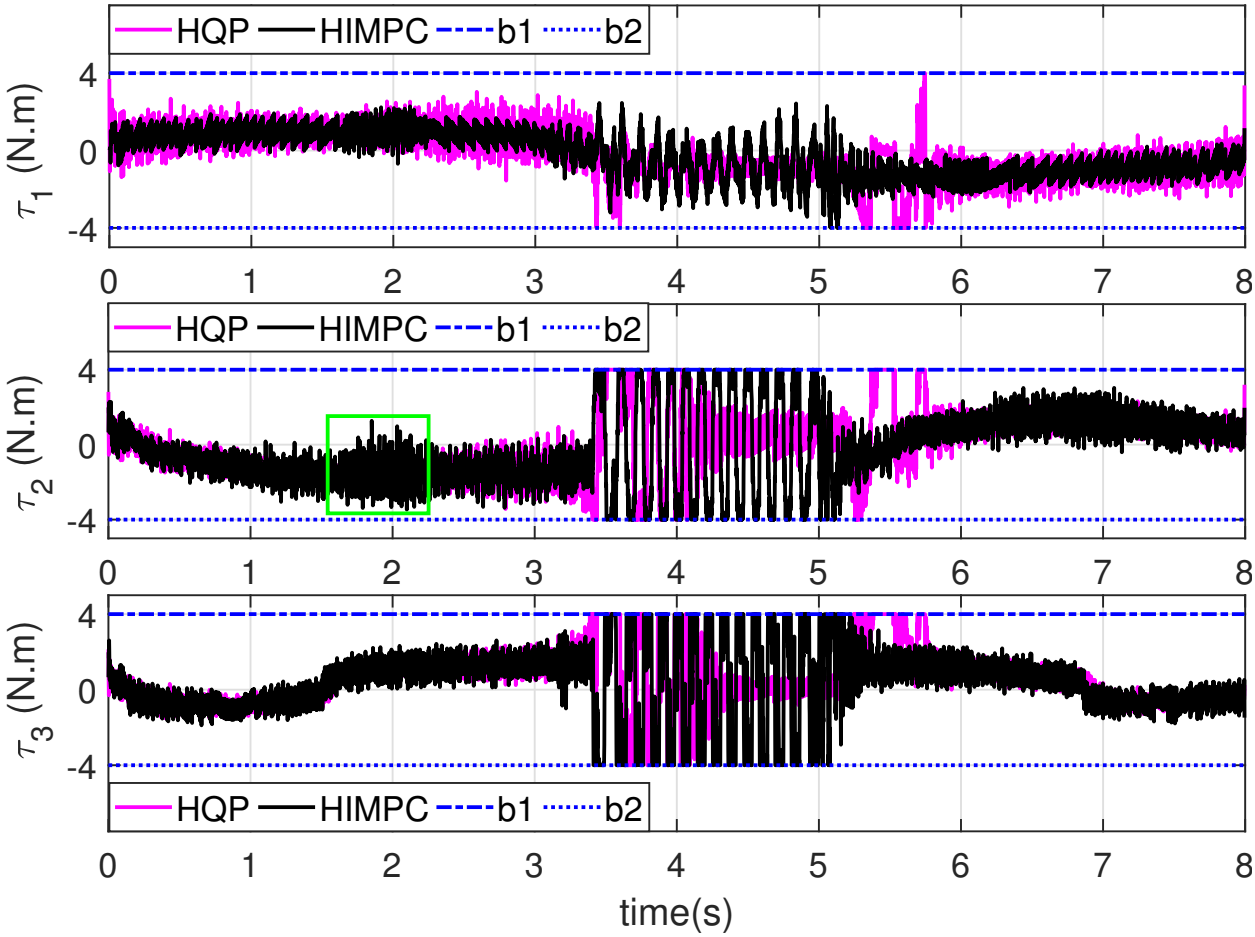

Figure 4.11: Experimental results of *Scenario 2*: Torque inputs of three joints (the reference trajectory is RT2), where b_* denotes the corresponding torque bound.

TDEOSF, are likely to suffer from algorithmic singularity problems when tasks conflict with each other. For security, we did numerical simulations to implement OSF and TDEOSF. Consistent with theoretical analysis, the values of $\mathbf{J}_{2|\mathrm{p}}\mathbf{M}^{-1}\mathbf{J}_{2|\mathrm{p}}^{\top}$ and $\mathbf{J}_{2|\mathrm{p}}\bar{\mathbf{M}}^{-1}\mathbf{J}_{2|\mathrm{p}}^{\top}$ ($\mathbf{J}_{2|\mathrm{p}}$ is the prioritized Jacobian matrix) under the action of OSF and TDEOSF tend to be 0 at around 3.3s. In other words, the prioritized Jacobian matrix $\mathbf{J}_{2|\mathrm{p}}$ loses its rank (and is a null vector here). Then, the corresponding prioritized inertia matrices, $(\mathbf{J}_{2|\mathrm{p}}\mathbf{M}^{-1}\mathbf{J}_{2|\mathrm{p}}^{\top})^{-1}$ and $(\mathbf{J}_{2|\mathrm{p}}\bar{\mathbf{M}}^{-1}\mathbf{J}_{2|\mathrm{p}}^{\top})^{-1}$, tend to infinity and undesired (large-value) control signals are obtained. As a result, the system will be unstable. Note that in the context of task definitions (see Table 4.1), $\mathbf{J}_2 = [1, 0, 0]$ is a constant vector. Thus, at this moment the system is not kinematically singular, but it is attributed to the prioritized Jacobian matrix (null-space projection idea), i.e., it is the algorithmic singularity. For HQP and HIMPC, equality constraints are employed to realize task hierarchy, and no prioritized inertia matrices are involved. Thus, algorithmic singularity is avoided in HQP and HIMPC.

iii) We finally verify that HIMPC is still applicable when the robot manipulator passes the kinematically singular configuration in *Scenario 2*, and the reference trajectory RT3 (see Figure 4.8) is considered. OSF, TDEOSF, and HQP cannot be implemented because of kinematic singularity in the intial configuration. The experimental results are shown in Figures 4.13 and 4.14. As shown in Figure 4.14, the tracking accuracy of HIMPC is still high.

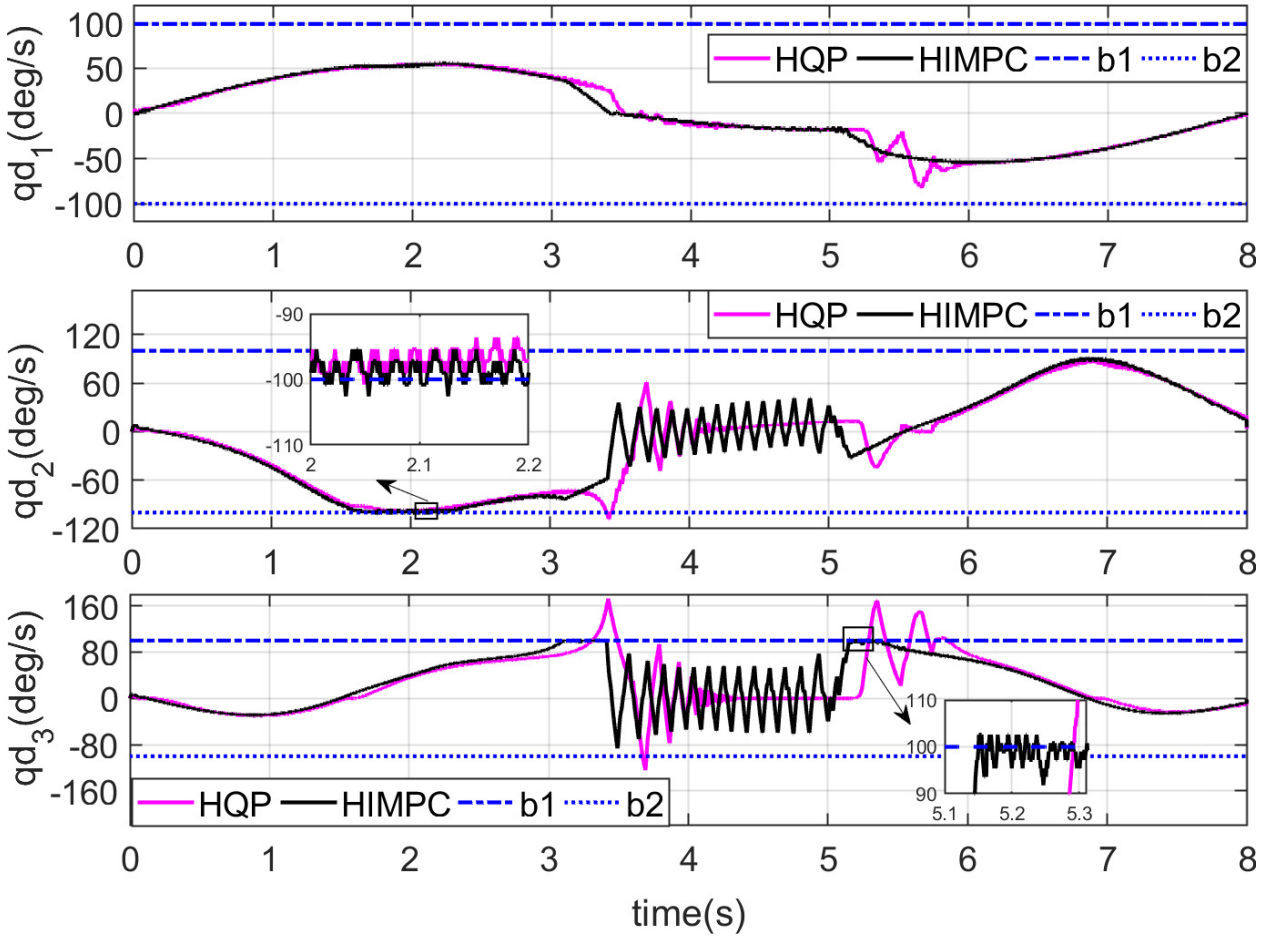

Figure 4.12: Experimental results *Scenario 2*: Joint velocities of three joints (the reference trajectory is RT2), where b_* denotes the corresponding joint velocity bound.

Table 4.4: Comparison Between the Proposed HIMPC and State-of-the-Art Controllers

Property	**OSF**	**TDEOSF**	**HQP**	**HIMPC**
Robust	×	✓	×	✓
Dynamic Consistency	×	✓	×	✓
Singularity-Free	×	×	×	✓
Input Constraints	×	×	✓	✓
State Constraints	×	×	×	✓

It verifies that HIMPC is kinematically singularity-free. Note that tracking errors of tasks (especially e_y shown in Figure 4.14) are slightly larger at the beginning and around 8s. This is because the control degrees of freedom are partially lost when the robot manipulator is kinematically singular. Nevertheless, HIMPC guarantees that the system passes the singular region safely.

Finally, we summarize the results of the experimental evaluation in Table 4.4.

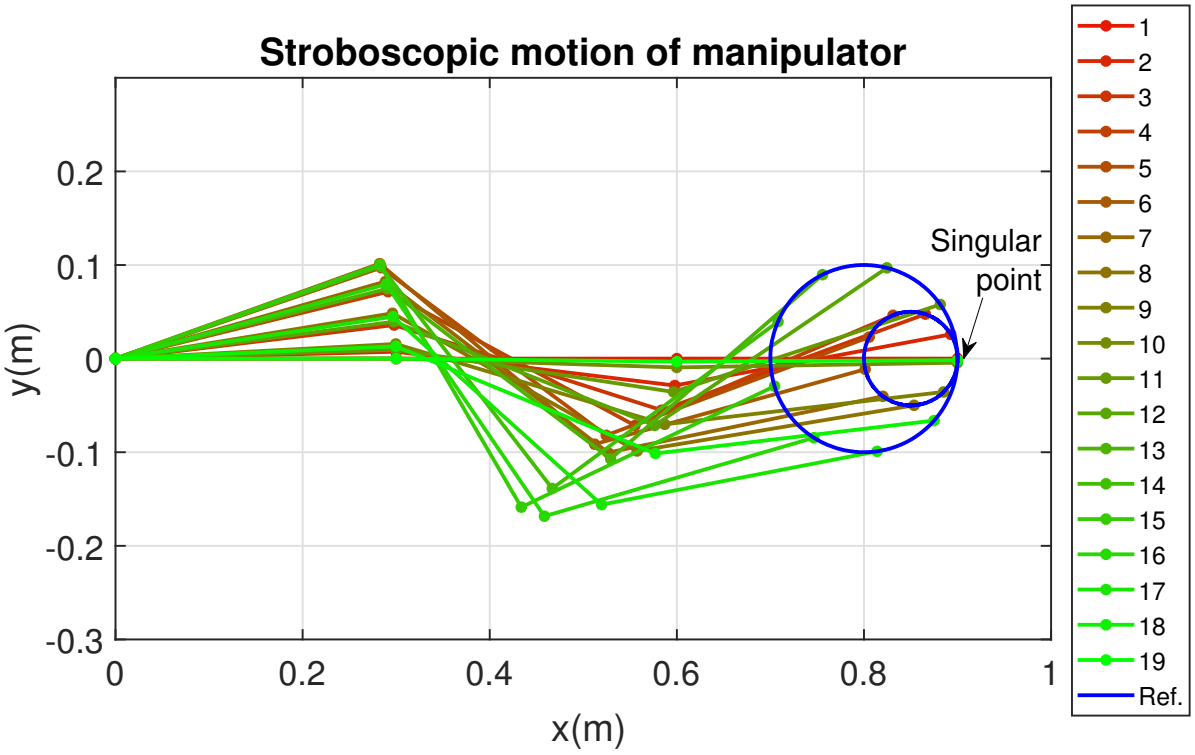

Figure 4.13: Experimental results of *Scenario 2*: Stroboscopic motion of the robot manipulator using the proposed HIMPC (the reference trajectory is RT3), and the robot manipulator is kinematically singular at the 1st, 10th, and 21st points.

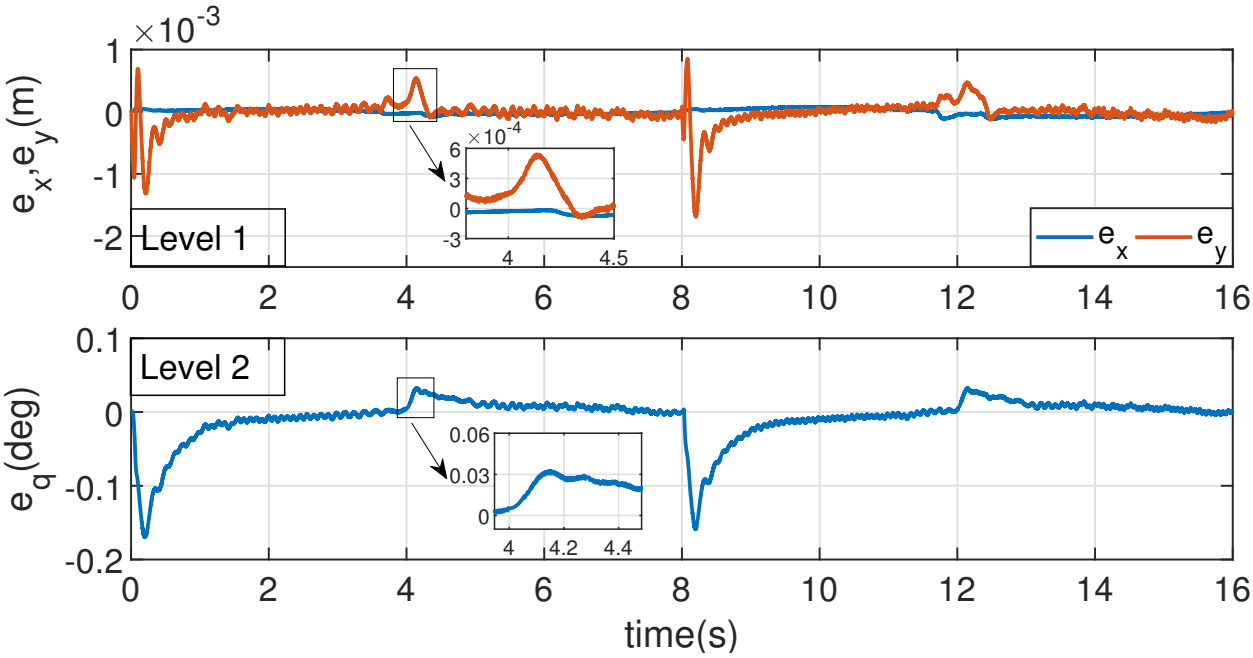

Figure 4.14: Experimental results of *Scenario 2*: Tracking errors of HIMPC (the reference trajectory is RT3).

Table 4.5: Task Definitions and Control Gains for Simulations

Level	Task Definition	Stiffness	Damping
1	TCP position in x	200 N/m	10 Ns/m
1	TCP position in y	200 N/m	10 Ns/m
1	TCP position in z	200 N/m	10 Ns/m
2	TCP orientation (o_X)	50 Nm/rad	5 Nms/rad
2	TCP orientation (o_Y)	50 Nm/rad	5 Nms/rad
2	TCP orientation (o_Z)	50 Nm/rad	5 Nms/rad
3	Joint position q_1	50 Nm/rad	5 Nms/rad

4.6 Simulation of a 7-DoF KUKA Robot

The effectiveness of HIMPC is now in addition validated by simulations of control performance for a higher-degree-of-freedom robot manipulator that allows for a task hierarchy with more than two task levels.

4.6.1 Simulation Setup

We simulate a 7-DoF KUKA LBR iiwa 14 R820 [180] using the Matlab Robotics System Toolbox [181] on a PC with Intel® Core™ CPU (i7 8550U @1.80 GHz). The sampling rate is 1 kHz.

A task hierarchy with 3 priority levels (see Figure 4.15) is implemented with task definitions and control gains in the target motion dynamics (4.3) from Table 4.5. We introduce the tool center point (TCP) and x, y, and z denote its Cartesian coordinates in the body frame, while o_X, o_Y, and o_Z are its orientation w.r.t. the X-, Y- and Z-axes. A reference trajectory RT4 is defined, see Figure 4.16. The initial configuration of the robot manipulator is $\mathbf{q}_0 = [0, 60, 0, 60, 0, 0, 0]^\top$deg. The prediction horizon of HIMPC is $N = 5$, and weighting matrices are chosen as $\mathbf{Q}_i := 200\mathbf{I}$ and $\mathbf{R}_i := 10\mathbf{I}$ for $i = 1, 2, 3$. Constraints for joint position, velocity, and torques are chosen according to [180]. The constrained OCPs in HIMPC are solved by `qpOASES` [174]. According to **Remark 23**, the diagonal matrix is chosen as $\bar{\mathbf{M}} = \mathrm{diag}(0.1, 0.21, 0.033, 0.042, 0.001, 0.001, 0.0003)$.

The reference trajectory RT4 is designed such that low-priority tasks conflict with high-priority tasks. The successful realization of the task hierarchy is investigated by measuring whether tracking performance of high-priority tasks is affected by low-priority tasks. Also, the computational complexity of HIMPC is investigated by monitoring the computation time for each prediction. Finally, it is verified that singularities are successfully avoided.

4.6.2 Simulation Results

The simulation results are displayed in Figure 4.17. We observe that the low-priority task (Level 3) "sacrifices" itself to guarantee the task hierarchy, while tracking performance of high-priority tasks is almost not affected. For [3.8s, 4s], tracking errors of Level 2 tasks (especially the orientation of the TCP w.r.t. Y-axis) slightly increase. This is mainly because

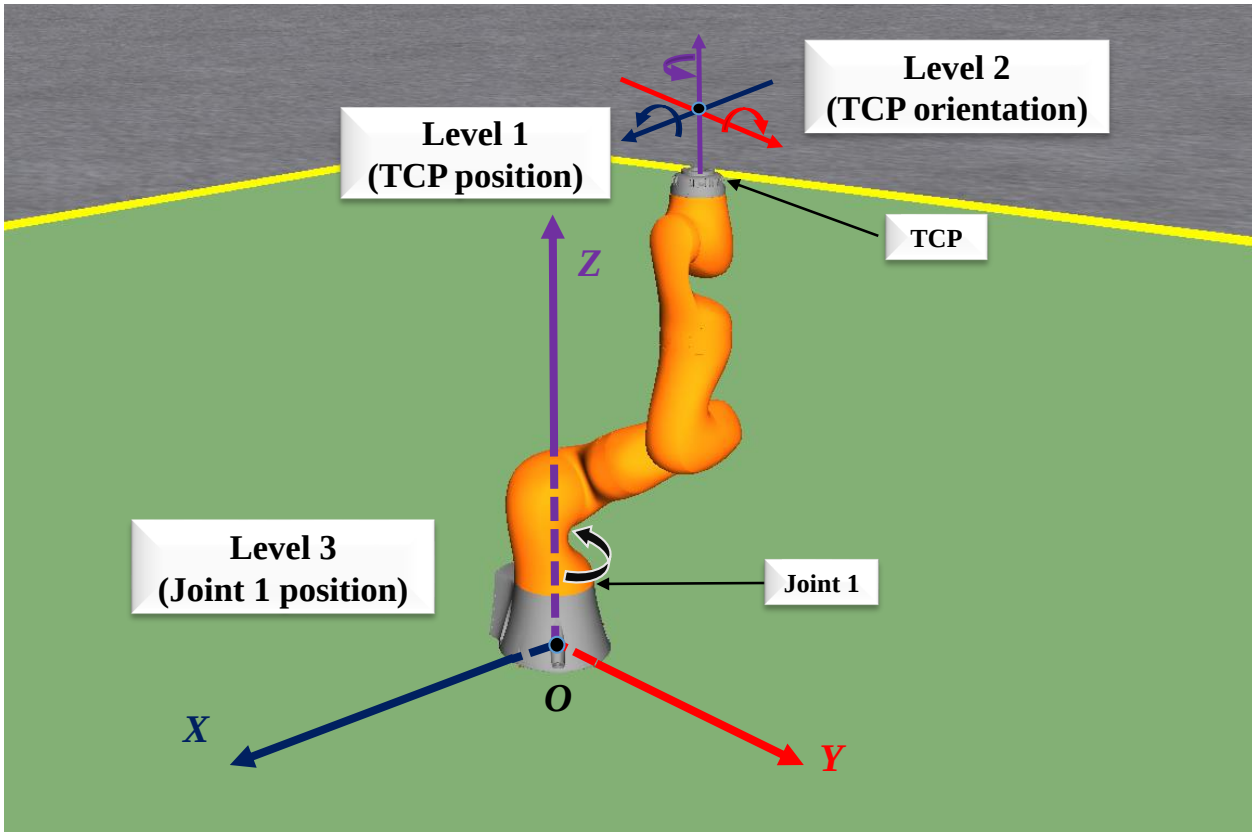

Figure 4.15: Simulation setup of the 7-DoF manipulator (KUKA LBR iiwa) with three-level task hierarchy.

the joint positions are constrained.

However, for OSF, TDEOSF, and HQP, the controlled system is unstable for reference trajectory RT4. This is because in the initial configuration, the system is kinematically singular, i.e., the Jacobian matrix loses its rank ($\text{rank}(\text{col}(\mathbf{J}_1, \mathbf{J}_2, \mathbf{J}_3)) = 6 < 7$). For HIMPC, we see that tracking errors of the level 3 task (position of joint 1) are slightly larger in the first 0.2 seconds. This is because the robot manipulator is kinematically singular and the control degrees of freedom of the system are partially lost during this time period. Nevertheless, the system passes the singular region safely.

4.7 Summary

In this chapter, the hierarchical incremental model predictive control (HIMPC) is proposed for robot manipulators to execute multiple tasks simultaneously, where singularity problems of task-space control are addressed.

To reduce dependency on an accurate mathematical model, equations of motion and system dynamics are approximated by incremental systems using time-delay estimation (TDE). It improves robustness of the controller against modelling errors and disturbances. The HIMPC is proposed by developing a series of constrained optimization control problems (OCPs), where task hierarchy is realized by equality constraints, which are set based on *dynamic consistency* principle instead of using the null-space projection. Besides, inverse

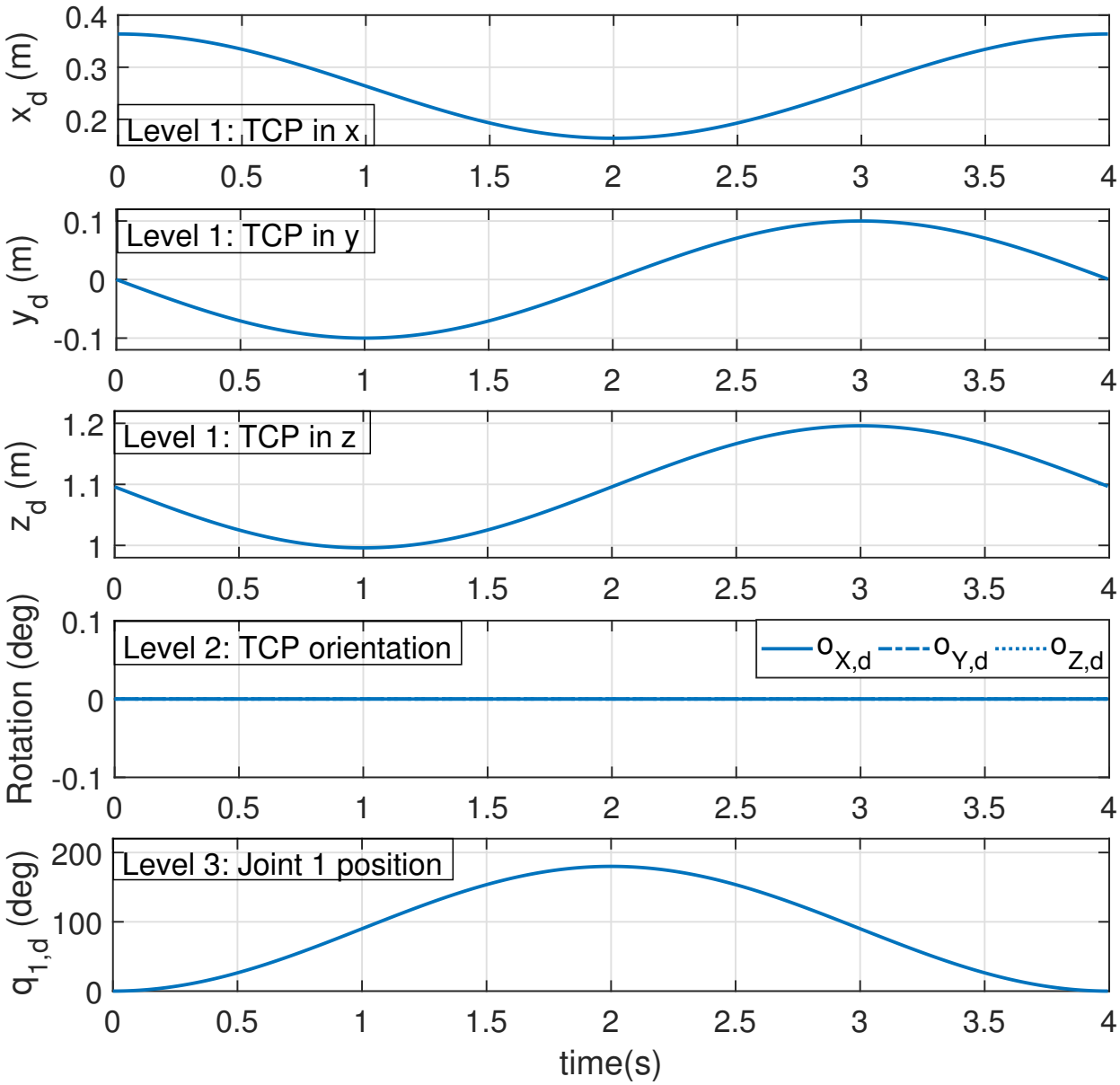

Figure 4.16: Reference trajectory RT4. The reference geometric curve of TCP is a "circle" with a radius of 10 cm (level 1), and the orientation of TCP is assigned to be maintained (level 2). Moreover, the first joint is commanded to move in a range of 180 deg (level 3).

calculation of terms w.r.t. Jacobian matrices is not involved and Hessian matrices of constrained OCPs are always positive definite. As a result, the proposed HIMPC guarantees both algorithmic and kinematic singularity-free capability. In addition, HIMPC is formulated as a linear MPC. Compared with nonlinear MPC, computational complexity of HIMPC dramatically decreases, which enables the controller run with a sampling time of 1 millisecond. Finally, simulations and experiments were conducted, and the efficacy of HIMPC is validated.

Future research will be devoted to extensive experimental evaluations of the controller and extend to the impedance control case when dynamic interaction is required. Besides, the

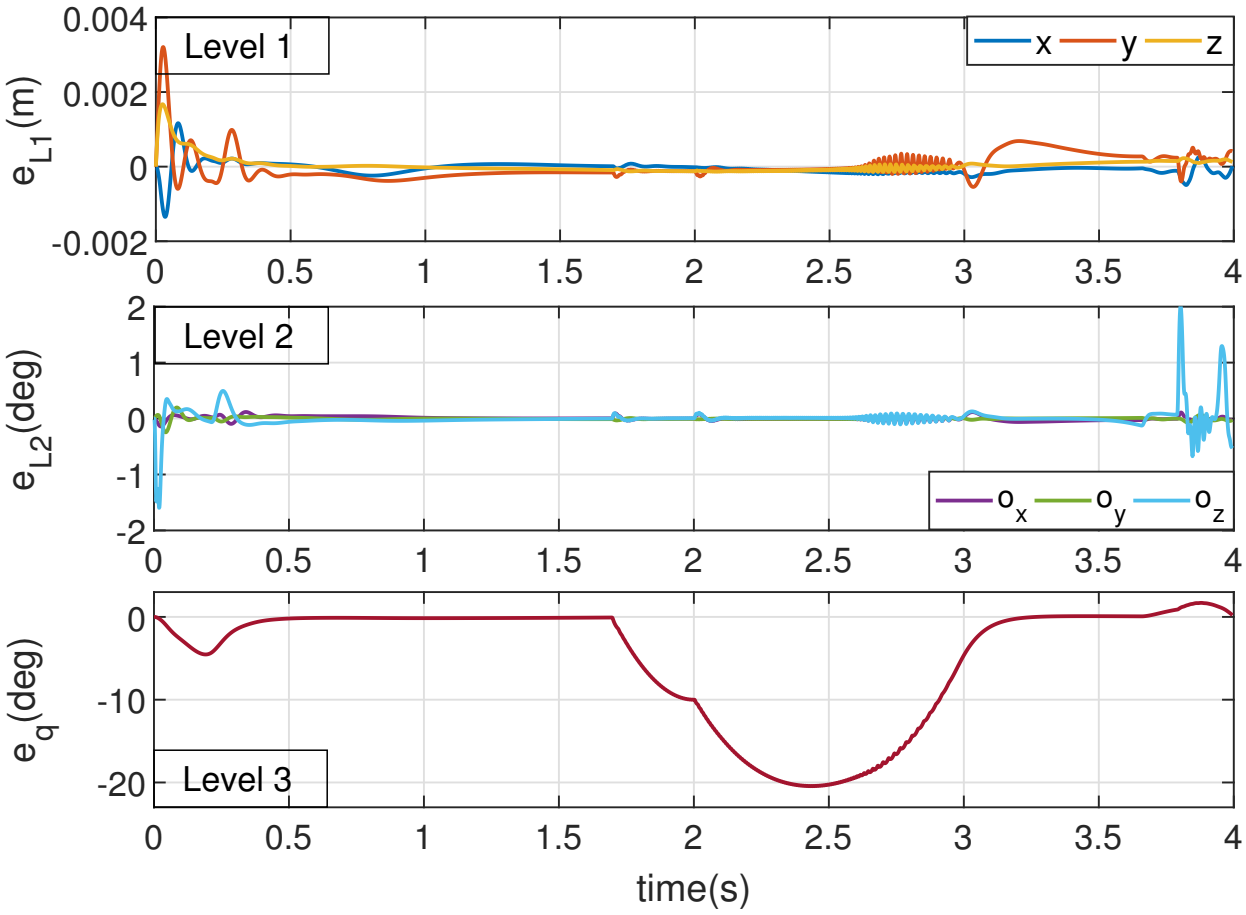

Figure 4.17: Simulation results: Tracking errors of HIMPC for the 7-DoF KUKA robot.

TDE error and strict state constraints will be addressed.

5 Conclusions and Outlook

5.1 Conclusions

In this dissertation, we develop the joint-space and task-space controllers for robot manipulators, addressing uncertainties, input and state constraints, and singularities, respectively. Here, we conclude the dissertation by chapters.

In Chapter 2, an adaptive incremental sliding mode control is proposed to address modeling errors and external disturbances. First, the time delay estimation (TDE) technique is employed to approximate the uncertain and complex mathematical model of the robot manipulator. It significantly reduces dependency on the mathematical model. However, the TDE error is introduced, which adversely affects the tracking performance if a constant diagonal decoupling inertia matrix is adopted. To compensate for the TDE error and then further enhance robustness of the controller, sliding mode control is combined with TDE. The novel positive semi-definite barrier function based sliding mode controller is designed to prevent switching gains from being over-estimated and under-estimated. It results in attenuating chattering and increasing tracking accuracy simultaneously. This is the main contribution of this chapter. Although the first challenge (listed in Section 1.2) is addressed, it also has the drawback, i.e., the input and state constraints are not considered.

In Chapter 3, an incremental model predictive control (IMPC) for the robot manipulator was developed. First, an approximation discrete-time linear system with the incremental control signal is derived using TDE and discretization. Based on the approximated discrete-time linear system, the IMPC is proposed through constructing a constrained optimal control problem (OCP). Thus, input and state constraints are addressed without the concrete mathematical model. This is the main contribution of this chapter. Moreover, considering the bounded TDE error as the disturbance, the input-to-state stability (ISS) of IMPC is confirmed. Different from conventional methods, ISS is analyzed utilizing the continuity of the value function, and over-conservative *cumulative error bound* is avoided. From ISS, it is theoretically inferred that increasing the prediction horizon decreases tracking errors and enlarges the region of attraction. This is the main theoretical contribution of this chapter. In addition, in practice, the IMPC is a linear MPC owing to the adopted linear incremental system, and the constrained OCP is a quadratic programming problem. Compared with nonlinear MPC schemes, computational complexity decreases significantly.

In Chapter 4, a robust and singularity-free task-prioritized controller, the hierarchical incremental model predictive controller (HIMPC), was proposed for a kinematically redundant robot manipulator. Multiple tasks are considered simultaneously and ordered by priority levels. At first, the incremental approximation is developed that approximates equations of motion of tasks and also uncertain system dynamics with high approximation accuracy. Then the HIMPC framework was developed based on multi-layer constrained OCPs, where the

task hierarchy is realized by equality constraints on control signals for lower-priority tasks, based on *dynamic consistency* principle. Moreover, the hierarchical feasibility of HIMPC and the uniqueness of its solution is theoretically analyzed. Finally, the effectiveness of the proposed HIMPC is demonstrated by numerical simulations and real-time experiments. Compared with state-of-the-art task-prioritized control schemes, the developed HIMPC shows strong robustness against uncertainties and external disturbances and *dynamic consistency* is also enhanced, owing to the introduced incremental approximation. Besides, the proposed HIMPC is singularity-free, which is the main contribution of this chapter. The reasons are twofold: (1) Inverse matrix calculation is not involved in HIMPC; (2) For each considered OCP in HIMPC, the Hessian matrix is positive definite, and numerical weakness is avoided.

5.2 Outlook

While the practical robust and optimal controllers are proposed for the robot manipulator, it also leaves some open problems to be investigated. In what follows, several potential interesting fields for incremental model predictive control methods are listed.

Incremental Model Predictive Control with an Adaptive TDE Parameter

In the incremental model predictive controllers in Chapters 3 and 4, a constant decoupled inertia matrix (TDE parameter) is employed and it is tuned manually. However, a constant TDE parameter introduces a large TDE error in some configurations of the robot manipulator. Thus, it still may result in poor tracking performance. As a potential development, the optimal TDE parameter can be obtained online through an efficient data-driven algorithm with a properly minimized data set.

In the data-driven algorithm, inevitable measurement noises will be considered since second-order derivatives are required in the incremental control scheme. Thus, dedicated filters and/or observers will be employed to estimate $\dot{\mathbf{q}}$ and $\ddot{\mathbf{q}}$. Besides, the the updating law of the TDE parameter will not be designed according to the tracking error. This is because with the state constraints, tracking error may increase when the robot manipulator stick to one configuration. In addition, for adaptive algorithm, the persistent-excitation (PE) condition should be satisfied. Otherwise, the controller will be singular and the system will be unstable. Therefore, to guarantee safety and system stability, the PE condition will be relaxed in the data-driven algorithm.

Incremental Model Predictive Impedance Control

In Chapter 4, the task-space controller is merely considered in the free space. In practice, the interaction between the robot manipulator and the environment is necessary. There is a trade-off to be made between allowable interface forces and allowable deviations from the desired positions. Impedance control is required so that the control objective should not track the position only but rather involve the regulation of impedance of the robot manipulator. Therefore, considering the target impedance control dynamics as part of the cost function, incremental predictive impedance control can be a potential field to be studied.

Besides, the force sensor output is adversely affected by disturbances and the interaction process and it is also a costly installation from an economic viewpoint. To realize the impedance control without force sensors, a practical force observer should be developed to estimate interaction forces merely according to end-effector positions and torques, i.e., the

sensor-less impedance control scheme is proposed. The major challenge is the design of the force observer without concrete mathematical model of the robot manipulator.

Incremental Model Predictive Control for a Flexible Joint Robot Manipulator and/or a General System

In this dissertation, the rigid robot manipulator is considered, which is modelled by the Euler-Lagrange equation. Flexible joint robot manipulators exhibit plenty of advantages over their rigid counterparts, such as less material, lighter weight, higher manipulation speed, lower power consumption, smaller actuators, more manoeuvrable and transportable, safer to operate owing to reduced weight, etc. However, the control for the flexible joint robot manipulator is also more challenging since the system dynamics is highly nonlinear and complex. Besides, the accurate model of the flexible joint robot manipulator is more difficult to be obtained. Thus, as a promising controller, a novel incremental model predictive controller for the more general system can be developed. First, a cascaded incremental system will be developed where the torques due to the joint compliance will be considered as an intermediate control law. Then the incremental model predictive controller for the flexible joint robot manipulator will be developed on the basis of the cascaded incremental system.

For robot manipulators, they can be modelled as Euler-Lagrange equations. The TDE technique can be employed to obtain the incremental systems and then IMPC is constructed. However, for a general system, such as non-Euler-Lagrange and non-affine system, it is challenging to apply TDE directly Since input matrix is not always positive definite or input matrix does not exist. Therefore, a general procedure should be developed to use the time-delay estimation and approximate the uncertain nonlinear and general dynamical systems.

Strict State Constraint Satisfaction

In the developed incremental model predictive control, the system dynamics (and also equations of motion of tasks in Chapter 4) is approximated by nominal incremental systems. However, the TDE error is ignored. Then, there are prediction errors of state variables. As a result, strict constraint satisfaction is not guaranteed. Although the huge deterioration of strongly violating constraints is avoided, the system suffers from the risk of constraint violation. This is an open problem for MPC when the uncertain system is considered. The learning method is really an effective method to deal with the unpredictable TDE error and measurement noises.

As a future development, we will take the strict state constraint satisfaction into consideration. The tube-based MPC, data-driven and safe learning methods can be employed. However, it is time-consuming to calculate tightened constraints in the tube-based MPC. Although recently the efficient method to calculate tightened constraints has been developed, it is still challenging to apply it on fast-dynamics systems. Thus, developing an effective algorithm to determine tightened constraints for tube-based MPC is one of our research directions.

Preliminaries

A

In this chapter, preliminaries, such as dynamic model of the robot manipulator and time-delay estimation technique, will be introduced. First, dynamic model of an n-link robot manipulator is modelled by an Euler-Lagrange equation. However, modelling errors and external disturbances are inevitable. To reduce dependence on the concrete mathematical model and approximate uncertain system dynamics, time-delay estimation (TDE) technique is introduced, which is also a basis to develop controllers in Chapters 2-4.

A.1 Modeling of the Robot Manipulator

The dynamic model of an n-link robot manipulator is given as an Euler-Lagrange equation [65], [182]:

$$\mathbf{M}(\mathbf{q})\ddot{\mathbf{q}} + \mathbf{C}(\mathbf{q}, \dot{\mathbf{q}})\dot{\mathbf{q}} + \mathbf{G}(\mathbf{q}) + \mathbf{F}(\dot{\mathbf{q}}) = \boldsymbol{\tau}, \tag{A.1}$$

where $\mathbf{q} \in \mathbb{R}^n$ is the vector of joint angles, $\mathbf{M}(\mathbf{q}) \in \mathbb{R}^{n\times n}$ is the symmetric positive definite inertia matrix, $\mathbf{C}(\mathbf{q}, \dot{\mathbf{q}}) \in \mathbb{R}^{n\times n}$ is a matrix of centrifugal and Coriolis terms, $\mathbf{G}(\mathbf{q}) \in \mathbb{R}^n$ contains the gravitational terms exerting on the robot manipulator, $\mathbf{F}(\dot{\mathbf{q}}) \in \mathbb{R}^n$ denotes viscous friction, $\boldsymbol{\tau} \in \mathbb{R}^n$ is the input applied to the joints.

For the Euler-Lagrange system (A.1), the uniform positive definiteness of the inertia matrix $\mathbf{M}(\mathbf{q})$ is introduced in the following. Later we will need positive definiteness of $\mathbf{M}(\mathbf{q})$ to determine design parameters (see **Remark 23**).

Property 1 (Positive Definite Inertia Matrix [79])**.** *The matrix* $\mathbf{M}(\mathbf{q})$ *is uniformly positively definite and there exist* μ_1, $\mu_2 \in \mathbb{R}_{>0}$ *such that* $\mu_1\mathbf{I} \leq \mathbf{M}(\mathbf{q}) \leq \mu_2\mathbf{I}$, *where* $\mathbf{I} \in \mathbb{R}^{n\times n}$ *is the* n*-dimensional identity matrix.*

Note that due to inevitable modeling errors, the inertia matrix $\mathbf{M}(\mathbf{q})$, and other nonlinear dynamics terms $\mathbf{C}(\mathbf{q}, \dot{\mathbf{q}})$, $\mathbf{G}(\mathbf{q})$, and $\mathbf{F}(\dot{\mathbf{q}})$ are considered to be unknown/uncertain in this dissertation.

A.2 Time-Delay Estimation

In this subsection, TDE will be introduced. Using the time-delay signals to estimate the lumped dynamics, TDE guarantees an attractive model-free structure for controllers [28]–[36]. To enhance robustness of the controller, the uncertain system dynamics will be approximated by TDE, which is the fundamental work to develop the incremental controllers in this dissertation.

Let $\mathbf{x}_1 = \mathbf{q}$, $\mathbf{x}_2 = \dot{\mathbf{q}}$, and $\mathbf{x} = \text{col}(\mathbf{x}_1, \mathbf{x}_2)$, the dynamics (A.1) is transformed into an affine nonlinear form:

$$\dot{\mathbf{x}}_1 = \mathbf{x}_2 \tag{A.2a}$$
$$\dot{\mathbf{x}}_2 = \mathbf{f}(\mathbf{x}) + \mathbf{g}(\mathbf{x})\mathbf{u}, \tag{A.2b}$$

where $\mathbf{f}(\mathbf{x}) = -\mathbf{M}^{-1}(\mathbf{q})(\mathbf{C}(\mathbf{q}, \dot{\mathbf{q}})\dot{\mathbf{q}} + \mathbf{G}(\mathbf{q}) + \mathbf{F}\dot{\mathbf{q}})$, $\mathbf{g}(\mathbf{x}) = \mathbf{M}^{-1}(\mathbf{q})$ and $\mathbf{u} = \boldsymbol{\tau}$.

According to [103], [183], $\mathbf{M}(\mathbf{q})$, $\mathbf{C}(\mathbf{q}, \dot{\mathbf{q}})$, $\mathbf{G}(\mathbf{q})$, and $\mathbf{F}(\dot{\mathbf{q}})$ are all upper bounded. Thus, the following assumption is made for $\mathbf{f}(\mathbf{x})$ in an admissible set $\mathbb{D}_{\mathbf{x}} \subset \mathbb{R}^{2n}$.

Assumption 5 (Boundedness Property of $\mathbf{f}(\mathbf{x})$)**.** $\mathbf{f}(\mathbf{x})$ *with* $\mathbf{f}(\mathbf{0}) = \mathbf{0}$ *is upper bounded in* $\mathbb{D}_{\mathbf{x}}$*, with constants* $f_{\max}, f_0 \in \mathbb{R}_{>0}$*, that is,*

$$\|\mathbf{f}(\mathbf{x})\| \leq f_{\max}\|\mathbf{x}\| + f_0, \quad \forall \mathbf{x} \in \mathbb{D}_{\mathbf{x}}. \tag{A.3}$$

To reduce dependence on the mathematical model, such as $\mathbf{f}(\mathbf{x})$ and $\mathbf{g}(\mathbf{x})$, TDE technique is applied on the second subsystem (A.2b), and an incremental system will be obtained.

Introducing a constant diagonal matrix $\bar{\mathbf{g}}$, one obtains another expression of (A.2b) as follows:

$$\bar{\mathbf{g}}^{-1}\dot{\mathbf{x}}_2 = \mathbf{H}(\mathbf{x}, \dot{\mathbf{x}}) + \mathbf{u}, \tag{A.4}$$

where $\mathbf{H}(\mathbf{x}, \dot{\mathbf{x}}) = (\bar{\mathbf{g}}^{-1} - \mathbf{g}^{-1}(\mathbf{x}))\,\dot{\mathbf{x}}_2 + \mathbf{g}^{-1}(\mathbf{x})\mathbf{f}(\mathbf{x})$ is a lump nonlinear function. In practice, when the sampling rate is sufficiently high, $\mathbf{H}(\mathbf{x}, \dot{\mathbf{x}})$ can be estimated by its time-delay value [28]–[36] as

$$\hat{\mathbf{H}}(\mathbf{x}, \dot{\mathbf{x}}) = \mathbf{H}(\mathbf{x}_0, \dot{\mathbf{x}}_0) = \bar{\mathbf{g}}^{-1}\dot{\mathbf{x}}_{2,0} - \mathbf{u}_0, \tag{A.5}$$

where $\mathbf{x}_0$, $\mathbf{x}_{2,0}$ and $\mathbf{u}_0$ are the values of the states $\mathbf{x}$, $\mathbf{x}_2$ and controller $\mathbf{u}$ at the previous sampling time, respectively. In practice, a digital control system behaves reasonably close to a continuous system if the sampling rate is faster than 30 times the system bandwidth [134]. Thus, with sufficiently high sampling rate, the lump nonlinear function is estimated by TDE [31].

From (A.4) and (A.5), we obtain the following system with the incremental controller $\Delta\mathbf{u}$:

$$\dot{\mathbf{x}}_2 = \dot{\mathbf{x}}_{2,0} + \bar{\mathbf{g}}\Delta\mathbf{u} + \boldsymbol{\epsilon} \tag{A.6}$$

where $\Delta\mathbf{u} = \mathbf{u} - \mathbf{u}_0$, $\boldsymbol{\epsilon} = \bar{\mathbf{g}}\left(\mathbf{H}(\mathbf{x}, \dot{\mathbf{x}}) - \hat{\mathbf{H}}(\mathbf{x}, \dot{\mathbf{x}})\right)$ is the TDE error. The TDE error is related to the designed controller [31]. We will analyze its boundedness in **Lemma 1**, **Lemma 2**, and **Lemma 6** with different controllers.

As a result, (A.2) is transformed into the following new *strict-feedback* system using TDE:

$$\dot{\mathbf{x}}_1 = \mathbf{x}_2 \tag{A.7a}$$
$$\dot{\mathbf{x}}_2 = \dot{\mathbf{x}}_{2,0} + \bar{\mathbf{g}}\Delta\mathbf{u} + \boldsymbol{\epsilon} \tag{A.7b}$$

We can observe that $\bar{\mathbf{g}}$ is the only parameter in the new *strict-feedback* system (A.7). For a specific robot manipulator, we can determine the diagonal matrix $\bar{\mathbf{g}}$ as follows.

Remark 23 (How to Determine the Diagonal Matrix $\bar{\mathbf{g}}$?)**.** *According to* ***Property 1****, there exist* $\mu_1, \mu_2 \in \mathbb{R}_{>0}$ *such that* $0 < \frac{1}{\mu_2} \leq \lambda_i \leq \frac{1}{\mu_1}$ *since* $\mathbf{g}(\mathbf{x}) = \mathbf{M}^{-1}(\mathbf{x})$*, where* $\mathbf{M}(\mathbf{x})$ *is the inertia matrix and* λ_i *is the eigenvalue of* $\mathbf{g}(\mathbf{x})$*. Suppose* $\bar{g}_i$ *is the diagonal element of* $\bar{\mathbf{g}}$*,*

$\left(1-\frac{\lambda_i}{\bar{g}_i}\right)$ *is the eigenvalue of* $(\mathbf{I}-\mathbf{g}(\mathbf{x})\bar{\mathbf{g}}^{-1})$. *If* $|1-\frac{\lambda_i}{\bar{g}_i}|<1$, *then* $\|\mathbf{I}-\mathbf{g}(\mathbf{x})\bar{\mathbf{g}}^{-1}\|_2<1$ *holds, i.e., if* $\bar{g}_i$ *satisfies* $\bar{g}_i>\frac{\lambda_i}{2}$, *then* $\|\mathbf{I}-\mathbf{g}(\mathbf{x})\bar{\mathbf{g}}^{-1}\|_2<1$ *holds. Theoretically, we fix* $\bar{g}_i$ *after we have determined the maximum eigenvalue of* $\mathbf{g}(\mathbf{x})$, *noted as* $\lambda_{i,\max}$, *and let* $\bar{g}_i>\frac{\lambda_{i,\max}}{2}$. *In practice,* $\bar{\mathbf{g}}$ *is selected by a manual tuning process. If* $\bar{g}_i$ *is sufficiently large,* $\bar{g}_i>\frac{\lambda_{i,\max}}{2}$ *holds. Generally, large* $\bar{\mathbf{g}}$ *results in large TDE errors while small* $\bar{\mathbf{g}}$ *causes noisy responses. The constant* $\bar{\mathbf{g}}:=\mathrm{diag}(\bar{g}_1,\cdots,\bar{g}_n)$ *is selected following the procedures in [184] (The TDE parameter* $\bar{\mathbf{g}}$ *is corresponding to the inverse of* $\bar{\mathbf{M}}$ *in [184]): (1) start with a sufficiently large positive value for* $\bar{g}_i$ *to guarantee stability; (2) decrease* $\bar{g}_i$ *until the closed-loop system almost shows a noisy response. Following the aforementioned procedures, the TDE parameter* $\bar{\mathbf{g}}$ *is tuned without any information about the plant dynamics.*

Remark 24 ($\bar{\mathbf{g}}$ is Robust Against Payload Variations)**.** $\bar{\mathbf{g}}$ *determined for the no-load case also makes* $\|\mathbf{I}-\mathbf{g}(\mathbf{x})\bar{\mathbf{g}}^{-1}\|_2<1$ *hold under payload variations. This is because the eigenvalues of* $\mathbf{M}(\mathbf{x})$ *increase when the robot manipulator carries some payloads while the eigenvalues of* $\mathbf{g}(\mathbf{x})$ *decrease. That is,* $\lambda_i>\lambda_i^*$, *supposing* λ_i^* *is the eigenvalue of* $\mathbf{g}(\mathbf{x})$ *when it carries some payloads. Thus,* $\bar{g}_i>\frac{\lambda_i^*}{2}$ *still holds.*

Parameters in Eq. (4.34)

B

$\mathcal{Q}_i := \bar{\mathbf{B}}_{1i}^\top \bar{\mathbf{Q}}_i \bar{\mathbf{B}}_{1i} + \bar{\mathbf{R}}_i$; $\mathcal{L}_i := 2\bar{\mathbf{B}}_{1i}^\top \bar{\mathbf{Q}}_i (\bar{\mathbf{A}}_1 \vec{\mathbf{x}}_i(k) - \mathbf{X}_{\mathrm{id}})$; $\bar{\mathbf{Q}}_i := \mathrm{diag}\left(\bar{\mathbf{K}}_i^\top \mathbf{Q}_i \bar{\mathbf{K}}_i, \cdots, \bar{\mathbf{K}}_i^\top \mathbf{Q}_i \bar{\mathbf{K}}_i\right)$;

$$\bar{\mathbf{B}}_{1i} := \begin{bmatrix} \mathbf{B}_{1i} & & & & \\ \mathbf{A}_1\mathbf{B}_{1i} & \mathbf{B}_{1i} & & & \\ \mathbf{A}_1^2\mathbf{B}_{1i} & \mathbf{A}_1\mathbf{B}_{1i} & \mathbf{B}_{1i} & & \\ \cdots & & & & \\ \mathbf{A}_1^{N-1}\mathbf{B}_{1i} & \mathbf{A}_1^{N-2}\mathbf{B}_{1i} & \mathbf{A}_1^{N-3}\mathbf{B}_{1i} & \cdots & \mathbf{B}_{1i} \end{bmatrix};$$

$\mathbf{X}_{i\mathrm{d}} := \mathrm{col}(\bar{\mathbf{x}}_{i\mathrm{d}}(k+1), \cdots, \bar{\mathbf{x}}_{i\mathrm{d}}(k+N))$; $\bar{\mathbf{R}}_i := \mathrm{diag}(\mathbf{R}_i, \cdots, \mathbf{R}_i)$; $\bar{\mathbf{K}}_i := [\mathbf{K}_i, \mathbf{O}]$;

$\bar{\mathbf{A}}_1 := \mathrm{col}\left(\mathbf{A}_1, \mathbf{A}_1^2, \cdots, \mathbf{A}_1^N\right)$; $\mathbf{C}_{i1} := \mathrm{col}(-\mathbf{c}_{i1}, \mathbf{c}_{i1})$; $\mathbf{D}_{i1} := \begin{bmatrix} -\bar{\mathbf{L}}_1 \vec{\mathbf{q}}(k) + \bar{\mathbf{q}}_{\min} \\ \bar{\mathbf{L}}_1 \vec{\mathbf{q}}(k) - \bar{\mathbf{q}}_{\max} \end{bmatrix}$;

$$\mathbf{c}_{i1} := \begin{bmatrix} \mathbf{L}_1\mathbf{B}_2 & & & & \\ \mathbf{L}_1\mathbf{A}_2\mathbf{B}_2 & \mathbf{L}_1\mathbf{B}_2 & & & \\ \mathbf{L}_1\mathbf{A}_2^2\mathbf{B}_2 & \mathbf{L}_1\mathbf{A}_2\mathbf{B}_2 & \mathbf{L}_1\mathbf{B}_2 & & \\ \cdots & & & & \\ \mathbf{L}_1\mathbf{A}_2^{N-1}\mathbf{B}_2 & \mathbf{L}_1\mathbf{A}_2^{N-2}\mathbf{B}_2 & \mathbf{L}_1\mathbf{A}_2^{N-3}\mathbf{B}_2 & \cdots & \mathbf{L}_1\mathbf{B}_2 \end{bmatrix};$$

$\bar{\mathbf{L}}_1 := \mathrm{col}\left(\mathbf{L}_1\mathbf{A}_2, \mathbf{L}_1\mathbf{A}_2^2, \cdots, \mathbf{L}_1\mathbf{A}_2^N\right)$; $\bar{\mathbf{q}}_{\min} := \mathrm{col}\left(\mathbf{q}_{\min}, \cdots, \mathbf{q}_{\min}\right)$;

$\bar{\mathbf{q}}_{\max} := \mathrm{col}\left(\mathbf{q}_{\max}, \cdots, \mathbf{q}_{\max}\right)$; $\mathbf{L}_1 := [\mathbf{I}, \mathbf{O}, \mathbf{O}, \mathbf{O}]$; $\mathbf{C}_{i2} := \mathrm{col}(-\mathbf{c}_{i2}, \mathbf{c}_{i2})$;

$\mathbf{D}_{i2} := \begin{bmatrix} -\bar{\mathbf{L}}_2 \vec{\mathbf{q}}(k) + \bar{\dot{\mathbf{q}}}_{\min} \\ \bar{\mathbf{L}}_2 \vec{\mathbf{q}}(k) - \bar{\dot{\mathbf{q}}}_{\max} \end{bmatrix}$; $\bar{\mathbf{L}}_2 := \mathrm{col}\left(\mathbf{L}_2\mathbf{A}_2, \mathbf{L}_2\mathbf{A}_2^2, \cdots, \mathbf{L}_2\mathbf{A}_2^N\right)$;

$$\mathbf{c}_{i2} := \begin{bmatrix} \mathbf{L}_2\mathbf{B}_2 & & & & \\ \mathbf{L}_2\mathbf{A}_2\mathbf{B}_2 & \mathbf{L}_2\mathbf{B}_2 & & & \\ \mathbf{L}_2\mathbf{A}_2^2\mathbf{B}_2 & \mathbf{L}_2\mathbf{A}_2\mathbf{B}_2 & \mathbf{L}_2\mathbf{B}_2 & & \\ \cdots & & & & \\ \mathbf{L}_2\mathbf{A}_2^{N-1}\mathbf{B}_2 & \mathbf{L}_2\mathbf{A}_2^{N-2}\mathbf{B}_2 & \mathbf{L}_2\mathbf{A}_2^{N-3}\mathbf{B}_2 & \cdots & \mathbf{L}_2\mathbf{B}_2 \end{bmatrix}; \ \mathbf{L}_2 := [\mathbf{O}, \mathbf{I}, \mathbf{O}, \mathbf{O}];$$

$\bar{\dot{\mathbf{q}}}_{\min} := \mathrm{col}\left(\dot{\mathbf{q}}_{\min}, \cdots, \dot{\mathbf{q}}_{\min}\right)$; $\bar{\dot{\mathbf{q}}}_{\max} := \mathrm{col}\left(\dot{\mathbf{q}}_{\max}, \cdots, \dot{\mathbf{q}}_{\max}\right)$; $\mathbf{C}_{i3} := \mathrm{col}(-\bar{\mathbf{I}}, \bar{\mathbf{I}})$;

$$\mathbf{D}_{i3} := \begin{bmatrix} -\bar{\boldsymbol{\tau}}_0 + \bar{\boldsymbol{\tau}}_{\min} \\ \bar{\boldsymbol{\tau}}_0 - \bar{\boldsymbol{\tau}}_{\max} \end{bmatrix}; \ \bar{\mathbf{I}} := \begin{bmatrix} \mathbf{I} & & & \\ \mathbf{I} & \mathbf{I} & & \\ \cdots & & & \\ \mathbf{I} & \mathbf{I} & \cdots & \mathbf{I} \end{bmatrix}; \ \bar{\boldsymbol{\tau}}_0 := \mathrm{col}\left(\boldsymbol{\tau}_0, \cdots, \boldsymbol{\tau}_0\right);$$

$\bar{\boldsymbol{\tau}}_{\min} := \mathrm{col}\left(\boldsymbol{\tau}_{\min}, \cdots, \boldsymbol{\tau}_{\min}\right)$; $\bar{\boldsymbol{\tau}}_{\max} := \mathrm{col}\left(\boldsymbol{\tau}_{\max}, \cdots, \boldsymbol{\tau}_{\max}\right)$; $\mathbf{a}_{ip}^\top := \bar{\mathbf{J}}_{p,k}$; $\mathbf{b}_{ip} := \bar{\mathbf{J}}_{p,k}\mathbf{U}_p^*$;

$\bar{\mathbf{J}}_{p,k} := \mathrm{diag}\left(\mathbf{J}_{p,k}\bar{\mathbf{M}}^{-1}, \cdots, \mathbf{J}_{p,k}\bar{\mathbf{M}}^{-1}\right)$; $\mathbf{U}_p^* := \mathrm{col}\left(\Delta\boldsymbol{\tau}_{p,k|k}^*, \cdots, \Delta\boldsymbol{\tau}_{p,k+N-1|k}^*\right)$.

Definitions and Properties of Comparison Functions

C

The comparison functions $\mathcal{K}$, $\mathcal{K}_\infty$ and $\mathcal{KL}$ are introduced in **Definition 5** and **Definition 6** [185].

Definition 5 ($\mathcal{K}$ Function)**.** *A continuous function $\alpha : [0, a) \to \mathbb{R}_{\geq 0}$, for some $a > 0$, is said to belong to class $\mathcal{K}$ if it is zero at zero and strictly increasing. Moreover, $\alpha(\cdot)$ is said to belong to class $\mathcal{K}_\infty$ if it is a class $\mathcal{K}$ function with $a = \infty$, and radially unbounded, i.e., $\alpha(x) \to \infty$ as $x \to \infty$.*

Definition 6 ($\mathcal{KL}$ Function)**.** *A continuous function $\sigma : \mathbb{R}_{>0} \to \mathbb{R}_{\geq 0}$ is said to belong to class $\mathcal{L}$ if it decreases with $\lim_{k\to\infty} \sigma(k) = 0$. A continuous function $\beta : [0, a) \times [0, \infty) \to [0, \infty)$ is said to belong to class $\mathcal{KL}$ if, for each fixed s, the mapping $\beta(r, s)$ belongs to class $\mathcal{K}$ with respect to r and, for each fixed r, the mapping $\beta(r, s)$ belongs to class $\mathcal{L}$.*

The following lemma states some properties of comparison functions, which are used in Chapter 4 for ISS analysis of IMPC.

Lemma 11 (Properties of Comparison Functions)**.** *Let α_1 and α_2 be $\mathcal{K}$ functions on $[0, a)$, α_3 and α_4 be $\mathcal{K}_\infty$, and β be a $\mathcal{KL}$ function. Denote the inverse of α_i by α_i^{-1}. Then,*

1) α_1^{-1} is defined on $[0, \alpha_1(a))$ and is a $\mathcal{K}$ function;

2) α_3^{-1} is defined on $[0, \infty)$ and is a $\mathcal{K}_\infty$ function;

3) $\alpha_1 \circ \alpha_2$ is a $\mathcal{K}$ function;

4) $\alpha_3 \circ \alpha_4$ is a $\mathcal{K}_\infty$ function;

5) $\sigma(r, s) = \alpha_1(\beta(\alpha_2(r), s))$ is a $\mathcal{KL}$ function.

Note that $\circ$ denotes composition of two functions. The composition of functions $f_1 : \mathbb{S}_1 \to \mathbb{S}_2$ and $f_2 : \mathbb{S}_1 \to \mathbb{S}_3$, $(f_2 \circ f_1)(\cdot)$ are functions, then the function $f_2 \circ f_1 := f_2(f_1(\cdot))$, where $\mathbb{S}_1$, $\mathbb{S}_2$, and $\mathbb{S}_3$ are any sets.

Bibliography

[1] J. Z. Sasiadek, "Space robotics—present and past challenges", in *Proc. 19th International Conference on Methods and Models in Automation and Robotics (MMAR)*, 2014, pp. 926–929.

[2] J. Li, T. Zhang, X. Liu, Y. Guan, and D. Wang, "A survey of robotic polishing", in *Proc. IEEE International Conference on Robotics and Biomimetics (ROBIO)*, 2018, pp. 2125–2132.

[3] D. Deng, J. W. Polden, J. Dong, and P. Y. Tao, "Sensor guided robot path generation for surface repair tasks on a large-scale buoyancy module", *IEEE/ASME Transactions on Mechatronics*, vol. 23, no. 2, pp. 636–645, 2018.

[4] B. H. Wilcox, T. Litwin, J. Biesiadecki, J. Matthews, M. Heverly, J. Morrison, J. Townsend, N. Ahmad, A. Sirota, and B. Cooper, "ATHLETE: A cargo handling and manipulation robot for the moon", *Journal of Field Robotics*, vol. 24, no. 5, pp. 421–434, 2007.

[5] L. Halt, F. Nagele, P. Tenbrock, and A. Pott, "Intuitive constraint-based robot programming for robotic assembly tasks", in *Proc. IEEE International Conference on Robotics and Automation (ICRA)*, 2018, pp. 520–526.

[6] J. Burgner, D. C. Rucker, H. B. Gilbert, P. J. Swaney, P. T. Russell, K. D. Weaver, and R. J. Webster, "A telerobotic system for transnasal surgery", *IEEE/ASME Transactions on Mechatronics*, vol. 19, no. 3, pp. 996–1006, 2013.

[7] J. Lee, N. Deshpande, D. G. Caldwell, and L. S. Mattos, "Microscale precision control of a computer-assisted transoral laser microsurgery system", *IEEE/ASME Transactions on Mechatronics*, vol. 25, no. 2, pp. 604–615, 2020.

[8] A. C. Bittencourt and S. Gunnarsson, "Static friction in a robot joint—modeling and identification of load and temperature effects", *Journal of Dynamic Systems, Measurement, and Control*, vol. 134, no. 5, p. 051 013, 2012.

[9] D. A. Haessig Jr and B. Friedland, "On the modeling and simulation of friction", *Journal of Dynamic Systems, Measurement, and Control*, vol. 113, no. 3, pp. 354–362, 1991.

[10] J. Swevers, F. Al-Bender, C. G. Ganseman, and T. Projogo, "An integrated friction model structure with improved presliding behavior for accurate friction compensation", *IEEE Transactions on Automatic Control*, vol. 45, no. 4, pp. 675–686, 2000.

[11] W. He, Y. Dong, and C. Sun, "Adaptive neural impedance control of a robotic manipulator with input saturation", *IEEE Transactions on Systems, Man, and Cybernetics: Systems*, vol. 46, no. 3, pp. 334–344, 2015.

[12] W. He, Y. Sun, Z. Yan, C. Yang, Z. Li, and O. Kaynak, "Disturbance observer-based neural network control of cooperative multiple manipulators with input saturation", *IEEE Transactions on Neural Networks and Learning Systems*, vol. 31, no. 5, pp. 1735–1746, 2019.

[13] Y. Liu, S. Lu, D. Li, and S. Tong, "Adaptive controller design-based ABLF for a class of nonlinear time-varying state constraint systems", *IEEE Transactions on Systems, Man, and Cybernetics: Systems*, vol. 47, no. 7, pp. 1546–1553, 2016.

[14] R. Kikuuwe, "A sliding-mode-like position controller for admittance control with bounded actuator force", *IEEE/ASME Transactions on Mechatronics*, vol. 19, no. 5, pp. 1489–1500, 2014.

[15] H. M. Wang, Y. P. Pan, S. H. Li, and H. Y. Yu, "Robust sliding mode control for robots driven by compliant actuators", *IEEE Transactions on Control Systems Technology*, vol. 27, no. 3, pp. 1259–1266, 2019.

[16] Q. Hu, L. Xu, and A. Zhang, "Adaptive backstepping trajectory tracking control of robot manipulator", *Journal of the Franklin Institute*, vol. 349, no. 3, pp. 1087–1105, 2012.

[17] N. Nikdel, M. Badamchizadeh, V. Azimirad, and M. A. Nazari, "Fractional-order adaptive backstepping control of robotic manipulators in the presence of model uncertainties and external disturbances", *IEEE Transactions on Industrial Electronics*, vol. 63, no. 10, pp. 6249–6256, 2016.

[18] B. S. Park, S. J. Yoo, J. B. Park, and Y. H. Choi, "Adaptive neural sliding mode control of nonholonomic wheeled mobile robots with model uncertainties", *IEEE Transactions on Control Systems Technology*, vol. 17, no. 1, pp. 207–214, 2009.

[19] L. Yu, S. Fei, L. Sun, J. Huang, and G. Yang, "Design of robust adaptive neural switching controller for robotic manipulators with uncertainty and disturbances", *Journal of Intelligent and Robotic Systems*, vol. 77, pp. 571–581, 2015.

[20] B. K. Yoo and W. C. Ham, "Adaptive control of robot manipulator using fuzzy compensator", *IEEE Transactions on Fuzzy Systems*, vol. 8, no. 2, pp. 186–199, 2000.

[21] B. M. Yilmaz, E. Tatlicioglu, A. Savran, and M. Alci, "Self-adjusting fuzzy logic based control of robot manipulators in task space", *IEEE Transactions on Industrial Electronics*, vol. 69, no. 2, pp. 1620–1629, 2021.

[22] H. Sasaki and T. Matsubara, "Variational policy search using sparse gaussian process priors for learning multimodal optimal actions", *Neural Networks*, vol. 143, pp. 291–302, 2021.

[23] E. Sariyildiz, R. Oboe, and K. Ohnishi, "Disturbance observer-based robust control and its applications: 35th anniversary overview", *IEEE Transactions on Industrial Electronics*, vol. 67, no. 3, pp. 2042–2053, 2020.

[24] M. J. Kim and W. K. Chung, "Disturbance-observer-based pd control of flexible joint robots for asymptotic convergence", *IEEE Transactions on Robotics*, vol. 31, no. 6, pp. 1508–1516, 2016.

[25] E. Sariyildiz and K. Ohnishi, "Stability and robustness of disturbance observer-based motion control systems", *IEEE Transactions on Industrial Electronics*, vol. 62, no. 1, pp. 414–422, 2015.

[26] E. Sariyildiz, H. Sekiguchi, T. Nozaki, B. Ugurlu, and K. Ohnishi, "A stability analysis for the acceleration-based robust position control of robot manipulators via disturbance observer", *IEEE/ASME Transactions on Mechatronics*, vol. 23, no. 5, pp. 2369–2378, 2018.

[27] W. H. Chen, D. J. Ballance, P. J. Gawthrop, and J. O'Reilly, "A nonlinear disturbance observer for robotic manipulators", *IEEE Transactions on Industrial Electronics*, vol. 47, no. 4, pp. 932–938, 2000.

[28] T. C. Hsia and L. S. Gao, "Robot manipulator control using decentralized linear time-invariant time-delayed joint controllers", in *Proc. IEEE International Conference on Robotics and Automation (ICRA)*, 1990, pp. 2070–2075.

[29] J. Baek, M. Jin, and S. Han, "A new adaptive sliding-mode control scheme for application to robot manipulators", *IEEE Transactions on Industrial Electronics*, vol. 63, no. 6, pp. 3628–3637, 2016.

[30] S. Cho, M. Jin, T. Kuo, and J. Lee, "Stability guaranteed auto-tuning algorithm of a time-delay controller using a modified Nussbaum function", *International Journal of Control*, vol. 87, no. 9, pp. 1926–1935, 2014.

[31] M. Jin, J. Lee, P. H. Chang, and C. Choi, "Practical nonsingular terminal sliding-mode control of robot manipulators for high-accuracy tracking control", *IEEE Transactions on Industrial Electronics*, vol. 56, no. 9, pp. 3593–3601, 2009.

[32] M. Jin, J. Lee, and N. G. Tsagarakis, "Model-free adaptive control of humanoid robots with flexible joints", *IEEE Transactions on Industrial Electronics*, vol. 64, no. 2, pp. 1706–1715, 2017.

[33] J. Lee, P. H. Chang, and M. Jin, "Adaptive integral sliding mode control with time-delay estimation for robot manipulators", *IEEE Transactions on Industrial Electronics*, vol. 64, no. 8, pp. 6796–6804, 2017.

[34] J. Lee, M. L. Jin, N. Kashiri, D. G. Caldwell, and N. G. Tsagarakis, "Inversion-free force tracking control of piezoelectric actuators using fast finite-time integral sliding-mode", *Mechatronics*, vol. 57, pp. 39–50, 2019.

[35] Y. Wang, F. Yan, J. Chen, F. Ju, and B. Chen, "A new adaptive time-delay control scheme for cable-driven manipulators", *IEEE Transactions on Industrial Informatics*, vol. 15, no. 6, pp. 3469–3481, 2019.

[36] K. Youcef-Toumi and S. T. Wu, "Input/Ooutput linearization using time delay control", *Journal of System Dynamics, Measurement, and Control*, vol. 114, no. 1, pp. 10–19, 1992.

[37] Y. J. Huang, T. C. Kuo, and S. H. Chang, "Adaptive sliding-mode control for nonlinear systems with uncertain parameters", *IEEE Transactions on Systems, Man, and Cybernetics, Part B (Cybernetics)*, vol. 38, no. 2, pp. 534–539, 2008.

[38] K. Shao, R. Tang, F. Xu, X. Wang, and J. Zheng, "Adaptive sliding mode control for uncertain Euler–Lagrange systems with input saturation", *Journal of the Franklin Institute*, vol. 358, no. 16, pp. 8356–8376, 2021.

[39] C. Yang, D. Huang, W. He, and L. Cheng, "Neural control of robot manipulators with trajectory tracking constraints and input saturation", *IEEE Transactions on Neural Networks and Learning Systems*, vol. 32, no. 9, pp. 4231–4242, 2020.

[40] E. Arefinia, H. A. Talebi, and A. Doustmohammadi, "A robust adaptive model reference impedance control of a robotic manipulator with actuator saturation", *IEEE Transactions on Systems, Man, and Cybernetics: Systems*, vol. 50, no. 2, pp. 409–420, 2017.

[41] C. Li, F. Liu, Y. Wang, and M. Buss, "Concurrent learning-based adaptive control of an uncertain robot manipulator with guaranteed safety and performance", *IEEE Transactions on Systems, Man, and Cybernetics: Systems*, 2021. DOI: 10.1109/TSMC.2021.3064971.

[42] D. Q. Mayne, J. B. Rawlings, C. V. Rao, and P. O. Scokaert, "Constrained model predictive control: Stability and optimality", *Automatica*, vol. 36, no. 6, pp. 789–814, 2000.

[43] G. P. Incremona, A. Ferrara, and L. Magni, "MPC for robot manipulators with integral sliding modes generation", *IEEE/ASME Transactions on Mechatronics*, vol. 22, no. 3, pp. 1299–1307, 2017.

[44] N. Nikdel, P. Nikdel, M. A. Badamchizadeh, and I. Hassanzadeh, "Using neural network model predictive control for controlling shape memory alloy-based manipulator", *IEEE Transactions on Industrial Electronics*, vol. 61, no. 3, pp. 1394–1401, 2013.

[45] J. Nubert, J. Köhler, V. Berenz, F. Allgöwer, and S. Trimpe, "Safe and fast tracking on a robot manipulator: Robust MPC and neural network control", *IEEE Robotics and Automation Letters*, vol. 5, no. 2, pp. 3050–3057, 2020.

[46] A. Carron, E. Arcari, M. Wermelinger, L. Hewing, M. Hutter, and M. N. Zeilinger, "Data-driven model predictive control for trajectory tracking with a robotic arm", *IEEE Robotics and Automation Letters*, vol. 4, no. 4, pp. 3758–3765, 2019.

[47] I. Mitsioni, Y. Karayiannidis, J. A. Stork, and D. Kragic, "Data-driven model predictive control for the contact-rich task of food cutting", in *Proc. IEEE-RAS 19th International Conference on Humanoid Robots (Humanoids)*, 2019, pp. 244–250.

[48] J. Matschek, R. Jordanowa, and R. Findeisen, "Direct force feedback using Gaussian process based model predictive control", in *2020 IEEE Conference on Control Technology and Applications (CCTA)*, 2020, pp. 8–13.

[49] Z. Jin, J. Wu, A. Liu, W.-A. Zhang, and L. Yu, "Gaussian process-based nonlinear predictive control for visual servoing of constrained mobile robots with unknown dynamics", *Robotics and Autonomous Systems*, vol. 136, p. 103 712, 2021.

[50] Y. Cao, J. Huang, H. Ru, W. Chen, and C.-H. Xiong, "A visual servo-based predictive control with echo state Gaussian process for soft bending actuator", *IEEE/ASME Transactions on Mechatronics*, vol. 26, no. 1, pp. 574–585, 2020.

[51] I. Lenz, R. A. Knepper, and A. Saxena, "DeepMPC: Learning deep latent features for model predictive control", in *Robotics: Science and Systems*, 2015.

[52] Z. Q. Tang, H. L. Heung, K. Y. Tong, and Z. Li, "A novel iterative learning model predictive control method for soft bending actuators", in *Proc. IEEE International Conference on Robotics and Automation (ICRA)*, 2019, pp. 4004–4010.

[53] S. Chiaverini, "Singularity-robust task-priority redundancy resolution for real-time kinematic control of robot manipulators", *IEEE Transactions on Robotics and Automation*, vol. 13, no. 3, pp. 398–410, 1997.

[54] Y. Nakamura and H. Hanafusa, "Inverse kinematic solutions with singularity robustness for robot manipulator control", *Journal of Dynamic Systems, Measurement, and Control*, vol. 108, no. 3, pp. 163–171, 1986.

[55] A. A. Maciejewski and C. A. Klein, "Numerical filtering for the operation of robotic manipulators through kinematically singular configurations", *Journal of Robotic systems*, vol. 5, no. 6, pp. 527–552, 1988.

[56] K. Pfeiffer, A. Escande, and A. Kheddar, "Singularity resolution in equality and inequality constrained hierarchical task-space control by adaptive nonlinear least squares", *IEEE Robotics and Automation Letters*, vol. 3, no. 4, pp. 3630–3637, 2018.

[57] V. Ortenzi, N. Marturi, V. Rajasekaran, M. Adjigble, and R. Stolkin, "Singularity-robust inverse kinematics solver for tele-manipulation", in *Proc. IEEE 15th International Conference on Automation Science and Engineering (CASE)*, 2019, pp. 1821–1828.

[58] C. C. Cheah and X. Li, "Singularity-robust task-space tracking control of robot", in *Proc. IEEE International Conference on Robotics and Automation (ICRA)*, 2011, pp. 5819–5824.

[59] H. Gao, W. Bi, X. Wu, Z. Li, Z. Kan, and Y. Kang, "Adaptive fuzzy region-based control of Euler-Lagrange systems with kinematically singular configurations", *IEEE Transactions on Fuzzy Systems*, vol. 29, no. 8, pp. 2169–2179, 2020.

[60] A. Dietrich, A. Albu-Schäffer, and G. Hirzinger, "On continuous null space projections for torque-based, hierarchical, multi-objective manipulation", in *Proc. IEEE International Conference on Robotics and Automation (ICRA)*, 2012, pp. 2978–2985.

[61] E. M. Hoffman, A. Laurenzi, L. Muratore, N. G. Tsagarakis, and D. G. Caldwell, "Multi-priority Cartesian impedance control based on quadratic programming optimization", in *Proc. IEEE International Conference on Robotics and Automation (ICRA)*, 2018, pp. 309–315.

[62] Y. Wang, Z. Zhang, C. Li, and M. Buss, "Adaptive incremental sliding mode control for a robot manipulator", *Mechatronics*, vol. 82, p. 102 717, 2022.

[63] Y. Wang, M. Leibold, J. Lee, W. Ye, J. Xie, and M. Buss, "Incremental model predictive control exploiting time delay estimation for a robot manipulator", *IEEE Transactions on Control Systems Technology*, 2022. DOI: 10.1109/TCST.2022.3142629.

[64] J. J. Craig, *Introduction to robotics: Mechanics and control*, Pearson Prentice Hall Upper Saddle River, 2005.

[65] R. Hayat and M. Buss, "Model identification for robot manipulators using regressor-free adaptive control", in *Proc. UKACC 11th International Conference on Control*, 2016, pp. 1–7.

[66] R. P. Pagilla and M. Tomizuka, "An adaptive output feedback controller for robot arms: Stability and experiments", *Automatica*, vol. 37, no. 7, pp. 983–995, 2001.

[67] H. Wang, "Adaptive control of robot manipulators with uncertain kinematics and dynamics", *IEEE Transactions on Automatic Control*, vol. 62, no. 2, pp. 948–954, 2017.

[68] K. Kaltsoukalas, S. Makris, and G. Chryssolouris, "On generating the motion of industrial robot manipulators", *Robotics and Computer-Integrated Manufacturing*, vol. 32, pp. 65–71, 2015.

[69] Z. Ma and P. Huang, "Discrete-time sliding mode control for deployment of tethered space robot with only length and angle measurement", *IEEE Transactions on Aerospace and Electronic Systems*, vol. 56, no. 1, pp. 585–596, 2019.

[70] W. Khalil and E. Dombre, *Modeling, identification and control of robots*, Butterworth, 2004.

[71] M. I. Ullah, S. A. Ajwad, R. U. Islam, U. Iqbal, and J. Iqbal, "Modeling and computed torque control of a 6 degree of freedom robotic arm", in *Proc. International Conference on Robotics and Emerging Allied Technologies in Engineering*, 2014, pp. 133–138.

[72] B. Brahmi, M. Saad, C. Ochoa-Luna, M. H. Rahman, and A. Brahmi, "Adaptive tracking control of an exoskeleton robot with uncertain dynamics based on estimated time-delay control", *IEEE/ASME Transactions on Mechatronics*, vol. 23, no. 2, pp. 575–585, 2018.

[73] J. H. Oh and J. S. Lee, "Control of flexible joint robot system by backstepping design approach", *Intelligent Automation and Soft Computing*, vol. 5, no. 4, pp. 267–278, 1999.

[74] Y. P. Pan, H. M. Wang, X. Li, and H. Y. Yu, "Adaptive command-filtered backstepping control of robot arms with compliant actuators", *IEEE Transactions on Control Systems Technology*, vol. 26, no. 3, pp. 1149–1156, 2018.

[75] M. J. Kim, W. Lee, J. Y. Choi, G. Chung, K. Han, I. S. Choi, C. Ott, and W. K. Chung, "A passivity-based nonlinear admittance control with application to powered upper-limb control under unknown environmental interactions", *IEEE/ASME Transactions on Mechatronics*, vol. 24, no. 4, pp. 1473–1484, 2019.

[76] A. Del Prete and N. Mansard, "Robustness to joint-torque-tracking errors in task-space inverse dynamics", *IEEE Transactions on Robotics*, vol. 32, no. 5, pp. 1091–1105, 2016.

[77] M. J. Kim, Y. Choi, and W. K. Chung, "Bringing nonlinear $h\infty$ optimality to robot controllers", *IEEE Transactions on Robotics*, vol. 31, no. 3, pp. 682–698, 2015.

[78] J. Park and W. K. Chung, "Analytic nonlinear $h\infty$ inverse-optimal control for Euler-Lagrange system", *IEEE Transactions on Robotics and Automation*, vol. 16, no. 4, pp. 847–854, 2000.

[79] S. Roy, S. B. Roy, J. Lee, and S. Baldi, "Overcoming the underestimation and overestimation problems in adaptive sliding mode control", *IEEE/ASME Transactions on Mechatronics*, vol. 24, no. 5, pp. 2031–2039, 2019.

[80] A. Saghafinia, H. W. Ping, M. N. Uddin, and K. S. Gaeid, "Adaptive fuzzy sliding-mode control into chattering-free IM drive", *IEEE Transactions on Industry Applications*, vol. 51, no. 1, pp. 692–701, 2015. DOI: 10.1109/TIA.2014.2328711.

[81] W. He, Z. Yan, and Y. Chen, "Adaptive neural network control of a flapping wing micro aerial vehicle with disturbance observer", *IEEE Transactions on Cybernetics*, vol. 47, no. 10, pp. 3452–3465, 2017.

[82] A. Ait Haddou Ali, Q. P. Chu, E. van Kampen, and C. C. de Visser, "Exploring adaptive incremental backstepping using immersion and invariance for an F-16 aircraft", in *Proc. AIAA Guidance, Navigation, and Control Conference*, 2014, pp. 1–32.

[83] X. Wang, E. Kampen, Q. Chu, and P. Lu, "Incremental sliding-mode fault-tolerant flight control", *Journal of Guidance, Control, and Dynamics*, vol. 42, no. 2, pp. 244–259, 2019.

[84] P. Lu and E. van Kampen, "Active fault-tolerant control system using incremental backstepping approach", in *Proc. AIAA Guidance, Navigation, and Control Conference*, 2015, pp. 1–17.

[85] Y. Wang, W. Chen, S. Zhang, J. Zhu, and L. Cao, "Command-filtered incremental backstepping controller for small unmanned aerial vehicles", *Journal of Guidance, Control, and Dynamics*, vol. 41, no. 4, pp. 954–967, 2018.

[86] Q. Shen, D. Wang, S. Zhu, and E. K. Poh, "Integral-type sliding mode fault-tolerant control for attitude stabilization of spacecraft", *IEEE Transactions on Control Systems Technology*, vol. 23, no. 3, pp. 1131–1138, 2015.

[87] A. Kawamura, H. Itoh, and K. Sakamoto, "Chattering reduction of disturbance observer based sliding mode control", *IEEE Transactions on Industry Applications*, vol. 30, no. 2, pp. 456–461, 1994.

[88] H. Obeid, L. M. Fridman, S. Laghrouche, and M. Harmouche, "Barrier function-based adaptive sliding mode control", *Automatica*, vol. 93, pp. 540–544, 2018.

[89] C. Shen, Y. Shi, and B. Buckham, "Trajectory tracking control of an autonomous underwater vehicle using Lyapunov-based model predictive control", *IEEE Transactions on Industrial Electronics*, vol. 65, no. 7, pp. 5796–5805, 2018.

[90] Y. Wang, L. Cao, S. Zhang, X. Hu, and F. Yu, "Command-filtered adaptive fuzzy backstepping control method of uncertain non-linear systems", *IET Control Theory and Applications*, vol. 10, no. 10, pp. 1134–1141, 2016.

[91] X. Li, X. Zhang, C. Yang, and W. Gui, "Exponential stability analysis for delayed semi-Markovian recurrent neural networks: A homogeneous polynomial approach", *IEEE Transactions on Neural Networks and Learning Systems*, vol. 29, no. 12, pp. 6374–6384, 2018.

[92] Y. Jin, P. H. Chang, M. Jin, and D. G. Gweon, "Stability guaranteed time-delay control of manipulators using nonlinear damping and terminal sliding mode", *IEEE Transactions on Industrial Electronics*, vol. 60, no. 8, pp. 3304–3317, 2013.

[93] G. P. Incremona, A. Ferrara, and L. Magni, "MPC for robot manipulators with integral sliding modes generation", *IEEE/ASME Transactions on Mechatronics*, vol. 22, no. 3, pp. 1299–1307, 2017.

[94] Z. Zhang, M. Leibold, and D. Wollherr, "Integral sliding-mode observer-based disturbance estimation for Euler-Lagrangian systems", *IEEE Transactions on Control Systems Technology*, vol. 28, no. 6, pp. 2377–2389, 2020.

[95] F. Castanos and L. Fridman, "Analysis and design of integral sliding manifold for systems with unmatched perturbations", *IEEE Transactions on Automatic Control*, vol. 51, no. 5, pp. 853–858, 2006.

[96] J. Qin, Q. Ma, H. Gao, and W. X. Zheng, "Fault-tolerant cooperative tracking control via integral sliding mode control technique", *IEEE/ASME Transactions on Mechatronics*, vol. 23, no. 1, pp. 342–351, 2018.

[97] F. Plestan, Y. Shtessel, V. Bregeault, and A. Poznyak, "New methodologies for adaptive sliding mode control", *International Journal of Control*, vol. 83, no. 9, pp. 1907–1919, 2010.

[98] J. Lee, H. Dallali, M. Jin, D. G. Caldwell, and N. G. Tsagarakis, "Robust and adaptive dynamic controller for fully-actuated robots in operational space under uncertainties", *Autonomous Robots*, vol. 43, pp. 1023–1040, 2019.

[99] P. H. Chang and J. H. Jung, "A systematic method for gain selection of robust PID control for nonlinear plants of second order controller canonical form", *IEEE Transactions on Control Systems Technology*, vol. 17, no. 2, pp. 473–483, 2009.

[100] H. S. Jeong and C. W. Lee, "Time delay control with state feedback for Azimuth motion of the frictionless positioning device", *IEEE/ASME Transactions on Mechatronics*, vol. 2, no. 3, pp. 161–168, 1997.

[101] R. Middletone and G. C. Goodwin, "Adaptive computed torque control for rigid link manipulators", in *25th IEEE Conference on Decision and Control (CDC)*, 1986, pp. 68–73.

[102] B. Brahmi, M. Saad, C. Ochoa-Luna, M. H. Rahman, and A. Brahmi, "Adaptive tracking control of an exoskeleton robot with uncertain dynamics based on estimated time-delay control", *IEEE/ASME Transactions on Mechatronics*, vol. 23, no. 2, pp. 575–585, 2018.

[103] Y. Feng, X. Yu, and Z. Man, "Non-singular terminal sliding mode control of rigid manipulators", *Automatica*, vol. 38, no. 12, pp. 2159–2167, 2002.

[104] M. J. Er and S. H. Chin, "Hybrid adaptive fuzzy controllers of robot manipulators with bounds estimation", *IEEE Transactions on Industrial Electronics*, vol. 47, no. 5, pp. 1151–1160, 2000.

[105] R.-J. Wai and R. Muthusamy, "Fuzzy-neural-network inherited sliding-mode control for robot manipulator including actuator dynamics", *IEEE Transactions on Neural Networks and Learning Systems*, vol. 24, no. 2, pp. 274–287, 2012.

[106] H. Michalska and D. Q. Mayne, "Robust receding horizon control of constrained nonlinear systems", *IEEE Transactions on Automatic Control*, vol. 38, no. 11, pp. 1623–1633, 1993.

[107] L. Grüne, "Economic receding horizon control without terminal constraints", *Automatica*, vol. 49, no. 3, pp. 725–734, 2013.

[108] M. B. Kane, J. P. Lynch, and J. Scruggs, "Run-time efficiency of bilinear model predictive control using variational methods, with applications to hydronic cooling", *IEEE/ASME Transactions on Mechatronics*, vol. 24, no. 2, pp. 718–728, 2019.

[109] D. Tavernini, M. Metzler, P. Gruber, and A. Sorniotti, "Explicit nonlinear model predictive control for electric vehicle traction control", *IEEE Transactions on Control Systems Technology*, vol. 27, no. 4, pp. 1438–1451, 2018.

[110] L. Grüne, "Nmpc without terminal constraints", *IFAC Proceedings Volumes*, vol. 45, no. 17, pp. 1–13, 2012.

[111] J. Köhler, M. A. Müller, and F. Allgöwer, "Nonlinear reference tracking: An economic model predictive control perspective", *IEEE Transactions on Automatic Control*, vol. 64, no. 1, pp. 254–269, 2019.

[112] J. Köhler, R. Soloperto, M. A. Müller, and F. Allgöwer, "A computationally efficient robust model predictive control framework for uncertain nonlinear systems", *IEEE Transactions on Automatic Control*, vol. 66, no. 2, pp. 794–801, 2020.

[113] J. Seo, S. Lee, J. Lee, and J. Choi, "Nonaffine helicopter control design and implementation based on a robust explicit nonlinear model predictive control", *IEEE Transactions on Control Systems Technology*, vol. 30, no. 2, pp. 811–818, 2022.

[114] L. Hewing, J. Kabzan, and M. N. Zeilinger, "Cautious model predictive control using Gaussian process regression", *IEEE Transactions on Control Systems Technology*, vol. 28, no. 6, pp. 2736–2743, 2019.

[115] J. Huang, Y. Cao, C. Xiong, and H.-T. Zhang, "An echo state gaussian process-based nonlinear model predictive control for pneumatic muscle actuators", *IEEE Transactions on Automation Science and Engineering*, vol. 16, no. 3, pp. 1071–1084, 2019.

[116] X. Xu, H. Chen, C. Lian, and D. Li, "Learning-based predictive control for discrete-time nonlinear systems with stochastic disturbances", *IEEE Transactions on Neural Networks and Learning Systems*, vol. 29, no. 12, pp. 6202–6213, 2018.

[117] J. M. Manzano, D. Limon, D. M. de la Peña, and J.-P. Calliess, "Robust learning-based MPC for nonlinear constrained systems", *Automatica*, vol. 117, p. 108 948, 2020.

[118] P. O. Scokaert and D. Q. Mayne, "Min-max feedback model predictive control for constrained linear systems", *IEEE Transactions on Automatic Control*, vol. 43, no. 8, pp. 1136–1142, 1998.

[119] O. Khan, G. Mustafa, A. Q. Khan, M. Abid, and M. Ali, "Fault-tolerant robust model predictive control of uncertain time-delay systems subject to disturbances", *IEEE Transactions on Industrial Electronics*, vol. 68, no. 11, pp. 11 400–11 408, 2021.

[120] M. Rubagotti, D. M. Raimondo, A. Ferrara, and L. Magni, "Robust model predictive control with integral sliding mode in continuous-time sampled-data nonlinear systems", *IEEE Transactions on Automatic Control*, vol. 56, no. 3, pp. 556–570, 2010.

[121] F. Bayat, "Model predictive sliding control for finite-time three-axis spacecraft attitude tracking", *IEEE Transactions on Industrial Electronics*, vol. 66, no. 10, pp. 7986–7996, 2019.

[122] N. O. Ghahramani and F. Towhidkhah, "Constrained incremental predictive controller design for a flexible joint robot", *ISA Transactions*, vol. 48, no. 3, pp. 321–326, 2009.

[123] D. L. Marruedo, T. Alamo, and E. Camacho, "Input-to-state stable MPC for constrained discrete-time nonlinear systems with bounded additive uncertainties", in *Proc. 41st IEEE Conference on Decision and Control (CDC)*, vol. 4, 2002, pp. 4619–4624.

[124] S. Heshmati-Alamdari, G. C. Karras, P. Marantos, and K. J. Kyriakopoulos, "A robust predictive control approach for underwater robotic vehicles", *IEEE Transactions on Control Systems Technology*, vol. 28, no. 6, pp. 2352–2363, 2019.

[125] Z. Li and J. Sun, "Disturbance compensating model predictive control with application to ship heading control", *IEEE Transactions on Control Systems Technology*, vol. 20, no. 1, pp. 257–265, 2012.

[126] L. Grüne and P. Jürgen, *Nonlinear model predictive control theory and algorithms*. New York, USA: Springer, 2011.

[127] L. Grüne and V. G. Palma, "Robustness of performance and stability for multistep and updated multistep MPC schemes", *Discrete and Continuous Dynamical Systems*, vol. 35, no. 9, pp. 4385–4414, 2015.

[128] ——, "On the benefit of re-optimization in optimal control under perturbations", in *Proc. 21st International Symposium on Mathematical Theory of Networks and Systems*, 2014, pp. 439–446.

[129] S. Rastegarpour, S. Gros, and L. Ferrarini, "MPC approaches for modulating air-to-water heat pumps in radiant-floor buildings", *Control Engineering Practice*, vol. 95, p. 104 209, 2020.

[130] Y. Fang and A. Armaou, "Nonlinear model predictive control using a bilinear Carleman linearization-based formulation for chemical processes", in *Proc. American Control Conference (ACC)*, 2015, pp. 5629–5634.

[131] J. Köhler, M. A. Müller, and F. Allgöwer, "A nonlinear model predictive control framework using reference generic terminal ingredients", *IEEE Transactions on Automatic Control*, vol. 65, no. 8, pp. 3576–3583, 2019.

[132] D. Limon, A. Ferramosca, I. Alvarado, and T. Alamo, "Nonlinear MPC for tracking piece-wise constant reference signals", *IEEE Transactions on Automatic Control*, vol. 63, no. 11, pp. 3735–3750, 2018.

[133] M. Jin, J. Lee, P. H. Chang, and C. Choi, "Practical nonsingular terminal sliding-mode control of robot manipulators for high-accuracy tracking control", *IEEE Transactions on Industrial Electronics*, vol. 56, no. 9, pp. 3593–3601, 2009.

[134] G. F. Franklin, J. Powell, and M. Workman, *Digital Control of Dynamic Systems*. Englewood Cliffs, NJ: Prentice Hall, 1997.

[135] Z.-P. Jiang and Y. Wang, "Input-to-state stability for discrete-time nonlinear systems", *Automatica*, vol. 37, no. 6, pp. 857–869, 2001.

[136] H. J. Ferreau, C. Kirches, A. Potschka, H. G. Bock, and M. Diehl, "qpOASES: A parametric active-set algorithm for quadratic programming", *Mathematical Programming Computation*, vol. 6, no. 4, pp. 327–363, 2014.

[137] S. Roy, S. B. Roy, J. Lee, and S. Baldi, "Overcoming the underestimation and overestimation problems in adaptive sliding mode control", *IEEE/ASME Transactions on Mechatronics*, vol. 24, no. 5, pp. 2031–2039, 2019.

[138] X. Liang, H. Wang, Y.-H. Liu, W. Chen, G. Hu, and J. Zhao, "Adaptive task-space cooperative tracking control of networked robotic manipulators without task-space velocity measurements", *IEEE Transactions on Cybernetics*, vol. 46, no. 10, pp. 2386–2398, 2016. DOI: 10.1109/TCYB.2015.2477606.

[139] F. Flacco, A. De Luca, and O. Khatib, "Control of redundant robots under hard joint constraints: Saturation in the null space", *IEEE Transactions on Robotics*, vol. 31, no. 3, pp. 637–654, 2015.

[140] A. Escande, N. Mansard, and P.-B. Wieber, "Hierarchical quadratic programming: Fast online humanoid-robot motion generation", *The International Journal of Robotics Research*, vol. 33, no. 7, pp. 1006–1028, 2014.

[141] K. Al Khudir, G. Halvorsen, L. Lanari, and A. De Luca, "Stable torque optimization for redundant robots using a short preview", *IEEE Robotics and Automation Letters*, vol. 4, no. 2, pp. 2046–2053, 2019.

[142] O. Khatib, "A unified approach for motion and force control of robot manipulators: The operational space formulation", *IEEE Journal on Robotics and Automation*, vol. 3, no. 1, pp. 43–53, 1987.

[143] ——, "Inertial properties in robotic manipulation: An object-level framework", *The International Journal of Robotics Research*, vol. 14, no. 1, pp. 19–36, 1995.

[144] J. Nakanishi, R. Cory, M. Mistry, J. Peters, and S. Schaal, "Operational space control: A theoretical and empirical comparison", *The International Journal of Robotics Research*, vol. 27, no. 6, pp. 737–757, 2008.

[145] P. H. Chang and J. W. Jeong, "Enhanced operational space formulation for multiple tasks by using time-delay estimation", *IEEE Transactions on Robotics*, vol. 28, no. 4, pp. 773–786, 2012.

[146] J. Lee, H. Dallali, M. Jin, D. G. Caldwell, and N. G. Tsagarakis, "Robust and adaptive dynamic controller for fully-actuated robots in operational space under uncertainties", *Autonomous Robots*, vol. 43, no. 4, pp. 1023–1040, 2019.

[147] J. Lee, H. Dallali, M. Jin, D. Caldwell, and N. Tsagarakis, "Robust and adaptive whole-body controller for humanoids with multiple tasks under uncertain disturbances", in *Proc. IEEE International Conference on Robotics and Automation (ICRA)*, 2016, pp. 5683–5689.

[148] A. Dietrich, C. Ott, and J. Park, "The hierarchical operational space formulation: Stability analysis for the regulation case", *IEEE Robotics and Automation Letters*, vol. 3, no. 2, pp. 1120–1127, 2018.

[149] C. Ott, A. Dietrich, and A. Albu-Schäffer, "Prioritized multi-task compliance control of redundant manipulators", *Automatica*, vol. 53, pp. 416–423, 2015.

[150] A. Dietrich and C. Ott, "Hierarchical impedance-based tracking control of kinematically redundant robots", *IEEE Transactions on Robotics*, vol. 36, no. 1, pp. 204–221, 2020.

[151] D. Nicolis, F. Allevi, and P. Rocco, "Robust impedance shaping of redundant teleoperators with time-delay via sliding mode control", in *Proc. IEEE/RSJ International Conference on Intelligent Robots and Systems (IROS)*, 2019, pp. 2740–2747.

[152] L. Saab, O. E. Ramos, F. Keith, N. Mansard, P. Soueres, and J.-Y. Fourquet, "Dynamic whole-body motion generation under rigid contacts and other unilateral constraints", *IEEE Transactions on Robotics*, vol. 29, no. 2, pp. 346–362, 2013.

[153] J. D. M. Osorio, A. Abdelazim, F. Allmendinger, and U. E. Zimmermann, "Unilateral constraints for torque-based whole-body control", in *Proc. IEEE/RSJ International Conference on Intelligent Robots and Systems (IROS)*, 2020, pp. 7623–7628.

[154] D. Nicolis, F. Allevi, and P. Rocco, "Operational space model predictive sliding mode control for redundant manipulators", *IEEE Transactions on Robotics*, vol. 36, no. 4, pp. 1348–1355, 2020.

[155] J. Lee, S. H. Bang, E. Bakolas, and L. Sentis, "MPC-based hierarchical task space control of underactuated and constrained robots for execution of multiple tasks", in *Proc. 59th IEEE Conference on Decision and Control (CDC)*, 2020, pp. 5942–5949.

[156] J. Hollerbach and K. Suh, "Redundancy resolution of manipulators through torque optimization", *IEEE Journal on Robotics and Automation*, vol. 3, no. 4, pp. 308–316, 1987.

[157] A. Karami, H. Sadeghian, M. Keshmiri, and G. Oriolo, "Hierarchical tracking task control in redundant manipulators with compliance control in the null-space", *Mechatronics*, vol. 55, pp. 171–179, 2018.

[158] K. P. Tee and R. Yan, "Adaptive operational space control of redundant robot manipulators", in *Proc. American Control Conference (ACC)*, 2011, pp. 1742–1747.

[159] J. Peters and S. Schaal, "Learning to control in operational space", *The International Journal of Robotics Research*, vol. 27, no. 2, pp. 197–212, 2008.

[160] O. Kanoun, F. Lamiraux, and P.-B. Wieber, "Kinematic control of redundant manipulators: Generalizing the task-priority framework to inequality task", *IEEE Transactions on Robotics*, vol. 27, no. 4, pp. 785–792, 2011.

[161] M. Faroni, M. Beschi, N. Pedrocchi, and A. Visioli, "Predictive inverse kinematics for redundant manipulators with task scaling and kinematic constraints", *IEEE Transactions on Robotics*, vol. 35, no. 1, pp. 278–285, 2019.

[162] M. Faroni, M. Beschi, and N. Pedrocchi, "Inverse kinematics of redundant manipulators with dynamic bounds on joint movements", *IEEE Robot. Autom. Lett.*, vol. 5, no. 4, pp. 6435–6442, 2020.

[163] D. Q. Mayne, "Model predictive control: Recent developments and future promise", *Automatica*, vol. 50, no. 12, pp. 2967–2986, 2014.

[164] L. Grüne, "Economic receding horizon control without terminal constraints", *Automatica*, vol. 49, no. 3, pp. 725–734, 2013.

[165] K. Bouyarmane and A. Kheddar, "On weight-prioritized multitask control of humanoid robots", *IEEE Transactions on Automatic Control*, vol. 63, no. 6, pp. 1632–1647, 2018.

[166] A. Wächter and L. T. Biegler, "On the implementation of an interior-point filter line-search algorithm for large-scale nonlinear programming", *Mathematical programming*, vol. 106, no. 1, pp. 25–57, 2006.

[167] R. J. Vanderbei and D. F. Shanno, "An interior-point algorithm for nonconvex nonlinear programming", *Computational Optimization and Applications*, vol. 13, no. 1, pp. 231–252, 1999.

[168] C. Büskens and H. Maurer, "SQP-methods for solving optimal control problems with control and state constraints: Adjoint variables, sensitivity analysis and real-time control", *Journal of computational and applied mathematics*, vol. 120, no. 1-2, pp. 85–108, 2000.

[169] A. Astudillo, J. Gillis, M. Diehl, W. Decré, G. Pipeleers, and J. Swevers, "Position and orientation tunnel-following NMPC of robot manipulators based on symbolic linearization in sequential convex quadratic programming", *IEEE Robot. Autom. Lett.*, vol. 7, no. 2, pp. 2867–2874, 2022.

[170] M. V. Minniti, R. Grandia, F. Farshidian, and M. Hutter, "Adaptive CLF-MPC with application to quadrupedal robots", *IEEE Robotics and Automation Letters*, vol. 7, no. 1, pp. 565–572, 2022.

[171] T. Faulwasser, T. Weber, P. Zometa, and R. Findeisen, "Implementation of nonlinear model predictive path-following control for an industrial robot", *IEEE Transactions on Control Systems Technology*, vol. 25, no. 4, pp. 1505–1511, 2016.

[172] S. Gros, M. Zanon, R. Quirynen, A. Bemporad, and M. Diehl, "From linear to nonlinear MPC: Bridging the gap via the real-time iteration", *International Journal of Control*, vol. 93, no. 1, pp. 62–80, 2020.

[173] A. Zanelli, A. Domahidi, J. Jerez, and M. Morari, "FORCES NLP: An efficient implementation of interior-point methods for multistage nonlinear nonconvex programs", *International Journal of Control*, vol. 93, no. 1, pp. 13–29, 2020.

[174] H. J. Ferreau, C. Kirches, A. Potschka, B. H. Georg, and M. Diehl, "QpOASES: A parametric active-set algorithm for quadratic programming", *Mathematical Programming Computation*, vol. 6, no. 4, pp. 327–363, 2014.

[175] K. Cheshmi, D. M. Kaufman, S. Kamil, and M. M. Dehnavi, "NASOQ: Numerically accurate sparsity-oriented QP solver", *ACM Transactions on Graphics*, vol. 39, no. 4, pp. 1–17, 2020.

[176] D. He, L. Wang, and J. Sun, "On stability of multiobjective nmpc with objective prioritization", *Automatica*, vol. 57, pp. 189–198, 2015.

[177] S. Boyd and L. Vandenberghe, *Convex Optimization*. Cambridge, UK: Cambridge Univ. Press, 2004.

[178] P. Falugi and D. Q. Mayne, "Getting robustness against unstructured uncertainty: A tube-based MPC approach", *IEEE Transactions on Automatic Control*, vol. 59, no. 5, pp. 1290–1295, 2014.

[179] H. Lukas, W. L. P., M. Marcel, and Z. M. N., "Learning-based model predictive control: Toward safe learning in control", *Annual Review of Control, Robotics, and Autonomous Systems*, vol. 3, pp. 269–296, 2020.

[180] K. R. Group, *LBR iiwa 7 R800, LBR iiwa 14 R820 specification, 5th edition*. Augusburg, Germany, 2015.

[181] P. Corke, "Robot manipulator capability in MATLAB: A tutorial on using the robotics system toolbox [tutorial]", *IEEE Robotics and Automation Magazine*, vol. 24, no. 3, pp. 165–166, 2017.

[182] R. Hayat, M. Leibold, and M. Buss, "Robust-adaptive controller design for robot manipulator using the $h\infty$ approach", *IEEE Access*, vol. 6, pp. 51 626–51 639, 2018.

[183] W. M. Grimm, "Robot non-linearity bounds evaluation techniques for robust control", *International Journal of Adaptive Control and Signal Processing*, vol. 4, no. 6, pp. 501–522, 1990.

[184] G. R. Cho, P. H. Chang, S. H. Park, and M. Jin, "Robust tracking under nonlinear friction using time-delay control with internal model", *IEEE Transactions on Control Systems Technology*, vol. 17, no. 6, pp. 1406–1414, 2009.

[185] H. Khalil, *Nonlinear systems*, Englewood Cliffs, NJ: Prentice Hall, 2002.